CHARACTERISTICS OF DIAGENETIC FLUIDS AFFECTING TWO MAJOR CARBONATE UNITS ON VICTORIA ISLAND, NORTHWEST TERRITORIES

By

Jordan-Paul Mathieu

A thesis submitted in partial fulfilment
of the requirements for the degree of
Master of Science (MSc) in Geology

The School of Graduate Studies
Laurentian University
Sudbury, Ontario, Canada

THESIS DEFENCE COMMITTEE/COMITÉ DE SOUTENANCE DE THÈSE

Laurentian Université/Université Laurentienne
School of Graduate Studies/École des études supérieures

Title of Thesis Titre de la thèse	CHARACTERISTICS OF DIAGENETIC FLUIDS AFFECTING TWO MAJOR CARBONATE UNITS ON VICTORIA ISLAND, NORTHWEST TERRITORIES
Name of Candidate Nom du candidat	Mathieu, Jordan-Paul
Degree Diplôme	Master of Science
Department/Program Département/Programme	Geology
Date of Defence Date de la soutenance	February 27, 2014

APPROVED/APPROUVÉ

Thesis Examiners/Examinateurs de thèse:

Dr. Elizabeth C. Turner
(Co-supervisor/Co-directrice de thèse)

Dr. Daniel J. Kontak
(Co-supervisor/Co-directeur de thèse)

Dr. Darrel G. F. Long
(Committee member/Membre du comité)

Dr. Keith Dewing
(External Examiner/Examinateur externe)

Approved for the School of Graduate Studies
Approuvé pour l'École des études supérieures
Dr. David Lesbarrères
M. David Lesbarrères
Director, School of Graduate Studies
Directeur, École des études supérieures

ACCESSIBILITY CLAUSE AND PERMISSION TO USE

ABSTRACT

Diagenetic histories of Proterozoic and Paleozoic carbonate strata on Victoria Island, in the Canadian arctic, are poorly understood, and their potential to be associated with base metals or petroleum is unknown. Using fluid inclusion and geochemical techniques, it was determined that the diagenetic fluid compositions of two major carbonate units, the Wynniatt Formation and the "Victoria Island formation", were largely controlled by fluid-rock reactions in reservoirs and by mixing of multiple fluids. Diagenesis of the Wynniatt Formation resulted from the progression from a shale-dominant fluid mixture to a meteoric-dominant mixture. Fluid composition of "Victoria Island formation" was a shale-dominant mixture. A change in fluid:rock from low to high was recorded during diagenesis of both units. Metals and hydrocarbons transported to the study sites were acquired by the fluids during interaction with the respective source reservoirs. Mixing of diagenetic fluids follows the established 'mixing model' used to explain many other mineralised locations. The diagenetic fluids that affected the strata in this study were comparable to those that produced the Polaris Zn-Pb deposit. This similarity suggests that there is potential for mineralisation on Victoria Island.

Keywords: carbonate diagenesis, fluid origin, fluid inclusion, evaporate mounds, SIMS, isotopes, rare-earth elements, Franklinian Basin, Shaler Supergroup, Victoria Island, Wynniatt Formation, "Victoria Island formation", karst

CO-AUTHORSHIP STATEMENT

Chapter 2 was co-authored with E.C. Turner and R.H. Rainbird. Fieldwork, major interpretations, and the first draft of the manuscript were done by the candidate. The co-authors concieved the project and edited the manuscript, adding their experience and knowledge. Chapter 3 and 4 were co-authored with D.J. Kontak and E.C. Turner. Fieldwork was done by the candidate and Dr. E. Turner. Both projects were conceived by the co-authors. Under the supervision of Drs. Turner and Kontak, analytical procedeures were done by the candidate. Guidence and training was provided by the co-authors, but the main interpretations and conclusions were made by the candidate. The first drafts of both manuscripts were done by the candidate with editing done by the co-authors.

ACKNOWLEDGEMENTS

First and foremost I would like to thank my supervisors Drs. Elizabeth Turner and Daniel Kontak for their expertise, guidance, and patience as well as for the opportunity to undertake this project; much appreciation is given to them for allowing me the freedom to work primarily from home. Thanks are also given to the Geological Survey of Canada (GSC) for funding and organising the field portion of this study.

Thanks to my two girls Raffles and Battosai for their unwavering patience and motivation throughout the duration of the project. I would like to offer my immeasurable gratitude to my sister Koral Blais for providing me with a place to live to finish this project. Many thanks are extended to Ryan Auld, Teresa Rzezniczak, and Jose Knee for providing essential breaks and entertainment, in addition to providing a place to sleep when needed.

TABLE OF CONTENTS

LIST OF FIGURES

LIST OF TABLES

CHAPTER 1 - INTRODUCTION

1.1 Introduction

The Canadian Arctic islands contain numerous carbonate-hosted mineralised (Zn-Pb) and hydrocarbon-bearing (oil, gas, and bitumen) areas. In addition to the Polaris and Nanisivik Zn-Pb deposits on Little Cornwallis Island and Baffin Island, respectively (Dewing *et al.*, 2007a; Dewing *et al.,* 2007b), Zn-Pb showings have been documented on Ellesmere (in Cape Clay and Hazen formations; Harrison *et al.,* 1999), Bathurst (Blue Fiord and Thumb Mountain formations; Anglin & Harrison 1999), Cornwallis (Thumb Mountain and Barlow Inlet formations; Turner 2001, Turner & Dewing 2004), and Baffin (Society Cliffs Formation/Nanisivik Formation; Sangster 1998, Turner 2011) islands. With the exception of the showings on Baffin Island (Proterozoic), showings are predominantly in lower to middle Paleozoic (O-D) formations and are of similar age and tectonic environment to the Cambro-Ordovician "Victoria Island formation" dolostone of Dewing *et al.* (2013) (formerly map-unit 10b of Thorsteinsson and Tozer, 1962) on Victoria Island. In addition to similarities with other Zn-Pb-hosting units, stream and sediment samples from Victoria Island suggest the possibility of Zn and Pb mineralisation (detrital sphalerite and galena) in the area of Minto Inlet (McCurdy *et al.,* 2013). Multiple oil and gas wells have been drilled in the Arctic with little success in the Paleozoic strata (Obermajer *et al.,* 2010); the West Bent Horn well on Cameron Island was one of the successful wells and produced 2.02 million barrels of oil. This deposit is hosted by the Devonian Blue Fiord Formation with a possible source in the Cape Phillips Formation

(Obermajer *et al.,* 2010). There has been greater success in drilling in the late Paleozoic to Mesozoic Sverdrup basin, (Harrison 1994; Gentzis *et al.,* 1996; Chen *et al.,* 2000). Bitumen showings have been documented on Victoria (Thorsteinsson and Tozer 1962), Melville (Harrison 1994), and Cornwallis (Turner 2001) islands.

Despite the abundance of showings in the Arctic, new exploration is conservative because of high costs of exploration. One of the aims of the Geological Survey of Canada's geomapping for energy and minerals (GEM) program was to provide information to enhance exploration target selection. This study was part of the Victoria Island GEM project (2010-2013) and is focused on the base-metal potential of two major carbonate units – the Neoproterozoic Wynniatt Formation, a shallow marine intertidal dolostone (Thomson *et al.,* 2014) and the Paleozoic "Victoria Island formation", a fabric-destructive dolostone (Dewing *et al.,* 2013). Both these units contain Paleozoic-aged diagenetic cements that could have been influenced by, or related to, the same events that lead to the mineralisation elsewhere in the archipelago.

Diagenetic cements in these two units recorded information regarding the evolution of the basins in which they formed, specifically, the fluid composition and evolution. The composition, evolution, timing, and mechanism of emplacement of the fluid allows for the assessment of its potential to transport economic commodities to an area. There are several analytical techniques to acquire this information such as: stratigraphy, petrography, fluid inclusion microthermometry, evaporate mound SEM-EDS, stable isotopes, and laser-ablation inductively-coupled mass-spectrometry (LA ICP-MS).

Most diagenetic studies involve the use of petrography, isotopes, and trace element analysis (e.g., Banner *et al.,* 1988; Qing and Mountjoy, 1994; Madden and Wilson

2012). Some studies incorporate fluid inclusion microthermometry to determine diagenetic fluid characteristics (e.g., Kontak and Jackson, 1995; Machel and Buschkoehle, 2008; Haeri-Ardakani *et al.*, 2013). The complementary analysis of evaporate mounds provides additional details on the diagenetic fluid chemistry. This study incorporates all of the aforementioned techniques to analyse and characterise the diagenetic fluids responsible for the diagenetic history of two carbonate units: the "Victoria Island formation" and the Wynniatt Formation, on Victoria Island, Northwest Territories, Canada. This information is used here to assess the economic potential of these units on Victoria Island.

1.2 Structure of thesis

This thesis consists of a general introduction that describes the rationale, objectives and methods for this project, followed by three related manuscripts in formats that reflect their respective (target) journals. The concluding chapter summarises the preceding chapters and acknowledges any differences in interpretations that occurred between the manuscripts. The following is a summary of the purpose and objectives of the following chapters.

Chapter 2 was published as a current research report (Mathieu *et al.*, 2013a) and involves a detailed mapping project of a preserved paleokarst between the Neoproterozoic Wynniatt Formation and the Cambrian "Clastic unit". This study involved recording the type and location of karst feature present in the Wynniatt Formation and sand volcano pipes in the Cambrian clastic unit; possible environmental setting and source of the sand volcanoes were also established for this locality. Wynniatt Formation samples were collected at this site for the diagenetic portion of this study. Temporal constraints of cement

precipitation were established based on spatial relationships between the Wynniatt Formation, the Cambrian clastic unit, and the diagenetic cements.

Chapter 3 was published in a special PACROFI fluid inclusion volume of *Geofluids* (Mathieu *et al.*, 2013b). Following the methods of Goldstein and Reynolds (1994) and Kontak (2004) for fluid inclusion microthermometry and evaporate mound analysis, respectively, fluid chemistry was determined for fluid inclusions in diagenetic cements hosted in the Wynniatt Formation and "Victoria Island formation". This chapter establishes thermal conditions (via homogenisation temperatures (T_h)), salinity and ion content of the fluid. These were used as guides for interpretations in chapter 4.

Chapter 4 is formatted for submission to the journal *Chemical Geology*. This paper uses *in situ* measurements of both stable isotopes (O, S), using the SIMS technique, and REE analyses, measured using an LA ICP-MS method, to build on fluid source and evolution constraints established in chapter 3. Samples to be analysed for oxygen isotopes were sent to University of Manitoba, samples for sulphur isotope analyses were sent to Memorial University, and LA ICP-MS analyses were done at Laurentian University.

1.3 Methods

1.3.1 Fluid inclusion microthermometry

Since Roedder (1968) utilised fluid inclusions to characterise the fluids at the Pine Point Zn-Pb deposit in the Northwest territories, Canada, fluid inclusions have been readily incorporated into the study of basin analysis (e.g., McNaughton and Smith, 1986; Goldstein, 1990; Kontak, 1995; Bril *et al.*, 1996; Lonnee and Machel, 2006; Machel and

Buschkoehle, 2008; Appold and Wenz, 2011; Dolnicek *et al.*, 2012; Haeri-Ardakani *et al.*, 2013). Fluid inclusions are aliquots of fluid trapped in crystals. A group of fluid inclusions that were trapped at the same time and display similar characteristics are referred to as fluid inclusion assemblages (FIA; Goldstein and Reynolds, 1994). Goldstein and Reynolds (1994), advancing on the earlier work of Roedder (1984), classified FIAs as primary, secondary, or pseudo-secondary depending on their entrapment timing relative to crystal growth. Primary FIAs are those which are trapped during crystal growth and represent the precipitating fluid. Secondary FIAs post-date crystal-precipitation and are located along cross-cutting fractures; these fluids do not, therefore, represent the original precipitating fluid. Pseudo-secondary FIAs are formed along healed fractures that formed in a crystal during its precipitation, and may represent the fluid from which the crystal precipitated. Fluid inclusion assemblages are used instead of individual fluid inclusions because (1) they can be identified with temporal relationships, (2) they provide a way to identify post-entrapment alteration that may have occurred (e.g., necking), and (3) they are more statistically meaningful than a single inclusion. In order for FIAs to be effective, they must adhere to "Roedder's rules" (Bodnar, 2003) in that they represent (1) a homogeneous fluid, (2) an isochoric (constant density) system, and (3) a chemically closed system.

Petrography identifies the type of FIA and establishes its timing in the paragenetic sequence. It is also used to determine whether the fluid inclusions have been necked, whether secondary phases are present in the inclusion (e.g., halite), and whether the fluid was trapped as a homogeneous fluid (i.e., whether boiling occurred).

Freezing and melting experiments on FIAs provides information on the salinity and dissolved ion content of the fluid. Because of a fluid's ability to be metastable at temperatures below its freezing point, more useful temperatures (rather than freezing temperature) are the eutectic and final ice-melting temperatures (T_e and T_m, respectively). The eutectic melting temperature is that at which the frozen fluid (i.e., single or mixed solid phases) first starts to melt. This temperature is a function of the composition of the fluid's solutes. Pure water, for example, would have a T_e of 0°C because it contains no solutes (e.g., NaCl). The most common dissolved ions in precipitating fluids are Na, K, Ca, and Mg (McCaffrey *et al.*, 1987; Hanor, 1994; Shepherd *et al.*, 1998; Bukowski *et al.*, 2000; Lowenstein *et al.*, 2005). These ions depress T_e to different extents: Na and K depress it the least, whereas Ca can depress the T_e to -52°C (Goldstein and Reynolds, 1994). The final dissolution temperature of ice in a fluid inclusion, referred to as the temperature of ice melting (T_m), is a function of the fluid's salinity. A high-salinity fluid has a lower T_m than a low-salinity fluid. For example, meteoric (i.e., fresh) water has a T_m at 0°C because it lacks salinity.

Homogenisation temperature (T_h) of a fluid inclusion records the minimum temperature of entrapment (Goldstein and Reynolds, 1994). This temperature is determined by heating the inclusion until the two-phase (liquid and vapour) fluid becomes a single-phase (homogeneous)fluid. True trapping temperature is not recorded by T_h because T_h only represents the temperature at which the fluid moves off of the liquid-vapour line, above the solvus in T-density space, and into the one-phase field; the true trapping temperature is a function of the pressure at the time of entrapment (Roedder and Bodnar, 1980). With an independent estimate of the pressure at the time of fluid entrapment (e.g.,

known thickness of overlying strata), the true trapping temperature can be calculated (Roedder and Bodnar, 1980) and the difference between the homogenisation and trapping temperatures is referred to as the "pressure correction" (Goldstein and Reynolds, 1994)

1.3.2 Evaporate mound analysis

Decrepitation of fluid inclusions occurs when the internal pressure of the fluid inclusion surpasses the confining pressure of the crystal as the temperature of the fluid inclusion is increased. As a result of decrepitation, the fluid moves along microfractures to the surface of the fluid inclusion wafer where it is evaporated, leaving precipitated solutes behind (typically chlorides) as mounds. Each mound produced is representative of either a single fluid inclusion or fluids from several inclusions, and is related to both the inclusion's volume and the concentration of dissolved ions in the trapped fluid (Haynes *et al.*, 1988), and can be used qualitatively to determine salinity. Such evaporate mounds can be analysed semi-quantitatively with a scanning electron microscope (SEM) that is coupled with an electron dispersion spectrometer (EDS) to determine the composition of both cations (e.g., Na, Ca, K, Mg, Mn) and anions (e.g., Cl, S) present in the fluid (Haynes and Kesler, 1987; Haynes *et al.*, 1988; Heinrich and Cousens, 1989; Kontak, 2004). If the salinity of the fluid is known (e.g., 20 wt. % eq. NaCl), a good approximation of the elemental concentrations can also be quantified.

Artificially decrepitated fluid inclusions (i.e., fluid inclusions decrepitated in the lab) have been used to study fluid composition for sedimentary-hosted base-metal deposits (e.g., Haynes and Kesler, 1987; Haynes *et al.*, 1988; Savard and Chi, 1998; Kesler *et al.*, 2007; Fischer 2012; Kontak, 2013) and magmatic deposits (e.g., Kontak 2004;

Tweedale *et al.*, 2013). This study demonstrates the utility of this method by applying it to samples that would otherwise provide no (or very little) information on fluid composition, including the observation of sulphide nanoparticles in fluid inclusions, a phenomenon that has not been documented previously.

1.3.3 Stable isotopes

Stable isotopes are a standard tool used in studying carbonate-rock diagenesis (e.g., Andrews *et al.*, 1987; Banner *et al.*, 1988; Qing, 1998; Adams *et al.*, 2000; Savard *et al.*, 2000; Lonnee and Machel, 2006; Reid *et al.*, 2013). Fractionation of different isotopes is controlled by isotope-specific factors. Oxygen isotopes, for example, fractionate primarily by temperature; higher temperature result in less fractionation. This temperature dependence provides a geothermometer for diagenetic phases. Fractionation of oxygen is also dependant on latitude and elevation of meteoric fluid (Dansgaard, 1964; Hitchon and Krouse, 1972). Seawater is a common fluid involved in diagenesis. The $\delta^{18}O$ of the oceans has been relatively constant for geologic history (Veizer et al 1997, 1999), therefore ocean water provides an excellent standard (SMOW).

The sulphur isotope value of seawater is a balance of input and output of sulphur from various processes: magmatic processes and erosion introduce S, whereas subduction and precipitation of sulphate minerals remove S from the seawater reservoir. As a result, seawater sulphate typically has a stable isotopic signature of +20‰ (CDT) for most of the Phanerozoic (Ohmoto and Rye, 1979).Kinetic fractionation is one of the main causes of fractionation of sulphur isotopes. Sulphate reduction by bacterial (BSR) and thermochemical (TSR) processes are among the most conspicuous causes at diagenetic tempera-

tures. The distinction between these two processes is a function of temperature. Bacterial sulphate reduction can only occur at temperatures at which sulphur-reducing bacteria can metabolise; although BSR can occur at temperatures near 100°C, the majority of BSR occurs at temperatures <80°C (Ohmoto and Rye, 1979; Jørgensen *et al.*, 1992; Machel 2001). There is evidence that some sulphur-reducing bacteria can metabolise at temperatures above 100°C (but still below 120°C; Jørgensen *et al.*, 1991; Stetter *et al.*, 1993). Bacteria reduce sulphate by oxidising organic matter through a series of irreversible reactions (Ohmoto and Rye, 1979; Machel, 2001). Sulphur-reducing bacteria, such as *Desulfovibrio desulfuricans*, prefer ^{32}S over ^{34}S, which causes a "vital effect" in isotope fractionation (Ohmoto and Rye, 1979?), similar to that caused by organisms that preferentially use lighter carbon isotopes in their structures (e.g., plants, O'Leary, 1981). Fractionation as a result of BSR is -45 +/- 20‰, which produces the characteristic isotopically light sulphide species (e.g., H_2S, or HS^-) that are commonly negative relative to the Canyon Diablo troilite (CDT) standard (Ohmoto and Rye, 1979; Machel, 2001; Seal, 2006). Although not exclusive to BSR, pyrite framboids are typical end products associated with BSR (Machel *et al.*, 1995; Riciputi *et al.*, 1996; Machel, 2001; Ohfuji and Rickard, 2005).

Temperatures beyond the BSR range (i.e., >100°C) are dominated by TSR. The lower temperature limit of TSR is not well defined (Machel *et al.*, 1995), but typically is considered to be approximately 100°C to 140°C (Machel *et al.*, 1995; Machel, 2001). Thermodynamically, TSR can occur at temperatures as low as 25°C (Worden and Smalley, 1996); however, below approximately 100°C, the reaction kinetics are too low for TSR to be significant (Machel, 2001). Sulphur is reduced via the thermal maturation

of organic matter and causes a fractionation of -15 +/- 5‰ (Ohmoto and Rye, 1979; Machel *et al.*, 1995).

Another factor in sulphur fractionation is the openness of a system. Systems closed to sulphate will result in the reduced sulphur attaining the same isotopic signature of the sulphate it was reduced from (Orr, 1974). If a system is closed to H_2S, that is to say that reduced sulphur is being produced faster than it is being removed, BSR will cease once H_2S levels are high enough to be toxic to the bacteria species (Reis *et al.*, 1992; Machel, 2001). Systems closed to H_2S do not affect the TSR reactions. Reduced sulphur will react with transition metals (if present) immediately, precipitating insoluble sulphides (Ohmoto and Rye, 1979; Lloyd *et al.*, 2001; Ohfuji and Rickard, 2005; Moreau *et al.*, 2007) and removing aqueous H_2S.

Typically, isotopes are addressed as bulk analyses of major phases (e.g., Qing, 1998; Lonnee and Machel, 2006; Heba *et al.*, 2009). Although in general this method is feasible, it assumes that the samples analysed are homogeneous, and cannot identify variations within individual phases. Valley and Graham (1991) showed, using secondary ion mass spectrometry (SIMS), that isotopic composition can vary during the growth of an individual crystal. Because of the microscopic changes that can occur within and between diagenetic cements, SIMS analyses were undertaken in this study in order to track the evolution of fluid via isotopic signatures of phases formed during precipitation.

1.3.4 Trace and rare earth elements

Rare earth elements (REE) are very useful tracers of origin and process because they are similar to each other, and behave in a predictable manner (Elderfield, 1988). In

addition, they are among the most immobile elements (Banner *et al.*, 1988; Elderfield, 1988; Qing and Mountjoy, 1994) - that is to say that they partition into mineral phases rather than being complexed by fluids. Consequently, typical REE patterns are essentially exclusive to specific phases and/or environments. Seawater, although low in elemental concentrations, has a standard REE pattern (Nozaki *et al.*, 1997; Kawabe *et al.*, 1998; Alibo and Nozaki, 1999), which can also resemble that of meteoric water. Because partition coefficients are so much higher in mineral phases than water, large volumes of fluid are required to alter rock REE signatures, or for precipitating phases to inherit the REE signal of the fluid rather than the rock (Banner *et al.*, 1988; Qing and Mountjoy, 1994). Carbonate rocks are several orders of magnitude enriched in REE over seawater (Banner *et al.*, 1988; Nothdurft *et al.*, 2004; Tanaka and Kawabe, 2006) and display a pattern that is typically depleted in light rare earth element (LREE) relative to heavy rare earth element (HREE), when normalised to Post Archean Australian Shale from Pourmand *et al.* (2012) (e.g., Bau *et al.*, 2003; Nothdurft *et al.*, 2004; Wilkinson *et al.*, 2011; Haeri-Ardakari *et al.*, 2013). Anomalies (positive and negative) are a function of enrichment or depletion of a phase relative to a standard and can be used to track the history of a fluid.

Cerium and Eu, unlike other REE, have two valence states, and therefore are redox-sensitive. The valence state of REEs is +3, but Ce also has a +4 state which reacts with oxygen to produce CeO_2 which is insoluble, in which case it is precipitated out, depleting the Ce content of oxidised fluids (De Baar *et al.*, 1983; Elderfield, 1988; German *et al.*, 1995). This depletion is evident on a standard REE plot as a negative Ce anomaly relative to its neighbouring elements La and Pr. In addition to its +3 valence, Eu has a +2 valence, which preferentially substitutes for Ca in plagioclase. Fractionation of Eu occurs

at temperatures that are hotter than typical seawater (Elderfield, 1988). Hydrothermal vent fluids and their related precipitates typically have a positive Eu anomaly due to the temperature dependence of Eu^{2+} (e.g., Wheat *et al.*, 2002; Bao et al 2008; Tang *et al.*, 2013). Groundwater that has interacted with sulphide ore bodies, which presumably formed at high temperatures, may also acquire a positive Eu signature (e.g., Leybourne *et al.*, 2000).

1.3 Statement of responsibilities

Field mapping and sample collection were conducted by the candidate with the assistance of Andrew Durbano. Wynniatt Formation samples used in chapter 3 and 4 were collected at the site described in Chapter 2, and the "Victoria Island formation" samples were collected by Dr. Elizabeth Turner. Samples were cut by the candidate and thin sections were made by Willard Desjardins at Laurentian University. Petrography, microthermometry and SEM-EDS were conducted by the candidate at Laurentian University. Trace and rare earth elements were analysed in the Geochemical Fingerprinting Laboratory at Laurentian University using the LA ICP-MS equipment with Joe Petrus. Although interpretation of the laser results was done by the candidate, raw data reduction was done by Joe Petrus. Samples for SIMS oxygen isotope analysis were prepared by Craig Stewart and analysed by Ryan Sharp at the University of Manitoba. Framboidal pyrite samples were sent to and prepared at Memorial University, Newfoundland, to be analysed for sulphur isotopes by SIMS. This project was designed by Drs. Turner, Kontak, and Rainbird. First drafts of manuscripts for chapters 2, 3, and 4 were written by the candidate. Intellectual input and edits for revised manuscript drafts were provided by co-

authors Drs. Turner, Rainbird and from Drs. Long, and Dewing for chapter 2, Drs. Kontak and Turner (co-authors) for chapters 3 and 4, with edits from reviewers and editor for chapter 3.

CHAPTER 2 - *SEDIMENTARY ARCHITECTURE OF A DEEPLY KARSTED PRECAMBRIAN-CAMBRIAN UNCONFORMITY, VICTORIA ISLAND, NORTH-WEST TERRITORIES*

J. Mathieu[1], E.C. Turner[1] and R.H. Rainbird[2]

[1]*Department of Earth Sciences, Laurentian University, 935 Ramsey Lake Road, Sudbury, Ontario, Canada, P3E 2C6*

[2]*Geological Survey of Canada, 615 Booth Street, Ottawa, Ontario, Canada K1A 0E9*

Abstract

A deeply karsted unconformity separates Proterozoic carbonate rocks of the Wynniatt Formation from overlying Cambrian sandstone near the head of Minto Inlet on Victoria Island, Arctic Canada. Sandstone-filled paleo-caverns, hundreds of metres wide and tens of metres high, are present approximately 10 to 15 m stratigraphically below the nominal stratigraphic contact between Proterozoic and Cambrian rocks; the paleo-caves' position relative to the main unconformity surface suggests development along a paleo-interface possibly associated with the water table. Gryke networks and karstic towers are present in the Wynniatt Formation at the unconformity. Cross-bedded sandstone that overlies the unconformity contains unusual, vertical columnar sandstone structures, decimetres to metres in diameter, which cut sharply across bedding and contains weak concentric layering. These pillar-like structures are attributed to water-escape through

submarine springs, where groundwater flowing through the karst network emerged onto the Cambrian seafloor. The pillars are most densely clustered in the most northern exposure of the sandstone, and diminish in abundance southward, suggesting that the coastline, and source of hydraulic head, were to the north of the study area.

2.1 Introduction

Victoria Island (Fig. 2.1) is underlain by strata of the Neoproterozoic Shaler Supergroup and poorly known, informally defined Cambrian to Devonian sedimentary units dominated by carbonate rocks and subordinate quartzose sandstone. The two successions are separated by a hiatus of approximately 200 million years.

The unconformity between Proterozoic and lower Paleozoic strata locally cuts down to the level of the Wynniatt Formation. This implies removal of 1 to 2 km of strata. The unconformity is locally well exposed and preserves clear evidence of deep karstification. The focus of this project is to document these karst-related features present in the Wynniatt Formation and its effect on deposition of overlying Cambrian sandstone.

2.2 Regional Geology

The bedrock geology of Victoria Island is divided into two main regions (Fig. 2.1): a central core of weakly metamorphosed and broadly folded Neoproterozoic strata, known as the Minto Inlier, and large flanking areas underlain by poorly exposed, mainly flat-lying, largely undescribed Paleozoic rocks. The geology of Victoria Island was first described by Washburn (1947) in a report that dealt mainly with glaciation and geomorphology. A more comprehensive description of the bedrock geology, including definition of Proterozoic sedimentary rocks of the Shaler Group and a 1:1 000 000 geological map, was produced by Thorsteinsson and Tozer (1962). The Shaler Group was studied in more detail by Young (see Young, 1981 and references therein) and then by Rainbird (e.g., Rainbird, 1991, 1992a), who further subdivided the stratigraphy and elevated the Shaler

Group to Supergroup (Rainbird *et al.*, 1994). The Shaler Supergroup consists of the Rae Group (previously the Glenelg Formation of Thorsteinsson and Tozer, 1962), the Reynolds Point Group, and the Minto, Wynniatt, Kilian, Kuujjua, and Natkusiak formations.

The Wynniatt Formation is a succession of shallow-marine limestone and dolostone that was divided into four informal members (Rainbird, 1991): the 'lower', 'shale', 'stromatolitic', and 'upper' members. The Kilian Formation consists of evaporite rocks interlayered with shale, sandstone and limestone, and was divided into eight informal members that form three complete upward-shallowing sequences. The Kuujjua Formation consists mainly of coarse-grained quartz arenite that was deposited in a broad fluvial braid-plain (Rainbird, 1992a). The uppermost unit of the Shaler Supergroup is the Natkusiak Formation, a 1100 m-thick flood basalt that is part of the Franklin igneous event (~720 Ma; Heaman et al., 1992). Two regional folds affect the Proterozoic succession on Victoria Island, the northeast-trending Walker Bay anticline and Holman Island syncline. Neither of these folds causes inclination of strata to exceed 10°. Phanerozoic strata are not affected by these folds (Thorsteinsson and Tozer, 1962).

The Shaler Supergroup is considered to be of early Neoproterozoic age based on detrital zircon geochronology (Rainbird et al., 1992; 1997) and has been correlated with the Mackenzie Mountains supergroup (Rainbird, 1992b; Rainbird *et al.*, 1996; 1997; Long *et al.*, 2008; Jones *et al.*, 2010). The Shaler Supergroup is unconformably overlain by Phanerozoic strata including Cambrian to Silurian rocks (based on fossil assemblages) mapped as units 10a and 10b by Thorsteinsson and Tozer (1962). Map-unit 10a, the basal unit, was described as sandstone with dolostone and shale. Map-unit 10b was de-

scribed as a fairly uniform succession of Ordovician to Silurian dolostone and is the most common bedrock type on the island.

2.3 Methods

An area approximately 1.5 km^2 was mapped near the head of the Minto Inlet (Fig. 2.1) where the karsted unconformity is exposed. This area represents a site in which one to two kilometres of subaerial erosion occurred prior to the preservation of the paleo-karst by burial under younger strata. Collection of geographic coordinates for all exposed karst and cylindrical sandstone structures was achieved using a portable computer/GPS (GETAC) unit. Accuracy of the GPS coordinates was within a few metres.

2.4 Results

The detailed map region contains exposures of the "upper carbonate member" of the Wynniatt Formation in the north, and the "lower clastic" and "tan" Cambrian units [map unit 10a of Thorsteinsson and Tozer (1962)] toward the south (Fig. 2.2). It should be noted that within the mapped area there are several areas of Quaternary cover. The contact between Proterozoic and Paleozoic units trends northeast. Strata of the Wynniatt Formation are sub-horizontal and Paleozoic strata are almost flat-lying; the land surface rises to the southeast such that progressively younger Paleozoic strata are preserved.

2.4.1 Wynniatt Formation

The upper carbonate member of the Wynniatt Formation in the study area is a pale tan- to grey-weathering, finely to medium crystalline dolostone that is thickly laminated to medium-bedded at a centimetre to decimetre scale (Fig. 2.3a). Bedding dips five to seven degrees to the southeast. Along the north edge of the mapped area, the dolostone is pale grey and has wavy laminations and thin bedding. Molar-tooth structure, intraclasts, zebra dolomite (Fig. 2.3b), chert nodules (Fig. 2.3c), and columnar branching stromatolites (Fig. 2.3d) typify the Wynniatt Formation at this location. Hydrothermal dolomite veins and masses locally are conspicuous.

Sparry dolomite is present throughout the Wynniatt Formation regionally, but seems to be more abundant in the vicinity of the paleokarst surface. At outcrop scale, the dolomite exhibits three phases: tan-coloured, white, and brown saddle dolomite (Fig. 2.4a). The dolomite occupies veins that are parallel to, and at various orientations to bedding (Figs. 3b and 4b). Local breccia masses (Fig. 2.4c) and small amounts of sulphide minerals (pyrite; Fig. 2.4d) are associated with the dolomite. It was difficult to assess in the field if the sparry dolomite masses and veins cut across the unconformity owing to the contrasting composition of the overlying material (sandstone).

2.4.2 Lower Cambrian "clastic member"

The Cambrian clastic member is divided here for simplicity into three sections at this site: basal cross-bedded, bioturbated, and upper cross-bedded sandstone. The basal cross-bedded section is a mature, purple-red (weathered) and pale grey-purple (fresh), medium-grained, well-sorted, rounded, cross-bedded sandstone with coarse-grained fore-

sets (Fig. 2.5a). The base of this section at this site includes approximately 0.1 to 0.5 m of poorly sorted quartz-pebble conglomerate (Fig. 2.5b). The bioturbated interval is grey-red, fine- to medium-grained, well-sorted, rounded sandstone with vertical burrows (Fig. 2.5c; possibly *Skolithos,* A. Durbano pers. comm., 2011). The upper cross-bedded section is grey to grey-tan, medium-grained, well-sorted, rounded, cross-bedded sandstone (Fig. 2.5 d). The upper contact with the "tan carbonate" member is concealed by Quaternary cover at this location, but elsewhere it is sharp.

2.4.3 Sandstone Cylinders

The basal cross-bedded sandstone in the study area contains numerous large cylindrical sand structures. These cylinders have circular cross-sections with diameters of 10 cm to 14 m (Fig. 2.6a-6d) and sharply cut across the bedding of the sandstone. The vertical cylinder walls are of unknown height (the greatest height observed was approximately 1.5 m). The size and location of 382 of these structures was recorded (Fig. 2.2; Table 2.1). The mode and average diameter of all the cylinders is 130 cm and 60 cm, respectively, with a range between 10 cm and 16 m. The cylinders are exposed in an area of approximately 120 000 m^2 and are most abundant in the northern part (292 cylinders) of the sandstone unit and diminish in number (but not size) to the southwest (30 cylinders; Fig. 2.2). The average diameter of the cylinders from the southern exposure of the sandstone unit is 190 cm with a mode of 100 cm (10 counts) and a range from 10 cm to 970 cm. In the northern exposure of the sandstone unit the average diameter of the cylinders is 120 cm with a mode of 40 and 60 cm (24 counts each) and a range from 10 cm to 16 m.

The core of these structures is moderately to well-sorted, medium-grained sandstone, with centimetre-scale concentric banding. Many of these structures include one band of gravel- to pebble-sized clasts; a few have more than one band of coarse material. These bands of coarse material are not preferentially located within the circular cross-section; central, marginal and intermediate positions were all documented. Cylinders locally cut across other cylinders. Rarely, a small cylinder is present inside a larger one, cross-cutting the larger structure's concentric laminae. Small (approximately 10 cm diameter), steep-sided cone structures with a relief of approximately 3 cm above the bedding-plane of the sandstone are locally preserved (Fig. 2.6c). Cylindrical structures are absent in the bioturbated and upper cross-bedded sections.

2.4.4 Unconformity

The base of the Cambrian sandstone is represented by an irregular unconformity surface in sharp contact with underlying strata of the Wynniatt Formation. Paleokarst features such as grykes, caverns, pans, and towers are preserved locally within the Wynniatt Formation. Grykes, solution-widened joints in carbonate rocks created via interaction with meteoric water (James and Choquette, 1990), locally penetrate the upper surface of the Wynniatt Formation and are both parallel to and perpendicular to dolostone bedding (Fig. 2.7a) creating a complex network. These networks are filled with medium-grained hematitic sandstone. Individual grykes are from one centimetre to several decimetres wide and one metre to decimetres deep. Similar gryke networks in dolostone have also been documented below the base of the Cambrian sandstone elsewhere on Victoria Island.

Sandstone-filled paleo-caverns are present along the edge of a northwest-striking ridge of Wynniatt Formation over a distance of approximately one kilometre (Fig. 2.2 and 7b). The paleocaverns are roughly circular in cross-section, with apparent "diameters" of approximately 30 to 100 m (Fig. 2.7d). Surfaces within these paleocaverns have concave dish-shaped depressions, which may be preserved dissolution pans (James and Choquette, 1990; Fig. 2.7c). The caverns' paleo-floors are not exposed; their paleo-rooves are approximately 10 to 15 m below the main surface of the unconformity. Recent erosion has cut obliquely across the sand-filled caverns, providing exposures of their walls and ceilings. The walls display overhanging remnants of cave walls (Fig. 2.7b). The fill of these features is dominated by sandstone and pebbly sandstone that is identical to that in the basal Cambrian sandstone. Blocks of Wynniatt Formation and sediment of any composition other than sandstone are lacking.

There are two isolated, narrow, relatively high-relief (4 to 5 metres above the stratigraphic contact), units of Wynniatt Fm. upper carbonate that protrude above the nominal stratigraphic level of the unconformity into the Cambrian sandstone (Fig. 2.2); these could possibly be remnants of paleokarst towers (Sweeting, 1972).

2.5 Interpretation

2.5.1 Cylindrical structures

These structures are interpreted as feeder conduits for sand volcanoes. The cylinders formed after the sand was deposited over the karst surface but before the sand lithified. Pulses of water from submarine springs fluidised sediment, moving it upward and through the unconsolidated sand. This truncated bedding and created sand volcanoes

on the seafloor. The inconsistent strength of the water movement caused concentric rings of coarse material to rise in the feeder-zone pipes of the volcanoes. The coarser bands represent pulses of higher water flow and the finer bands pulses of lower water flow. Because the water appears to have come from the underlying Wynniatt Formation karst reservoir, gravel-grade material from the base of the sandstone was carried up the pipes when fluid flow rates were great enough to transport it.

Numerous studies have documented cylindrical structures in a variety of settings. Cylinders have been documented from the Cambrian Potsdam Formation (Hawley and Hart, 1934; Sanford and Arnott, 2010), Permian Talchir Formation (Van Loon and Maulik, 2011), younger rocks from Colorado (Gabelman, 1955) and Nebraska (Guhman and Pederson, 1992), and in modern sediment along the Mississpipi River (Li *et al.,* 1996) and in Tuchodi Lake, British Columbia (Long and Donaldson, 2005). The means by which these cylinders developed is controversial, particularly with respect to the mechanism of fluidisation. Experimental studies of fluidisation have attempted to recreate cylindrical structures in sediment (Hawley and Hart, 1934; Nichols *et al.,* 1994; Owen, 1996; Buck and Goldring, 2003; Kadau *et al.,* 2009; Ross *et al.,* 2011) with variable success.

Sand volcanoes in the Talchir Formation, India, (Van Loon and Maulik, 2011) resemble the Minto Inlet structures, but occupy a smaller geographic area (50 m^2 vs. 120 000 m^2). Sediment liquefaction in the Indian example was attributed to a seismic event. Because a seismic event would normally have caused soft sediment deformation, it was argued that the area was far enough away from the epicentre of the shock as to liquefy the sand, but not create seismites. Because a sand-volcano field like the one described by

Van Loon and Maulik (2011) was produced at the Victoria Island location, and no other soft-sediment deformation is evident, a similar trigger could be invoked for the Minto Inlet structures. However, the pulsing nature of the fluidised sediment, suggested by the concentric rings of coarser material, together with the local cross-cutting relationships between pipes, cannot be explained by a single, instantaneous fluidisation caused by a single seismic event. It could be argued that multiple seismic events could account for the pulsing flow or the cross-cutting relationships between cylinders. However the spatial distribution of the cylinders - that is, decreasing from north to south - must also be taken into consideration. If multiple seismic events occurred as a result of movements along the nearby faults (Fig. 2.1c) the expected distribution should be either even or showing a decrease in abundance from south to north (because the nearest fault is just to the south of the study area).

Clustered cylindrical dewatering structures in a Pleistocene calcarenite that overlies karsted carbonate rock in Salento, Italy were documented by Massari *et al.* (2001). These cylinders were interpreted to have formed when water upwelled from an underlying karst reservoir. Because the cylinders were clustered, had circular cross-sections, and were composed of sand capable of dispersing excess pore pressure, Massari *et al.* (2001) rejected a seismic model. The lack of concentric downfaulting or association with soft-sediment deformation led Massari *et al.* (2001) to reject a model involving collapse of caves to infill the underlying karst. The Minto Inlet cylinders, like the Italian structures, are clustered, circular in cross-section, lack concentric downfaulting patterns or soft-sediment deformation (with one exception), and formed in a pressure-dispersing medium. Because of the similarities, the arguments against seismic and/or cave collapse origins

could similarly be made here. There is one large cylinder among the Victoria Island cylinders that displays an apparent dipping of beds in towards the centre of the structure; concentric banding was not observed in this structure due to vegetative cover. This single occurrence may have been formed through collapse of an underlying karst feature and would then be considered an isolated event.

Li *et al.* (1996) discussed conical extrusive structures with cylindrical structures under them in sands alongside the levees of the Mississippi River. They interpreted the structures as sand boils formed by the flooding of the Mississippi River in 1993. They determined that the large hydraulic head caused by the high artificial levee caused fluid flow under the levee to produce sand boils on the floodplain. The boils were most densely distributed close to the levee, and diminished in both size and number away from the levee (maximum distance from levee was ~100 m). The concentration of the Minto Inlet volcanoes is highest in the northern part of the mapped area and decreases to the southwest, resembling the distribution noted Li *et al.* (1996). Submarine springs appear to exhibit the same spatial distribution as the sand boils of a flooding river: they are most abundant closest to the shore (Fritz and Bahun, 1997; Bayari and Kurttas, 2002; Bayari *et al.*, 2011). In the study of Fritz and Bahun (1997), groundwater was transported through a paleokarst network to submarine springs.

Repeated upward movement of sediment in the Minto Inlet cylinders is indicated by the presence of gravel in the concentric bands of the cylinders (probably derived from a base of clastic unit; Fig. 2.6a and b), along with the single small group of sand volcanoes preserved on a bedding plane (Fig. 2.6c). This provides evidence against models which involve collapse of overlying sands into voids as the mechanism to create these

cylinders. The nonlinear distribution of the cylinders, their circular cross-sections, the well to moderate sorting of the sand, and the southwestward decrease in abundance (Fig. 2.2b), are some of the criteria of Li *et al.* (1996) used in arguing against seismically induced cylinder formation. Although there are faults present around the study area that are assumed to have been active in the Cambrian (Fig. 2.1c) and could be responsible for some isolated instances, the arguments presented here favour a different mechanism of formation for the whole area. The Minto Inlet cylinders more closely resemble the sand volcanoes produced by Mississippi River flooding (Li *et al.*, 1996) and the submarine springs of Fritz and Bahun (1997); these are interpreted as the result of meteoric groundwater flow, concentrated within karst features in the Wynniatt Formation. The flow was driven by a hydraulic head, produced by accumulation of rainwater beneath the nearby carbonate land surface (a freshwater lens) at the time when basal Cambrian sand had just begun to accumulate over the unconformity. The water emerged onto the shallow seafloor as point-sources of fresh water (subaqueous springs). The fresh water rose through the sandy sediment and overlying salt water in a temporally variable manner (pulsing), driven by pressure variations in the hydraulic head. The rising fresh water plume fluidised the sandy sediment, caused upward migration of sand to produce cylindrical channels with crude concentric lamination, and forced pebbles to rise from their position near the basal contact. Conical sand volcanoes would have been expected to develop on the upper surface of the sand (which are rare here due to erosion).

2.5.2 Hydrothermal Dolomite

Field observations of the apparent truncation of hydrothermal dolomite veins by karst features, and hydrothermal dolomite occupying void space around sand fill, provide ambiguous evidence regarding the temporal relationship between the dolomitising hydrothermal fluid and paleokarst development: there appears to be evidence for migration of hydrothermal fluid both before and after development of the unconformity. The timing and origin of the dolomite phases are consequently unknown, and will be addressed by further study.

2.5.3 Karst evolution

During the early Neoproterozoic, when the Shaler Supergroup was deposited, and in the early Cambrian, Laurentia was at a low latitude (~10°; Park, 1994; Irving *et al.*, 2004). There is evidence of both arid climates (Kilian Formation sabkha evaporites; Young 1981) and humid climates (Kuujjua Formation fluvial sandstone; Rainbird, 1992a, 1993). After eruption of the Natkusiak Formation lavas on top of the Kuujjua and Kilian formations at~ 720 Ma (Heaman *et al.*, 1992), there was folding and uplift followed by erosional removal of several kilometres of Neoproterozoic strata, which exposed the upper Wynniatt Formation in the study area. Rainwater and groundwater gradually dissolved the carbonate bedrock of the Wynniatt Formation to form karst features such as grykes, towers, and caverns (Fig. 2.8a). Karstification occurred either late in the Neoproterozoic or, more probably, early in the Cambrian, just prior to transgression and deposition of the sandstone, accounting for preservation of the karst features. Preservation of the cavern system at a stratigraphic position several tens of metres below the unconform-

ity strongly suggests its development at a water table that was associated with a freshwater lens, shortly before deposition of the sandstone. Relative sea level rose, submerging the karstified surface of the Wynniatt Formation and filling the caverns and grykes with quartzose sand, and deposited sandstone layers above the unconforminty. Fresh water was collected over exposed land immediately north of the mapped area and moved through the Wynniatt Formation using the joints and karst features as conduits to feed the submarine springs. The hydraulic head in the karst network was sufficient to fluidise the sediment in and above the karst and mobilize it to propagate upwards towards the sea floor, where it produced submarine springs and sand volcanoes (Fig. 2.8b). The presence of bioturbation in fine- to medium-grained sandstone that overlies the cylinder-bearing interval suggests a sea level rise, placing this location into an open marine, subtidal setting. The extended distance from the coastline produced by seal level rise subdued the topographically driven hydraulic head, and springs in the area became inactive, as low flows would have diffused through unconsolidated sands.

2.6 Conclusions

A deeply karstified unconformity separates the Neoproterozoic Wynniatt Formation (dolostone) from lower Cambrian sandstone. Several common karst features are well developed: dissolution pans on the surface of the Wynniatt Formation, gryke networks, towers, and paleo-caverns. The contact with the overlying Cambrian marine sandstone is sharp and well exposed in some areas. The Cambrian sandstone unit contains cylindrical structures, decimetres to metres in diameter, which cross-cut bedding perpendicularly. The cylinders are interpreted as the pipes that developed below sand volcanoes. The cyl-

inders formed where groundwater flowing through karstic-prepared permeability pathways in the dolostone passed through unconsolidated sand, and emerged onto the shallow seafloor, creating submarine springs and sand volcanoes.

Veins of hydrothermal dolomite are spatially associated with the paleokarst. The temporal relationship between the unconformity and hydrothermal fluid migration is ambiguous, and further research will be conducted to answer this question.

Acknowledgements

The Geological Survey of Canada GEM Victoria Island project supported the field research. Andrew Durbano provided assistance in the field and helpful discussion as well as sharing his photos. Danielle Thomson, Dr. Darrel Long, and Dr. Keith Dewing provided valuable instruction and advice.

References

Bayari, C.S. and Kurttas, T.

2002: Coastal and submarine karstic discharges in the Gokova Bay, SW Turkey; Quarterly Journal of Engineering Geology and Hydrogeology, v. 35, p. 381-390.

Bayari, C.S., Ozyurt, N.N., Oztan, M., Bastanlar, Y., Varinlioglu, G., Koyuneu, H., Ulkenli, H., and Hamarat, S.

2011: Submarine and coastal karstic groundwater discharges along the southwestern Mediterranean coast of Turkey; Hydrogeology Journal, v. 19, p. 399-414.

Buck, S.G. and Goldring, R.

2003: Conical sedimentary structures, trace fossils or not? Observations, experiments, and review; Journal of Sedimentary Research v. 73(3), p. 338-353.

Fritz, F. and Bahun, S.

1997: The morphogenesis of submarine springs in the Bay of Kastela, Croatia; Geology Croatia, v. 50(1) p. 105-110.

Gabelman, J.W.

1955: Cylindrical structures in Permian(?) siltstone, Eagle County, Colorado; The Journal of Geology, v. 63(3), p. 214-227.

Guhman, A.I. and Pederson, D.T.

1992: Boiling sand springs, Dismal River, Nebraska Agents for formation of vertical cylindrical structures and geomorphic change; Geology, v. 20, p. 8-10.

Hawley, J.E. and Hart, R.C.

1934: Cylindrical structures in sandstones; Geological Society of America Bulletin, v. 45, p. 1017-1034.

Heaman, L.M., LeCheminant, A.N., and Rainbird, R.H.

1992: Nature and timing of Franklin igneous events, Canada; implications for a late Proterozoic mantle plume and the break-up of Laurentia; Earth and Planetary Science Letters, v. 109(1-2), p. 117-131.

Irving, E., Baker, J., Hamiltoon, M., and Wynne, P.J.

2004: Early Proterozoic geomagnetic field in western Laurentia: implications for paleo-latitudes, local rotations and stratigraphy; Precambrian Research, v. 129, p. 251-270.

James, N.P. and Choquette, P.W.

1990: Limestones – the meteoric diagenetic environment; in Geoscience Canada reprint series 4, Diagenesis, (ed.) I.A. McIlreath and D.W. Morrow, p.35-74.

Jones, D.S., Maloof, A.C., Hurtgen, M.T., Rainbird, R.H., and Schrag, D.P.

2010: Regional and global chemostratigraphic correlation of the early Neoproterozoic Shaler Supergroup, Victoria Island, Northwestern Canada; Precambrian Research, v. 181, p. 43-63.

Kadau, D., Herrmann, H.J., Andrade, J.S., Araujo, A.D., Bezerra, L.J.C., and Mala, L.P.

2009: Living quicksand; Granular Matter, v. 11, p. 67-71.

Li, Y., Craven, J., Schweig, E.S., and Obermeier, S.F.

1996: Sand boils induced by the 1993 Mississippi River flood: Could they one day be misinterpreted as earthquake-induced liquefaction?; Geology, v. 24(2), p. 171-174.

Long, D.G.F. and Donaldson, J.A.

2005: Modern and Ancient Clastic Sedimentary Environments: A collection of field photographs; GAC CSRG CD-1.

Long, D.G.F., Rainbird, R.H., Turner, E.C., and MacNaughton, R.B.

2008: Early Neoproterozoic strata (Sequence B) of mainland northern Canada and Victoria and Banks islands: a contribution to the Geological Atlas of the Northern

Canadian Mainland Sedimentary Basin; Geological Survey of Canada, Open file report 5700, 27 p.

Massari, F., Ghibaudo, G., D'Alessandro, A., and Davaud, E.

2001: Water-upwelling pipes and soft-sediment-deformation structures in lower Pleistocene calcarenites (Salento, southern Italy); Geological Society of America Bulletin, v. 113 (5), p. 545-560.

Nichols, R.J., Sparks, R.S.J., and Wilson, C.J.N.

1994: Experimental studies of the fluidization of layered sediments and the formation of fluid escape structures; Sedimentology, v. 41, p. 233-253.

Owen, G.

1996: Experimental soft-sediment deformation: structures formed by the liquefaction of unconsolidated sands and some ancient examples; Sedimentology, v. 43, p. 279-293.

Park, J.K.

1994: Paleomagnetic constraints on the position of Laurentia from middle Neoproterozoic to Early Cambrian times; Precambrian Research, v. 69, p. 95-112.

Rainbird, R.

1991: Stratigraphy, sedimentology, and tectonic setting of the upper Shaler Group, Victoria Island, Northwest Territories; Unpublished Ph.D. Thesis, University of Western Ontario, London, Ontario.

1992a: Anatomy of a large-scale braid-plain quartzarenite from the Neoproterozoic Shaler Group, Victoria Island, NorthWest Territories, Canada; Canadian Journal of Earth Sciences, v. 29, p. 2537-2550.

1992b: Stratigraphy and correlation of the Neoproterozoic Shaler Supergroup, Amundsen Basin, Northwestern Canada; in Proceedings of the International Conference on Arctic Margins, (ed.) D.K. Thurston and K. Fujita; Anchorage, Alaska, p. 1-10.

1993: The Sedimentary Record of Mantle Plume Uplift Preceding Eruption of the Neoproterozoic Natkusiak Flood Basalt; The Journal of Geology, v. 101 (3), p. 305-318.

Rainbird, R.H., Heaman, L.M., and Young, G.

1992: Sampling Laurentia: Detrital zircon geochronology offers evidence for an extensive Neoproterozoic river system originating from the Grenville orogen; Geology, v. 20, p. 351-354.

Rainbird, R.H., Jefferson, C.W., Hildebrand, R.S., and Worth, J.K.

1994: The Shaler Supergroup and revision of Neoproterozoic stratigraphy in Amundsen Basin, Northwest Territories; in Current Research, Part C; Geological Survey of Canada, Paper 94-01C, p. 61-70.

Rainbird, R.H., Jefferson, C.W., and Young, G.M.

1996: The early Neoproterozoic sedimentary Succession B of northwestern Laurentia: Correlations and paleogeographic significance; Geological Society of America Bulletin, v. 108(4), p. 454-470.

Rainbird, R.H., McNicoll, V.J., Theriault, R.J., Heaman, L.M., Abbott, J.G., Long, D.G.F., and Thorkelson, D.J.

1997: Pan-continental river system draining Grenville orogen recorded by U-Pb and Sm-Nd geochronology of Neoproterozoic quartzarenites and mudrocks, northwestern Canada; The Journal of Geology, v. 105, p. 1-17.

Ross, J.A., Peakall, J., and Keevil, G.M.

2011: An integrated model of extrusive sand injectites in cohesionless sediments; Sedimentology, v. 58, p. 1693-1715.

Sanford, B.V., and Arnott, R.W.C.

2010: Stratigraphic and structural framework of the Potsdam Group in eastern Ontario, western Quebec, and northern New York State; Geological Survey of Canada, Bulletin 597, 84 p.

Sweeting, M.M.

1972: Karst landforms; Macmillan Publishing Co. Ltd., London, 362 p.

Thorsteinsson, R. and Tozer, E.T.

1962: Banks, Victoria, and Stefansson Islands, Arctic Archipelago; Geological Survey of Canada, Memoir 330: 85 p.

Van Loon, A.J. and Maulik, P.

2011: Abraded sand volcanoes as a tool for recognizing paleo-earthquakes, with examples from the Cisuralian Talchir Formation near Angul (Orissa, eastern India); Sedimentary Geology, v. 238, p. 145-155.

Washburn, A.L.

1947: Reconnaissance geology of portions of Victoria Island and adjacent regions, Arctic Canada; Geological Society of America, Memoir 22. 142 p.

Young, G.M.

1981: The Amundsen Embayment, Northwest Territories; relevance to the upper Proterozoic evolution of North America; Geological Survey of Canada, Paper 81. p. 203-218.

Table 2.1. Diameter and UTM coordinates of dewatering cylinders in Cambrian sandstone near Minto Inlet.

Diameter (cm)	Easting	Northing
100	554396.23	7925567.22
160	554340.095	7925669.651
150	554494.86	7925724.06
480	554577.13	7925725.97
340	554518.13	7925722.42
120	554495.863	7925723.058
100	554493.383	7925724.032
95	554495.87	7925724.062
120	554557.39	7925707.61
560	554547.89	7925703.47
260	554547.1	7925687.83
340	554517.72	7925659.19
160	554518	7925659.19
120	554505.04	7925658.86
120	554490.88	7925665.76
200	554576.08	7925660.11
90	554493.88	7925665.76
90	554494	7925665.76
450	554554.65	7925572.54
90	554555	7925572.54
260	554649.84	7925635.95
90	554632	7925682.36
220	554664.49	7925747.16
300	554674.59	7925771.96
40	554672.59	7925771.96
160	554650.47	7925756.106
100	554626.04	7925779.28
140	554623.04	7925685.992
30	554618.6	7925801.4
150	554643.95	7925804.47
80	554615.6	7925801.4
60	554606.27	7925818.01
200	554855.52	7925691.59
150	554787.72	7925658.8
500	554815.92	7925689.28
970	554861.46	7925718.89
320	554850.16	7925785.18
190	554841.36	7925781.6
270	554836.89	7925775.91
110	554824.34	7925765.92
300	554823.34	7925766.92
130	554820.34	7925766.92
450	554817.34	7925766.92
220	554810.47	7925761.1
100	554798.39	7925749.27
90	554798.61	7925747.41
35	554790.27	7925751.66
50	554791.02	7925749.82
200	554717.64	7925736.05
120	554780.02	7925762.93
100	554787.88	7925759.23
100	554824.36	7925776.52
35	554832.49	7925813.55
25	554832.09	7925813.55
490	554778.87	7925791.72
200	554745.44	7925763.91
400	554745.04	7925763.91
270	554736.93	7925765.18
210	554743.7	7925760.33
55	554739.41	7925758.92
200	554735.22	7925755.65
120	554735.28	7925758.07
370	554732.02	7925778.81
390	554766.1	7925792.89
25	554796.72	7925823.79
190	554787.99	7925824.69
100	554786.44	7925825.02
130	554778.16	7925828.9
240	554776.26	7925821.97
70	554751.73	7925815.02
100	554696.93	7925825.53
25	554698.33	7925824.07
20	554734.05	7925817.92
30	554733.65	7925817.92

70	554728.58	7925825.59
100	554730.85	7925822.49
60	554727.57	7925837.28
40	554727.47	7925832.07
130	554740.1	7925827.18
60	554760.6	7925834.21
130	554769.48	7925834.81
130	554779.16	7925831.71
200	554791.19	7925833.88
170	554793.92	7925854.78
130	554794.01	7925844.36
160	554780.7	7925845.7
90	554776.91	7925845.42
60	554774.84	7925845.18
95	554774.44	7925845.58
55	554774.2	7925845.58
390	554744.7	7925828.04
50	554709.05	7925852.43
130	554716.11	7925856.7
170	554713.94	7925858.13
35	554726.4	7925853.05
35	554726.3	7925853.05
75	554730.28	7925858.92
130	554736.42	7925862.05
60	554742.2	7925856.25
40	554741.09	7925862.73
70	554741.09	7925864.23
220	554754.69	7925854.52
55	554775.12	7925871.59
55	554773.17	7925862.06
135	554780.4	7925859.45
60	554796.16	7925882.91
20	554798.86	7925886.33
35	554798.86	7925885.73
40	554799.36	7925885.13
15	554799.46	7925885.13
240	554803.41	7925882.35
30	554803.41	7925882.45
40	554798.79	7925875.36
60	554798.79	7925874.86
30	554798.79	7925874.56
120	554803.09	7925876.4
70	554804.35	7925873.45
60	554804.35	7925874.15
130	554807.76	7925878.93
250	554806	7925878.93
50	554810.16	7925880.3
70	554812.61	7925874.96
70	554807.96	7925868.9
220	554808.23	7925865.18
70	554810.77	7925865.43
130	554823.13	7925869.1
160	554823.69	7925863.35
60	554824.55	7925859.83
160	554827.12	7925856.55
60	554810.03	7925852.77
40	554808.52	7925854.03
60	554811.84	7925856.16
120	554811.84	7925856.26
200	554819.88	7925852.28
10	554818.32	7925836.8
70	554824.27	7925840.49
50	554824.63	7925840.5
120	554827.4	7925841.13
30	554821.46	7925846
100	554843.83	7925851.96
90	554838.48	7925852.57
160	554839.21	7925854.26
50	554837.51	7925853.47
40	554836.62	7925851.22
140	554833.12	7925851.5
50	554833.92	7925852.45
50	554837.07	7925856.81
110	554833.92	7925857.1
320	554833.54	7925862.85
30	554833.19	7925867.12
80	554833.13	7925871.96
80	554836.13	7925872.78
300	554828.19	7925877.22
40	554825.58	7925875.3
260	554817.34	7925896.28
150	554838.06	7925876.17
50	554838.06	7925876.37
140	554843.18	7925879.84
240	554843.58	7925873.52
420	554850.66	7925867.75

40	554849.98	7925864.2
60	554854.97	7925856.71
60	554854.87	7925856.71
100	554858.35	7925852.14
70	554862.88	7925855.61
190	554862.42	7925848.16
150	554863.02	7925847.99
30	554863.41	7925851.34
50	554863.94	7925844.29
560	554875.06	7925845.32
410	554880.19	7925851.03
160	554879.99	7925851.23
35	554877.64	7925853.38
80	554874.57	7925862.23
70	554874.87	7925862.23
130	554874.21	7925866.87
180	554871.66	7925869.22
60	554871.66	7925868.12
400	554839.1	7925897.96
40	554834.03	7925906.19
30	554834.63	7925906.19
120	554826.92	7925906.2
330	554823.77	7925904.45
100	554842.54	7925916.64
100	554839.52	7925918.79
110	554839	7925918.41
40	554839	7925917.51
30	554838.4	7925917.51
40	554838.4	7925917.11
20	554837.9	7925917.11
30	554837.5	7925916.71
50	554846.35	7925890.33
200	554891.19	7925842.57
80	554888.73	7925846.04
140	554894.78	7925855.31
20	554894.38	7925854.91
90	554888.31	7925860.35
50	554888.71	7925860.35
210	554886.79	7925868.86
90	554881.21	7925873.56
210	554882.39	7925876.37
90	554884.21	7925879.21
150	554885.13	7925887.23

60	554885	7925885.37
40	554885	7925884.77
70	554888.06	7925886.19
80	554880.2	7925892.5
50	554878.26	7925891.89
50	554883.73	7925895.75
60	554883.93	7925895.75
30	554884.93	7925895.75
20	554884.93	7925896.15
60	554879.21	7925896.19
150	554876.79	7925900.59
110	554874.01	7925904.8
110	554868.41	7925906.14
90	554863.85	7925903.61
50	554860.12	7925905.75
50	554862.61	7925905.81
100	554867.28	7925906.3
130	554866.01	7925909.43
360	554865.4	7925910.16
400	554864.26	7925922.4
310	554866.63	7925915.4
90	554868.03	7925911.53
310	554872.72	7925911.46
50	554872.22	7925911.96
50	554873.91	7925918
230	554880.05	7925918.9
90	554882.37	7925918.59
65	554882.93	7925903.72
30	554881.28	7925910.19
330	554893.42	7925903.81
130	554893.42	7925903.71
60	554898.79	7925899.85
60	554898.49	7925899.85
70	554898.65	7925891.48
120	554898.65	7925891.78
70	554898.65	7925892.48
90	554902.85	7925887.13
40	554905.62	7925885.71
180	554905.31	7925881.42
220	554909.68	7925879.68
70	554910	7925879.68
230	554909.68	7925879.58
160	554916.46	7925881.15

100	554916.69	7925885.99
60	554912.81	7925880.13
20	554911.81	7925880.13
40	554911.81	7925880.43
20	554911.61	7925880.43
100	554917.7	7925878.95
90	554917.7	7925879.45
320	554923	7925829.44
160	554924.1	7925829.44
320	554931.6	7925833.56
500	554938.8	7925858.11
110	554936.58	7925898.4
70	554933.41	7925906.5
170	554931.39	7925906.82
350	554930.49	7925909.78
70	554926.55	7925915.25
110	554922.85	7925914.04
280	554921.03	7925917.9
110	554920.46	7925921.61
90	554921.18	7925921.44
95	554921.18	7925922
60	554912.96	7925922.9
60	554912.96	7925922.4
55	554912.96	7925922.2
90	554904.86	7925919.91
45	554907.43	7925902.86
180	554904.87	7925901.12
140	554909.05	7925899.74
10	554908.05	7925899.74
350	554903.31	7925897.18
350	554915.44	7925906.97
90	554914.44	7925906.97
110	554913.54	7925906.97
80	554952.14	7925906.42
160	554955.34	7925901.86
230	554959.04	7925882.61
250	554963.38	7925870.45
35	554967.03	7925866.82
100	554968.53	7925866.82
30	554968.73	7925866.82
380	554966.95	7925860.68
80	554969.76	7925861.69
25	554969.76	7925861.59
25	554970.01	7925861.59
30	554971.8	7925863.39
240	554970.61	7925865.8
240	554978.25	7925868.41
70	554978.25	7925869.41
50	554978.35	7925869.51
30	554978.75	7925868.51
40	554980.15	7925869.51
100	554976.98	7925869.12
110	554980.67	7925866.43
130	554982	7925862.93
20	554982.3	7925862.63
40	554982.6	7925862.63
50	554981.1	7925861.13
30	554981.3	7925861.13
90	554977.21	7925860.39
60	554977.11	7925860.31
110	554977.41	7925860.39
160	554977.31	7925860.59
300	554977.73	7925858.36
320	554974.42	7925851.02
590	554986.11	7925829.75
370	555003.46	7925837.44
160	555008.38	7925841.85
100	555003.18	7925836.69
320	555009.32	7925844.66
80	554998.57	7925852.2
340	554996.72	7925850.66
360	554995.18	7925866.8
110	554995.58	7925867.2
40	554995.58	7925867.3
60	554981.58	7925877.05
230	554983.83	7925881.94
80	554975.17	7925898.09
140	554981.99	7925923.55
40	554996.93	7925962.61
160	554998.16	7925968.04
210	554998.02	7925959.3
100	554998.02	7925958.6
30	554989.09	7925930.8
140	554983.28	7925917.08
80	554985.89	7925898.36
150	554982.45	7925900.88

200	554987.64	7925885.58
40	554986.25	7925875.13
120	554986.31	7925870.66
220	554996.95	7925867.03
30	555019.41	7925859.98
140	555019.49	7925859.43
50	555021.26	7925859.66
60	555024.89	7925859.01
170	555025.64	7925857.72
140	555032.06	7925866.26
170	555028.41	7925869.88
40	555026.24	7925868.71
140	555026.24	7925869.71
100	555021.49	7925878.45
45	555021.2	7925878.45
90	555020.98	7925877.69
40	555021.98	7925878.69
90	555019	7925883.22
160	555017.31	7925891.36
65	555019.52	7925899.97
90	555023.28	7925949.9
40	555024.78	7925950.4
120	555031.85	7925945.84
180	555019.31	7925970.63
40	555031.81	7925977.45
270	555038.74	7925961.64
65	555039.83	7925963.16
260	555053.59	7925944.17
100	555050.63	7925946.14
110	555048.78	7925937.35
90	555055.48	7925937.52
125	555061.26	7925943.06
180	555057.13	7925961
70	555060.99	7925967.6
150	555057.88	7925970.87
280	555063.36	7925974.54
180	555038.93	7926009.81
140	555046.13	7926017.8
1600	555072.42	7926023.13
220	555138.06	7926051.96
40	555143.65	7926067.17
180	555141.52	7926069.53
60	555153.12	7926086.38

185	555151.58	7926083.73
110	555172.52	7926108.26
90	555173.52	7926109.26
60	555175.85	7926108.16
130	555178.72	7926111.58
40	555180.53	7926117.39
30	555180	7926117.39

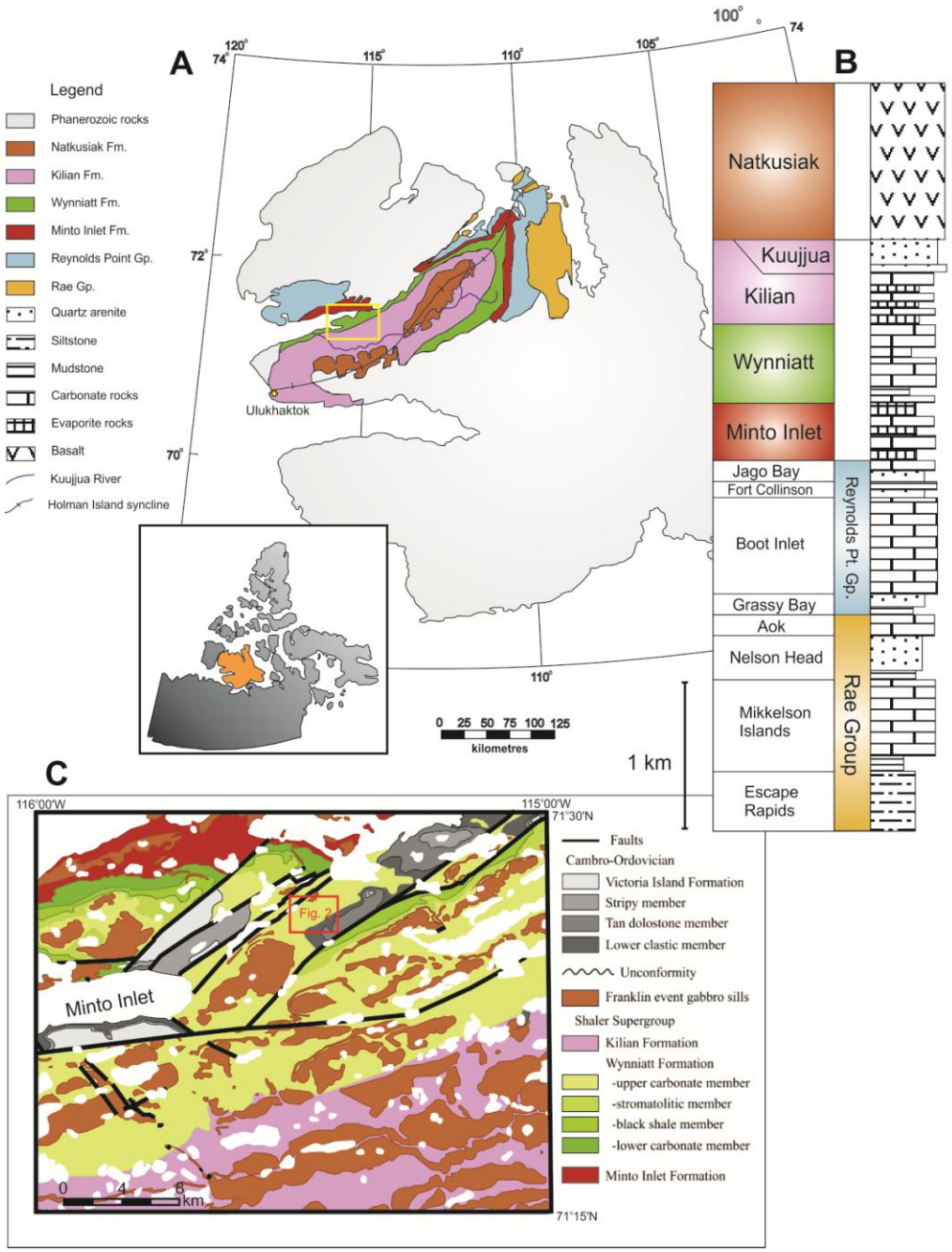

Figure 2.1. (A) Bedrock geology of Victoria Island after Thorsteinsson and Tozer (1962) highlighting the Minto Inlier (coloured). Inset shows location of Victoria Island in northern Canada. Colours on maps correspond to geological units in (B). (B) Composite stratigraphic section of the Shaler Supergroup (from Rainbird et al. 1994) and (C) Geology of NTS 87H/05 (box on A) (modified from Rainbird *et al.*, in press).

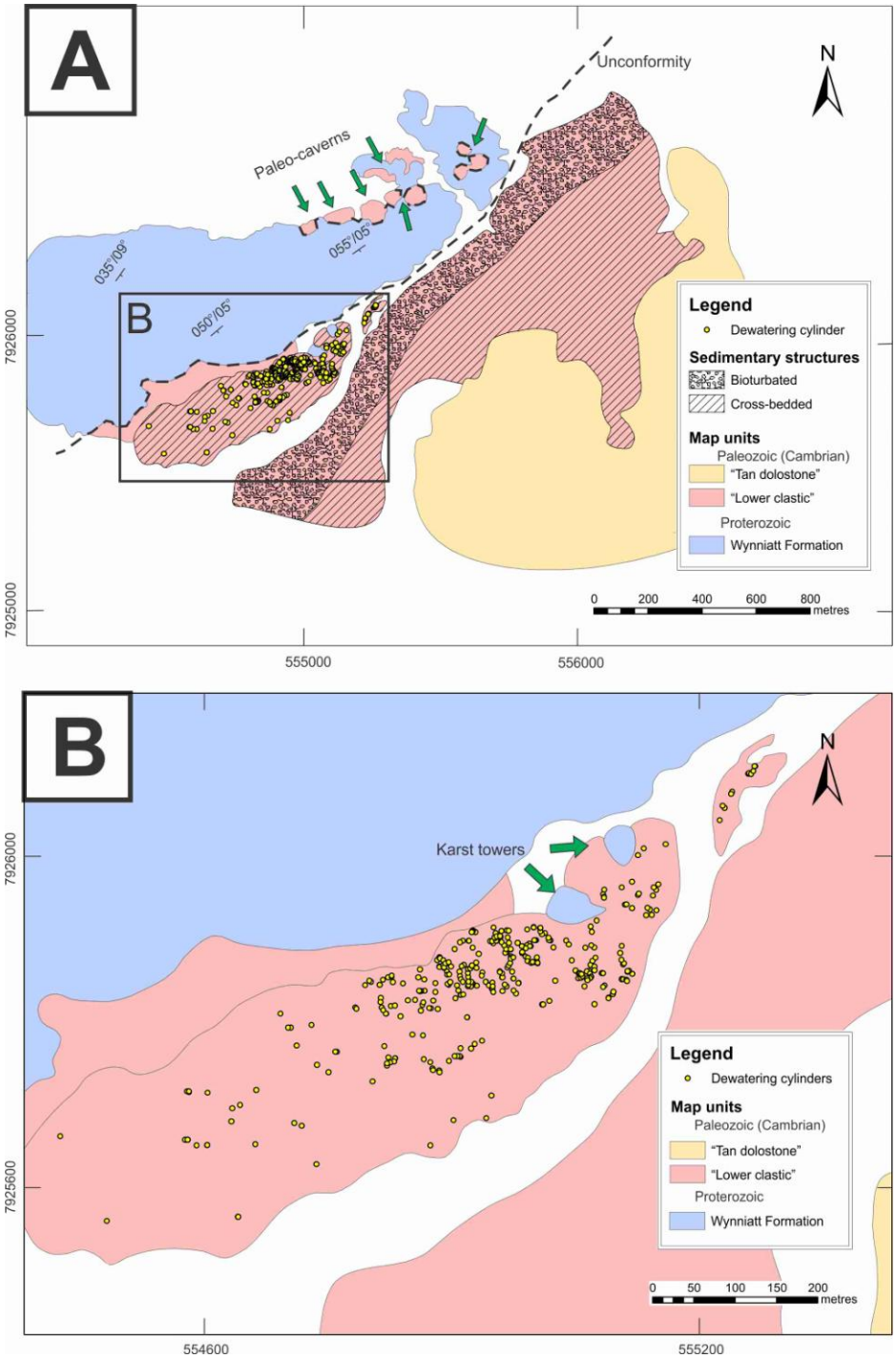

Figure 2.2. A. Map of the paleokarst area, showing distribution of paleo-caverns and dewatering cylinders. The un-patterned pink area between Wynniatt Fm. dolostone and cylinder-bearing sandstone is an area of frost-heaved sandstone rubble that could not be

mapped. B. Detailed map of cross-bedded sandstone unit showing sand cylinder distribution.

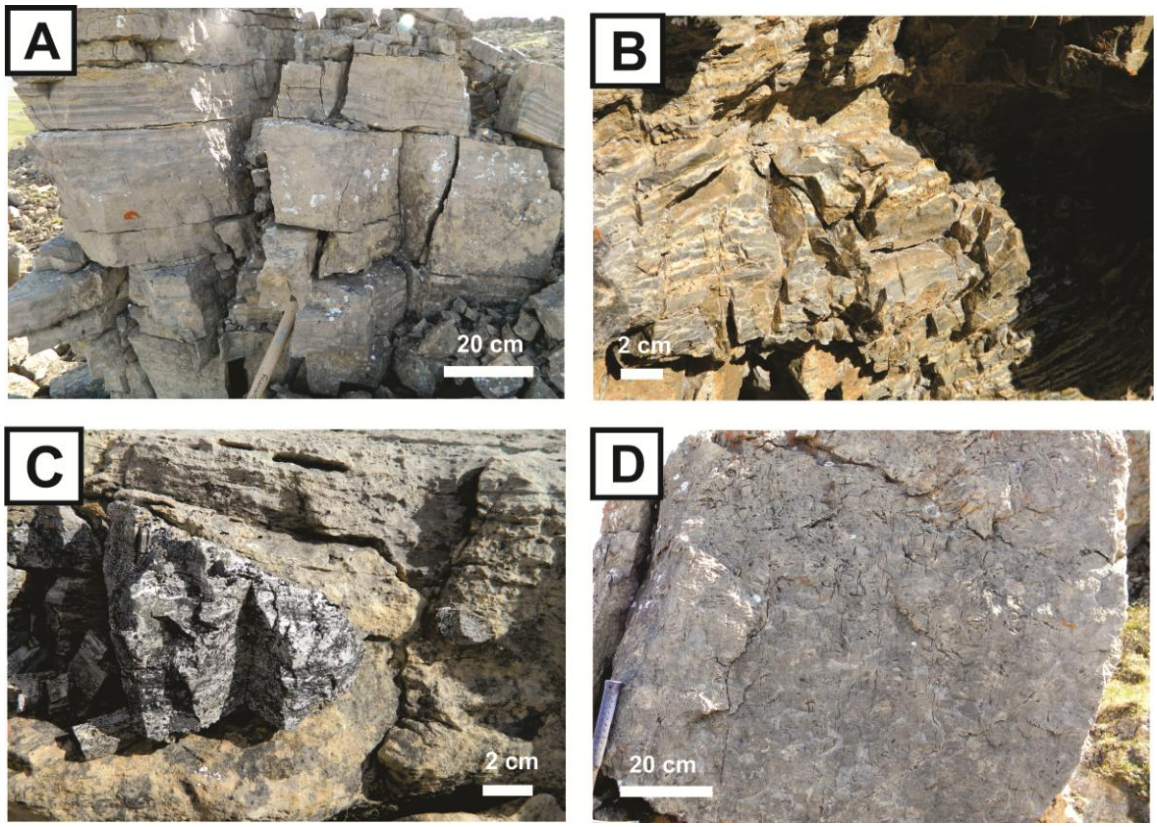

Figure 2.3. Typical features of the Wynniatt Formation in the study area. A. Pale grey dolostone with laminations and partings. B. Zebra dolomite. C. Chert nodules. D. Columnar branching stromatolites.

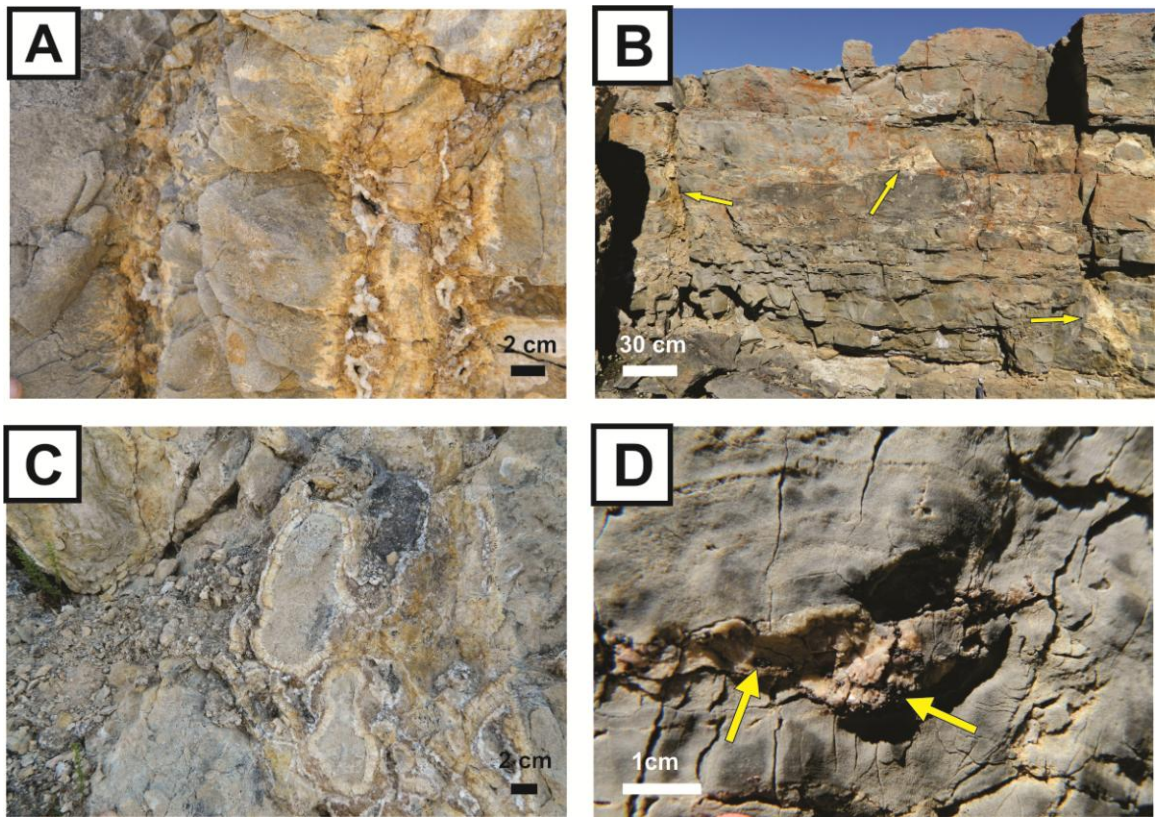

Figure 2.4. Hydrothermal dolomite appears to be particularly abundant in the vicinity of the unconformity. A. Three dolomite phases are distinguished in the field based on colour: tan, brown, and white. B. Large vertical and horizontal dolomite veins (arrows). C. Hydrothermal brecciation. D. Minor sulphide minerals (mostly pyrite?) in dolomite veins (arrow).

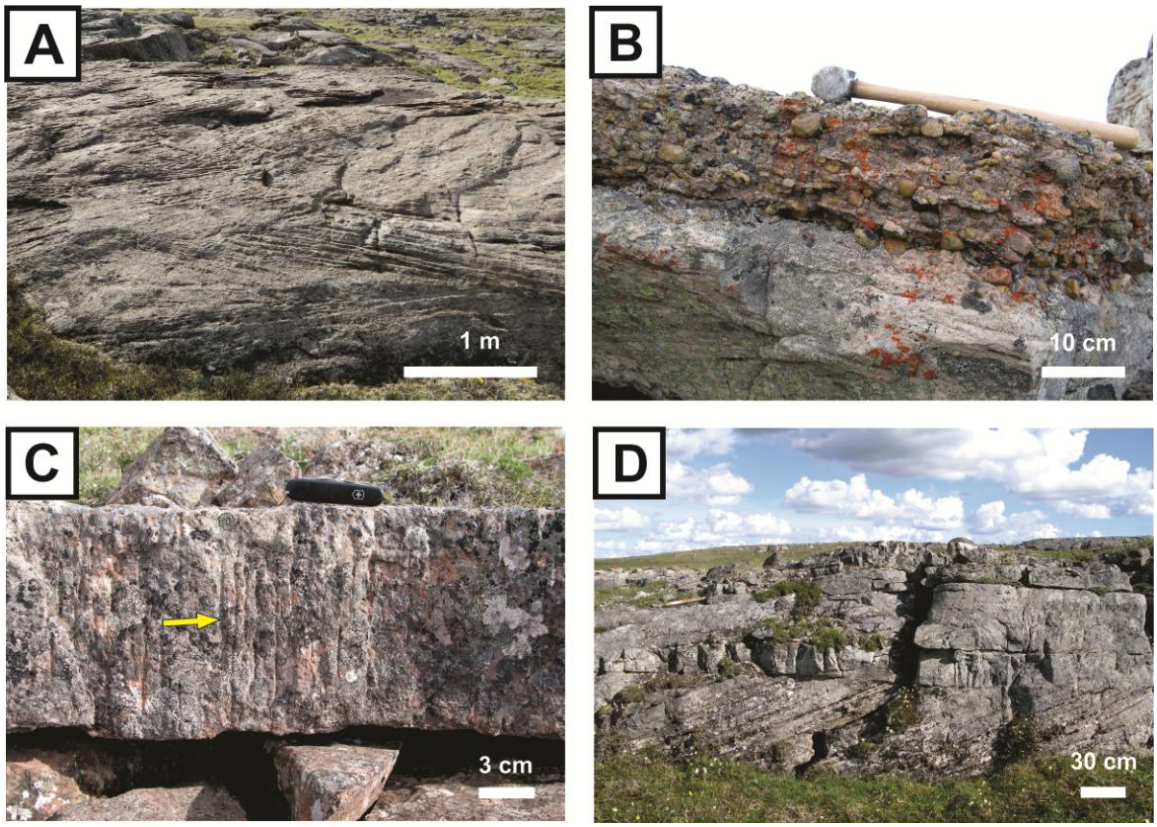

Figure 2.5. Cambrian "lower clastic member". A. Basal, planar cross-bedded quartz arenite. B. Conglomerate bed at the base of the cross-bedded quartz arenite. C. Bioturbated section with vertical burrows (*Skolithos*). D. Upper cross-bedded section above the bioturbated section (figures courtesy of Andrew Durbano).

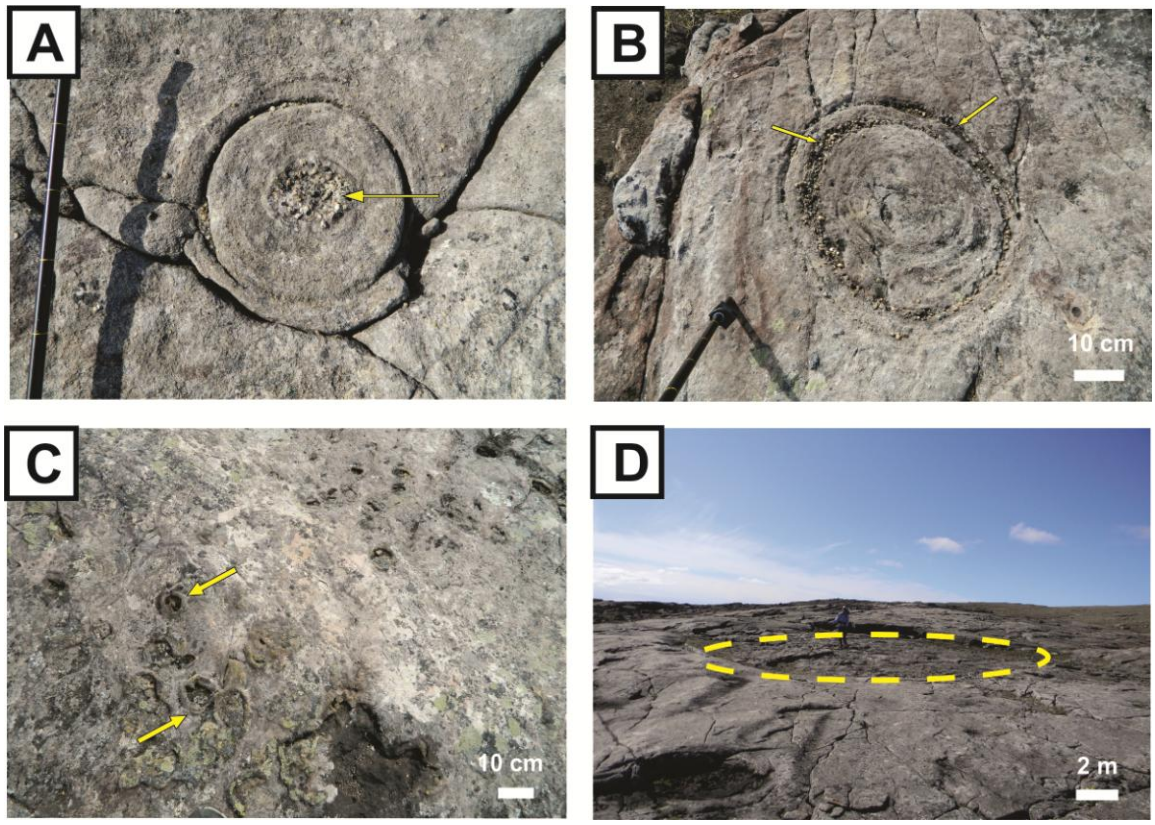

Figure 2.6. Cylinders in the Cambrian sandstone. A. Cross-section of cylindrical column with coarse gravel at its core (arrow). Pole is marked in 10 cm increments. B. Cross-section of column with two concentric zones of coarse gravel (arrows). C. Sand volcanoes on a bedding plane. D. Exposure of column approximately 15 m in diameter (person for scale).

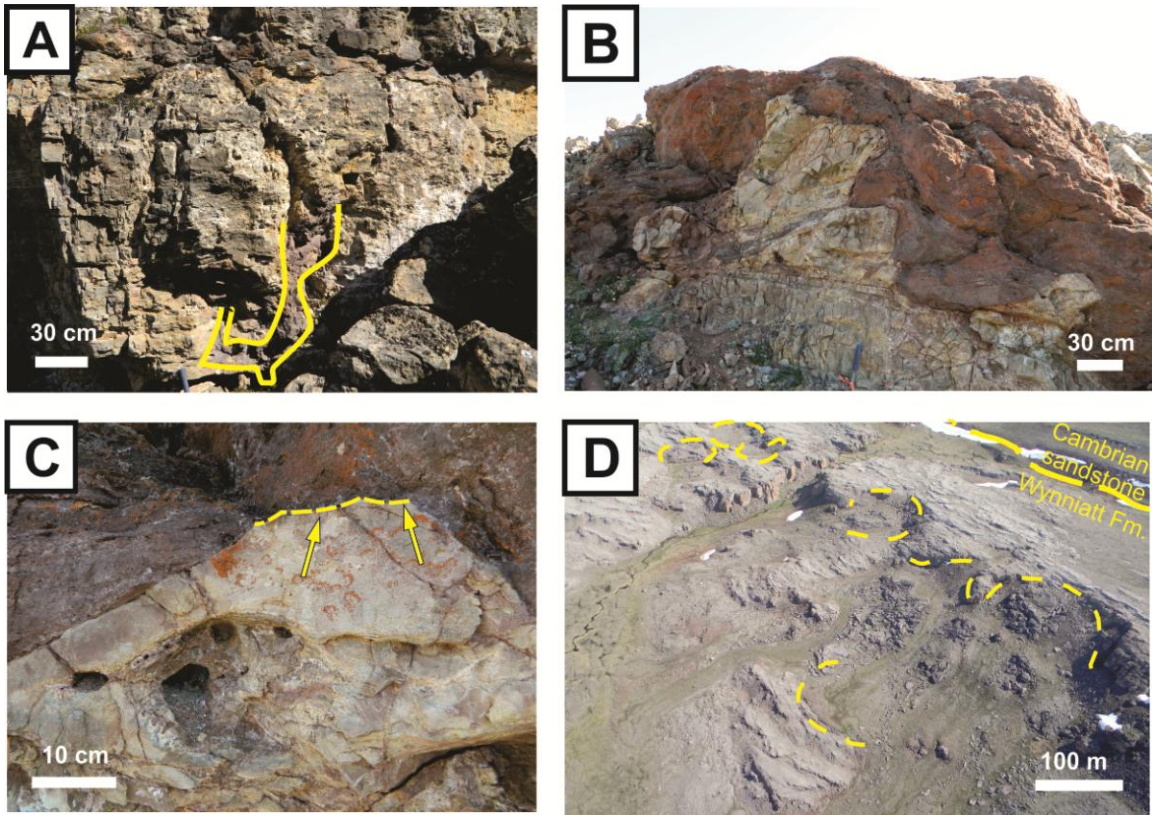

Figure 2.7. Karstic features below the Proterozoic – Cambrian unconformity. A.Vertical cross-section of a gryke that branches into vertical and horizontal orientations. B. Sharp, irregular paleocavern base and wall. C. Dissolutional scalloping on paleo-horizontal surface within a paleocavern (arrows). D. Aerial view of the karst area showing red sandstone-filled paleocaverns in Wynniatt Formation, well below the projected stratigraphic contact of Wynniatt Formation and red sandstone of the basal Cambrian unit.

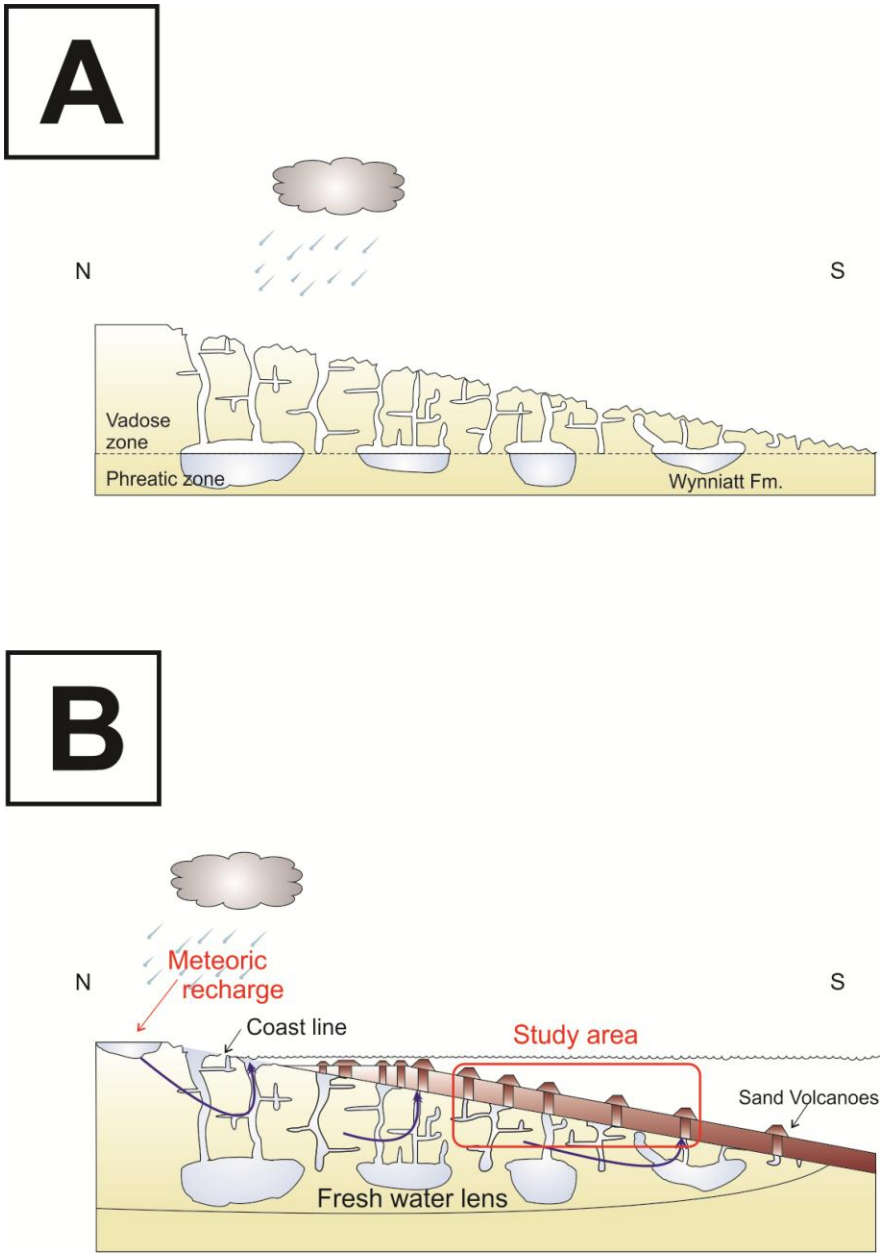

Figure 2.8. Interpretation of karsting and sand cylinder formation. A. Late Neoproterozoic or early Cambrian erosion of overlying formations to expose the Wynniatt Formation to meteoric dissolution creating a karst environment. B. Cambrian sand deposited over the karst surface was reworked locally by submarine springs caused by the hydraulic head to the north (left) of the coastline forcing water through the karst features as conduits.

CHAPTER 3 - *A FLUID INCLUSION STUDY OF DIAGENETIC FLUIDS IN PROTEROZOIC AND PALEOZOIC CARBONATE ROCKS, VICTORIA ISLAND, NWT.*

J. MATHIEU, D. J. KONTAK AND E. C. TURNER

Department of Earth Sciences, Laurentian University, Sudbury, Ontario, Canada P3E 2C6

ABSTRACT

Despite the presence of known economic resources in Canada's Arctic archipelago, Victoria Island remains understudied. This study addresses the fluid history and economic potential of two major carbonate units on Victoria Island by integrating fluid inclusion microthermometry with SEM-EDS analysis of evaporate mounds. Three cements containing fluid inclusion assemblages (FIA) occur in the Neoproterozoic Wynniatt Formation: saddle dolomite, brown dolomite, and calcite, in paragenetic order. The two dolomite-hosted cements have average homogenisation temperatures (T_h) for FIAs (n=3) of 108°C (saddle) and 101°C and 116°C, but metastability precluded determining salinities; most calcite-hosted fluid inclusions are too small and/or necked to obtain T_h values, but rare larger inclusions have salinities from 1.7 to 0.4 wt. % NaCl equiv. SEM-EDS analysis of evaporate mounds indicates the fluid changed from an early K-rich (saddle dolomite), to a later K+Na (brown dolomite), and finally Na-rich (calcite), which suggests mixing of two end-member fluids (i.e., Na-rich and K-rich). Dolostone of the lower Pa-

leozoic “Victoria Island formation” contains two cements: early quartz and late dolomite. Quartz-hosted FIAs (n=2) have an average T_h value of 126°C, and salinity of 23.2 wt. % NaCl equiv., whereas FIAs (n=3) in dolomite have average T_h values of 109°C, 116°C, and 124°C; metastability precluded determining salinity. Evaporate mound analysis for the cements indicates evolution from a Na-rich to a Na+K fluid through interaction with reservoir rocks. A reduced, metal-rich fluid was present during quartz precipitation, as implied by the presence of pyrite framboids along growth zones and nanoparticles of barite and sulphide minerals (Zn, Cu, and Pb) in evacuated inclusions, which suggests the area may have potential to host base-metal mineralisation. Importantly, distinguishing different fluid compositions in both of the case studies would not have been possible without evaporate mound analysis and, therefore, the results emphasise integrating this technique into diagenetic studies.

Key words: fluid inclusions, evaporate mounds, carbonate diagenesis, Victoria Island, Wynniatt Formation, “Victoria Island formation”, Shaler Supergroup, Franklinian Basin

3.1 INTRODUCTION

Victoria Island is a large island in the Canadian Arctic archipelago underlain by nearly undeformed Proterozoic and Paleozoic sedimentary rocks. Much of the island remains geologically unmapped and economically unexplored, but is known to have bitumen showings and native copper occurrences (Thorsteinsson and Tozer 1962, R. Rainbird pers. comm. 2012). Islands elsewhere in the Canadian Arctic archipelago (Fig. 3.1) contain oil and gas in Paleozoic and Mesozoic strata (Gentzis *et al.* 1996, Chen *et al.* 2000, Obermajer *et al.* 2010). Proterozoic strata on Baffin Island contain the Nanisivik Zn-Pb deposit (McNaughton & Smith 1986), and Paleozoic strata east of Victoria Island contain the Cornwallis Zn-Pb district (Fig. 3.1), which includes the Polaris deposit (mined 1976-2002, production ~20 million tonnes at ~17% Zn+Pb; Dewing *et al.* 2006, 2007a,b). Proterozoic and Paleozoic carbonate strata on Victoria Island contain multiple generations of cement that offer the opportunity to study their diagenetic history, and may help illuminate the area's economic potential.

This paper describes and characterises the fluids that were present during precipitation of late diagenetic cements in the Neoproterozoic Wynniatt Formation and the lower Paleozoic "Victoria Island formation" on Victoria Island, using standard microthermometry and SEM-EDS on evaporate mounds (e.g., Haynes & Kesler 1987, Haynes *et al.* 1988). The nature and origin of the fluids are interpreted in the context of the burial history of the rocks, and implications for base-metal and petroleum potential in the area are discussed. The material used was collected as part of a broad field program focussed on

the regional geology Victoria Island (Bedard *et al.* 2012, Rayner & Rainbird 2013, Rainbird *et al.* in press.).

3.2 GEOLOGICAL SETTING

The regional geology of Victoria Island was established by Thorsteinsson and Tozer (1962), who provided the first descriptions of Proterozoic and Paleozoic strata. More detailed descriptions of the Proterozoic units were provided by Young (1981), Rainbird (1991, 1992), and Rainbird *et al.* (1994); the Paleozoic units were informally named and described by Dewing *et al.* (2013).

The Neoproterozoic Shaler Supergroup was deposited in a poorly understood epicratonic basin (Rainbird *et al*. 1994, Long *et al.* 2008). The upper part of the Shaler Supergroup includes, in decreasing age, the Minto Inlet, Wynniatt, Kilian, and Kuujjua formations, which are overlain by the Natkusiak Formation flood basalt (Rainbird 1991), a volcanic unit associated with the ~ 723 Ma Franklin large igneous province (Heaman *et al*. 1992). The Holman Island syncline and Walker Bay anticline (Fig. 3.2A) are evidence of later Neoproterozoic deformation; structural dip is no more than 10°.

The Wynniatt Formation consists of shallow-marine limestone and dolostone of the informal "lower", "shale", "stromatolitic", and "upper" members (Rainbird 1991). This formation was locally karsted shortly before deposition of lower Paleozoic strata (Mathieu *et al.* 2013). Evidence for hydrothermal brecciation and cementation is present in the Wynniatt formation (Mathieu *et al.* 2013). The estimated thickness of Proterozoic strata now overlying the Wynniatt Formation ranges from 0 m (at the unconformity site)

to approximately 2000 m (where the Natkusiak Formation is well preserved; Rainbird 1991).

Latest Neoproterozoic to early Paleozoic rifting and transgression resulted in the development of an epicratonic sea over most of Laurentia, which in arctic Canada resulted in the early to middle Paleozoic Franklinian Basin, a broad, stable, crudely north-facing, carbonate-dominated passive-margin and contiguous epicratonic environment (Fig. 3.1). Paleozoic strata that underlie most of Victoria Island include Cambrian(?)-Silurian(?) carbonate and terrigenous clastic strata that were collectively known as map-unit 10 (Thorsteinsson & Tozer 1962), but which have since been divided into ten units (Dewing *et al.* 2013). The Cambro-Ordovician "Victoria Island formation" (formerly map-unit 10b; Thorsteinsson & Tozer, 1962) is a generally fabric-destructive, shallow-marine dolostone with intraclasts and locally preserved microbial structures. This unit is, at least in part, equivalent to the Franklin Mountain Formation on the northern Canadian mainland, which has similar age, tectonic setting, and geological characteristics (Norford & Macqueen 1975, Turner 2011). The age of the "Victoria Island formation" is constrained by Middle Cambrian trilobites in the underlying unit and Early Ordovician conodonts below the contact with the overlying unit (Dewing *et al.* 2013).

The Boothia Uplift, a north-trending, 250 km-wide structural zone that extends northward from the exposed craton on the mainland to Devon Island in the central Canadian Arctic islands, formed as a result of far-field compressional forces from the Caledonian Orogeny to the east in the late Silurian (Fig. 3.1; Miall 1986). Approximately 4-5 km of uplift occurred, resulting in north-trending faults and folds, and deposition of clastic wedges on both sides of the uplift (Okulitch *et al.* 1991).

The late Devonian Ellesmerian Orogeny produced a southeast–vergent deformation front and a thick clastic wedge (Fig. 3.1; Embry 1991a). The Boothia Uplift acted as a local buttress against the deformation front (Okulitch *et al.* 1991): interaction with the south-directed orogenic stress reactivated faults associated with the Boothia Uplift (Turner and Dewing 2004, Dewing *et al.* 2007a, Jober *et al.* 2007), and fluid movement through these faults was responsible for formation of Zn deposits in the Cornwallis District, including the Polaris Zn-Pb deposit (Dewing *et al.* 2007a). The Devonian clastic wedge is preserved on Banks (Thorsteinsson & Tozer 1962, Miall 1976), Melville (Harrison 1994) and Bathurst (Anglin & Harrison 1999) islands, but is absent on Victoria Island (Thorsteinsson & Tozer 1962). The proximity of these islands to Victoria Island allows for the assumption that this area was also part of the same fluvio-deltaic environment (Embry 1991a). The greatest preserved thickness of the clastic wedge (4 km) is on Banks Island, immediately west of Victoria Island (Miall 1976, Embry 1991a). Maturation of organic material from several islands suggests that approximately 4 km of Devonian strata were eroded during the Ellesmerian Orogeny (Dewing & Obermajer 2009). This thickness is probably an overestimation, because vitrinite reflectance records the highest temperature reached, whether it was from burial or some other cause. Jurassic extension on Banks Island probably caused a thermal pulse, which would have resulted in vitrinite reflectance indicating deeper burial than truly took place; this discrepancy is shown by vitrinite reflectance data that do not agree with the sonic velocity of shale in the Muskox D-87 drill hole on Banks Island (Dewing & Obermajer 2009). The maximum thickness of the Devonian clastic wedge is therefore assumed to have been between 4 and 8 km, although sonic velocities imply that the thickness was probably 6-7 km.

In the early Carboniferous, rifting and formation of the Sverdrup Basin in the northwestern Arctic islands (Fig. 3.1) marked the end of the Ellesmerian Orogeny (Davies & Nassichuk 1991), as indicated by extensional structures under the basin (Forsyth *et al.* 1979). The southern limit of the Sverdrup Basin is on Melville Island. The basin accumulated approximately 12 km of strata and became a predominantly deep-water basin (Embry 1991b). Southwest of the Sverdrup Basin, Jurassic extension produced the Canada Basin (part of the present Arctic Ocean) (Miall 1979) with strata preserved on land in grabens on Banks Island (Embry & Dixon 1992). Rifting in the Cretaceous emplaced flood basalts and sills in the Sverdrup Basin (Embry 1991b, Dewing *et al.* 2007b).

The Cretaceous to Oligocene Eurekan Orogeny was caused by counter-clockwise rotation of Greenland with respect to North America, which caused compression in the northern Arctic islands and extension in the southern islands (Okulitch & Trettin 1991): folds and thrust faults on Ellesmere Island, extension in Baffin Bay and Canada Basin, and normal faulting that produced islands and straits in the southern Arctic islands are Eurekan features. Isostatic uplift associated with the opening of Baffin Bay contributed to the present-day geography of the Arctic islands, and shifted the main sedimentary depocentre to the present-day continental margin northwest of the Arctic islands (Trettin 1991).

3.3 METHODS

Samples of cement-bearing carbonate rock were collected from the Neoproterozoic upper Wynniatt Formation, and from the Cambro-Ordovician “Victoria Island formation”

(Fig. 3.2B). Wynniatt Formation dolostone samples are from below a sub-Cambrian karst surface exposed at the head of Minto Inlet (Mathieu *et al.* 2013), and contain three late-stage cements in vugs and fractures (Fig. 3.3A, C). "Victoria Island formation" samples are from an area characterised by northeast-trending normal faults south of Minto Inlet; associated brecciation is limited to the immediate vicinity of present-day map traces of normal faults (Fig. 3.4A).

Polished thin sections (30 μm thick) were made from rock slabs and studied petrographically in both transmitted and reflected light using an Olympus BX-51 microscope. A single-wavelength ultraviolet (385 nm) light source was used to identify the fluorescence of hydrocarbons in the sample from the "Victoria Island formation". The fluorescence colour was compared to the American Petroleum Institute (API) gravity chart qualitatively.

Fluid inclusion microthermometry using 100 μm-thick, doubly polished thin sections was undertaken at Laurentian University, Sudbury, Ontario, using a Linkham THMSG600 heating-freezing stage with an automated controller unit and Olympus BX-51 microscope equipped with a Q-Imaging digital capture system. The heating-freezing stage calibration was checked using synthetic fluid inclusions: CO_2 (-56.6°C), the freezing point of H_2O (0°C), and critical point of H_2O (374°C). Inclusion salinities were calculated using final melting temperature of ice (T_m(ice)) for aqueous inclusions (Bodnar 1993). Fluid inclusions were homogenised repeatedly to test consistency. The fluid inclusions that froze were also reheated multiple times to ensure accurate and precise measurements and salinities.

Two procedures were used to prepare evaporate mounds for subsequent analysis. For quartz cement, chips were heated at a rate of 60°C/min to 350°C in order to induce decrepitation of fluid inclusions; samples were kept at 350°C for less than 2 minutes to obtain optimal amounts of evaporate mound residue produced from individual fluid inclusions (Haynes & Kesler 1987, Haynes *et al.* 1988). The quartz chips were then adhered to a glass slide with carbon tape and carbon-coated for SEM-EDS analysis. For carbonate cement, a Fisher Brand microscope cover glass was placed under the chip and the same heating rate used; after cooling to <50°C the chip was removed, leaving the debris and evaporate mounds on the glass surface of the cover slip; this procedure precluded any influence of the carbonate mineral substrate during SEM-EDS analysis. The glass cover slips used in this experiment were not pure silica, but contained, in addition to Si, consistent proportions of Na, K, Al, Ti, and Zn, as determined from SEM-EDS analysis. Frequent analysis of the glass slide was done to ensure both its compositional consistency and the accuracy of the testing. Final compositions of the evaporate mounds were calculated by subtracting the proportional amount of the contaminant (i.e., Na, K) in the glass based on the amount of Si detected in each analysis.

Imaging and analysis of fluid inclusion evaporate mounds was undertaken at Laurentian University using a JEOL 6400 scanning electron microscope running with a voltage of 20 kV, with an INCA EDS detector and software. The minimum detection limit for the operating conditions of this study was about 0.5 wt. %. Na+K, the latter of which accounted for >25% of the totals on an oxygen-free basis (i.e., Na, K, Cl, Si), which ensured minimal errors in estimating the Na:K ratios of the analysis. The apparent concentration of an element can be exaggerated by in situ fractionation during mound precipita-

tion (Haynes *et al*. 1988; Kontak 2004). This potential problem was avoided in two ways: (1) rastering over mounds that were of sufficient size (>10 µm), and (2) conducting multiple analyses of individual mounds where more than one mound was produced during decrepitation. The former provides bulk composition of mounds, eliminating the effect of spatial fractionation within a mound, whereas the latter was used to check for consistency among mounds. In any group of mounds the results were uniform, and large spatial excursions in elemental ratios (in this case Na:K) were absent, which agrees with previous studies that addressed the issue of fractionation in evaporate mounds (Haynes *et al*. 1988, Kontak 2004). These precautions are considered sufficient to preclude possible in situ fraction from influencing the present data, which is important given the unusual enrichment of K in some FIAs in this study.

The size and abundance of mounds generated by artificial decrepitation conveys useful information. Based on numerous integrated microthermometric and evaporate mound studies of samples from a wide variety of settings (e.g., Kontak *et al*. 2002, Kontak & Kyser 2011, Morden 2011, Burns *et al.* 2012, Kontak 2013, Tweedale *et al*. 2013), it is clear that moderate (10-20 wt. %) to high- (>25 wt. %) salinity inclusions produce abundant, medium- to large-sized mounds (>5-10 µm); this relationship was semi-quantified by Haynes *et al.* (1988; their Fig. 10). In contrast, low-salinity inclusions produce smaller and less abundant mounds. It is, therefore, possible to distinguish qualitatively between low- and higher-salinity fluids using visual documentation of mound populations. This type of assessment was necessary in this study because of fluid inclusion metastability which precluded salinity determinations for some cements.

3.4 RESULTS

3.4.1 Wynniatt Formation

3.4.1.1 Paragenesis

The upper Wynniatt Formation consists of finely crystalline anhedral dolomite crystals that are full of fluid inclusions that confer a dark grey-brown colour in plane-polarised light, and medium to pale grey in hand sample (Fig. 3.3A). Under cross-polarised light, the individual crystals exhibit uniform extinction. Deposition and dolomitisation of the Neoproterozoic Wynniatt Formation were followed by much later karsting and quartz sandstone deposition in the Cambrian. Karst features (paleo-caves and grykes) in the Wynniatt Formation were filled by quartz sand in the Cambrian; the void-filling sandstone is compositionally identical to that in Paleozoic map-unit 10a ("clastic unit" of Dewing *et al*. 2013), which directly overlies the unconformity at the study site (Mathieu *et al.* 2013). Cements in the Wynniatt Formation are saddle dolomite, brown dolomite, and calcite (Fig. 3.3A, B). Saddle dolomite cement has individual crystals up to several millimetres in diameter; these crystals have curved faces, show sweeping extinction under cross-polarised light, and contain abundant fluid inclusions. Brown dolomite cement consists of a narrow band of millimetric euhedral dolomite crystals with uniform extinction. The crystals are uniformly brown in hand sample, but brown and colourless microbanding is evident in thin section c owing to the presence of small (<1 μm) hematite inclusions. Fluid inclusions, although present, are not abundant in this cement stage. Calcite cement consists of millimetric, colourless, anhedral crystals that fill the remaining space.

This cement is nearly devoid of fluid inclusions and where present average <1 μm in diameter.

Precipitation of all cements is known to have taken place after sandstone deposition (Fig. 3.5), because where saddle-dolomite-filled veins reach the margins of karst voids, the dolomite encloses quartz grains (Fig. 3.3C, D). A younger age constraint could not be determined for these cements.

3.4.1.2 Fluid inclusion petrography

The three cement phases in the Wynniatt Formation contain well-defined, aqueous (A) fluid inclusion assemblages (FIAs) of primary and secondary origin, as defined by Goldstein and Reynolds (1994). Primary AFIAs are distributed along growth zones, whereas secondary AFIAs form both random groups of inclusions and clusters decorating healed fractures. Aqueous inclusions include L-V-types and monophase L- and V-types. Only the L-V-type inclusions conform to "Roedder's Rules" (Bodnar 2003): (1) they represent trapping of a homogeneous fluid; (2) they represent an isochoric (constant volume) system; and (3) they have not exchanged chemically since entrapment. The monophase L- and V-rich inclusions are considered to be artefacts of post-entrapment processes and, because they do not represent trapping of a homogeneous fluid, are not discussed further.

The aqueous fluid inclusions in the saddle dolomite are typically <10 μm (long axis), with the average size near 2-4 μm (Fig. 3.3E); some of these AFIAs display similar L:V ratios (85:15), whereas the majority have highly variable L:V ratios (70:30 to 90:10) due to necking. Inclusions in the brown dolomite are typically 1-3 μm in diameter and have relatively consistent L:V ratios (85:15). Few inclusions in the calcite are larger than 1-3

μm (Fig. 3.3G), which made it difficult to observe phase changes during microthermometry, and where inclusions were larger most of these are necked (Fig. 3.3F).

3.4.1.3 Microthermometry

Microthermometric data for the cements are limited (see Table 3.1), for reasons addressed below. Homogenisation data were collected only for FIAs with uniform L:V ratios (i.e., similar densities). The presence of abundant necking of FIAs in the host dolostone resulted, however, in highly variable L:V ratios for inclusions and precluded obtaining homogenisation data for these inclusions. Fluid inclusions in saddle dolomite and brown dolomite did not freeze, despite repeated attempts and holding at low temperatures (to -140°C) for several minutes, and so salinities could not be obtained.

Freezing data were obtained for two calcite-hosted FIAs; a single inclusion in each FIA froze. Because all of the fluid inclusions in an FIA must represent the same fluid, even if only a single fluid inclusion freezes, it must represent the fluid trapped in the FIA (Roedder 1984, Goldstein & Reynolds 1994). One of the FIAs froze at -60°C, with first and final melting at -36°C and -1°C, respectively (Table 3.1). In the other FIA, a single inclusion froze at -40°Cand first and final melting, both at -0.2°C (Table 3.1), occurred instantly with no visible phase change of the liquid during warming other than the vapour bubble instantly returning to its original size and shape.

Homogenisation temperatures (T_h) are available only for FIAs in the saddle and brown dolomite phases, because the small size and the necking of larger inclusions in the calcite cement precluded obtaining data. The FIA in the saddle dolomite had homogenisation temperatures from 105°C to 118°C (n=6), with an average of 108°C. The two FIAs

in the brown dolomite had homogenisation temperatures of 100 to 112°C, with averages of 101ºC (n=2) and 105°C (n=3).

3.4.1.4 Evaporate mound analysis

Evaporate mounds from brown dolomite and calcite cements in the Wynniatt Formation were produced on glass slides to avoid the inevitable contribution of the underlying carbonate phase that would have ensued if the mounds had been produced and analysed on their host phase. For comparative purposes, the mounds from the saddle dolomite cement were analyzed on the host phase. For all three cements, the mounds produced had a large range in size; shapes were equant to elongate (Fig. 3.3H), and in rare cases dendritic geometries were present (Fig. 3.3I). The results below follow the paragenetic sequence in Figure 3.5.

Analyses of mounds produced from the saddle dolomite show uniform Ca:Mg abundances, but varying Na+K (Fig. 3.7A), which reflects the contribution of Ca and Mg from the dolomite host, rather than the from the fluid. Removing the dolomite host contribution of Ca+Mg from the analyses indicates that the mounds have a uniform Na:K ratio, except for a single analysis with relative enrichment in Na (Fig. 3.7B). The mound data for the brown dolomite (Fig. 3.7C) also indicate depletion in both Ca and Mg, but more variable Na:K ratios that range from 60:40 to 90:10. Finally, the mound data for calcite cement (Fig. 3.7D) indicate a dominance of Na, with Na:K ratios greater than 90:10, and an absence of both Ca and Mg. In all of the mounds, Cl was the only anion detected.

3.4.2 "Victoria Island formation"

3.4.2.1 Paragenesis

Two cements are present in Paleozoic "Victoria Island formation" dolostone: quartz and dolomite (Fig. 3.4A, B). The quartz cement crystals are coarse, dark grey-brown (in hand sample and thin section), and euhedral, with conspicuous growth zones; fluid inclusions and framboidal pyrite nanoparticles are arrayed along growth zones (Fig. 3.4B, C, F). Liquid petroleum fluid inclusions are present in fractures in the quartz. The dolomite cement crystals, which fill space among fragments of host rock and quartz cement, are colourless, coarse, and anhedral, and contain abundant fluid inclusions. The paragenesis of the material studied (Fig. 3.6) includes Paleozoic deposition and dolomitisation of "Victoria Island formation", followed by its local silicification and coeval precipitation of quartz cement that contains pyrite framboids along growth zones. After precipitation of quartz cement had ceased, a liquid hydrocarbon migrated through the rock and was trapped along fractures in the quartz cement, but is absent from dolomite cement crystals. Dolomite cement followed at an uncertain, later time.

3.4.2.2 Fluid inclusion petrography

The two cement phases in the "Victoria Island formation" contain well-defined, abundant, primary and secondary AFIAs and secondary petroleum (P) FIAs, as defined by Goldstein and Reynolds (1994). Primary AFIAs are distributed along growth zones, whereas secondary AFIAs form both random groups of inclusions and clusters on healed fractures. Aqueous inclusion types include L-V-types with consistent L:V ratios, and mo-

nophase L- and V-types. For the same reasons noted above, only the L-V AFIAs are discussed further.

Aqueous FIAs in the quartz consist of equant to irregular fluid inclusions that are typically <10 μm (long axis, average size near 5-10 μm; Fig. 3.4C, D) with consistent L:V ratios (90:10). Liquid petroleum is present only as secondary FIAs in quartz (Fig. 3.4E). Elongate petroleum inclusions up to 25 μm long are nearly homogeneous, with about 5% of an aqueous phase present. No vapour phase was observed in the petroleum component of the inclusions. The petroleum inclusions exhibit a uniform pale green fluorescence under UV light (385 nm). The aqueous fluid inclusions in dolomite are equant, negative-shaped, and about 10 μm long, but inclusions >15-20 μm are common (Fig. 3.4G). Although there is some variability of L:V ratios in these FIAs due to necking, most show a consistent ratio.

3.4.2.3 Microthermometry

Single fluid inclusions in the FIAs in quartz cement exhibited the same temperatures for first and final melting during warming: -63°C and -21°C, respectively (Table 3.1). In addition, a single, mixed aqueous-petroleum inclusion in a PFIA froze. This single inclusion differed in size, shape, and petroleum:water ratio from the other inclusions in the same FIA: it is three to four times larger than the other fluid inclusions, has an irregular shape, and the petroleum component accounts for only approximately 20% of the inclusion. Freezing was detectable by movement of the petroleum phase in the inclusion. Upon warming, first melting occurred near -30°C, when the inclusion rapidly darkened, after which the aqueous component recrystallised into a fine mosaic. The ice slowly

melted first, followed by hydrohalite at -10°C. Thus, although V_{H2O} was absent in this inclusion and the assemblage L_{H2O}-hydrohalite is metastable at last melting, the inferred salinity of 23 wt. % equiv. NaCl is considered a good estimate and is similar to that obtained for the two aqueous inclusions in the quartz cement.

Homogenisation temperatures for the AFIAs in the quartz cement are similar both in their range (120° to 133°C) and average (126°C). The lack of a vapour phase in the PFIAs precluded measuring T_h values.

Dolomite-hosted inclusions did not freeze despite repeated attempts. Homogenisation data were obtained for three FIAs in the dolomite cement. For the first FIA, T_h values varied between 109°C and 121°C (Table 3.1) with an average of 116°C; the second FIA had T_h values from 120-124°C with an average of 123°C, and the third FIA had a uniform T_h of 109°C.

3.4.2.5 Evaporate mound analysis

Mound data were obtained for both the quartz and dolomite cements, the latter produced on a glass slide. Cation composition in quartz-hosted mounds ranged from Na-dominant to K-dominant, with the majority at 50:50 Na:K (Fig. 3.8). Where mounds were more K-rich, they generally had a complex, dendritic morphology. As expected, chlorine was the main anion in all mounds, although minor amounts of sulphur were present (<5% of the anion component) in a small number of analyses. Calcium was also detectable in some mounds, and in such cases S was also detected, but not all mounds with S had Ca. The mounds produced from the dolomite cement were oval (Fig. 3.4H) with a mixed Na-K composition (Fig. 3.8). These mounds were depleted in both Ca and Mg and had a

generally uniform Na:K ratio near 65:35. In addition to evaporate mounds, nanoparticles of barite and Pb-, Zn-, and Cu-sulphides were present in evacuated inclusions in the quartz cement (Fig. 3.4I).

3.5 INTERPRETATION

3.5.1 Wynniatt Formation

The sharp contacts between crystals of the dolostone host rock and crystals of void-filling saddle dolomite, as well as their different extinction patterns, suggest that these two phases did not form from the same fluid, or at least not at the same time. The contact between the saddle dolomite and the brown dolomite is gradational, and may represent a fluid that experienced a change after precipitation of the saddle dolomite. Banding in the brown dolomite is interpreted to have resulted from dissolution of the brown dolomite and precipitation of calcite, which implies the presence of a dolomite-undersaturated fluid during this time.

Even though almost no fluid inclusions froze, the cementing fluids can be inferred not to have been hypersaline (i.e., <26 wt. % equiv. NaCl) because halite is not present in the fluid inclusions at room temperature. The two fluid inclusions representing their respective FIAs measured in the calcite cement that froze (Table 3.1) provide the only insight into what the fluid salinity was during cementation. The final melting point of ice for these inclusions at -1 and -0.2°C reflect salinities of 1.74 and 0.35 wt. % equiv. NaCl, respectively (Bodnar 1993), which are values well below those of seawater. In contrast to

these salinities, the presence of evaporate mounds (see below) implies much higher salinities in the fluids (Haynes *et al*. 1988).

The burial depth in this part of the basin at the time of cementation is not well constrained by stratigraphic evidence because of the scarcity of regional stratigraphic information, and therefore a range from 0-9 km (precipitation shortly after Cambrian sandstone deposition to precipitation during the Ellesmerian Orogeny; see below) must be used. A value of 0 km would have no effect on the pressure correction of the T_h values for these FIAs, whereas a value of 9 km would have a great influence. Because salinity data for these fluids are sparse and high salinities are generally associated with diagenetic fluids, particularly with saddle dolomite (Davies & Smith 2006), a pressure correction calculated from Bodnar & Vityk (1994) is applied for a fluid of 2 wt. % equiv. NaCl (low salinity fluid observed) and 20 wt. % equiv. NaCl (assumed average fluid salinity) as an estimate to determine the possible range of trapping temperatures. For the inferred depth at the time of cement formation (0 - 9 km), the pressure correction for the fluid ranges from 0°C to ~140-160°C (depending on salinity), which results in estimated trapping temperature of 110°C to 250°C (Table 3.2).

The evaporate mound data for the three cements in the Wynniatt Formation differ from one another, implying a chemical evolution (Fig. 3.9) that proceeded from an early K-rich fluid (saddle dolomite), through a Na-K fluid (brown dolomite), to a late Na-rich fluid (calcite). This systematic change in composition suggests either that three distinct fluids migrated through this area, or that two end-member fluids mixed progressively in situ during cement precipitation.

3.5.2 "Victoria Island formation"

Salinity data for diagenetic fluids are limited to the quartz cement. The two FIAs in quartz had final ice melting temperatures between -21° and -22°C, which indicate a salinity of 23 wt. % equiv. NaCl (Bodnar 1993). The low eutectic temperature of -63°C for both of these FIAs indicates that a divalent cation, probably Ca, is present in the fluid, which is confirmed from analysis of evaporate mounds.

The homogenisation temperatures for fluid inclusions hosted by the quartz and dolomite cements are similar at 120º to 133°C and 109º to 124°C, respectively, but these results need to be pressure-corrected. Burial depth for "Victoria Island formation" is loosely constrained by petroleum maturation. A range in burial depth from 0-6 km requires a correction of about 93°C (i.e., 15.6°C/km), yielding formation temperatures of 125° to 225°C.

The lack of, and inability to artificially nucleate, a vapour bubble in any of the petroleum inclusions suggests that the petroleum is dead oil (no longer contains any dissolved volatiles). The final melting temperature of hydrohalite in the aqueous part of a single petroleum inclusion (-10°C) corresponds to a salinity of 23 wt. % NaCl (but see discussion above regarding this value). The petroleum was transported, therefore, by a fluid of similar salinity to that which formed the quartz cement, and it must have experienced either a large degree of evaporation or fluid-rock interaction along its flow path.

The evaporate mound data for quartz and calcite cements (Fig. 3.8) indicate Na-dominant Na-K mixtures. The quartz-hosted mounds contain Ca and Mg (Ca>>Mg). The barite and Pb-, Zn-, and Cu-sulphide nanoparticles present in the opened fluid inclusions may represent precipitates that formed when the supercritical fluid evaporated during de-

crepitation, or may have been nanoparticles transported in the fluid. Regardless of which of these interpretations is correct, they both imply that the fluid was metal-bearing.

3.6 DISCUSSION

3.6.1 Metastability of fluid inclusions

The absence of fluid inclusion freezing at temperatures as low as -140°C can be explained by either (1) metastability of the fluid, or (2) hypersalinity of the fluid. Fluid metastability can be caused by a lack of nucleation sites (i.e., very pure, solute-free water or very smooth inclusion walls; Roedder, 1968). However, even in pure water with no suspended particles, inclusion walls should eventually act as nucleation sites (Nitsch, 2009); also, once supercooled water reaches the homogeneous nucleation temperature, ice should nucleate itself. Fluid inclusions containing hypersaline fluids should contain solid halite at room temperature; because halite is absent from these fluid inclusions, the fluid cannot be considered hypersaline, but it may still be of comparatively high salinity, which is known to inhibit freezing. Inclusion morphology or size could also make phase changes undetectable, which may have been an issue in this study because of the small size of the inclusions (2-3 μm). There is no conclusive explanation for the lack of freezing of fluid inclusions in saddle dolomite and brown dolomite in the Wynniatt Formation, and in dolomite in the "Victoria Island formation". The inability of some fluid inclusions to freeze has been documented in other sedimentary rocks, such as the host rocks of the Pine Point Zn-Pb deposit (Roedder 1968).

3.6.2 Implications of evaporate mound analysis

Fluid inclusion studies, including those for sedimentary basins, typically rely on qualitative methods to determine fluid composition, such as the first melting of ice and ice-hydrohalite melting relationships in inclusions (Goldstein & Reynolds 1994). The documentation of multiple fluids or fluid events is commonly based on different T_h or salinity values, as is the case in many carbonate-hosted Zn-Pb settings (e.g., Roedder 1968, Appold *et al.* 1995, Chi & Savard 1995, Savard *et al.* 2000, Banks *et al.* 2002, Gleeson & Turner 2007, Persellin *et al.* 2010). Unfortunately, these types of studies are limited because they are indirect, and where similar T_h and salinities are present it is not possible to distinguish among fluid compositions. Furthermore, metastable fluid inclusions that resist freezing, such as those at Pine Point (Roedder 1968), preclude calculations of salinity values, such that cation presence cannot be inferred. In this study, a qualitative estimate of salinity and fluid composition in metastable FIAs can be established from the production of evaporate mounds. Production of evaporate mounds implies that the fluid contains dissolved ions (i.e., has salinity). The size of an evaporate mound is a function of the fluid's salinity and the volume of the fluid inclusion (Haynes *et al.* 1988). The application of evaporate mound analysis in this study demonstrates the utility of this efficient, inexpensive, and semi-quantitative analytical method in the study of fluid inclusions, particularly for diagenetic fluids.

3.6.2.1 Wynniatt Formation

Fluid inclusions in both saddle and brown dolomite cements of the Wynniatt Formation behaved metastably during freezing, thereby precluding salinity determination, but

have similar T_h values (Table 3.1), suggesting similar thermal histories. In contrast, the calcite cement has low-salinity FIAs for which no T_h values could be determined. Using the conventional approach for fluid inclusions, it would not have been possible to conclude that these three cements precipitated from fluids of different compositions. The application of evaporate mound SEM-EDS analysis on these samples, however, identified three distinct fluid compositions. Saddle and brown dolomite cements are distinct from the low-salinity FIAs in the calcite because the dolomite FIAs have higher salinities, as indicated by the larger mound size produced by these inclusions relative to those from calcite. The recognition of a different fluid composition in each paragenetic phase then allows for interpretation of the possible origin and evolution of these fluids, which is discussed in more detail below.

3.6.2.2 "Victoria Island formation"

Fluid inclusions hosted by quartz cement in "Victoria Island formation" produced evaporate mounds that allowed identification of two end-member fluids. These data imply a more complex fluid history than would have been traceable using standard microthermometric measurements, which would have resulted in a single fluid composition with relatively uniform T_h and salinity values (Table 3.1). Furthermore, the presence of barite and Pb-, Zn-, and Cu-sulphide nanoparticles in opened fluid inclusions would also have gone undetected. As is the case for some of the Wynniatt Formation cements, the fluid inclusions in the dolomite cement are metastable, which precluded salinity determination. The production of abundant evaporate mounds in the dolomite cement suggests that its fluid inclusions are of at least moderate salinity.

3.6.3 Nature and origin of fluid composition

3.6.3.1 Wynniatt Formation

Although salinity data could not be obtained for most of the cements through microthermometry, the production of evaporate mounds indicates that at least some of the fluid inclusions trapped saline water. The size and abundance of the mounds indicate moderately saline fluid (i.e., 10-20 wt. % equiv. NaCl; Haynes & Kesler 1987, Savard & Chi 1998, Kontak 2004, Morden 2011). Based on microthermometric data and evaporate mound analyses, three or four fluid compositions are recorded in cements from the Wynniatt Formation: three saline fluid compositions with different cation proportions (Na<K, Na>K, and Na>>K) based on evaporate mound composition (Fig. 3.9), and a fourth, low-salinity (<1.7 wt. % equiv. NaCl) fluid. Although it cannot be confirmed that the low-salinity fluid is distinct from the three fluid types identified from cation proportions, it is treated as distinct fluid type because of its low salinity. The presence of multiple distinct fluids is not unusual in MVT settings. For example, both Johnson *et al*. (2009) and Persellin *et al*. (2010) documented three distinct diagenetic fluids in cements from Lower Carboniferous rocks in Ireland, and Gleeson & Turner (2007) distinguished four fluids in dolomite cements of the Pine Point Zn-Pb district.

The fluid responsible for saddle dolomite cement in the Wynniatt Formation has a very low Na/K ratio, and Cl is the only detectable anion. This is atypical of brine compositions, which usually have subordinate proportions of K relative to Na and Mg (Shepherd *et al.* 1998, Bukowski *et al.* 2000, Lowenstein *et al.* 2005). The high amount of K in

the saline fluid can be explained by extreme evaporation of marine water or by interaction of subsurface fluids with a K-rich rock. In order for K to become the dominant cation in marine-derived fluid, a large degree of evaporation is needed to increase the salinity beyond halite saturation and to lower the Na content of the fluid (McCaffrey *et al.* 1987). Salinity several times greater than that of seawater is typical of fluids that precipitate hydrothermal saddle dolomite (Davies & Smith 2006, Lonnee & Machel 2006), but, as previously noted, no salinity data could be obtained for this cement. Another explanation for the high K content could be interaction between fluid and K-rich rocks, such as crystalline basement or a sedimentary derivative, during fluid migration (Savard & Chi 1998, Gleeson & Turner 2007, Johnson *et al.* 2009, Landis & Hofstra 2012).

The elevated Na over K in the fluid that formed the brown dolomite requires either a change in fluid composition or the introduction of a new, different fluid. If the existing fluid evolved to a new composition, one mechanism to account for the Na:K ratio is less interaction with the K-rich reservoir. If a new fluid was involved, it must have been enriched in Na or depleted in K, and must have had variable interaction with a K-bearing unit to account for the spread in Na:K values. Fluid interaction with evaporite units is generally invoked to explain an increase in the salinity of subsurface fluids (Hanor 1994, Lonnee & Machel 2006). Evaporite units present in the region may be a source for the salinity of hydrothermal-dolomite-related fluid. An example is the Neoproterozoic Kilian Formation (Fig. 3.2), which contains halite casts (Rainbird 1991).

The third saline fluid composition, recorded by calcite-hosted inclusions, may have been responsible for the dissolution of the brown dolomite: detailed petrographic and SEM-EDS analysis shows dissolution features at the contact between the two phases. The

calcite-precipitating fluid must, therefore, have been undersaturated with respect to dolomite. Dissolution of dolomite is commonly associated with fluids derived from interaction with subsurface evaporites (Lucia 1961, Warren 2006), which supports the above argument for subsurface fluid-rock interaction.

A simpler model to account for the change in cation proportions is to consider only two distinct fluids, one K-rich and the other Na-rich. In this case, progressive mixing of these fluids would account for the range of Na:K compositions in the mounds. Early stages of cement formation trapped a K-rich fluid, whereas later stages were dominated by a Na-rich fluid; fluid associated with the intermediate-stage brown dolomite had the largest Na:K range because of the mixing of the two fluids.

Finally, the only inclusions for which salinity could be measured had values of 0.4 to 1.7 wt. % NaCl (in calcite). Such low salinities are not unusual in dolomite cements (e.g., Johnson *et al*. 2009) and, although low-salinity fluids are not implicated in MVT mineralization (Basuki & Spooner 2002, Leach *et al*. 2005), they have been documented in mineralised settings (Gleeson & Turner 2007). Salinities below that of seawater indicate that this fluid must have had a component of surficial (i.e., meteoric) water.

In summary, the cement-precipitating fluids probably resulted from mixing of two saline fluids (K-rich and Na-rich) whose proportions changed through time (during precipitation of successive phases). The two fluids acquired their compositions through fluid-rock interactions as they migrated to the site of mixing and precipitation. The late incursion of a fluid with a meteoric component, which is inferred to have diluted the Na-rich fluid, is recorded by FIAs with low salinities in the calcite cement.

3.6.3.2 "Victoria Island formation"

The fluid evolution recorded in "Victoria Island formation" cements involves a fluid that was initially Na-K rich (variable proportions) with variable amounts of Ca (± Mg; early-stage quartz), which evolved into a fluid that was Na-K rich (consistent proportions) but Ca-Mg poor (late-stage dolomite). The quartz-precipitating fluid was highly saline and represents a typical burial fluid with an origin involving early evaporation or protracted fluid:rock interaction to increase its salinity. The range of fluid compositions documented in the quartz evaporate mounds can be explained by mixing of two fluids that experienced different fluid-rock interactions prior to mixing (Fig. 3.10). The K-rich fluid may have interacted with a K-rich reservoir, such as granitic basement or a clastic derivative, and carried metals. Another explanation could be that the fluid originated from the evaporation of seawater past the point of halite saturation. The former explanation is considered to be more probable because of the lack of hypersaline fluid inclusions. The Na-rich fluid may have originated as seawater that experienced evaporation that did not reach saturation with respect to halite, and probably transported the Ca because Ca is present only in Na-dominant evaporate mounds (Fig. 3.8).

The composition of the dolomite-hosted fluid inclusions indicates a Na-K composition with generally uniform Na:K of 60:40. Two explanations are offered for this fluid composition: (1) a single Na-fluid interacted with a K-rich reservoir, such as granitic basement or its clastic derivatives, or (2) mixing with a K-rich fluid. The former is considered simpler, and until more data are obtained, is the preferred interpretation.

Fluid inclusion data indicate that liquid petroleum migrated through the system during quartz cementation. Freezing data from the petroleum-aqueous H_2O inclusion suggests a

highly saline composition for the aqueous phase, which resembles the fluid in the quartz cement's primary fluid inclusions. This suggests that the petroleum migrated at the same time as the aqueous fluid and mixed either during transport or at the site where the cement grew. Although only one PFIA was documented in the material studied, liquid petroleum must have been present in the basin.

An important observation is the presence of nanoparticles of barite and base-metal sulphides (Pb, Zn, and Cu) in quartz-hosted inclusions. These particles may represent particulate matter carried by the fluid (which means the fluid was saturated in these phases), daughter phases formed during cooling of the trapped fluids, or particles that formed instantaneously when the inclusions were opened, due to fluid saturation. Such particles were not present in all of the opened inclusions, which argues against their being daughter phases, unless metastability was involved (Roedder 1984). The metal content of the fluid is unknown and so the other possibilities cannot be evaluated, but regardless of the explanation, the fluids must have been enriched in these metals. Metal nanoparticles are known to form in run-off waters and under a wide array of experimental conditions (Lloyd *et al*. 2001, Moreau *et al.* 2007). Sulphate-reducing bacteria species such as *Desulfovibrio desulfuricans* can produce sulphide nanoparticles (Lloyd *et al.* 2001) and Zn-binding proteins can bind with excess or bound Zn^{2+} to form ZnS (Moreau *et al.* 2007). Particles of this size can remain in suspension and be transported in a fluid (Honeyman 1999, Hochella 2002). Although sulphide nanoparticles have been documented in groundwater, there are no reported cases of sulphide nanoparticles (with the exception of pyrite) being preserved in diagenetic mineral phases.

The precipitation of framboidal pyrite during quartz growth implies a reduced environment, possibly with the presence of H_2S (Wilkin & Barnes 1997, Suits & Wilkin 1998). Experimental work has shown that pyrite-framboid-forming conditions can be highly variable, and the exact mechanism(s) and chemical reaction(s) cannot be determined with certainty (Ohfuji & Rickard 2005). In most cases an electron acceptor is required, one of the most effective being H_2S (Wilkin & Barnes 1997, Butler & Rickard 2000, Ohfuji & Rickard 2005).

The maturity of the liquid petroleum (i.e., API gravity index), as inferred based on the uniform fluorescence of the PFIA, as well as the absence of solid bitumen and natural gas in the inclusions, indicates that burial depth must not have exceeded the temperature of the oil window (approximately 150°C). Therefore, "Victoria Island formation" rocks could not have been buried deeper than 5-6 km (using a geothermal gradient of 25-30°C/km; Allen & Allen 2005).

In summary, the cements in "Victoria Island formation" record the incursion of a regional Na-rich fluid that experienced mixing of fluids during quartz precipitation enriching the fluid in K as well metals (Pb, Zn, and Cu) and petroleum, followed by evolution of the fluid by later interaction with a K-rich rock during dolomite precipitation. Reduced fluid (H_2S) was present during quartz precipitation and was responsible for the formation of pyrite framboids.

3.6.3.3 Origin of K-rich fluids

The above discussion shows that cement precipitation involved introduction of K-rich fluids at some time during the paragenetic evolution of both host rocks. Such fluids are

not typically documented in the fluid evolution of buried sedimentary basins, either barren (e.g., Hanor 1994) or mineralised (Chi & Savard 1998, Wilkinson 2010). In fact, the results of recent LA ICP-MS analysis of single fluid inclusions in a variety of mineralised MVT settings, generally considered to be the products of basin dewatering (Leach *et al*. 2005), confirm that elevated Na:K ratios of such fluids is the norm, with Ca also generally exceeding K (Stoffell *et al*. 20008, Wilkinson *et al*. 2009, Appold & Wenz 2011). There are, however, exceptions to this, in which K enrichment, expressed either as authigenic K-feldspar or illite, is present in a wide variety of settings that include both siliciclastic and carbonate successions (e.g., Buyce & Friedman 1975, Hearn *et al.* 1987, Fedo *et al.* 1995, Harper *et al*. 1995, Ziegler & Longstaffe 2000). In fact, Buyce & Friedman (1975) noted that authigenic K-feldspar, hitherto considered a rarity, is more common than once thought. Widespread K-rich fluids related to regional-scale fluid-flow coincident with regional tectonic events, as constrained by a variety of chronometers (Hearn *et al*. 1987, Harper *et al*. 1995, Elliot *et al.* 2002), is well established as a component of the general models for base-metal mineralisation in sedimentary basins (Leach *et al*. 2005, Paradis *et al.* 2007). Given the evidence for the presence of such fluids, one might wonder why they are not more commonly reported either in MVT or other sediment-hosted base-metal settings, such as red-bed copper deposits (e.g., Desouky *et al*. 2009). Two points may be relevant to this conundrum.

First, detection of K enrichment in fluids requires direct analysis of fluid inclusions, because ice melting, or in some cases ice-hydrate melting, is insufficient to quantify solute composition. Either in situ LA ICP-MS analysis or SEM-EDS analysis of evaporate mounds is required. Neither of these methods is routinely employed, and so most fluid

inclusion studies are not adequately designed to detect the presence of K. Is the apparent rarity of K-rich fluids in diagenetic studies real, or a reflection of the limitations of the methods used?

The second point is that K-rich fluids may require specific geological conditions. Several factors should be considered: (1) favourable aquifers or reservoirs (i.e., K-rich horizons; cf. Buyce & Friedman 1975); (2) fluid history (e.g., an evolved seawater with preferential loss of Na (halite precipitation) and Mg (dolomitisation)); or (3) appropriate tectonic settings. Until these factors have been addressed systematically, the extent, origin, and relevance of K-rich fluids to cement-forming processes will remain unresolved.

3.6.4 Evidence for hydrothermal fluid

In order to determine if the fluids responsible for cement precipitation in the Wynniatt Formation and "Victoria Island formation" were of hydrothermal origin, it must be demonstrated that the temperature of the fluid was at least 5°C greater than the ambient temperature of the host rocks at the time of entrapment (White 1957, Machel & Lonnee 2002). Because the FIAs reported here have relatively small vapour bubbles (i.e., have high density), the T_h cannot be assumed to be equal to the trapping temperature, and a pressure correction must be applied to establish the trapping temperature of the fluid (Goldstein & Reynolds 1994). The amount of thermometric data in this study is limited due to the quality of the fluid inclusions: post-entrapment changes (i.e., necking), dearth of FIAs, and small sizes were limiting factors. An independent source of pressure, such as stratigraphic thickness, is necessary to calculate a pressure correction (Goldstein & Reynolds 1994). The approximate burial depths of these samples, as outlined above, and

geothermal gradients typical of sedimentary basins (25-30°C/km; Allen & Allen 2005) were used for calculations.

For the Wynniatt Formation, the maximum burial depth of 9 km and a pressure correction for high-salinity (20 wt. % NaCl equiv.) and low-salinity (2 wt. % NaCl equiv.) fluids (15.6°C/km and 18.5°C/km respectively; using calculations from Bodnar & Vityk 1994) were used. Pressure-corrected fluid temperatures (Table 3.2) range from 110º to 250.4°C (high salinity) and 110° to-276.5°C (low salinity). The fluids were, therefore, of higher than ambient temperatures for all burial depths less than 7-8 km (Table 3.2, Fig. 3.11), depending on the salinity of the fluid and the geothermal gradient used. Because the maximum possible burial depth was 6-7 km, all pressure-corrected temperatures (220-240°C) are higher than ambient temperatures (<210°C), and the fluids should be interpreted as hydrothermal. The corrected temperatures may be a slight overestimation of the trapping temperature because the calculated values assume that fluid-flow took place at maximum burial depths.

The maturity of the liquid petroleum inclusions in the "Victoria Island formation" quartz restricts the burial depth imposed by overlying strata. The submaturity of the liquid petroleum suggests that the upper limit of the oil window (150°C) was not exceeded for extended lengths of time, and so the thickness of overlying strata was no more than 5-6 km (using a 25-30°C/km geothermal gradient; Allen & Allen 2005).

Applying a burial depth range of 0-6 km and a pressure correction for high salinities (23 wt. % NaCl equiv.), pressure-corrected temperatures for quartz-hosted FIAs are 126° to 219°C and 109º to 202°C for dolomite-hosted FIAs. The trapping conditions for all of the fluids exceed the ambient temperature of the buried strata for all depths, therefore im-

plying a hydrothermal origin for the fluids involved. The maximum temperature of fluid entrapment in dolomite exceeds the oil window. This could be explained by precipitation of dolomite in veins: the pressure correction used above is based on lithostatic pressure, whereas in a vein setting, a spectrum from lithostatic to hydrostatic pressures can be experienced (Roedder & Bodnar 1980). If pressure was in part hydrostatic, the trapping temperature would be overestimated in the calculation above.

The alternative explanation to a hydrothermal model involves hypersaline-basin-derived brine. Satisfying the temperature conditions in which the cements precipitated requires either a region with an elevated geothermal gradient or precipitation at great depth. Detailed stratigraphic study may eventually provide limits on cement formation conditions. Isotope and rare earth geochemistry are also needed to shed light on fluid derivation, but such analyses are beyond the scope of this study.

3.6.5 Implications for economic potential

Carbonate rocks of the Wynniatt Formation and "Victoria Island formation" exhibit features that are comparable to those of MVT deposits in general, and to known base-metal occurrences in the Arctic islands: (1) Victoria Island was part of the foreland basin of the Ellesmerian Orogen; (2) known faults in the study area could have focussed fluids, as was the case in the Polaris deposit; (3) fluid mixing took place between at least two fluid compositions in the Wynniatt Formation, and between a metal-rich fluid and a reduced sulphur-bearing fluid in the "Victoria Island formation"; and (4) fluid temperature and composition are consistent with those of other MVT deposits worldwide. In addition, the presence of liquid petroleum fluid inclusions in quartz cement indicates that hydro-

carbons migrated through faults that cross-cut the “Victoria Island formation”. The Arctic islands of Canada are known to contain numerous carbonate-hosted mineral showings (Zn-Pb) and hydrocarbon-bearing (oil, gas, and bitumen) areas; this study’s results may extend the prospective areas for each of these commodities.

3.7 CONCLUSIONS

Carbonate and quartz cements in the Proterozoic Wynniatt Formation and lower Paleozoic “Victoria Island formation” from Victoria Island in Canada’s Arctic archipelago contain primary and secondary fluid inclusions that provide information regarding the evolution of Phanerozoic diagenetic fluids. Analytical results suggest that multiple fluid compositions were involved in the precipitation of the diagenetic cements in both stratigraphic units. At least four fluid compositions were involved in the precipitation of the cements in the Wynniatt Formation. Of these, three resulted from variable mixing of two hydrothermal fluids, whereas the fourth was a meteoric fluid that mixed with the previous fluid during late cementation. Cements in the Paleozoic “Victoria Island formation” record several fluid compositions that resulted from two hydrothermal fluids, each with a separate flow path, mixing during early cementation of quartz. A NaCl-bearing fluid transported metals to a reduced environment at the site of precipitation. Following quartz precipitation, liquid petroleum was transported with a high-salinity fluid through the area, followed by a later, low-salinity fluid, recorded in the later dolomite cement. The petroleum fluid inclusion data agree with the geological context and suggest that this part of the lower Paleozoic succession did not experience conditions exceeding the oil window,

which in turn limits the total thickness of Paleozoic cover to <5-6 km. Both host rocks possess characteristics that resemble those of MVT settings. The "Victoria Island formation" is particularly interesting in this regard, because of presence of a metal-rich fluid that mixed with a reduced (H_2S) fluid during the unit's diagenetic history. Evidence for liquid-petroleum-bearing fluid in the "Victoria Island formation" implies that liquid petroleum migrated through faults, probably in the Paleozoic.

ACKNOWLEDGEMENTS

Field work was supported by the Geological Survey of Canada's Geomapping for Energy and Minerals (GEM) Victoria Island project. The fluid inclusion microthermometry laboratory at Laurentian University was funded by an NSERC grant to DJ Kontak.

REFERENCES

Allen PA, Allen JR (2005) *Basin Analysis: Principles and applications* (eds. Allen PA & Allen JR). Blackwell Publishing Ltd. Malden MA USA, p. 549.

Anderson GM (1975) Precipitation of Mississippi Valley-type ores. *Economic Geology*, **70**, 937-942.

Anglin CD, Harrison JC (1999) Mineral and energy resource assessment of Bathurst Island area, Nunavut. *Geological Survey of Canada Open-File* 3714.

Appold MS, Kesler SE, Alt JC (1995) Sulfur isotope and fluid inclusion constraints on the genesis of Mississippi Valley-Type mineralization in the Central Appalachians. *Economic Geology*, **90**, 902-919.

Appold MS, Wenz, ZJ (2011) Composition of ore fluid inclusions from the Viburnum Trend, Southeast Missouri District, United States: Implications for transport and precipitation mechanisms. *Economic Geology*, **106**, 55-78.

Ault AK, Flowers RM, Bowring SA (2009) Phanerozoic burial and unroofing history of the western Slave craton and Wopmay orogen from apatite (U-Th)/He thermochronometry. *Earth and Planetary Science Letters*, **284**, 1-11.

Banks DA, Boyce AJ, Samson IM (2002) Constraints on the Origins of Fluids Forming Irish Zn-Pb-Ba Deposits: Evidence from the composition of Fluid Inclusions. *Economic Geology*, **97**, 471-480.

Basuki NI, Spooner ETC (2002) A review of fluid inclusion temperatures and salinities in Mississippi Valley-type Zn-Pb deposits: Identifying thresholds for metal transport. *Exploration Mining Geology*, **11**, 1-17.

Bedard JH, Naslund HR, Nabelek P, Winpenny A, Hryciuk M, Macdonald W, Hayes B, Steigerwaldt K, Hadlari T, Rainbird R, Dewing K, Girard E (2012) Fault-mediated melt ascent in a Neoproterozoic continental flood basalt province, the Franklin sills, Victoria Island, Canada. *Geological Society of America Bulletin*, **124**, 723-736.

Bodnar RJ (1993) Revised equation and table for determining the freezing point depression of H2O-NaCl solutions. *Geochimica et Cosmochimica Acta*, **57,** 689-684.

Bodnar RJ (2003) Introduction to fluid inclusions. In: *Fluid inclusions: Analysis and interpretation* (eds Samson I *et al.*), Short course series vol. 32. Mineralogical Association of Canada, pp. 1-8.

Bodnar RJ, Vityk MO (1994) Interpretation of microthermometric data for H_2O-NaCl fluid inclusions. In: Fluid inclusions in minerals, methods and applications (eds. De Vivo B & Frezzotti ML). Virginia Tech, Blacksburg, VA, p. 117-130.

Bukowski K, Galamay AR, Goralski M (2000) Inclusion brine chemistry of Badenian salt from Wieliczka. *Journal of Geochemical Exploration*, **69-70**, 87-90.

Burns M, Kontak,DJ, Barrett, TJ (2012) Fluids in the Montclerg Archean mesothermal gold system: An SEM-EDS evaporate mound approach to unravelling the chemistry and origin of different fluids. Program with Abstracts, 11th Pan-American Current Research on Fluid Inclusions Conference, Windsor, ON, 13-14.

Butler IB, Rickard D (2000) Framboidal pyrite formation via the oxidation of iron (II) monosulphide by hydrogen sulphide. *Geochimica Acta,* **64,** 2665-2672.

Buyce MR, Friedman, GM (1975) Significance of authigenic K-feldspar in Cambrian-Ordovician carbonate rocks of the proto-Atlantic Shelf in North America. *Journal Sedimentary Research* **45**, 808-821.

Carpenter AB, Trout ML, Pickett EE (1974) Preliminary report on the origin and chemical evolution of lead-and zinc-rich oil field brines in Central Mississippi. *Economic geology*, **69,** 1191-1206.

Chen Z, Osadetz KG, Embry AF, Gao H, Hannigan PK (2000) Petroleum potential in western Sverdrup Basin, Canadian Arctic Archipelago. *Bulletin of Canadian Petroleum Geology*, **48**, 323-338.

Chi GX, Savard MM (1995) Fluid evolution and mixing in the Gays River carbonate-hosted Zn-Pb deposit and its surrounding barren areas, Nova Scotia. *Atlantic Geology*, **31**, 141-152.

Corbella M, Ayora C, Cardellach E (2004) Hydrothermal mixing, carbonate dissolution and sulfide precipitation in Mississippi Valley-type deposits. *Mineralium Deposita*, **39**, 344-357.

Davies GR, Nassichuk WW (1991) Carboniferous and Permian history of the Sverdrup Basin, Arctic Islands. In: *Geology of the Innuitian Orogen and Arctic Platform of Canada and Greenland* (ed. Trettin HP), no. 3. Geological Survey of Canada, Geology of Canada, pp.345-368.

Davies GR, Smith LB (2006) Structurally controlled hydrothermal dolomite reservoir facies: An overview. *AAPG Bulletin,* **90,** 1641-1690.

Dewing K, Obermajer M (2009) Lower Paleozoic thermal maturity and hydrocarbon potential of the Canadian Arctic Archipelago. *Bulletin of Canadian Petroleum Geology*, **57,** 141-166.

Dewing K, Sharp RJ, Muraro T (2006) Exploration history and mineral potential of the central Arctic Zn-Pb district, Nunavut. *Arctic*, **59,** 415-427.

Dewing K, Sharp RJ, Turner E (2007a) Synopsis of the Polaris Zn-Pb district, Canadian Arctic Islands, Nunavut. In: *Mineral Deposits of Canada: A synthesis of Major deposit-types, district metallogeny, the evolution of geological provinces, and exploration methods* (ed. Goodfellow WD) no. 5. Geological Association of Canada, Mineral Deposits division, Special publication, pp. 655-672.

Dewing K, Turner E, Harrison JC (2007b) Geological history, mineral occurrences, and mineral potential of the sedimentary rocks of the Canadian Arctic archipelago. In: *Mineral Deposits of Canada: A synthesis of Major deposit-types, district metallogeny, the evolution of geological provinces, and exploration methods* (ed. Goodfellow WD) no. 5. Geological Association of Canada, Mineral Deposits division, Special publication, pp. 733-753.

Dewing K, Pratt BR, Hadlari T, Brent T, Bedard J, Rainbird RH (2013) Newly identified "Tunnunik" impact structure, Prince Albert Peninsula, northwestern Victoria Island, Arctic Canada. *Meteorics and Planetary Sciences*, **48,** 211-223.

El Desouky HA, Muchez, P, Cailteux, J (2009) Two Cu-Co sulfide phases and contrasting fluid systems in the Katanga Copperbelt, Democratic Republic of Congo. *Ore Geology Reviews*, **36**, 315-332.

Elliot WC, Haynes, JT (2002) The chemical character of fluids forming diagenetic illite in teh Southern Appalachian Basin. *American Mineralogist*, **87**, 1519-1527.

Embry AF (1991a) Middle-Upper Devonian clastic wedge of the Arctic Islands. In: *Geology of the Innuitian Orogen and Arctic Platform of Canada and Greenland* (ed. Trettin HP), no. 3. Geological Survey of Canada, Geology of Canada, pp. 261-291.

Embry AF (1991b) Mesozoic history of the Arctic Islands. In: *Geology of the Innuitian Orogen and Arctic Platform of Canada and Greenland* (ed. Trettin HP), no. 3. Geological Survey of Canada, Geology of Canada, pp. 369-433.

Embry AF, Dixon J (1992) The breakup unconformity of the Amerasia Basin, Arctic Ocean: Evidence from Arctic Canada. *Geological Society of America Bulletin*, **102**, 1526-1534.

Fedo CM, Nesbitt, HW, Young, GM (1995) Unravelling the effects of potassium metasomatism in sedimentary rocks and paleosols, with implications for paleoweathering conditions and provenance. *Geology,* **23**, 921-924.

Forsyth DA, Mair JA, Fraser I (1979) Crustal structure of the central Sverdrup Basin. *Canadian Journal of Earth Science,* **16**, 1581-1598.

Garven G, Freeze RA (1984) Theoretical analysis of the role of groundwater in the genesis of stratabound ore deposits, *American Journal of Science* **284**, p. 1085-1124.

Gentzis T, Goodarzi F, Embry AF (1996) Thermal maturation, potential source rocks and hydrocarbon generation in Mesozoic rocks, Lougheed Island area, Central Canadian Arctic archipelago. *Marine and Petroleum Geology,* **13,** 879-905.

Gleeson SA, Turner WA (2007) Fluid inclusion constraints on the origin of the brines responsible for Pb-Zn mineralization at Pine Point and coarse non-saddle and saddle dolomite formation in southern Northwest Territories. *Geofluids,* **7,** 51-68.

Goldstein RH, Reynolds TJ (1994) Systematics of fluid inclusions in diagenetic minerals. Society for Sedimentary Geology Short Course 31, 199 p.

Hanor JS (1994) Origin of saline fluids in sedimentary basins. *In* Geofluids: Origin, migration and evolution of fluids in sedimentary basins (J. Parnell, ed.). *Geological Society Special Publication* **78,** 151-174.

Harper DA, Longstaffe, F, Wadleigh, MA, McNut, RH (1995) Secondary K-feldspar at the Precambrian-Paleozoic unconformity. southwestern Ontario. *Canadian Journal of Earth Sciences,* **32**, 1432-1450.

Harrison JC (1994) Melville Island and adjacent smaller islands, Canadian Arctic Archipelago. M*ap 1844A* 1:250000 Geological Survey of Canada.

Haynes FM, Kesler SE (1987) Chemical evolution of brines during Mississippi Valley-Type mineralization: evidence from East Tennessee and Pine Point. *Economic Geology,* **82**, 53-71.

Haynes FM, Sterner, SM, Bodnar RJ (1988) Synthetic fluid inclusions in natural quartz. IV. Chemical analyses of fluid inclusions by SEM/EDA: Evaluation of method. *Geochimica Cosmochimica Acta,* **52**, 969-977.

Heaman LM, Lecheminant AN, Rainbird RH (1992) Nature and timing of Franklin igneous events, Canada: implications for a late Proterozoic mantle plume and the break-up of Laurentia. *Earth and Planetary Science Letters,* **109**, 117-131.

Hearn PP, Sutter, JF, Belkin, HE (1987) Evidence for late-Paleozoic brine migration in Cambrian carbonate rocks of the Central and Southern Appalachians: Impications for Mississippi Valley-Type sulphide mineralization. *Geochimica Cosmochimica Acta,* **51**, 13231334.

Hochella MF (2002) There's plenty of room at the bottom: nanoscience in geochemistry. *Geochimica Cosmochimica Acta,* **66**, 735-743.

Honeyman BD (1999) Colloidal culprits in contamination. *Nature*, **397**, 23-24.

Jober S, Dewing K, White JC (2007) Structural geology and Zn-Pb mineral occurrences of northeastern Cornwallis Island: implications for exploration of the Cornwallis Fold Belt, northern Nunavut. *Bulletin of Canadian Petroleum Geology*, **55**, 138-159.

Johnson AW, Shelton KL, Gregg JM, Somerville ID, Wright WR, Nagy ZR (2009) Regional studies of dolomites and their included fluids: recognizing multiple chemically distinct fluids during the complex diagenetic history of Lower Carboniferous (Mississippian) rocks of the Irish Zn-Pb ore field. *Mineralogy & Petrology*, **96**, 1–18

Kerr JM (1977a) Cornwallis Fold Belt and the mechanism of basement uplift. *Canadian Journal of Earth Science*, **14,** 1374-1401.

Kerr JM (1977b) Cornwallis Lead-Zinc District; Mississippi Valley-type deposits controlled by stratigraphy and tectonics. *Canadian Journal of Earth Science*, **14,** 1402-1426.

Kesler SE, Reich M, Jean M (2007) Geochemistry of fluid inclusion brines from Earth's oldest Mississippi Valley-type (MVT) deposits, Transvaal Supergroup, South Africa. *Chemical Geology*, **237,** 274-288.

Kontak DJ (1995) A study of fluid inclusions in sulfide and nonsulfide mineral phases from a carbonate-hosted Zn-Pb deposit, Gays River, Nova Scotia, Canada. *Economic Geology*, **93,** 793-817.

Kontak DJ (2004) Analysis of evaporate mounds as a complement to fluid-inclusion thermometric data: case studies from granitic environments in Nova Scotia and Peru. *The Canadian Mineralogist*, **42,** 1315-1329.

Kontak DJ (2013) Fluid inclusion evaporate mound analysis: A rapid, efficient and informative means of determining fluid chemistry in hydrothermal systems. Atlantic Geology, **49**, p. 34

Kontak DJ, Dostal, J, Kyser, K, Archibald, DA (2002) A petrological, geochemical, isotopic and fluid inclusion study of 370 Ma Pegmatite-Aplite Sheets, Peggy's Cove, Nova Scotia, Canada. *Canadian Mineralogist*, **40**, 1249-1286.

Kontak DJ, Kyser K (2011) A fluid inclusion and isotopic study of an intrusion-related gold deposit (IRGD) setting in the 380 Ma South Mountain Batholith, Nova Scotia, Canada: evidence for multiple fluid reservoirs. *Mineralium Deposita*, **46**, 337-363.

Landis GP, Hofstra AH (2012) Ore genesis constraints on the Idaho Cobalt Belt from fluid inclusion gas, noble gas isotope, and ion ratio analyses. *Economic Geology*, **107**, 1189-1205.

Leach DL, Sangster DF, Kelley KD, Large RR, Garven G, Allen CR, Gutzmer J, Walters S (2005) Sediment-hosted lead-zinc deposits; a global perspective. In: *Economic Geology; One Hundredth Anniversary Volume, 1905-2005* (eds Hedenquist JW *et al.*), pp. 561-607. Society of Economic Geologists, Littleton, Colorado.

Lloyd JR, Williams DR, Macaskie LE (2001) Metal reduction by sulphate-reducing bacteria: physiological diversity and metal specificity. *Hydrometallurgy*, **59**, 327-337.

Long DGF, Rainbird RH, Turner EC, MacNaughton RB (2008) Early Neoproterozoic strata (Sequence B) of mainland northern Canada and Victoria and Banks islands: a contribution to the Geological Atlas of the Northern Canadian Mainland Sedimentary Basin. *Geological Survey of Canada, Open File* 5700 27p.

Lonnee J, Machel HG (2006) Pervasive dolomitization with subsequent hydrothermal alteration in the Clarke Lake gas field, Middle Devonian Slave Point Formation, British Columbia, Canada. *The American Association of Petroleum Geologists Bulletin,* **90,** 1739-1761.

Lowenstein TK, Timofeef MN, Kovalevych VM, Horita J (2005) The major-ion composition of Permian seawater. *Geochimica et Cosmochimica Acta*, **69**, 1701-1719.

Lucia FJ (1961) Dedolomitization in the Tansill (Permian) Formation. *Geological Society of America Bulletin,* **72**, 1107-1110.

Machel HG, Lonnee J (2002) Hydrothermal dolomite – a product of poor definition and imagination. *Sedimentary Geology*, **152**, 163-171.

Mathieu J, Turner EC, Rainbird RH (2013) Sedimentary architecture of a deeply karsted Precambrian – Cambrian unconformity, Victoria Island, NWT. *Geological Survey of Canada Current Research,* 2013-1, 15p.

McCaffrey MA, Lazar B, Holland HD (1987) The evaporation path of sea water and the coprecipitation of Br- and K+ with halite. *Journal of Sedimentary Petrology*, **57,** 928-937.

McNaughton K, Smith TE (1986) A fluid inclusion study of sphalerite and dolomite from the Nanisivik lead-zinc deposit, Baffin Island, Northwest Territories, Canada. *Economic Geology*, **81**, 713-720.

Miall AD (1976) Devonian geology of Banks Island, Arctic Canada, and its bearing on the tectonic development of the circum-Arctic region. *Geological Society of America Bulletin*, **87**, 1599-1608.

Miall AD (1979) Mesozoic and Tertiary geology of Banks Island, Arctic Canada. *Geological Survey of Canada Memoir*, **387**, 235 p.

Miall AD (1986) Effects of Caledonian tectonism in Arctic Canada. *Geology*, **14**, 904-907.

Morden R (2011) A fluid inclusion study of the Nanisivik Zn-Pb deposit, Nunavut, with implications for the origin of mineralization. Unpublished B.Sc. thesis, Laurentian University, Sudbury, Ontario, Canada, 40 p.

Moreau JW, Weber PK, Martin MC, Gilbert B, Huteon ID, Banfield JF (2007) Extracellular proteins limit the dispersal of biogenic nanoparticles. *Science*, **316**, 1600-1603.

Nitsch K (2009) Thermal analysis study on water freezing and supercooling. *Journal of Thermal Analysis and Calorimetry*, **95,** 11-14.

Norford BS, Macqueen RW (1975) Lower Paleozoic Franklin Mountain and Mount Kindle formations, district Mackenzie: Their type sections and regional development. *Geological Survey of Canada Paper*, **74-34.**

Obermajer M, Dewing K, Fowler MG (2010) Geochemistry of crude oil from Bent Horn field (Canadian Arctic Archipelago) and its possible Paleozoic origin. *Organic Geochemistry,* **41**, 986-996.

Ohfuji H, Rickard D (2005) Experimental synthesis of framboids – a review. *Earth Science Reviews,* **71,** 147-170.

Okulitch AV, Trettin HP (1991) Late Cretaceous – Early Tertiary deformation, Arctic Islands. In: *Geology of the Innuitian Orogen and Arctic Platform of Canada and Greenland* (ed. Trettin HP), no. 3. Geological Survey of Canada, Geology of Canada, pp. 469-490.

Okulitch AV, Packard JJ, Zolnai AI (1991) Late Silurian - Early Devonian deformation of the Boothia Uplift. In: *Geology of the Innuitian Orogen and Arctic Platform of Canada and Greenland* (ed. Trettin HP), no. 3. Geological Survey of Canada, Geology of Canada, pp. 302-307.

Paradis S, Hannigan P, Dewing K (2007) Mississippi Valley-Type lead-zinc deposits. In: *Mineral Deposits of Canada: A synthesis of Major deposit-types, district metallogeny, the evolution of geological provinces, and exploration methods* (ed. Goodfellow WD) no. 5. Geological Association of Canada, Mineral Deposits division, Special publication, pp. 185-203.

Persellin CJ, Gregg JM, Shelton KL, Somerville, Atekwana EA (2010) Base Metal Sulfide Mineralization in Lower Carboniferous Strata, Northwest Ireland. *Exploration and Mining Geology*, **19**, 35-54.

Qing H, Mountjoy EW (1994) Origin of dissolution vugs, caverns, and breccias in the Middle Devonian Presqu'ile Barrier, host of Pine Point Mississippi Valley-type deposits. *Economic Geology*, **89**, 858-876.

Rainbird R (1991) Stratigraphy, sedimentology, and tectonic setting of the upper Shaler Group, Victoria Island, Northwest Territories; Unpublished Ph.D. Thesis, University of Western Ontario, London, Ontario.

Rainbird R (1992) Anatomy of a large-scale braid-plain quartz arenite from the Neoproterozoic Shaler Group, Victoria Island, Northwest Territories, Canada. *Canadian Journal of Earth Sciences*, **29**, 2537-2550.

Rainbird RH, Jefferson CW, Hildebrand RS, Worth JK (1994) The Shaler Supergroup and revision of Neoproterozoic stratigraphy in Amundsen Basin, Northwest Territories; in Current Research, Part C; *Geological Survey of Canada, Paper* 94-01C, pp. 61-70.

Rainbird RH, Bedard JH, Dewing K, Hadlari T (in press) Geology, Minto Inlet, Victoria Island, Northwest Territories. *Geological Survey of Canada,* Geoscience Map 82 (preliminary) 1:50 000.

Rayner NM, Rainbird RH (2013) u-Pb Geochronology of the Shaler Supergroup, Victoria Island, northwest Canada: 2009-2013. *Geological Survey of Canada Open File* 7419, 62 p.

Rhodes D, Lantos EA, Lantos JA, Webb RJ, Owens DC (1984) Pine Point ore bodies and their relationship to the stratigraphy, structures, dolomitisation and karstification on the Middle Devonian Barrier Complex. *Economic Geology*, **79,** 991-1055.

Roedder E (1968) Temperature, salinity, and origin of the ore-forming fluids at Pine Point, Northwest Territories, Canada, from fluid inclusion studies. *Economic Geology*, **63,** 439-450.

Roedder E (1984) *Fluid inclusions: an introduction to studies of all types of fluid inclusions, gas, liquid or melt, trapped in materials from earth and space, and their application to the understanding of geologic processes* (ed Roedder E), Vol. 12. Mineralogical Society of America, Washington, DC, pp. 644.

Roedder E, Bodnar RJ (1980) Geologica pressure determinations from fluid inclusion studies. *Annual Review of Earth and Planetary Sciences*, **8**, 263-301.

Savard MM, Chi G (1998) Cation study of fluid inclusion decrepitates in the Jubilee and Gays River (Canada) Zn-Pb deposits – Characterization of ore-forming brines. *Economic Geology*, **93,** 920-931.

Savard MM, Chi G, Sami T, Williams-Jones AE, Leigh K (2000) Fluid inclusion and carbon, oxygen, and strontium isotope study of the Polaris Mississippi Valley-type Zn-Pb deposit, Canadian Arctic Archipelago: implications for ore genesis. *Mineralium Deposita*, **35,** 495-510.

Shepherd TJ, Ayora C, Cendon DI, Chenery SR, Moissette A (1998) Quantitative solute analysis of single fluid inclusions in halite by LA-ICP-MS and cryo-SEM-EDS: complementary microbeam techniques. *European Journal of Mineralogy*, **10**, 1097-1108.

Stoffel B, Appold, MS, Wilkinson, JJ, McClean, NA, Jeffries, TE (2008) Geochemistry and evolution of Mississippi Valley-Type and northern Arkansas districts determined by LA ICP-MS microanalysis of fluid inclusions. *Economic Geology*, **103**, 1422-1435.

Suits NS, Wilkin RT (1998) Pyrite formation in the water column and sediments of a meromictic lake. *Geology*, **26,** 1099-1102.

Thorsteinsson R, Tozer ET (1962) Banks, Victoria, and Stefansson Islands, Arctic archipelago. *Geological Survey of Canada Memoir* **330,** 85 p.

Trettin HP (1991) Middle and Late Tertiary tectonic and physiographic developments. In: *Geology of the Innuitian Orogen and Arctic Platform of Canada and Greenland* (ed. Trettin HP), no. 3. Geological Survey of Canada, Geology of Canada, pp. 493-496.

Trettin HP, Mayr U, Long GDF, Packard JJ (1991) Cambrian to Early Devonian basin development, sedimentation and volcanism. In: *Geology of the Innuitian Orogen and Arctic Platform of Canada and Greenland* (ed. Trettin HP), no. 3. Geological Survey of Canada, Geology of Canada, pp. 163-238.

Turner EC (2011) A lithostratigraphic transect through the Cambro-Ordovician Franklin Mountain Formation in NTS 96D (Carcajou Canyon) and 96E (Norman Wells), NWT. Geological Survey of Canada Open File 6994 28 p.

Turner EC, Dewing K (2004) Geology of Little Cornwallis Island and Rookery Creek (Cornwallis Island), Nunavut. *Geological Survey of Canada Open File* 1780, scale 1:50,000.

Tweedale F, Hanley, J, Kontak, DJ, Rogers, N (2013) Evaporate analysis of quartz-hosted fluid inclusions by SEM/EDS: Evaluation and application of the method to as-

sess granite metal fertility. Geological Association of Canada-Mineralogical Association of Canada Annual Meeting, Program with Abstracts, vol. 37.

Warren JK (2006) *Evaporites: Sediments, resources and hydrocarbons* (ed Warren JK). Springer, Verlag Berlin Heidelberg, p. 1035.

White DE (1957) Thermal waters of volcanic origin. *Geological Society of America Bulletin,* **68,** 1637-1658**.**

Wilkin RT, Barnes HL (1997) Pyrite formation in an anoxic estuarine basin. *American Journal of Science*, **297,** 620-650.

Wilkinson JJ (2001) Fluid inclusions in hydrothermal ore deposits. *Lithos*, **55,** 229-272.

Wilkinson JJ (2010) A review of fluid inclusion constraints on mineralization in the Irish ore field and implications for the genesis of sediment-hosted Zn-Ob deposits. *Economic Geology*, **105**, 417-443.

Wilkinson JJ, Stoffell, B, Wilkinson, CC, Jeffries, TE, Appold, MS (2009) Anomalously metal-rich fluids form hydrothermal ore deposits. *Science*, **323**, 764-768.

Young GM (1981) The Amundsen Embayment, Northwest Territories; relevance to the upper Proterozoic evolution of North America; *Geological Survey of Canada*, *Paper* **81.** p. 203-218.

Ziegler K, Longstaffe, FJ (2000) Clay mineral authigenesis along a mid-continental scale fluid conduit in Palaeozoic sedimentary rocs from southern Ontario. *Clay Minerals*, **35**, 239-260.

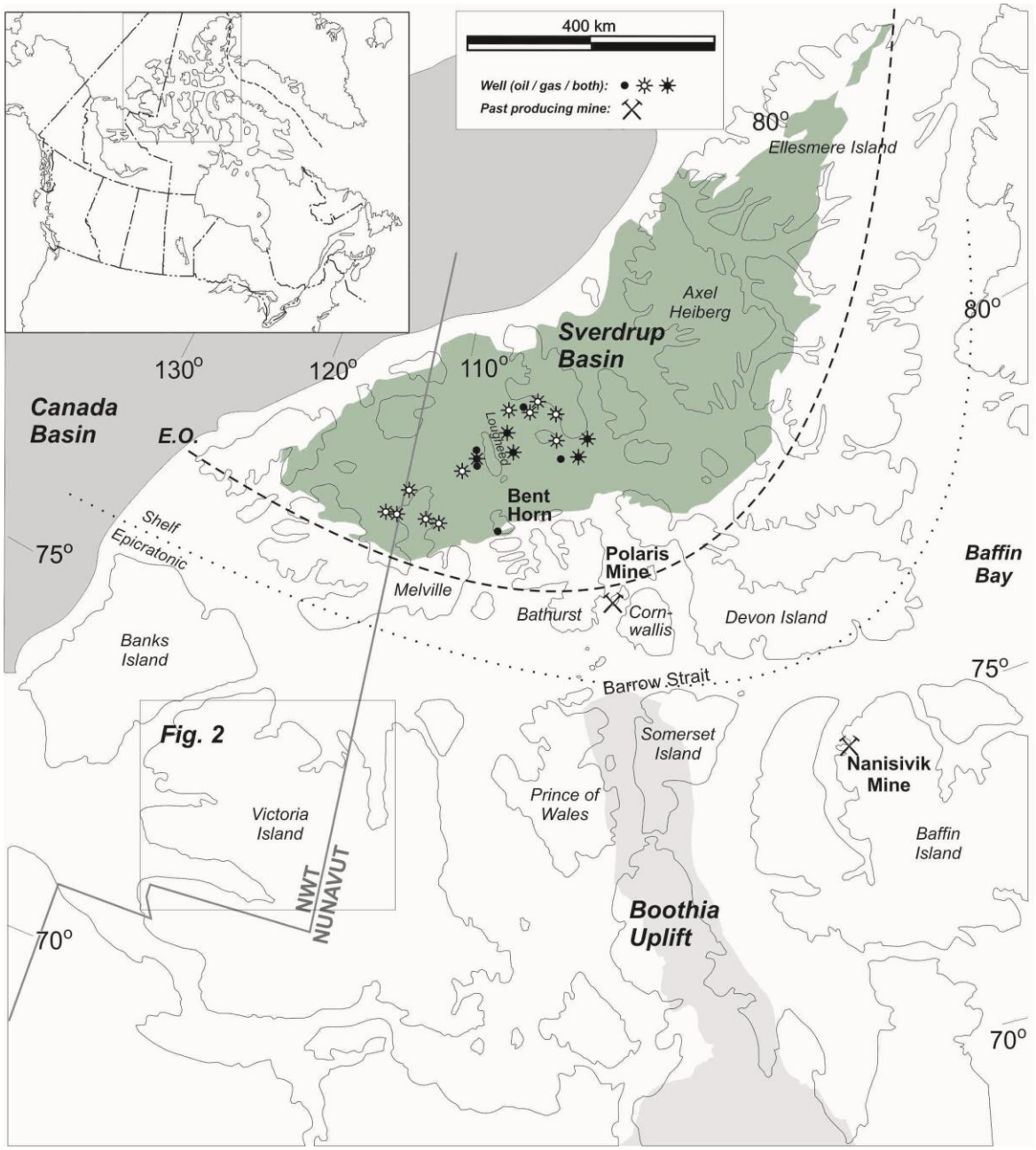

Fig. 3.1. Map of the Arctic archipelago highlighting features relevant to this study, modified after Dewing *et al*. (2007b). The Sverdrup and Canada basins and Baffin Bay are shaded areas. The southern limit of the Ellesmerian fold-thrust belt (E.O.), the location of the lower Paleozoic transition from epicratonic (south and east) to continental shelf (north

and west) settings of the Franklinian Basin, the locations of the Polaris and Nanisivik Zn deposits, and oil and gas wells, including Bent Horn, are also shown.

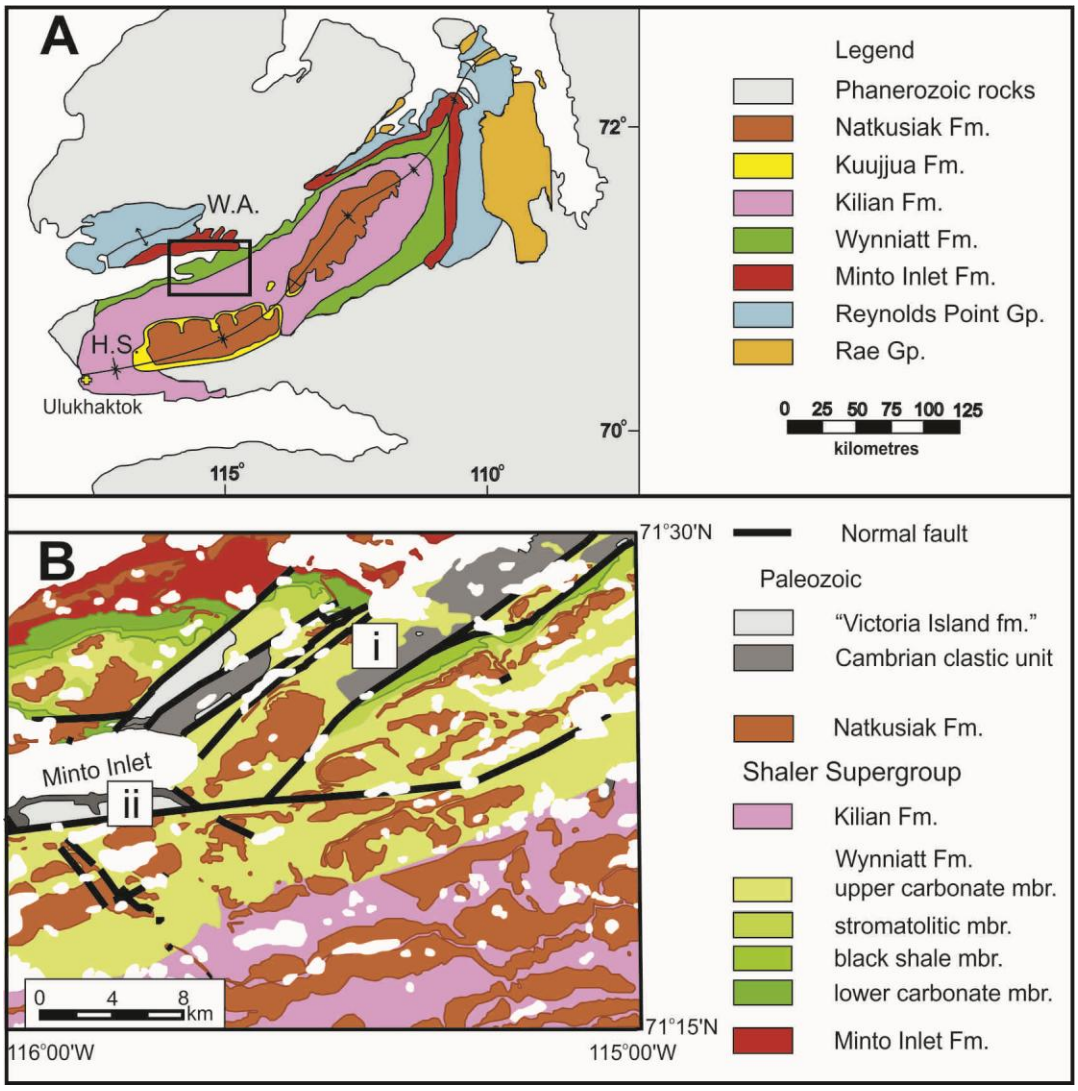

Fig. 3.2. (A) Bedrock geology of part of Victoria Island, after Thorsteinsson and Tozer (1962), highlighting Minto Inlier (coloured), Walker Bay anticline (W.A.), and the Holman Island syncline (H.S.). Yellow rectangle indicates area enlarged in (B). (B) Detailed geology of Minto Inlet (from Rainbird *et al.* in press) showing the locations of (i) Proterozoic and (ii) Paleozoic samples addressed by this paper.

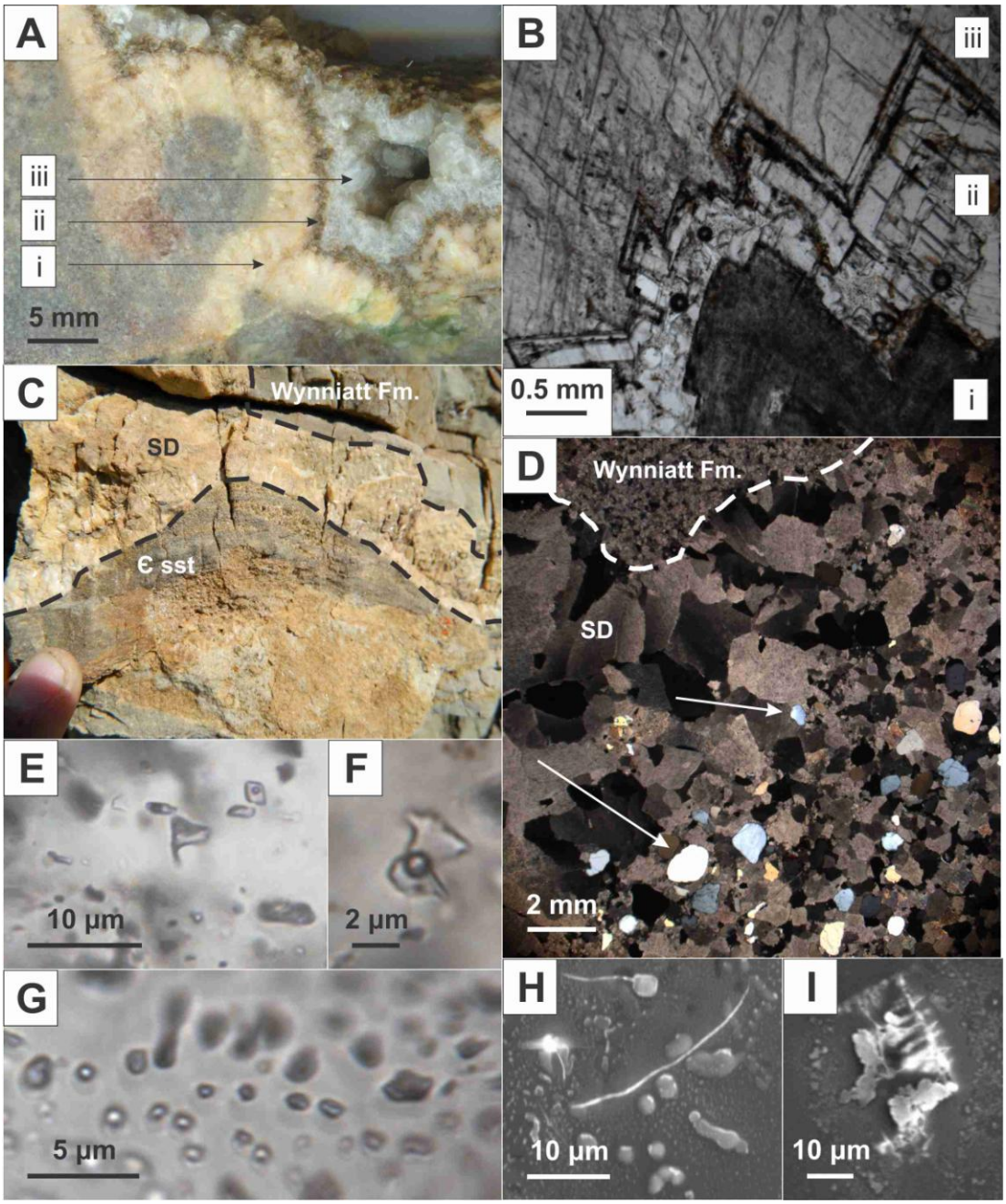

Fig. 3.3. Wynniatt Formation cements and their fluid inclusions. (A) Cut rock slab showing the typical appearance of three cements: (i) saddle dolomite, (ii) brown dolomite, and (iii) calcite. (B) Photomicrograph of cements (i) to (iii) in plane-polarised light. (C) Hand sample of Wynniatt Formation with Cambrian quartz sandstone filling a karst void fol-

lowed by saddle dolomite (SD) cement. (D) Photomicrograph in cross-polarised light of saddle dolomite (SD) cement surrounding quartz sand grains (arrows) inferred to be derived from overlying Cambrian map-unit 10a, which provides a maximum age for cement precipitation. (E) Typical aqueous FIA in the saddle dolomite in plane-polarised light showing uniform L-V ratios indicative of low-T inclusions. (F) A large fluid inclusion, part of a larger population, in calcite cement with a shape indicative of necking (G) Crystallographic plane decorated by small (<1-3 μm) aqueous fluid inclusions; the small size of these inclusions made microthermometry difficult. (H) Back-scattered electron (BSE) image showing the typical size and shape of evaporate mounds produced from the saddle dolomite. (I) BSE image of partly dendritic evaporate mounds produced from the brown dolomite.

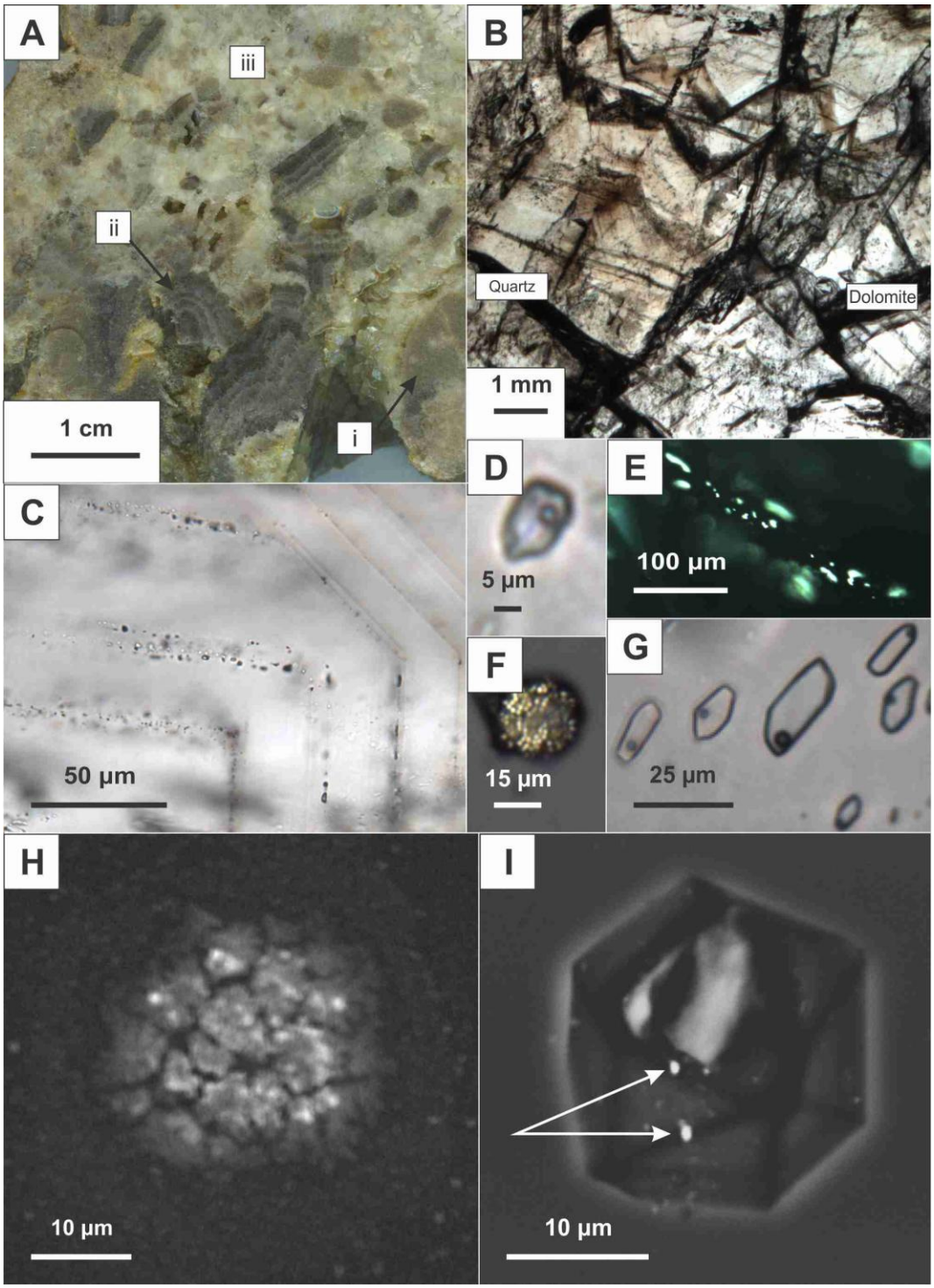

Fig. 3.4. Cements and fluid inclusions from "Victoria Island formation". (A) Cut rock slab showing the paragenetic relationship among (i) silicified and brecciated host rock,

(ii) brecciated quartz cement, and (iii) dolomite cement. (B) Quartz and dolomite cements in plane-polarised light showing growth bands in quartz. (C) Primary FIAs along growth zones in quartz cement. The small size of these inclusions precluded collection of thermometric data. (D) Atypical, unusually large aqueous fluid inclusion in the quartz cement. (E) Photomicrograph, taken under UV light (385 nm), showing fluorescence of secondary petroleum fluid inclusions in quartz cement. (F) Reflected-light photomicrograph of a single pyrite framboid on a growth surface in quartz cement. (G) Typical primary aqueous FIA in dolomite cement, taken in plane-polarised light, showing evidence of constant density, as represented by the uniform L-V ratios. (H) Back-scattered electron (BSE) image showing a typical evaporate mound hosted by dolomite cement. (I) BSE image showing an evacuated fluid inclusion in quartz cement containing nanoparticles (arrows) of lead sulphide phases.

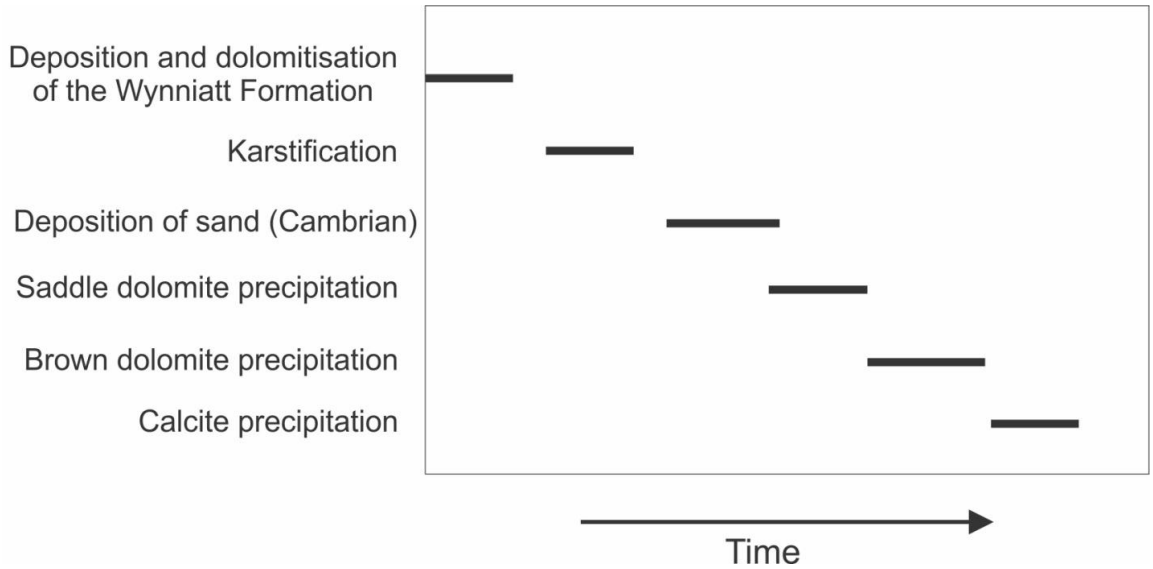

Fig. 3.5. Paragenesis of cements hosted by the Wynniatt Formation.

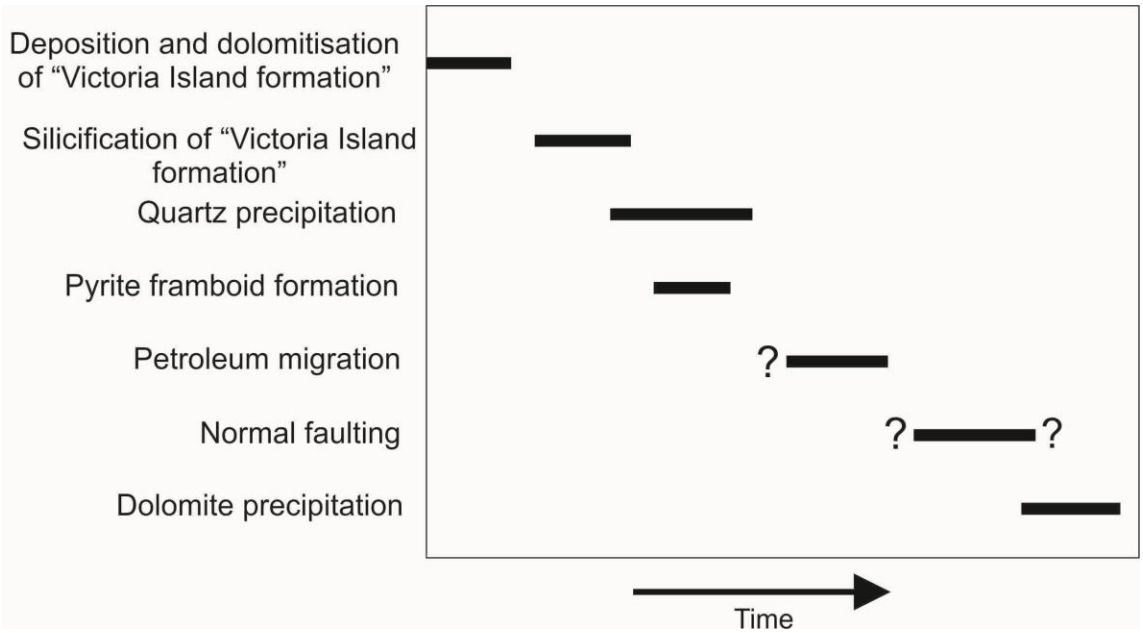

Fig. 3.6. Paragenesis of cements hosted by "Victoria Island formation".

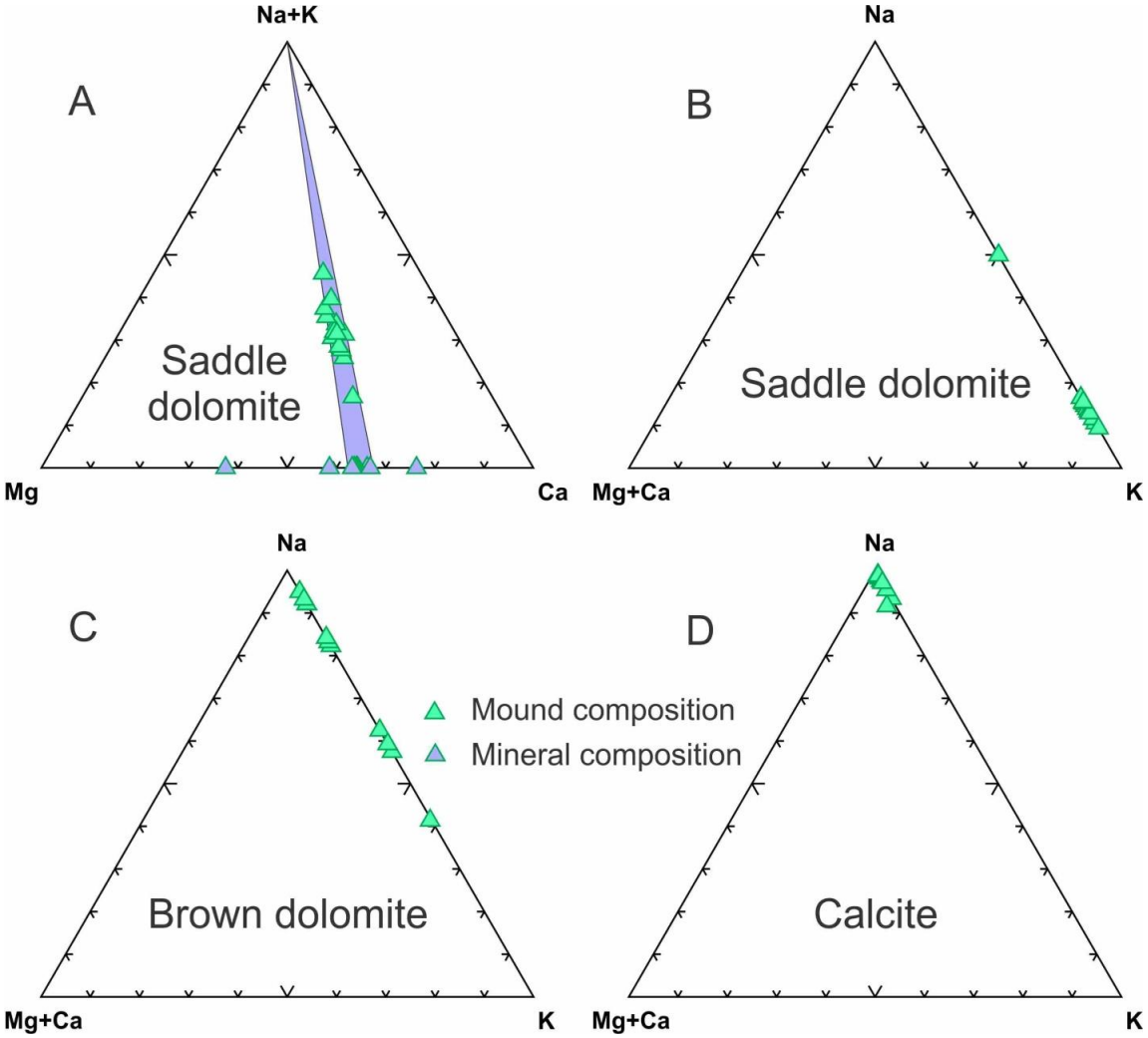

Fig. 3.7. Results of SEM-EDS analysis for evaporate mounds from Wynniatt Formation cements plotted in ternary compositional space (Mg+Ca-Na-K). (A, B) Mound data for saddle dolomite cement. The blue field in (A) represents the projected Mg:Ca ratio of the saddle dolomite with added Na+K, which overlaps the evaporate mound data and suggests that their Ca+Mg values are inherited from the host dolomite. (B) Data from Figure 3.7A, re-plotted without their Ca+Mg component, show a consistent, low Na:K ratio. (C) Mound data from the brown dolomite cement showing a range of Na:K ratios. (D) Mound data from the calcite cement showing high Na:K ratio.

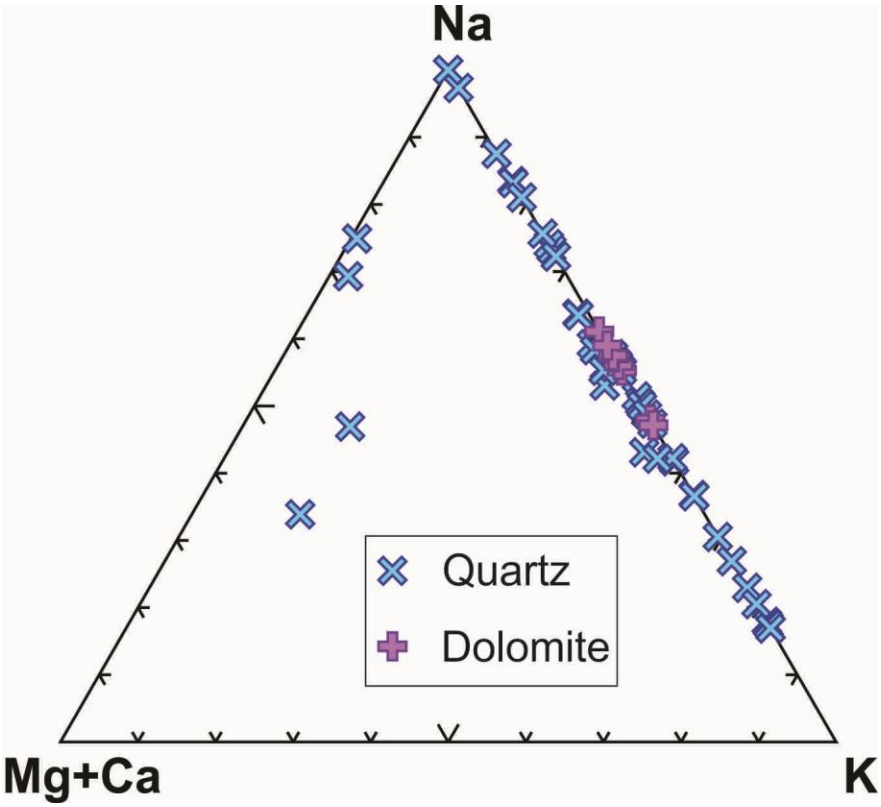

Fig. 3.8. Results of SEM-EDS analysis of evaporate mounds from "Victoria Island formation" cements plotted in a Mg+Ca-Na-K ternary diagram. Note that the Na:K ratios for quartz cement are variable, but those for dolomite cement show minimal variation.

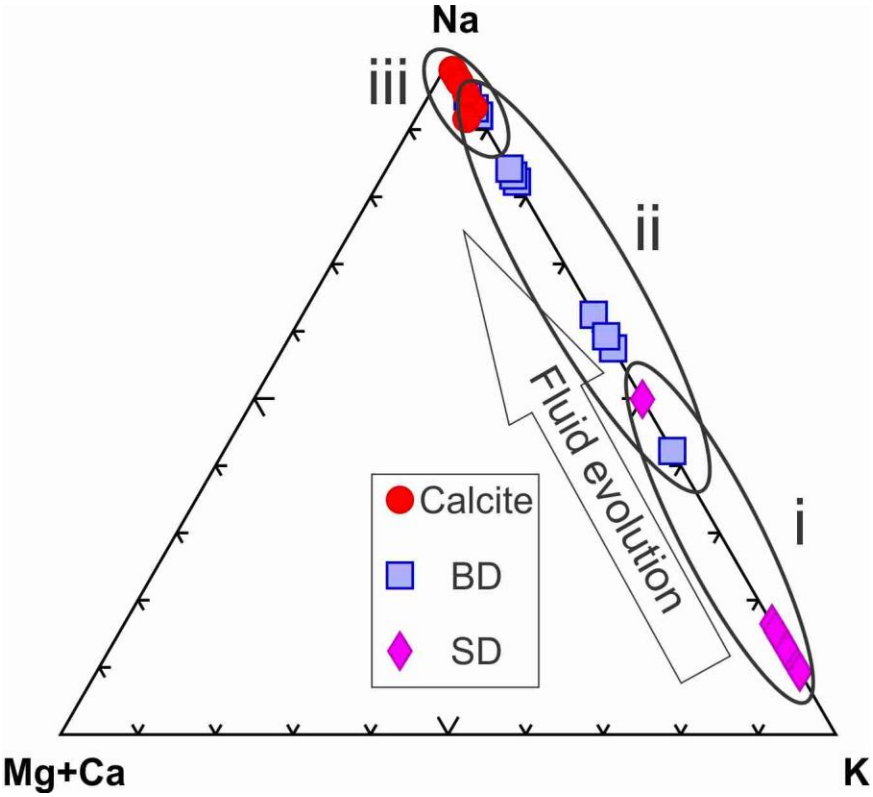

Fig. 3.9. Summary plot of evaporate mound analyses for fluid inclusions from Wynniatt Formation cements, with suggested evolution. As discussed in the text, fluid-rock interaction and fluid mixing caused fluid composition to evolve from (i) a K-rich fluid for the saddle dolomite to (ii) a Na+K fluid for the brown dolomite, followed by (iii) a Na-rich fluid during calcite cementation.

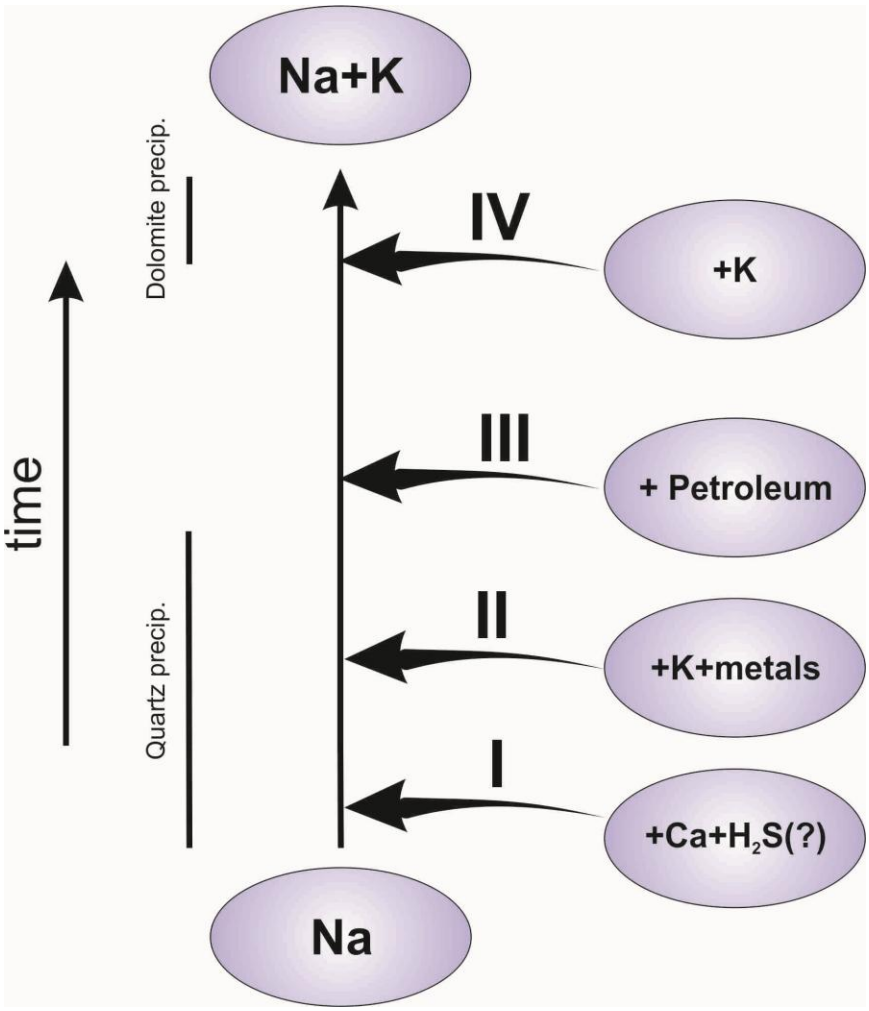

Fig. 3.10. Suggested evolution of the hydrothermal fluid responsible for "Victoria Island formation" cements. (I) A Na-dominant fluid experienced fluid-rock interactions with a carbonate rock to gain Ca. (II) The Na-Ca fluid then mixed with a K-rich, metal-rich fluid to generate the range in fluid compositions and trap sulphide nanoparticles in quartz cement. (III) Migration of petroleum and mixing with the Na-dominant fluid. (IV) The Na-dominant fluid interacted with a K-rich reservoir to gain K (dolomite cement).

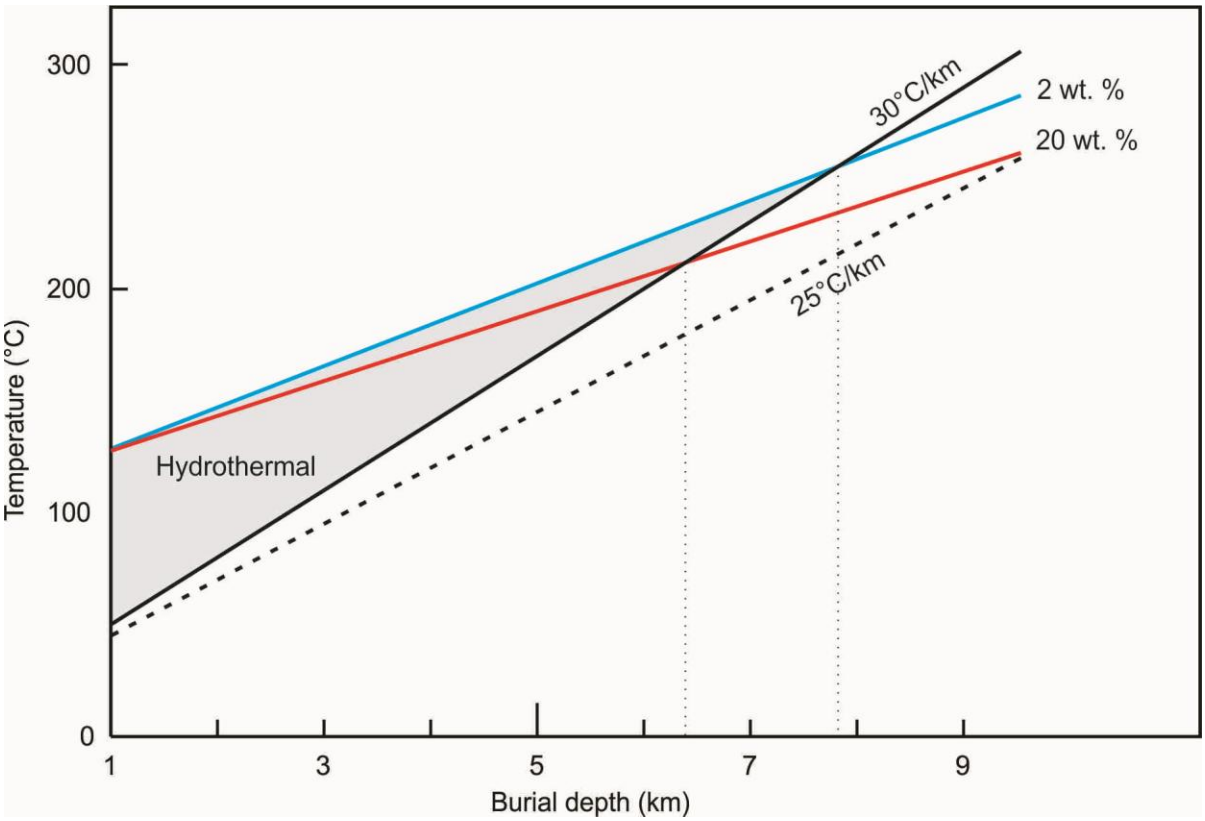

Fig. 3.11. Plot of fluid temperature versus burial depth for fluids of 2 and 20 wt. % equiv. NaCl with homogenisation temperatures of 110°C (see text for discussion of pressure corrections). In this plot, the areas above the average geothermal gradients of 25° and 30°C/km (Allen & Allen 2005) for given burial depths are considered to be hydrothermal (grey region in diagram using the 30°C gradient). In this diagram, fluids of two different salinities (2 and 20 wt. % equiv. NaCl) are used to illustrate that such fluids can be considered hydrothermal until burial exceeds 7.8 km with a geothermal gradient of 30°C/km, or 9 km for a 25°C/km gradient.

Table 3.1. Microthermometry results for cements from both host rocks. SD = saddle dolomite, BD = brown dolomite, Th = homogenisation temperature, Te = eutectic temperature, and Tm = temperature of final melt. Salinity is in wt. % NaCl equivalent.

Host	Cement	FIA#	Th range	Th average	Te	Tm	Salinity (wt %)	Fluid comp
Wynniatt Fm.	SD	1	105-115	108 (n=6)	NA	NA	NA	K-rich (20:80 to 10:90)
	BD	1	112-117	116 (n=3)	NA	NA	NA	K+Na (40:60 to 95:5)
	BD	2	100-102	101 (n=2)	NA	NA	NA	K+Na (40:60 to 95:5)
	Calcite	1	NA		-0.2	-0.2	0.4	Na-rich (90:10 to 100)
	Calcite	2	NA		-36	-1	1.7	Na-rich (90:10 to 100)
"Victoria Island fm."	Quartz	1	120-130	123 (n=3)	-63	-22	23.2	K+Na+Ca (variable)
	Quartz	1	120-133	128 (n=3)	-65	-21	23.1	K+Na+Ca (variable)
	Dolomite	1	109-122	116 (n=7)	NA	NA	NA	K+Na (50:50 to 60:40)
	Dolomite	2	109	109 (n=5)	NA	NA	NA	K+Na (50:50 to 60:40)
	Dolomite	3	120-124	123 (n=6)	NA	NA	NA	K+Na (50:50 to 60:40)

Table 3.2. Pressure-corrected temperatures of fluids in diagenetic cements of the Wyniatt Formation at different depths, using two end-member salinities. Tth = temperature of high-salinity fluid (20 wt. % NaCl equiv.), Ttl = temperature of low-salinity fluid (2 wt. % NaCl equiv.), Tamin = minimum ambient temperature using 25°C/km geothermal gradient, Tamax = maximum ambient temperature using 30°C/km geothermal gradient.

Burial depth (km)	Tth (°C)	Ttl (°C)	Tamin (°C)	Tamax (°C)
0	110	110	0	0
1	125.	6 128.5	25	30
2	141.	2 147	50	60
3	156.	8 165.5	75	90
4	172.	4 184	100	120
5	188	202.5	125	150
6	203.	6 221	150	180
7	219.	2 239.5	175	210
8	234.	8 258	200	240
9	250.	4 276.5	225	270

Tth = temperature of high-salinity fluid (20 wt. % NaCl equiv.), Ttl = temperature of low-salinity fluid (2 wt. % NaCl equiv.), Tamin = minimum ambient temperature using 25°C km^{-1} geothermal gradient, Tamax = maximum ambient temperature using 30°C km^{-1} geothermal gradient.

CHAPTER 4 - *GEOCHEMISTRY OF PHANEROZOIC DIAGENESIS ON VICTORIA ISLAND, NWT*

J. Mathieu, D. J. Kontak and E. C. Turner

Department of Earth Sciences, Laurentian University, Sudbury, Ontario, Canada P3E 2C6

ABSTRACT

The Neoproterozoic Wynniatt Formation dolostone contains four Phanerozoic cements: saddle dolomite, brown dolomite, replacive calcite and late calcite. Cambro-Ordovician "Victoria Island formation" dolostone contains two cements: quartz and dolomite. In situ isotopic (O and S) analysis by SIMS was used to assess microscopic changes in the diagenetic phases. Average oxygen isotopic values of Wynniatt Formation saddle and brown dolomite, replacive calcite, and late calcite cements are 24.7‰, 7.7‰, and 6.9‰ (SMOW), respectively. Rare earth element patterns of Wynniatt Formation dolostone, dolomite, and replacive calcite are smooth and flat with slightly positive Ce and Y anomalies and MREE-enriched when normalised to PAAS; late calcite cement, in contrast, has negative Ce and positive Y anomalies. Recrystallisation of the Wynniatt Formation dolostone by the reduced saddle-dolomite-precipitating fluid in a fluid-dominated system altered the isotopic and REE pattern of the dolostone to saddle dolomite values. This fluid interacted with a shale unit at depth and mixed with a relatively high-salinity fluid. Brown dolomite precipitated from this fluid after a decrease in salinity. Oxygenated

meteoric water infiltrated the system and precipitated the calcite cements. “Victoria Island formation” dolostone, quartz, and dolomite have average oxygen isotope values of 31.7‰, 18.7‰, and 18.6‰ (SMOW), respectively. The $\delta^{34}S$ for framboidal pyrite in quartz averages -7.5‰ (CDT). “Victoria Island formation” dolostone has flat REE patterns with a positive Eu anomaly, no Ce anomaly, and zig-zagged HREE. Dolomite cements have two patterns: one similar to the dolostone, and the other with LREE enrichment, and negative La and Eu anomalies. Reduced hydrothermal fluids altered and partially silicified the “Victoria Island formation” dolostone. Quartz precipitated from a seawater-sourced fluid that incorporated metals at depth and mixed with bacterially reduced sulphur at the site of precipitation. Dolomite cement records the change from a rock-dominant system, inheriting precursor signatures to a fluid-dominant system reflecting fluid composition. This fluid was sourced from seawater and interacted with REE-phosphate minerals. Similarities with the Polaris Zn-Pb deposit may suggest that Victoria Island has or had the potential to host base-metal mineralisation.

4.1 INTRODUCTION

Despite the presence of past-producing ore deposits and oil fields in the surrounding islands (Chen et al., 2000; Dewing et al., 2007) (Fig. 4.1), geological research and mineral exploration on Victoria Island has been minimal. Because the formation of sediment-hosted base-metal (e.g., Zn-Pb) ore deposits is primarily controlled by fluids (e.g., Leach et al., 2005), understanding a sedimentary basin's fluid history is essential in assessing its economic potential. Arctic exploration is expensive, and so any method that can contribute to identifying potential target areas is potentially beneficial. The study reported here forms part of the GEM (Geomapping for Energy and Minerals) program of the Geological Survey of Canada, a segment of which was directed towards evaluating the potential of Victoria Island for base metal and energy resources.

Stable isotopes, including those of oxygen and sulphur, provide indirect information regarding the history of fluids that precipitate minerals, and are among the most widely used geochemical indicators in the study of sedimentary basins (e.g., Qing, 1998; Savard and Kontak, 1998; Adams et al., 2000; Savard et al., 2000; Dolnicek et al., 2012). Because the fractionation of many isotopes is temperature-sensitive, the oxygen isotopic values of mineral phases can be used both as a geothermometers, and as a way of determining the source of a fluid. For example, stable oxygen isotopic data can be used to distinguish between sources such as seawater and meteoric water (and their possible latitudes/elevations). Seawater, a common source of diagenetic fluids, yields a relatively

constant stable oxygen isotopic signal throughout geologic time (Veizer et al., 1997; Veizer et al., 1999). Combining isotopic data with independently derived estimates for temperature and fluid composition from fluid inclusion studies on host and cement samples provides a means of evaluating the burial and diagenetic history of a basin in terms of its thermal history and source of circulating fluids. Because the ratio of diagenetic fluid volume to rock volume influences isotopic signatures (Banner et al., 1988), this provides an indirect means of assessing the scale of fluid movement, or openness, of a diagenetic system.

Conventional isotopic analyses in diagenetic studies have traditionally been undertaken either on whole-rock or whole-mineral samples, which are adequate for relatively large, homogeneous phases, but, this method provides little information about the isotopic variation acquired during crystal growth. Secondary ion mass spectrometry (SIMS) can be used to analyse isotopes *in situ* at a spatial resolution of microns. This allows for refined microscopic resolution of isotopic variation within single crystals (Valley and Graham, 1991; Xiao et al., 2010; Gabitov et al., 2012). This approach is especially useful when the diagenetic and alteration phases are microscopic (Shotyk and Metson, 1994; Xiao et al., 2010).

Unlike oxygen and sulphur isotopes and other trace elements, rare earth elements (REE) are generally immobile so large degrees of fluid:rock interaction (i.e., ($>10^4$) are required to alter the REE signature of carbonate rocks (Banner et al., 1988). The REEs therefore provide a useful means for understanding the origin of fluids, their evolution through fluid:rock interaction, and their redox conditions (Graf, 1984; Banner et al., 1988; Kontak and Jackson, 1995; Qing, 1998; Bau et al., 2003; Staude et al., 2012). This

aspect of the REE chemistry of carbonate rocks provides a means to: (1) determine the chemistry of ancient seawater, as preserved in carbonate rocks (Elderfield and Greaves, 1982; Elderfield, 1988; Nothdurft et al., 2004; Tanaka and Kawabe, 2006; Qu et al., 2009; Azmy et al., 2011); (2) identify the source of the precipitating fluid (marine or non-marine) (Tlig and M'Rabet, 1985; Banner et al., 1988; Nozaki et al., 1997); and (3) assess the amount of fluid interaction that occurred (Banner et al., 1988; Qing and Mountjoy, 1994). The partitioning of REEs into carbonate minerals is several orders of magnitude greater than their concentration in seawater; hence carbonate minerals become enriched in REEs relative to seawater (Banner et al., 1988; Kawabe et al., 1998). Because the HREE radii are more similar to that of Mg than that of Ca, dolomite/dolostone has a greater enrichment in HREE than associated calcite/limestone; nonetheless, dolomite/dolostone generally inherits the REE signature of the precursor carbonate rock during dissolution and precipitation under low fluid:rock ratios (Banner et al., 1988; Qing and Mountjoy, 1994). Although the volume of diagenetic fluid required for dolomitisation is insufficient to alter the REE content of pre-existing carbonate phases, fluid volumes associated with MVT deposits are large and can be sufficient to alter REE patterns (Graf, 1984; Banner et al., 1988; Qing and Mountjoy, 1994; Qing, 1998).

This study of a small suite of samples combines fluid inclusion data and fluid chemistry information from samples examined in a previous study (Mathieu et al., 2013a) with new isotopic (O, S) and trace element (including the REE) data, to unravel the nature and origin of fluids responsible for initial dolomitisation of the host carbonate rock and precipitation of subsequent cement in voids and fractures. This study integrates multiple micro-analytical methods: secondary electron microscopy (SEM) for textural and par-

agenetic information, SIMS for oxygen and sulphur isotopic analysis, and laser ablation inductively coupled mass spectrometry (LA ICP-MS) for trace elements - together, these methods permit resolution of chemical changes at a micron-scale during diagenesis. The results, incorporating fluid inclusion data from an earlier phase of the study (Mathieu et al., 2013a), demonstrate that combining different types of micron-scale analyses can unravel the evolution of a basin's fluid chemistry in a level of detail that has not been attained in previous diagenetic studies.

4.2 GEOLOGY

4.2.1 Tectonic framework

The rocks addressed in this study are from Victoria Island, in the southwestern part of Canada's Arctic archipelago. The island's geology is dominated by lower Paleozoic carbonate rocks, but also exposes Proterozoic strata. This study addresses Phanerozoic diagenetic events that affected both Proterozoic and Paleozoic carbonate strata, and so it is the Phanerozoic tectonostratigraphic history of the islands that is of primary interest in terms of interpreting the cements that are the focus of this study.

The Neoproterozoic Shaler Supergroup was deposited in the Amundsen Basin of northwestern (present geography) Laurentia. A combination of different geochronological methods provide an age constraint for the deposition of the supergroup between 1151 and 723 Ma (Heaman et al., 1992; Rayner and Rainbird, 2013), which is within the time span of the Grenville Orogeny (~1100 to 980 Ma; Hynes and Rivers, 2010) as well as Rodinia's assembly (~1300 to 900 Ma) and disassembly (825 to 740 Ma; Li et al., 2008).

Detrital zircon grains sourced from the Grenville Orogeny are common in the supergroup (Rainbird et al., 1997a; Rayner and Rainbird, 2013). The Amundsen Basin was separated from the Mackenzie Basin by the Great Bear Arch (Young, 1981). Intermittent isolation of the basin precipitated basin-central evaporite deposits. During deposition of the Wynniatt Formation, the Amundsen Basin experienced depocentre migration from the southwest to the northeast and then back to the southwest (Thomson et al., 2014). Rhenium-osmium dating of black shale in the Wynniatt Formation (van Acken et al., 2013) reveals that early Wynniatt Formation members were deposited during the quiescence of the assembled Rodinia (~850 Ma), whereas later Wynniatt Formation members were deposited during the initial rifting of Rodinia (~740 Ma).

The Franklinian Basin refers to the latest Neoproterozoic to middle Paleozoic sedimentary rocks of Canada's Arctic archipelago and parts of the adjacent mainland. This succession records a complete Wilson cycle, beginning with the rifting of Rodinia in the late Neoproterozoic and ending with the Ellesmerian Orogeny (late Devonian). The Franklinian Basin consists of a southern and eastern shallow-marine area underlain by cratonic basement, and a deep-marine area in the northern and western parts of the islands (Trettin et al., 1991). Several kilometres of carbonate and evaporite strata were deposited during the Ordovician-Devonian, including the Thumb Mountain Formation, which hosts the Polaris Zn-Pb deposit (Kerr, 1977; Trettin et al., 1991; Savard et al., 2000; Jober et al., 2007; Dewing et al., 2007b) and the Cape Phillips Formation, which was the hydrocarbon source rock for the Bent Horn oil field on Cameron Island (Obermajer et al., 2010).

The closure of the Iapetus Ocean during the collision of Baltica and Laurentia in the Silurian-Devonian resulted in the Caledonian Orogeny, which is prominent in eastern Laurentia and Scotland (Miall 1986; Oliver 2001; Morris et al., 2005). The Boothia Uplift, a north-trending structural zone that extends from the exposed craton to Devon Island (central high Arctic), formed as a result of far-field compressional forces from the Caledonian Orogeny from the distant east in the late Silurian (Miall 1986). No record of structural deformation related to the Caledonian Orogeny is known to be present west of the Boothia Uplift.

Collision between Laurentia and an unknown landmass in the Devonian resulted in the Ellesmerian Orogeny, which was expressed as a southeastward-advancing deformation front (Embry 1991a). Large fold belts parallel to the deformation front reached as far south as the Parry Islands (Melville, Bathurst, and Cornwallis islands; Fig. 4.1; Okulitch et al., 1991). No Ellesmerian structures are developed on Banks Island (Miall 1976), or south of the Parry Islands. Ellesmerian stresses reactivated Boothia-aged structures in the central Arctic islands, and this event is considered to have been responsible for mobilising metalliferous fluids which resulted in the formation of the Cornwallis Zn-Pb district (Turner and Dewing 2004, Dewing et al., 2007b, Jober et al., 2007). Although there are no structural effects of the Ellesmerian Orogeny south of the Parry Islands, a large clastic wedge deposited in the orogen's foreland basin covered a broad area that reached as far south as Banks Island (Embry 1991a), where up to 9 km (4 km preserved) of strata accumulated (Miall 1976, Dewing and Obermajer 2009). On Victoria Island, the clastic wedge probably reached a thickness comparable to that on Banks Island (~9 km).

The Sverdrup Basin, a large intraplate basin in the northern Arctic islands (Fig. 4.1), contains sub-basin faults (Forsyth et al., 1979) associated with extension that began after waning of the Ellesmerian Orogeny in the Early Carboniferous (Davies and Nassichuk, 1991). The basin represents the main depocentre for much of the northern Arctic islands, but subsidence exceeded sediment supply and the basin eventually became a deep marine basin (Embry 1991b). During most of the Sverdrup Basin's depositional history, Victoria Island experienced erosion, and acted as a sediment source area, rather than a depocentre (Embry 1991b). Cretaceous flood basalts and sills are associated with extension in the Sverdrup Basin (Embry, 1991b; Dewing et al., 2007a).

Extension in the Canada basin west of the Arctic islands probably started in the Jurassic, as suggested by strata preserved in the Banks Island graben (Miall 1979). A break-up unconformity underlying the Isachsen Formation (Hauterivian) is recorded in the Banks basin (Embry and Dixon 1992), which confirms the time of rifting. Extension on and near Banks Island was associated with an anomalously high temperature flux, as recorded by vitrinite reflectance values that exceed those expected for the amount of burial suggested by sonic interval transit time (Dewing and Obermajer, 2009). Because of the proximity of Victoria Island to Banks Island, the thermal anomaly could have had an effect on the thermal regime of buried strata on Victoria Island.

The Cretaceous to Oligocene Eurekan Orogeny was a compressive event caused by the counter-clockwise rotation of Greenland relative to Laurentia (Kerr 1967; Tegner et al., 2011). This orogen affected primarily the northern- and eastern-most islands, producing structures that typically are parallel to or reactivated older structural features, such as those of the Ellesmerian Orogeny (Okulitch and Trettin 1991). The rotational movement

caused extension in the south, and associated opening of Baffin Bay, but compression in the north, on Ellesmere Island (Okulitch and Trettin 1991; Oakley and Stephenson, 2008; Tegner et al., 2011). The Sverdrup Basin became divided into several smaller basins. The Eureka Sound Group, a syntectonic deltaic deposit, accumulated in local basins over much of the islands, including at least 1 km of thickness on Banks Island (Miall 1979); the area of the former Franklinian shelf (including Victoria Island) was predominantly a positive geographic feature during this time (Miall 1991). Stresses related to the orogen reactivated faults, which resulted in the formation of grabens and straits, where post-Eurekan (Tertiary) sediment accumulated (Okulitch and Trettin, 1991). Following the compressive phase of the Eurekan Orogeny (Miall 1991), isostatic uplift resulting from erosion produced the present-day geomorphology of the Arctic islands and shifted the main sedimentary depocentre from intracratonic basins to the present-day continental margins (Canada and Baffin basins; Trettin 1991).

4.2.2 Local geology

The oldest strata on Victoria Island are exposed on the northeastern part of the island (Thorsteinsson and Tozer, 1962). These strata consist of quartzite (map-unit 1) of un-known age, and granitic rocks (map-unit 2), thought to be of Paleoproterozoic age based on conventional K-Ar dates (Thorsteinsson and Tozer, 1962).

The Early Neoproterozoic Shaler Supergroup (Sequence B) is exposed in the Duke of York and Minto inliers of southern and central Victoria Island (Thorsteinsson and Tozer, 1962; Rainbird et al., 1994, 1996). It is also exposed or correlated to strata in the Cop-permine River area and in the northern Cordillera (Mackenzie Mountain Supergroup) of

the Northwest Territories and Nunavut (Rainbird et al., 1996; Long et al., 2008). The strata of this supergroup were deposited in the epicratonic Amundsen Basin (Rainbird et al., 1994, Long et al., 2008) and comprise, in stratigraphic order, the Rae and Reynolds Point groups, and the Minto Inlet, Wynniatt, Killian, and Kuujjua formations (Thorsteinsson and Tozer, 1962; Young 1981; Rainbird 1991; Rainbird et al., 1996). These units are overlain by the Natkusiak Formation, a 1 km-thick flood basalt associated with the ~723 Ma Franklin large igneous province (Heaman et al., 1992). The Holman Island syncline and the Walker Bay anticline, which span Victoria Island (Fig. 4.2), exhibit structural dips no greater than 10°, and appear to be the only evidence of late Neoproterozoic deformation (Thorsteinsson and Tozer 1962; Harrison et al., 2013). Exposure of the Shaler Supergroup in the Duke of York Inlier is limited to formations of the Rae Group (Mikkelsen Island, Nelson Head, and Aok) that are unconformably overlain by Paleozoic strata (Cambrian quartz arenite; Thorsteinsson and Tozer, 1962; Rainbird et al., 1994, 1997b), whereas the Minto Inlier contains the entire supergroup (Fig. 4.2), which is overlain by Cambrian siliciclastic sediment (Thorsteinsson and Tozer, 1962; Rainbird et al., 1994, 1996). The Wynniatt Formation consists of shallow-marine limestone and dolostone divided into the informal Lower Carbonate, Shale, Stromatolitic, and Upper Carbonate members (Rainbird 1991; Rayner and Rainbird 2013; Thomson et al., 2014). Shortly before deposition of the basal Cambrian clastic unit, the upper Wynniatt Formation was subaerially exposed and karsted (Mathieu et al., 2013b). The estimated total thickness of Proterozoic strata overlying the Wynniatt Formation is from 0 m (at the unconformity site) to 1000-2000 m (where the Natkusiak Formation is well preserved; Rainbird 1991).

Most of the Paleozoic strata underlying Victoria Island are Franklinian epicratonic rocks that were divided into four informal groups by Thorsteinsson and Tozer (1962) based largely on fossil assemblages. More recently, Dewing et al. (2013) described and informally named several units from northwestern Victoria Island: Cambrian "clastic" and "stripy" units, Cambro-Ordovician "Victoria Island formation", Ordovician-Silurian Thumb Mountain and Allen Bay formations, unnamed Silurian shale, and Devonian Blue Fiord and Kitson formations. The Cambrian clastic unit is described as a cross-bedded marine quartz arenite that was largely deposited in a shallow tidally dominated inner-shelf environment (Durbano in prep.). Some of the stratigraphic units on Victoria Island are stratigraphically equivalent to units associated with mineralisation in the Cornwallis Zn-Pb district and to the source rock for the Bent Horn oil field on Cameron Island (Fig. 4.1). On northwestern Victoria Island, an impact crater formed by an impactor with a 2 km diameter sometime between the Devonian and Cretaceous, probably during the Mesozoic (Dewing et al., 2013). This impact crater exposes Proterozoic strata and shatter cones.

4.3 METHODS

4.3.1 Sample locations

Carbonate rocks from two locations near the head of Minto Inlet on Victoria Island (Fig. 4.2) were used in this study: (1) Neoproterozoic Wynniatt Formation dolostone and cements are from below an unconformity between the "upper carbonate member" of the Wynniatt Formation and the Cambrian clastic unit (map-unit 10a from Thorsteinsson and

Tozer, 1962; Mathieu et al., 2013b); and (2) the Paleozoic "Victoria Island formation" (formerly map-unit 10b from Thorsteinsson and Tozer, 1962) dolostone and cements are from an area that is bounded by present-day traces of faults south of Minto Inlet (Fig. 4.2).The samples used were the same as those used in a previous, related fluid inclusion study (Mathieu et al., 2013a).

4.3.2 Secondary ion mass spectrometry (SIMS)

Samples that represented all of the known diagenetic phases were selected for in-situ oxygen isotope analysis by SIMS at the University of Manitoba (Winnipeg, Manitoba). Samples were analysed with a spot size of ~10 μm, with a 10 kV source, and detected on a Balzers SEV 1217 electron multiplier, coupled with an ion counting system. Standard deviations of reproducibility for dolomite, calcite, and quartz were ±0.7‰, ±0.5‰, and ±0.6‰, respectively. Sulphur isotopes of pyrite framboids were analysed in-situ at Memorial University (Newfoundland, Canada).

4.3.3 Laser ablation inductively coupled plasma mass spectrometry (LA ICP-MS)

Samples were analysed for minor and trace elements using a Resonetics RESOlution M-50, ArF excimer laser with a 193 nm wavelength and two-volume chamber (Laurin Technic) and a Thermo X Series II (quadruple) ICP-MS in the Department of Earth Sciences, Laurentian University (Sudbury, Ontario, Canada). Samples were first characterised petrographically using transmitted and reflected light methods followed by imaging and analysis using a JEOL SEM-EDS system (Department of Earth Sciences, Laurentian University). The external standard used was the NIST 610 glass and the internal standard

used (e.g., Ca) depended on the phase being analysed (e.g., dolomite, calcite) and was based on the SEM-EDS analysis. The LA ICP-MS analyses were done with beam sizes between 19 μm and 124 μm at 5 Hz and approximately 7 J/cm2, 650 ml/min He, 700 ml/min Ar, and 6 ml/min $_{N2}$. Smaller beam sizes were used where necessary to analyse micrometre-scale features, and larger beams were used, when appropriate, to enhance rare earth element signals. Precision error is estimated, based on counting statistics, to be typically <10% for trace elements.

4.3.4 Scanning electron microscopy (SEM)

The paragenesis of the cements, their texture and chemistry, was determined using an SEM at Laurentian University. The instrument used was a JEOL 6400 SEM with an INCA EDS detector and software system. X-ray mapping was also used, in addition to point analysis, to assess chemical variation within each cement phase. Analytical conditions employed were accelerating voltage of 20 keV, beam current of 1 Amps, and 5 second counting rate.

4.4 RESULTS

4.4.1 Wynniatt Formation

4.4.1.1 Petrography

The Wynniatt Formation dolostone consists of planar dolomite crystals ranging from fine- to medium-crystalline. Displacive replacement of the original limestone by replacive dolomite concentrated relatively insoluble material around the dolomite crystal

faces. Individual matrix crystals of dolomite have a concentration of inclusions (solid and fluid) at their centres and are limpid at their edges. The Wynniatt Formation dolostone contains four types of pore-filling diagenetic cements: saddle dolomite (SD), brown dolomite (BD), replacive calcite (RC), and late-stage calcite (LC) (Fig. 4.3). Along the contact between the dolostone and the SD, as well as in patches within the dolostone, de-dolomite is present and contains disseminated hematite.

Saddle dolomite crystals at the margins of voids are several millimetres long, have curved crystal faces and abundant fluid inclusions, and exhibit sweeping extinction in cross-polarised light (Fig. 4.3). Saddle dolomite crystals are also present within host dolostone, and, like the cement, exhibit sweeping extinction, but are small and lack a well-developed crystal habit.

Brown dolomite cement has straight euhedral crystal faces and crystals up to several millimetres in size. The brown colour of the crystals, in hand sample, is caused by disseminated hematite that is associated with RC (or dedolomite; Fig. 4.3). The dolomite crystals are colourless and essentially free of inclusions, but for clarity will be referred to as "brown dolomite" in this study. There is fine banding of alternating brown dolomite and replacive calcite. Bands are of uneven width and have irregular boundaries, but roughly follow growth zonation of the BD crystals and typically are present on their outermost surfaces (Fig. 4.3C). Microfractures cross-cut BD and RC and contain hematite.

Late-stage calcite is a colourless, blocky, medium- to coarse-grained, anhedral, pore-filling cement with some inclusions (Fig. 4.3). No fractures are apparent in the crystals, and they contain no disseminated hematite.

4.4.1.2 Paragenesis

Limestone of the Wynniatt Formation was deposited in the Neoproterozoic. In the late Neoproterozoic to early Cambrian, subaerial exposure removed approximately 1 km of strata and caused karsting of the limestone. Prior to karst features being entirely eroded, shallow marine sandstone was deposited, preserving the karst features (Mathieu et al., 2013b), but it is unclear whether dolomitisation of the limestone occurred prior to karsting or after. Saddle dolomite cement precipitated some unknown amount of time after sandstone deposition, locally incorporating sand grains into the cement (Fig. 4.3D). After BD precipitated, a dolomite-undersaturated fluid dissolved some of the BD and precipitated RC followed by LC cement (Fig. 4.4). Part of this stage also involved precipitation of hematite, which defines the boundary between RC and LC cement (Fig. 4.3C). Because sand grains from the "Cambrian clastic" unit are enclosed by crystals of the oldest void-filling cement phase (saddle dolomite; Fig. 4.3D), the age of the diagenetic cements can be no older than Cambrian.

4.4.1.3 Stable isotopes

The Upper Carbonate member of the Wynniatt Formation has $\delta^{18}O$ values that range between approximately 22.6 and 25.7‰ (SMOW; Thomson pers. Comm. 2014) with a mean of approximately 24.2‰. The $\delta^{18}O$ values for SD cement range from 23.1 to 26.3‰, with a mean of 24.7 ‰ (SMOW). Brown dolomite cement has a similar range and mean of $\delta^{18}O$ values as SD, from 23.3 to 26.5‰, with a mean of 24.7‰. Replacive calcite cement cements have $\delta^{18}O$ values of 6.7 to 9.5‰, with a mean of 7.7‰, and LC $\delta^{18}O$ values are 3.1 to 9.8‰, with a mean of 6.9‰ (Table 4.1).

Because no homogenisation temperature (T_h) values could be determined for fluid inclusions in Wynniatt Formation dolostone or calcite cements (Mathieu et al., 2013a), bounding temperatures for carbonate formation are estimated at 20°C to 120°C, based on the possibility of dolomitising/precipitating at or near surface or at temperatures that were similar to those of the preceding/succeeding (saddle dolomite-precipitating) fluid (using fluid inclusion thermometric data). This large range of possible temperatures results from the lack of stratigraphic constraints on the timing of dolomitisation/precipitation. Fractionation equations from Land (1985) and O'Neil (1969) for dolomite and calcite phases, respectively, yield average $\delta^{18}O_{H2O}$ values of -8.6‰ (using 20°C) and 3.8‰ (using 120°C) for Wynniatt Formation dolostone, 4.6‰ for SD, 4.8‰ for BD, -21.7‰ (using 20°C) and -9.3‰ (using 120°C) for RC, and -22.6‰ (using 20°C) and -10.2‰ (using 120°C) for LC (Table 4.1; Fig. 4.5).

4.4.1.4 Trace and rare earth elements

Trace and rare earth element concentrations for each diagenetic phase are summarised in Table 2, and REE data, normalised to Post Archean Australian Shale (PAAS) from Pourmand et al. (2012), are shown in Figure 4.6. It appears that there is a general increase in ΣREE+Y from the host dolostone (3.28 to 4.82 ppm, average 3.92 ppm, n=8) to the SD (2.23 to 20.31 ppm, average 6.69, n=11), BD (6.69 to 14.14 ppm, average 10.35, n=6), and RC phases (2.35 to 19.27 ppm, average 8.21, n=8), followed by a decrease to the lowest ΣREE+Y in the LC (1.05 to 5.57 ppm, average 3.01, n=5). The REE plots also show a gradual increase in the degree of MREE enrichment for both the SD and BD and also for some of the RC. The latest calcite is, however, distinct from all other cements

and is instead characterised by its pronounced anomalies. Dolostone through to RC phases have no La anomaly, and a slight positive Ce anomaly in some samples, whereas the LC has a strong positive La anomaly and a well-developed negative Ce anomaly; one analysis of RC has a REE pattern similar to that of LC, with regards to anomalies (Fig. 4.7). Lanthanum and Ce anomalies were verified using a Pr/Pr* versus Ce/Ce* plot (Fig. 4.8) from Bau et al. (1997). All phases, with the exception of RC, possess superchondritic Y/Ho values (i.e., >28; McDonnough and Sun, 1995); replacive calcite has Y/Ho of 17.04 to 36.55 (average 26.37, n=8).

Samples change from Fe- and Mn-rich (>2000 ppm and >200 ppm, respectively), in the dolostone and dolomite phases, to Fe- and Mn-poor (<100 ppm and <50 ppm, respectively) in the LC phase; replacive calcite possesses the highest range and highest values of both Fe (130.78 to 17155.4 ppm, average 4021.77 ppm, n=8) and Mn (8.02 to 1500.1 ppm, average 597.40 ppm, n=8) (Fig. 4.9). The Na, Al, and K concentrations decrease from the host dolostone (~115 ppm, ~250 ppm, and ~150 ppm, respectively) to the SD (~44.89 ppm, ~54.70 ppm, ~25.06 ppm, respectively), BD (~2.37 ppm, ~34.90 ppm, ~1.26 ppm, respectively), RC (~14.50 ppm, ~124.01 ppm, ~4.95 ppm, respectively), aand LC cement (~0.24 ppm, ~0.3 ppm, and ~0.55 ppm, respectively) (Fig. 4.9). Ratios of Ca and Mg are approximately 65:35 for all dolomite phases. Both calcite phases have the same composition, and there does not appear to be any partitioning of major elements or compositional zoning between RC and LC cements, as indicated from SEM mapping.

4.4.2 “Victoria Island formation”

4.4.2.1 Petrography

Dolostone of the "Victoria Island formation" contains three pore-filling diagenetic cements: quartz and two different dolomite cements (Fig. 4.10A and B). The dolostone ranges from fine- to medium-crystalline planar to nonplanar dolomite (Fig. 4.10). Silicification of the dolostone is shown by a replacement texture of dolomite by quartz (Fig. 4.10C).

The quartz cement has chevron-shaped zoning outlined by an abundance of inclusions (solid and fluid) and is brown-grey, euhedral, and medium-grained (Fig. 4.10A-D). The crystals are stained along some growth zones, probably owing to micro-inclusions of an iron phase. Pyrite framboids are also present, primarily in the earlier zones, and have generally been oxidised to an iron-oxide phase (hematite) (Fig. 4.10D-G). Pyrite framboids are brass-coloured in reflected light and consist of discrete crystal aggregates, whereas framboidal hematite is grey in reflected light and does not exhibit discrete crystals (Fig. 4.10E). It appears, therefore, that oxidation was not uniform in the framboids. Oxidation occurred both from the inside out and from the outside in, and some framboids were oxidised on one surface only. The two dolomite cements (D1 and D2) are essentially indistinguishable from each other and are colourless, anhedral, coarse-grained pore-filling cements with an abundance of large primary fluid inclusions. Separation of dolomite cement into two varieties is based on REE compositions (see section 4.2.4). Fragments of dolostone and quartz cement are 'suspended' in the dolomite cement (Fig 4.10A).

4.4.2.2 Paragenesis

After deposition in the Paleozoic, the limestone was dolomitised and silicified. It is unknown whether dolostone replacement by quartz and quartz cement precipitation were related. The framboidal pyrite is inferred to reflect co-precipitation during the early stage of quartz formation (see Fig. 4.10D). Hydrothermal brecciation of both dolostone and quartz is associated with dolomite precipitation (D1 and D2) (Fig. 4.11).

4.4.2.3 Stable isotopes

"Victoria Island formation" dolostone has $\delta^{18}O$ values that range from 27.6 to 35.8‰, with a mean of 31.7‰ (SMOW), whereas the $\delta^{18}O$ values of the quartz cement range from 16.6 to 21.2‰, with a mean of 18.7‰, and the dolomite cement has a $\delta^{18}O$ value of 18.6‰ (Fig. 4.12). The $\delta^{34}S$ values for pyrite framboids range from -11.7 to -4.0‰ (CDT) with two apparent clusters of -4 to -6‰ and -9 to -11‰ (Table 4.1).

Because no T_h values could be determined for fluid inclusions in the "Victoria Island formation" dolostone, bounding values of 20°C to 120°Care used for the temperature of formation. These temperatures are based on the possibility of dolomitisation at or near surface or at temperatures that were similar to the succeeding (quartz-precipitating) fluid. The large temperature range is due to the lack of stratigraphic constraints on the timing of dolomitisation. Using the dolomite-water fractionation equation of Land (1985) and the quartz-water fractionation of Sharp and Kirschner (1994), the calculated $\delta^{18}O_{H2O}$ values for the cement phases average -1.6‰ (using 20°C) and 12.8‰ (using 120°C) for "Victoria Island formation" dolostone, -1.3‰ for quartz, and -0.8‰ for dolomite (Fig. 4.12).

4.4.2.4 Trace and rare earth elements

Trace and rare-earth element concentrations for each diagenetic phase are summarised in Table 4.2, and shale-normalised REE patterns are shown in Figure 4.13. The REE profiles for all analyses of the "Victoria Island formation" dolostone are subparallel, with a slight LREE enrichment and (slight) positive Ce and Eu anomalies (average Ce/Ce*= 1.06 and Eu/Eu*=1.58, n=6), and a slightly zig-zag HREE pattern. Quartz failed to ablate properly, and so only incomplete elemental concentrations were acquired; incomplete REE patterns appear to be zig-zagged, with no Ce anomaly and a positive Eu anomaly. The results of the LA ICP-MS analysis indicate that two dolomite cements can be distinguished based on their REE chemistry (D1 and D2), but these two cement phases were not distinguishable using either optical properties or SEM-EDS imaging and analysis. Adjacent crystals have contrasting REE patterns that do not appear to display any change inherited from when they were precipitated (Fig. 4.14). In terms of the REE data, the two types of dolomite cement are characterised as follows: D1 has a flat to slightly fractionated (i.e., $(Nd/Yb)_{SN}>1$) REE pattern, no La or Ce anomalies (Fig. 4.13), a slight positive Eu anomaly (Eu/Eu*=2.15, n=8), and comparatively low ΣREE+Y (average 2.20 ppm, n=8), whereas D2 has a negatively sloped REE pattern with average $(Nd/Yb)_{SN}$ = 4.00 (n=8), negative La, Ce, and Eu (Eu/Eu*= 0.83, n=8) anomalies, and comparatively higher ΣREE+Y (average 3.13 ppm, n=8). Anomalies of Ce and La were verified with the equations from Bau et al. (1997) (Fig. 4.15). All phases have variable Y/Ho values that range from sub- to superchondritic, but average 29.46 (n=6) for dolostone, 27.94 (n=9) for D1, and 27.40 (n=8) for D2. Where data are available, quartz cement has Y/Ho values that range from 23.16 to 30.56 and average 27 (n=3). There is an increase in Mn concentra-

tions from the dolostone (average 30.63 ppm, n=6) to the two dolomite cements (D1 average 37.13 ppm, n=9; D2 average 96.16 ppm, n=8). Iron does not change in a systematic manner between phases (average dolostone 477.3 ppm, D1 187.84 ppm, D2 1162.29 ppm). Quartz cement has much lower concentrations of Fe (average 23.92 ppm, n=5) and Mn (0.14 ppm, n=5) compared to the dolomite phases, but this may in part be because of the quartz's incomplete ablation. Dolostone and D1 cement have (relatively) high Pb contents (average 1.94 ppm and 0.929 ppm, respectively) compared to D2 (average 0.153 ppm). All dolomite phases have similar Ca:Mg of 65:35

4.5 INTERPRETATION

4.5.1 Wynniatt Formation

4.5.1.1 Isotopic composition of precipitating fluid

The calculated $\delta^{18}O_{H2O}$ values for the Wynniatt Formation dolostone (-8.6 to 3.8‰, Table 4.1, Fig. 4.5) indicate that dolomitising fluid could have had a low-latitude meteoric fluid component if dolomitisation occurred in a shallow to near-surface (less than 1 km) environment. Dolomitisation associated with meteoric water is known to occur in zones where meteoric ground water and seawater mix (Land, 1973; Ward and Halley, 1985). For burial temperatures greater than 60°C, the isotopic values indicate a seawater (or modified seawater) source. Assuming a seawater source ($\delta^{18}O = 0$) for the dolomitising/recrystallising fluid, the temperature of dolomitisation is restricted to a temperature between 62º and 84°C, which is equivalent to an approximate burial depth of 1.5 to 2.5 km if a reasonable geothermal gradient of 25°C/km (Allen and Allen, 2005) is used. This

burial depth is classified as intermediate to deep burial by Machel (1999) and is characterised as containing reduced fluids that can transport redox-sensitive metals (e.g., Fe and Mn; Machel, 1999; Budd, 1997). If the upper temperature limit (120°C) is assumed for dolomitisation, then the $\delta^{18}O_{H2O}$ is similar to that calculated for saddle-dolomite-precipitating fluid (Table 4.1). This similarity points to the possibility that the saddle-dolomite-precipitating fluid recrystallised the dolostone and effectively overwrote its $\delta^{18}O$ signature.

Evaporation can enrich fluids in heavier isotopes (by up to +6‰; Lloyd, 1966; Ward and Halley, 1985), but cannot fully account for the positive $\delta^{18}O$ values in the dolomite cements (SD and BD). The positive values for these cements could indicate instead that the fluid interacted with a siliciclastic unit to enrich the fluid in ^{18}O. Interaction with siliciclastic material was suggested by Mathieu et al. (2013a) based on the chemistry of fluid inclusions, which agrees with this interpretation (Table 4.3). The similarity in $\delta^{18}O_{H2O}$ values between SD and BD (Table 4.2) suggest that both of these cements may have precipitated from the same fluid.

Negative $\delta^{18}O$ values recorded for the fluids responsible for the calcite cements (RC and LC) (i.e., $\delta^{18}O_{H2O}$ = <-5‰; Table 4.1, Fig. 4.5) correspond to a meteoric fluid reservoir, which can be correlated to latitude and/or altitude (Dansgaard, 1964). Calculated $\delta^{18}O_{H2O}$ values for both calcite cements at all reasonable temperatures suggest that low-latitude meteoric fluid was responsible for their precipitation. This is in agreement with the low-salinity fluid inclusions (i.e., 0.4 to 1.7 wt. % eq. NaCl) recorded by Mathieu et al. (2013a) for the LC cement (Table 4.3) and the presence of hematite at the interface of

the BD and LC cements (Fig. 4.3C). The overlapping $\delta^{18}O_{H2O}$ values of RC and LC suggest precipitation from the same fluid.

4.5.1.2 REE patterns and trace elements

Even a small percentage of siliciclastic and/or oxyhydroxide contaminant can significantly affect REE abundances in carbonate phases (Nothdurft et al., 2004). Given that there are no correlations between Al, Fe, or Mn and ΣREE+Y in the data, it appears that any such contamination is insignificant.

Typical seawater, and by extension marine carbonate rocks, has REE patterns that are characterised by LREE depletion (relative to HREE), and negative Ce and positive La and Y anomalies, when standardised to PAAS (Nozaki et al., 1997; Kawabe et al., 1998; Alibo and Nozaki, 1999; Nothdurft et al., 2004; Wilkinson et al., 2011). The Wynniatt Formation dolostone and dolomites do not have these characteristics (Fig. 4.6); instead, enrichment of LREE and MREE, a negative La anomaly and positive Ce anomaly indicate that either the Wynniatt Formation limestone was not precipitated from normal marine water or that the dolomitising/recrystallising fluid altered the original REE signature of the dolostone. Groundwater and river water REE concentrations are largely influenced by lithological interaction (i.e., fluid-rock) and can produce similarly flat, convex patterns (e.g., Leybourne et al., 2000; Hannigan and Sholkovitz, 2001; Lawrence et al., 2006; Leybourne and Johannesson, 2008). Enrichment in MREE has been attributed to the weathering of phosphate minerals (Johannesson et al., 1996; Hannigan and Sholkovitz, 2001) or Fe-oxides (Haley et al., 2004), and may explain the MREE patterns documented here. Because the Upper Carbonate member of the Wynniatt Formation was largely de-

posited in a shallow-marine, intertidal zone (Thomson et al., 2014), estuarine and/or river water mixing with seawater could have influenced the REE pattern and diluted characteristic seawater anomalies, resulting in a smoother, relatively flat pattern (Leybourne et al., 2000; Webb and Kamber, 2000; Kamber and Webb, 2001; Lawrence et al., 2006). Positive to absent Ce anomalies indicate reduced fluids (Elderfield and Greaves, 1982; De Baar et al., 1983; Elderfield et al., 1988), and may suggest that the Wynniatt Formation formed in anoxic seawater, but the intertidal depositional environment of the Wynniatt Formation (Thomson et al., 2014) precludes reduced depositional conditions. The observed REE pattern is, therefore, the result of a diagenetic fluid that was reduced under a sufficiently high fluid-rock ratio to alter the marine REE pattern of the original rock.

Rare earth element patterns for the two dolomite cements (SD and BD) and some of the RC data display a similar pattern to that of the host dolostone, but with different concentrations (Fig. 4.6). The similarity of REE patterns of the host rock and these cements indicate that: (1) the cement REE patterns were inherited from the host rock in a rock-buffered or low fluid:rock system; (2) the cement REE record a chemistry that is similar to that of the dolomitising fluids; or (3) the hydrothermal fluid that precipitated SD overprinted and recrystallised the dolostone.

Replacive calcite cement has REE patterns that are generally similar to that of BD cement (Fig. 4.6), and indicate that the REE composition was inherited from dissolution of the BD cement. Inheritance of REE patterns of one carbonate mineral from another indicates a low fluid:rock ratio (Banner et al., 1988; Qing and Mountjoy, 1994). The LC cement and some of the RC data differ from the preceding phases and obtained their REE signatures from the precipitating fluid rather than the host rock, which indicates a rela-

tively high fluid:rock ratio for that fluid (Banner et al., 1988; Qing and Mountjoy, 1994). The LREE depletion, negative Ce and positive La and Y anomalies for the LC cement are characteristic of typical seawater chemistry (e.g., De Baar et al., 1983; Elderfield, 1988; German et al., 1995; Kawabe et al., 1998; Nothdurft et al., 2004; Tanaka and Kawabe, 2006). Because marine and meteoric water can have similar REE characteristics (Nozaki et al., 1997; Nozaki et al., 2000; Lawrence et al., 2006; Leybourne and Johannesson, 2008), either of the two fluids, or both, may have precipitated this cement. The negative Ce anomaly in calcite cement indicates an oxygenated fluid (De Baar et al., 1983; Elderfield, 1988; German et al., 1995), thus restricting cementation to shallow burial or near-surface depths (i.e., <1 km; Machel, 1999). The transition of RC from a reduced REE signal to an oxidised signal (i.e., change in the Ce anomaly from positive to negative; Fig. 4.7) suggests that the RC-precipitating fluid was, or became, predominantly oxidised. The location of the negative Ce anomaly REE pattern (Fig. 4.7) indicates that either there was a pulse of fluid during RC precipitation or that replacement of BD was not systematic (e.g., random point-locations of replacement). This RC-precipitating fluid would have oxidised the liberated iron, from dissolved BD, to hematite, which would explain the association of hematite with RC cement (Fig. 4.3).

Iron and Mn are redox-sensitive and require a reduced fluid for transportation (Budd, 1997). Carbonate material precipitated in oxygenated marine water should have low concentrations of both of these elements; those that have high concentrations of Fe and Mn require a reduced diagenetic fluid. A reduced fluid interacting with siliciclastic material could become enriched in Fe and Mn and thus capable of transporting them to the location of carbonate precipitation (Morrow, 1990; Budd, 1997). Because the dolostone and

dolomite phases are enriched in these metals and have positive Ce anomalies, a reduced fluid that interacted with a sedimentary unit may have precipitated these phases. The Y/Ho ratios for the dolostone host (33.86) and dolomite cements (37.15) are between those of typical shale (~26; e.g., Pourmand et al., 2012) and marine carbonates (~40; e.g., Möller et al., 2003; Nothdurft et al., 2004), suggesting that interaction of a marine fluid with a siliciclastic unit (e.g., shale) resulted in the ratio between the two end members; intermediate Y/Ho values between shale and carbonate have been attributed to mixing/interaction between the two in other studies (e.g., Nothdurft et al., 2004; Turner and Kamber (2012). Fluid-rock interaction has been inferred from fluid inclusion evaporate mound analyses for these cements (Table 4.3; Mathieu et al., 2013a). The low Fe and Mn content and marine Y/Ho values of the LC would be consistent with either oxygenated seawater or meteoric water.

The decrease of ΣREE+Y from the dolomite cement to the LC cement could suggest that an influx of dilute fluid (seawater or meteoric) mixed with the precipitating fluid, thereby reducing the REE content. Low-salinity fluid inclusions in the LC cement indicate that the precipitating fluid had a meteoric component (Table 4.3; Mathieu et al., 2013a) and would explain the negative $\delta^{18}O$ values, diluted ΣREE+Y, low Fe and Mn, and REE anomalies.

4.5.2 "Victoria Island formation"

4.5.2.1 Isotopic composition of precipitating fluid

If the temperature of dolomitisation is limited to surface temperature (20°C) and the T_h of later phases (~120°C; Mathieu et al., 2013a) is used for calculations, then the $\delta^{18}O_{H2O}$ for dolostone formation ranges between -1.4‰ and 15.5‰. This range includes fluids of meteoric and seawater origin, those that have interacted with sedimentary sources, or, alternatively, a mixture of different fluid reservoirs. In contrast, if one assumes that seawater was the source for "Victoria Island formation" dolostone's dolomitising fluid, using the fractionation factor of Land (1985), the temperature of formation ranges between 10° and 43°C. These low temperatures would suggest that dolomitisation occurred in the near-surface to shallow burial environment (<1 km depth).

The $\delta^{18}O_{H2O}$ values for the fluid in equilibrium with the quartz cement are near 0‰ (or slightly negative) and are consistent with Paleozoic seawater (Veizer et al., 1997, 1999). An alternative source for the fluid, based on these isotopic values, could be meteoric water, but fluid inclusion data for the quartz suggest a high salinity (23 wt. % NaCl equiv.) for the cementing fluid (Table 4.3; Mathieu et al., 2013a), which precludes a significant contribution from unmodified surficial water.

Negative $\delta^{34}S$ values typically indicate a biogenic reservoir for sulphur (e.g., Ohmoto and Rye, 1979; Kucha et al., 2010).The sulfur isotopic values for the pyrite framboids are much heavier than what is typical for biogenic sulphur (i.e., below -20‰), which suggests that there was a mixture of sulphur sources. A mixture between biogenic or thermochemical sulphur and seawater or mobilised evaporite sulphate would produce the slightly negative $\delta^{34}S$ values recorded here. The association between dissolved Ca with S in the quartz-precipitating fluid (Mathieu et al., 2013a) indicates that dissolution of evaporite phases may have occurred, but its low abundance in the fluids would indicate

that the main source for heavier (relative to biogenic) sulphur was probably seawater. The two clusters of data (around -5‰ and -10‰) suggest that the fluid was not a homogeneous mixture.

Dolomite cement was deposited from a fluid with $\delta^{18}O_{H2O}$ close to 0‰ using the T_h values, which suggest seawater as a probable reservoir, but given that salinity could not be determined from fluid inclusions due to metastability (Mathieu et al., 2013a), meteoric water cannot be excluded as a possible source.

4.5.2.2 REE patterns and trace elements

The REE pattern in the "Victoria Island formation" dolostone is similar (with respect to anomalies) to silicified dolomite of the Guanmenshan Formation in Korea, which has been interpreted as being the product of hydrothermal alteration and silicification (Tang et al., 2013). The sub-parallel REE patterns could suggest a source that was either from, or interacted with, a shale unit. The absence of a negative Ce anomaly suggests that the precipitating fluid was reduced, whereas the positive Eu anomaly may suggest some component of a hydrothermal vent fluid (Bao et al., 2008), or a subsurface interaction with sulphides (Leybourne et al., 2000). The limited REE information yielded from quartz indicates a mixture with a primarily reduced (no Ce anomaly) fluid. A possible hydrothermal component for the quartz-precipitating fluid is also suggested by the positive Eu anomalies (Bao et al., 2008), zonal texture of the quartz (Dong et al., 1995), and T_h values obtained by Mathieu et al. (2013a) (Table 4.3). The different REE patterns in the dolomite cement could suggest fluid mixing between two end-member fluids, but the

lack of a transitional pattern precludes such mixing. Alternatively, a change in fluid flow path, hence reservoirs which the fluids interacted with, and/or fluid volume (i.e., fluid:rock) could change the REE patterns. The positive Eu anomaly and (relatively) high Pb concentration (up to 2.20 ppm) for D1 cement may indicate subsurface interaction with sulphide minerals (Leybourne et al., 2000). The relative enrichment of LREE and MREE in the D2 cement may indicate fluid interaction with a REE-phosphate mineral (Hannigan and Sholkovitz, 2001; Köhler et al., 2005).The similarity between the REE pattern of D1 cement and the dolostone (Fig. 4.13) may suggest low fluid:rock ratios; D2 cements display REE patterns that differ from those of the preceding phases (Fig. 4.13), thereby suggesting high fluid-rock ratios. The different REE patterns of adjacent crystals without gradual transition from one to another (Fig. 4.14) may suggest that these patterns are not the product of fluid mixing, but instead, a change in fluid volume.

4.6 DISCUSSION

4.6.1 Origin of the replacive calcite

The origin of the replacive calcite in the Wynniatt Formation must be discussed in order to determine its role in the paragenesis, and whether it was precipitated from its own fluid, or was the product of another phase's precipitating fluid. Paragenetically (Fig. 4.4), RC post-dates BD, as is apparent from the dissolution features in the BD (Fig. 4.3). Petrographic features (e.g., crystal habit, extinction) of dedolomitised cement can be inherited by the replacive calcite (e.g., Qing and Mountjoy, 1994) and are present in these

cements, which would require a dolomite-undersaturated fluid. Replacive calcite has the same $\delta^{18}O$ values as the LC cement and suggests a meteoric source, which is known to dissolve dolomite (e.g., Al-Hashimi and Hemingway, 1973; Savard et al., 2000). It can then be inferred that the LC-precipitating fluid was also responsible for the dissolution of BD and precipitation of RC. Replacive calcite (dedolomite) and calcite at the Polaris deposit are also both accredited to the same post-mineralisation, meteoric fluid (Savard et al., 2000). Although there is no preferential partitioning of major elements between RC and LC, as inferred from SEM imaging and elemental X-ray maps, hematite is associated with the RC but is absent in LC. This latter discrepancy may be attributed to the insolubility of Fe in oxidised water, which would have limited transportation after dissolution of BD. The oxidised water of the calcite-precipitating fluid could have dissolved the BD while precipitating RC, which is reflected in the negative Ce anomaly of one of the REE patterns (Fig. 4.6 and 7). Dissolved iron liberated from the BD would have precipitated as hematite in the RC; similar processes could explain the Mn enrichment. Rare earth element patterns for the RC have similarities with both the BD and LC cements (Fig. 4.6 and 7) and suggests that RC is an intermediate phase between the two end-members: BD and LC. Replacive calcite, which precipitated from meteoric water, inherited REE signatures from dissolved BD. After dissolution of dolomite had ended, LC began to precipitate in the pore space with an REE pattern reflecting the precipitating fluid, with no further influence from REE liberated from BD.

4.6.2 Sources and interaction of fluids

The fluid sources that probably had an effect on the diagenesis of the study areas are seawater, meteoric water, and modified or basin-derived fluids. On Victoria Island there is no evidence of metamorphism or magmatism other than that associated with the Neoproterozoic Natkusiak flood basalt (Thorsteinsson and Tozer, 1962), which predates all of the diagenetic events described here. Fluids from these types of sources would, therefore, have had to migrated from other areas, such as Banks Island, which experienced rifting in the Jurassic (Embry and Dixon, 1992; Dewing and Obermajer, 2009), or the Sverdrup Basin, which experienced magmatism in the Mesozoic (Embry 1991b). Long-distance (several hundred kilometres) transport of a diagenetic fluid is not uncommon (e.g., Lonnee and Machel, 2006; Haeri-Ardakani et al., 2013) and remains a possibility for the phases in this study.

4.6.2.1 Wynniatt Formation

Dolostone and dolomite cements

Three possible arguments can be made to explain the observed characteristics of dolostone and dolomite cements in the Wynniatt Formation: (i) the Wynniatt Formation limestone was deposited in a river-influenced marine environment and was later recrystallised under low fluid:rock conditions, (ii) dolomitisation occurred with a high fluid:rock, but subsequent hydrothermal phases precipitated under rock-dominated conditions, or (iii) hydrothermal fluids influenced by high fluid:rock recrystallised and overprinted the dolostone's characteristics.

Possibility 1: If the sedimentary depositional environment caused the REE pattern in the dolostone (LREE- and MREE-enrichment from continental weathering), then dolo-

mitisation and cement precipitation were in rock-dominated systems and inherited the precursor REE signature. The Wynniatt Formation was largely deposited in an intertidal environment (Thomson et al., 2014); therefore, production of reduced REE patterns or high Fe and Mn concentrations is not probable because the marine water was probably oxygenated.

Possibility 2: High fluid:rock during dolomitisation would reset the rock's $\delta^{18}O$ value and impose the REE pattern of the dolomitising fluid on the dolostone produced (Banner et al., 1988). The dolomitising fluid may have been reduced groundwater, which would account for its positive Ce anomaly. Mixing of the reduced groundwater with seawater could have diluted $\delta^{18}O$ and REE anomalies (La and Y) to values in between typical sea-water and shale values. This dolomitising fluid would have enriched the dolostone in Fe, Mn, Al, K, and Na from rock interactions along its flow path. The dolostone was then recrystallised under the influence of the succeeding hydrothermal fluid, and cements precipitated under low fluid:rock and retained the dolostone REE pattern. The observed decrease in Al, K, and Na from dolostone to successive cements (Fig. 4.9) could have been from progressive dilution of the dolostone formation water by the hydrothermal fluid. Typically, however, dolomitisation does not occur under sufficiently high fluid-rock ratios to alter precursor REE patterns (Banner et al., 1988; Qing and Mountjoy, 1994).

Possibility 3: Recrystallisation by hydrothermal fluids under high fluid-rock ratios would overprint the signatures of preceding phases. The REE signature and $\delta^{18}O$ values would then reflect the hydrothermal fluid. This interpretation could explain the similarities of $\delta^{18}O$ values and REE patterns between the dolostone and the two dolomite cements. This type of explanation was argued by Savard et al. (2000) to explain the isotopic

composition of the Polaris Zn-Pb deposit. A fluid in isotopic equilibrium with dolostone at the T_h of the saddle dolomite-precipitating fluid (~120°C; Mathieu et al., 2013a) yields similar $\delta^{18}O$ values to those of the $\delta^{18}O_{H2O}$ of SD, which could indicate recrystallisation by such a fluid. The progressive decrease in Al, K, and Na from the dolostone to the succeeding phases could have been from the initial mixing between the hydrothermal fluid and another fluid. Because possibility #3 is the simplest explanation, it is the preferred one.

Although evaporation can enrich the $\delta^{18}O_{H2O}$ value of a fluid by up to +6‰ (Lloyd, 1966; Ward and Halley, 1985), interaction with a sedimentary unit could also have resulted in isotopic exchange with similar isotopic enrichment. Interaction with a terrigenous clastic sedimentary rock was inferred by Mathieu et al. (2013a) for the origin of dissolved cations in the precipitating fluid for these cements (Table 4.3) and has also been used to explain the relatively heavy $\delta^{18}O$ in MVT brines in the Appalachians (Kesler et al., 1997) and dolomite from southern Ontario (Haeri-Ardakani et al., 2013). Interaction with siliciclastic units in the subsurface is also implied by the trace and REE. Enrichment of the LREE and MREE can result from interaction with appropriate sedimentary units (Leybourne et al., 2000; Nothdurft et al., 2004; Lawrence et al., 2006); for example, the observed MREE-enrichment suggests that the fluid interacted with a phosphatic and/or Fe-oxide unit (Leybourne et al., 2000; Hannigan and Sholkovitz, 2001; Haley et al., 2004; Köhler et al., 2005). Intermediate Y/Ho values between those of shale and seawater also suggest exchange with a shale unit (Nothdurft et al., 2004; Turner and Kamber, 2012). High Fe and Mn concentration are the result of reduced fluids interacting with rocks such as shale (Budd, 1997), and fit with this explanation. Homogenisation

temperatures for fluid inclusions in SD and BD indicate that the hydrothermal fluid came from intermediate to deep burial depths (Mathieu et al., 2013a). These depth regimes correspond to reduced fluids (Machel, 1999), which is also reflected in the Ce anomaly (Table 4.3). Positive Ce anomalies suggest accumulation of oxidized Ce when the reduced fluid was exposed to oxygenated fluid. Enrichment of Ce is observed in stratified marine water below the oxic-anoxic interface (De Baar et al., 1983) and where reduced groundwater seeps meet surface water (Lawrence et al., 2006). Such evidence could then suggest that recrystallisation and precipitation were not necessarily at depths that are reduced (greater than 1 km), but instead occurred at shallow burial depths (<1 km). In summary, the hydrothermal fluid possibly originated as seawater, thermally equilibrated at depths >1 km, and interacted with a (phosphatic and/or Fe-oxide-bearing) shale unit to incorporate heavy isotopes and trace and rare earth elements.

Concentration of Na in the carbonate lattice can be a function of salinity of the precipitating fluid (Veizer et al., 1978); therefore, the decrease in Na concentration from saddle (44.90 ppm) to BD (2.37 ppm) (Fig. 4.9) may be because of salinity differences of their respective fluids; the salinity for these two cements could not be determined because of metastability (Mathieu et al., 2013a). Saddle dolomite typically precipitates from high-salinity fluids (Davies and Smith, 2006), which could explain the greater Na concentration in SD lattice than in BD. It is possible that a decrease in salinity caused the change from SD to BD, whereas other parameters (i.e., T_h, $\delta^{18}O$, and REE) remained similar. Although the concentration of Na is greater in SD than in BD, the Na/K proportion is higher in BD precipitating fluid (Mathieu et al., 2013a). Dilution of a Na-rich fluid with a low Na/K by a relatively Na-poor fluid with a high Na/K would simultaneously reduce salin-

ity (and Na content) and increase the Na/K. The relatively consistent Fe and Mn concentrations as the Na-poor fluid becomes more dominant (Fig. 4.9) suggest that this fluid was the main source of these metals. The increase in ΣREEY and MREE-enrichment from dolostone to BD could also reflect the progressive dominance of the (relatively) Na-poor fluid in the fluid mixture. The aforementioned elemental trends would then suggest that the dominant (relatively) Na-poor fluid was the one that interacted with the phosphatic/Fe-oxide unit.

Calcite cements

Because RC and LC precipitated from the same fluid (section 4.6.1), the difference in REE signatures between RC and LC must be due to different fluid:rock ratios. The majority of RC cements have a positive Ce anomaly and a REE signature that is similar to that of the BD cement (Fig. 4.6). This similarity suggests that the precipitating fluid dissolved the BD cement under low fluid:rock conditions (Banner et al., 1988; Qing and Mountjoy, 1994) and that the RC cement inherited the BD's REE composition. The REE patterns of LC and some RC, conversely, are different from preceding cements and represent high a fluid:rock system (Banner et al., 1988; Qing and Mountjoy, 1994). The negative Ce anomaly present in the LC and some RC cements indicate that they were precipitated under oxygenated conditions. According to Machel (1999), oxygenated subsurface fluids occur at depths less than 600 m (surface to shallow burial depths). At these shallow depths, $\delta^{18}O_{H2O}$ values are <-18‰, which correspond to high-latitude meteoric water. In order to get such O isotopic values that corresponds to seawater, burial depth would have to exceed 5 km, but because this depth involves reduced subsurface fluids (deep burial

zone; Machel, 1999) such an environment would preclude an oxidised REE pattern, and so only a meteoric fluid can explain the light isotope values of the LC and RC. Given that hematite is associated with RC rather than LC (Fig. 4.3), the RC-precipitating fluid must have been oxidised during dedolomitisation of BD. The apparent change in the Ce anomaly of the RC may, therefore, represent a change in the fluid:rock from rock-dominated to fluid-dominated, rather than a change in the redox-state of the RC-precipitating fluid. The low concentration of Na, K, Fe and Mn, the observed REE patterns, O isotopes, Y/Ho, and low-salinity of the calcite-precipitating fluid (Mathieu et al., 2013a) in these samples are all features that are typical of oxygenated meteoric water (e.g., Nozaki et al., 1997; Nozaki et al., 2000) (Table 4.3).

In summary, the chemical nature of the diagenetic fluids that affected the Wynniatt Formation changed from shale-dominated during dolomite precipitation, to meteoric-dominant during later-stage calcite precipitation. The recrystallising and dolomite-precipitating fluids were reduced seawater that interacted with phosphatic/Fe-oxide siliciclastic rocks in a fluid-dominated system; this interaction reset the chemical signatures of the earlier carbonate phases. Replacive and late-stage calcite precipitated in a fluid-dominated system from an oxygenated meteoric-dominated fluid.

4.6.2.2 "Victoria Island formation"

Poor age and burial depth constraints on the dolomitisation of the precursor limestone result in isotopic evidence that points to a wide variety of possible fluid sources. The lack of a negative Ce anomaly for the "Victoria Island formation" dolostone indicates that it formed under reduced conditions. Therefore, burial of the parent limestone must have

been deeper than 1 km (at least the intermediate burial zone; Machel, 1999); however, the temperature range (10° to 43°C) required to produce seawater $\delta^{18}O$ values suggests near-surface to shallow burial conditions (i.e., oxic). Together, the REE and isotopic data implies that seawater was not a major component of the dolomitising/recrystallising fluid. Instead, the heavy $\delta^{18}O_{H2O}$ signature indicates that the fluid was in equilibrium with a sedimentary rock (possibly shale), which is also suggested by the flat, sub-parallel shale-normalised REE patterns; all of this is consistent with the fact that subsurface brines interacting with shale is common (e.g., Kesler et al., 1997; Leybourne et al., 2000; Lawrence et al., 2006; Haeri-Ardakani et al., 2013). The positive Eu anomalies displayed by the dolostone are typical of hydrothermal fluids and have been documented in modern vent fluids (e.g., Bao et al., 2008). Positive Eu anomalies in carbonate minerals, although of lower magnitude than for vent fluid, can also indicate interaction of groundwater with sulphide bodies, and have been suggested to be of use in exploration (Leybourne et al., 2000). Silicification has been shown to alter original carbonate REE patterns, especially the HREE (Tang et al., 2013) and probably had an effect on the "Victoria Island formation" dolostone. The fluid that silicified the dolostone may have been related to the hydrothermal quartz-precipitating fluid, which was probably sourced from seawater, and may have interacted with buried sulphide materials.

A fluid sourced from seawater was the main component in the quartz-precipitating fluid, as indicated by its $\delta^{18}O_{H2O}$values. Erratic, incomplete REE patterns of quartz cement (Fig. 4.13) may indicate a reduced hydrothermal fluid by the absence of Ce anomalies and some positive Eu anomalies, respectively. A zoned texture displayed by quartz cement (see Fig. 4.10), which is typical of hydrothermal precipitation (Dong et al., 1995),

would agree with the high temperature (~130°C) and salinity (23 wt. % NaCl equiv.) of this fluid (Table 4.3; Mathieu et al., 2013a). Mixing of at least two different fluids was responsible for the quartz precipitation: a sulphur-rich fluid and a metal-rich, sulfur-poor fluid. Mixing is inferred to have taken place because of the mixed Na-K ratio of the precipitating fluid (Table 4.3; Mathieu et al., 2013a), the presence of associated framboidal pyrite (see 6.2.3 Pyrite framboids discussion), and the slightly negative sulphur isotope values for these pyrite framboids. The hydrothermal, metal-rich, sulphur-poor quartz-precipitating fluid mobilised transition metals at depth and transported them up to mix with a reduced sulphur-rich fluid at the site of precipitation.

The two populations of REE patterns for dolomite cement are interesting, given the cements' petrographic similarity and co-spatial relationship (Fig. 4.14). Based on the temperature of formation of these cements (i.e., T_h = 109-124°C) the $\delta^{18}O$ data indicate precipitation from marine water. This value probably reflects both D1 and D2 cement because (1) marine fluid is the most common diagenetic fluid that affects carbonate rocks, (2) fluid inclusion temperatures and chemistries of both cements are the same (Mathieu et al., 2013a), and (3) even with fluid-rock ratios that are too low to change REE, oxygen isotopes can still retain the fluid's signature (Banner et al., 1988). The REE patterns differ from one crystal to the next, rather than gradually within individual crystals (Fig. 4.14), which suggests that the change in fluid chemistry was not a gradual shift from one fluid end-member to another. Similarities of REE patterns between "Victoria Island formation" dolostone and D1 cement suggest that D1 cement precipitated from a marine fluid under low fluid:rock, and that D1 probably predates D2; D2 cement, in contrast, was precipitated under higher fluid:rock conditions. The change from a rock-dominated

to a fluid-dominated system suggests a large fluid flux along the faults and fractures in the area (Fig. 4.2). Therefore, both D1 and D2 cements may have been precipitated by the same marine fluid, but with very different fluid:rock conditions. Alternatively, the flow path of the fluid may have been altered, such that the fluid interacted with different rock types but at similar depths, to account for their similar T_h values. The REE patterns of D2 cement indicate rock-interaction along its fluid's flow path. Reduction of Y/Ho and LREE- and MREE-enrichment relative to typical marine values may suggest interaction with a shale source (Nothdurft et al., 2004). The depletion of La and Eu may indicate the removal of these elements prior to precipitation, or the retention of these elements in the rocks along the flow path.

4.6.2.3 Pyrite framboid formation

Although framboidal pyrite is typically associated with bacterial sulphate reduction (BSR) (Ohmoto and Rye, 1979; Machel et al., 1995; Machel, 2001), bacterial influence is not required for its precipitation, as supported by experimental studies (see Ohfuji and Rickard, 2005 for review). Therefore, the presence of framboidal pyrite in this study does not conclusively indicate BSR processes, because the slightly negative (-5 to -10‰) $\delta^{34}S$ values of the pyrite may suggest kinetic fractionation from BSR or thermochemical sulphate reduction (TSR; Ohmoto and Rye, 1979; Machel et al., 1995). Both BSR and TSR have been used to explain the presence of reduced sulphur in the Polaris Zn-Pb deposit (Kerr, 1977; Savard et al., 2000; Reid et al., 2013), which suggests that both processes can be important a single deposit.

Fractionation via TSR can depart by up to approximately -20‰ from the parent fluid (Ohmoto and Rye, 1979; Machel et al., 1995), and results in negative $\delta^{34}S$ if the parent

fluid is isotopically light enough. In order to produce sulphides with $\delta^{34}S$ values in the range of -5 to -10‰ by TSR, several criteria must be met: (1) the seawater sulphate isotopic signature has to be low (approximately 10‰), (2) the maximum possible fractionation by TSR (-20‰) must have occurred, and (3) the sulphide must incorporate S only from the H_2S produced through TSR, with no mixing of another S source (unless that source is biogenic). During the Permian, the seawater sulphur isotope value reached a low of 10‰ (Veizer et al., 1999) suggesting that unusual seawater values may have been the source. However, the aforementioned conditions are specific and inflexible. Also, TSR fractionation decreases with increasing temperature (Ohmoto and Rye, 1979; Machel et al., 1995), and the reaction rate of TSR is too slow to form large volumes of reduced sulphur (Machel, 2001), as would be required to explain the abundance of early framboidal pyrite observed here. Therefore, TSR is less probable than BSR as a mechanism for sulphate reduction.

Alternatively, BSR can fractionate -45 +/- 20‰ from the initial fluid (Ohmoto and Rye, 1979; Machel et al., 1995). This greater fractionation reduces the limiting conditions imposed by TSR. Any seawater isotopic composition in the Phanerozoic could be fractionated to produce negative values, and mixing of sulphur sources can occur in variable proportions that would still yield slightly negative values. Inhomogeneous sulphur isotopes have also been attributed to pyrite precipitated by BSR (e.g., Riciputi et al., 1996), which makes BSR a more plausible interpretation. However, the temperature range for BSR is strictly limited to low (<80°C) values (Ohmoto and Rye, 1979; Machel et al., 1995; Machel, 2001). This temperature range conflicts with T_h (120°-130°C) obtained from the cogenetic quartz cement (Mathieu et al., 2013a). Because the T_h of FIAs (fluid

inclusion assemblages) in quartz exceeds the metabolic threshold temperature for sulphate reducing bacteria (SRB), the precipitating fluid was probably not reduced on site during precipitation. It is possible, however, that an unknown microbial species existed in the past that could metabolise at higher temperatures. Auld et al. (2013) and Auld (2014) demonstrate that "rare" species can be easily overlooked in microbial community analyses, implying that there is a possibility that there are some SRB that can metabolise at the high temperatures recorded by quartz FIAs. Although unknown microbes are hypothetically possible, the existence of such microbes is not very probable because it would require more than a 20°C increase from the current metabolic threshold of SRB (Jørgensen et al., 1991; Stetter et al., 1993). Instead, sulphate reduction probably predated fluid transport and precipitation. Either the sulphate was reduced at the site of precipitation prior to the introduction of a metal-(Fe) bearing fluid, or the reduced S was transported away from the location where BSR took place and mixed with a fluid that was rich in Fe. The decreasing abundance of pyrite framboids from initial quartz precipitation to later quartz growth indicates that either Fe and/or reduced S were exhausted. Extremophile organisms have been shown to revert to a state of dormancy when environmental conditions are not favourable and begin metabolising again when appropriate conditions return (Auld, 2014). If sulphate was reduced at the site prior to the influx of metalliferous hydrothermal fluid, the increased temperature would halt the metabolising process (because the temperature would be too great) and stop the production of reduced sulphur; whatever reduced sulphur was present would precipitate pyrite framboids until the S concentration became insufficient. When the temperature returned to normal between fluid pulses, BSR would have continued, replenishing the reduced S. Conversely, if sulphate

was reduced off-site and transported to meet with a static volume of metalliferous fluid, iron would be exhausted owing to the precipitation of pyrite framboids. Because the quartz-precipitating fluid was metal-saturated (Mathieu et al., 2013a), reduced sulphide could not have been transported to the precipitation location with that fluid. Metal transport capabilities of sulphide fluids are insufficient to be metal-saturated (Anderson, 1975); therefore, sulphide must have been reduced at the site of pyrite precipitation.

In summary, the formation of framboidal pyrite was probably the result of hot metal-bearing fluid interacting with a cooler, reduced, sulphur-bearing fluid. Sulphur was reduced on-site by BSR and was temporarily halted when a flux of metal-bearing fluid increased the temperature to beyond the metabolic threshold of SRB, but recommenced when the temperature returned to "normal". Sulphur was the limiting reactant, as indicated by the initial abundance of pyrite which was succeeded by later sparse pyrite formation during continued growth of quartz.

Oxidation of pyrite framboids to "hematite framboids" has been documented from the Negaunee Iron formation in Michigan by Lougheed and Mancuso, (1973). By subjecting pyrite framboids to high (650°C) temperatures for several hours Lougheed and Mancuso (1973) were able to oxidize the pyrite to hematite, thereby determining that the hematite is indeed pseudomorphed after pyrite framboids. The hematite framboids in this study are, like those of Lougheed and Mancuso (1973), pseudomorphs of framboidal pyrite, which indicates that redox conditions changed from initially reducing to oxic.

4.6.3 Implications for economic potential

Mineralisation on Victoria Island, in the area near Minto Inlet, is indicated by anomalous concentrations of Zn and Pb sulphides in stream sediment samples (McCurdy et al., 2013), and merits further investigation. Using the Polaris Zn-Pb deposit as a guide to Zn-Pb exploration in the Arctic (Dewing et al., 2007b; Reid et al., 2013), features from both study sites on Victoria Island are compared with the Polaris deposit.

The Wynniatt Formation shares structural, paragenetic, and geochemical similarities with the Polaris deposit, with the exception that mineralisation is conspicuous in the latter. Fluid-focussing faults are considered to be one of the controls on mineralisation in the Cornwallis Zn-Pb district (e.g., Kerr, 1977; Turner and Dewing, 2004; Dewing et al., 2007b; Jober et al., 2007). The Wynniatt Formation sample site is close to faults that could have focussed fluids from the same (or similar) fluid-flow event as that responsible for the Cornwallis Zn-Pb district. Enhanced porosity associated with the Wynniatt Formation karst surface, which was a controlling factor in the case of the Pine Point deposit of northwestern Canada (Rhodes et al., 1984), may have been favourable for mineralisation. Both the Polaris deposit and the Wynniatt Formation site have dolostone that formed due to recrystallisation mediated by a hydrothermal fluid that also precipitated saddle dolomite (mineralisation is directly associated with this phase at Polaris). Oxygen isotopes for saddle dolomite suggest that, in the case of the Polaris deposit, the metal-bearing fluids interacted at depth with a sedimentary reservoir (Savard et al., 2000), and the same is indicated for the dolomite in the Wynniatt Formation. Although the salinity of Wynniatt Formation dolomitising fluid could not be quantified (Mathieu et al., 2013a), the fluid does have a similar T_h to the high-salinity fluid responsible for mineralisation at the Polaris deposit (Savard et al., 2000). Although not associated with mineralisation, the

meteoric fluid responsible for precipitation of paragenetically later calcite is present in both locations. The main difference between the two settings is, however, the lack of a suitable, impermeable shale cover (i.e., aquitard) overlying the Wynniatt Formation. Depending on the mineralisation model, the presence of an organic-rich host rock that acted as a reducing agent for the metal-sulphate fluids by TSR (in-situ model; Reid et al., 2013), like the Thumb Mountain Formation at the Polaris deposit, is absent in the Wynniatt Formation. The mixed model of Kerr (1977) and Savard et al. (2000) does not require in-situ reduction.

Tectonically driven fluid movement could have been initiated from any of the orogenic events that took place in the Arctic archipelago (section 4.2.2 - Tectonic framework), but the Ellesmerian Orogeny, which is associated with fluid movement for the Cornwallis Zn-Pb district (Kerr, 1977; Savard et al., 2000; Dewing et al., 2007b), is the most obvious among these candidates for fluid-flow on Victoria Island. Alternatively, thermal anomalies associated with rifting (Banks Island or Sverdrup Basin) could have been the fluid-driving mechanism; such a driving mechanism was used to explain hydrothermal fluid movement in the Michigan Basin (Haeri-ardakani et al., 2013). A high temperature flux from the meteorite impact in northwestern Victoria Island (Dewing et al., 2013) is another possible cause for localised fluid movement.

Similarities between the Wynniatt Formation and the Polaris deposit's fluid suggest that a mineralising fluid may also have been present on Victoria Island. Although the Wynniatt Formation is not stratigraphically favourable for deposition of sulphides from metalliferous fluids owing to the lack of an overlying aquitard, the fluid may have found appropriate mineralisation conditions in other stratigraphic units in the vicinity. "Victoria

Island formation" quartz cement was precipitated from a metal-rich hydrothermal fluid that probably moved through nearby faults and mixed with a reduced sulphur fluid. This combination is similar to the mixed model for Polaris mineralisation (e.g., Kerr, 1977; Savard et al., 2000) and could have produced mineralisation if a trapping site were available. The geochemistry of the dolomite cements indicates interaction with subsurface sedimentary units, and possibly even with sulphide ore bodies (positive Eu anomalies, and slightly increased Pb content). In addition, the high fluid:rock recorded in the D2 cement is favourable for mineralising potential.

4.7 CONCLUSIONS

Diagenetic cements examined in detail from two locations on Victoria Island record geochemical attributes, based on in situ microanalysis of isotopes ($\delta^{18}O$, $\delta^{34}S$) and trace elements, including REE, that reflect their fluid history. The Wynniatt Formation dolostone and dolomite cements record infiltration of a hydrothermal fluid that transported metals from a subsurface siliciclastic unit and mixed with a high-salinity fluid, whereas later calcite cements record influx of meteoric fluid that replaced dolomite with calcite (dedolomitisation). The similarities of the Wynniatt Formation diagenetic fluids to those of the Polaris Zn-Pb deposit suggest some potential for base-metal mineralisation in the area. The "Victoria Island formation" dolostone and cements, including early quartz and later dolomite, indicate a relatively complex fluid history that commenced with possible hydrothermal fluids that may have silicified the host dolostone. Subsequently, a quartz-precipitating fluid that interacted with a sedimentary source (shale) at depth mixed with a

reduced-sulphur-bearing fluid at higher levels to precipitate cogenetic quartz and framboidal pyrite. Sulphur isotopes indicate that BSR occurred near the site of sulphide precipitation. The later dolomite cements (D1 and D2) record a change from an initial rock-dominated system to a fluid-dominated system. The occurrence of a metal-rich fluid responsible for quartz precipitation and a fluid-dominated system for the late dolomite indicate the potential for base-metal mineralisation in this unit on Victoria Island.

ACKNOWLEDGEMENTS

Field work was funded by the Geological Survey of Canada's Geomapping for Energy and Minerals (GEM) Victoria Island project. Laser ablation work was done and processed by Joe Petrus at Laurentian University, Sudbury, Ontario using facilities established with a CFI grant to the Department of Earth Sciences. The in situ oxygen and sulphur isotope work was done at the University of Manitoba, Winnipeg, and Memorial University, St. John's, respectively, where the facilities are supported by funding to M. Fayek and G. Layne. Craig Stewart is thanked for assistance and analysis of the samples for oxygen isotopes.

REFERENCES

Adams, J.J., Rostron, B.J., Mendoza, C.A., 2000. Evidence for two-fluid mixing at Pine Point, NWT. Journal of Geochemical Exploration 69-70, 103-108.

Al-Hashimi, W.S., Hemingway, J.E., 1973. Recent dedolomitization and the origin of the rusty crusts of Northumberland. Journal of Sedimentary Petrology 43, 82-91.

Alibo, D.S., Nozaki, Y., 1999. Rare earth elements in seawater: Particle association, shale-normalization, and Ce oxidation. Geochimica et Cosmochimica Acta, 63(3/4), 363-372.

Allen, A.A., Allen, J.R., 2005. Basin analysis: Principles and applications. Blackwell Publishing. 549 pp.

Anderson, G.M., 1975. Precipitation of Mississippi Valley-type ores. Economic Geology, 70, 937-942.

Auld, R.R., 2014. Examining temporal and seasonal microbial acid mine drainage community variation. Unpublished M.Sc. thesis Laurentian University, Sudbury, Ontario, 101 p.

Auld, R.R., Myre, M., Mykytczuk, N.C., Leduc, L.G., Merritt, T.J., 2013. Characterization of the Microbial Acid Mine Drainage Microbial Community Using Culturing and Direct Sequencing Techniques. Journal of Microbiolical Techniques, 93(2), 108-115.

Azmy, K., Brand, U., Sylvester, P., Gleeson, S.A., Logan, A., Bitner, M.A., 2011. Biogenic and abiogenic low-Mg calcite (bLMC and aLMC): Evaluation of seawater-REE composition, water masses and carbonate diagenesis. Chemical Geology 280, 180-190.

Bao, S., Zhou, H., Peng, X., Ji, F., Yao, H., 2008. Geochemistry of REE and yttrium in hydrothermal fluids from the Endeavour segment, Juan de Fuca Ridge. Geochem. J. 42, 359-370.

Banner, J.L., Hanson, G.N., Meyers, W.J., 1988. Rare earth element and Nd isotopic variations in regionally extensive dolomites from the Burlington-Keokuk Formation (Mississippian): Implications for REE mobility during carbonate diagenesis. J. Sed. Pet. 58, 415-432.

Bau, M., Möller, P., Dulski, P., 1997. Yttrium and lanthanides in eastern Mediterranean seawater and their fractionation during redox cycling. Marine Chemistry, 56, 123-131.

Bau, M., Romer, R.L., Luders, V., Dulski, P., 2003. Tracing element sources of hydrothermal mineral deposits: REE and Y distribution and Sr-Nd-Pb isoptopes in fluorite from MVT deposits in the Pennine Orefield, England. Mineralium Deposita 38, 992-1008.

Budd, D.A., 1997. Cenozoic dolomites of carbonate islands: their attributes and origin. Earth-Science Reviews 42, 1-47.

Chen, Z., Osadetz, K.G., Embry, A.F., Gao, H., Hannigan, P.K., 2000. Petroleum potential in western Sverdrup Basin, Canadian Arctic Archipelago. Bulletin of Canadian Petroleum Geology 48, 323-338.

Dansgaard, W., 1964. Stable isotopes in precipitation. Tellus, 16(4), 436-468.

Davies, G.R., Nassichuk, W.W., 1991. Carboniferous and Permian history of the Sverdrup Basin, Arctic Islands, In: Trettin, H.P. (Ed.), Geology of the Innuitian Orogen and Arctic Platform of Canada and Greenland, Geological Survey of Canada, Geology of Canada 3, pp 345-368.

Davies, G.R., Smith, L.B., 2006. Structurally controlled hydrothermal dolomite reservoir facies: An overview. American Association of Petroleum Geologists 90, 1641-1690.

De Baar, H.J.W., Bacon, M.P., Brewer, P.G., 1983. Rare-earth distributions with a positive Ce anomaly in the Western North Atlantic Ocean. Nature 301, 324-327.

Dewing, K., Obermajer, M., 2009. Lower Paleozoic thermal maturity and hydrocarbon potential of the Canadian Arctic Archipelago. Bulletin of Canadian Petroleum Geology 57, 141-166.

Dewing, K., Turner, E., Harrison, J.C., 2007a. Geological history, mineral occurrences, and mineral potential of the sedimentary rocks of the Canadian Arctic archipelago, In: Goodfellow, W.D. (Ed.) Mineral Deposits of Canada: A synthesis of Major deposit-types, district metallogeny, the evolution of geological provinces, and exploration methods. Geological Association of Canada, Mineral Deposits division, Special publication 5, pp. 733-753.

Dewing, K., Sharp, R.J., Turner, E., 2007b. Synopsis of the Polaris Zn-Pb district, Canadian Arctic Islands, Nunavut, In: Goodfellow, W.D. (Ed.) Mineral Deposits of Canada: A synthesis of Major deposit-types, district metallogeny, the evolution of geological provinces, and exploration methods. Geological Association of Canada, Mineral Deposits division, Special publication 5, pp. 655-672.

Dewing K, Pratt BR, Hadlari T, Brent T, Bedard J, Rainbird RH (2013) Newly identified "Tunnunik" impact structure, Prince Albert Peninsula, northwestern Victoria Island, Arctic Canada. Meteorics and Planetary Sciences, 48, 211-223.

Dolnicek, Z., Kropac, K., Janickova, K., Urubek, T., 2012. Diagenetic source of fluids causing the hydrothermal alteration of teschenites in the Silesian Unit, Outer Western Carpathians, Czech Repupublic: Petroleum-bearing vein mineralization from the Stribrnik site. Marine and Petroleum Geology 37, 27-40.

Dong, G., Morrison, G., Jaireth, S., 1995. Quartz textures in epithermal veins, Queensland – classification, origin, and implication. Economic Geology, 90, 1841-1856.

Elderfield, H., 1988. The oceanic chemistry of the rare-earth elements. Philosophical Transactions of the Royal Society of London A 325, 105-126.

Elderfield, H., Greaves, M.J., 1982. The rare earth elements in seawater. Nature 296, 214-219.

Embry, A.F., 1991a. Middle-Upper Devonian clastic wedge of the Arctic Islands, In: Trettin, H.P. (Ed.), Geology of the Innuitian Orogen and Arctic Platform of Canada and Greenland, Geological Survey of Canada, Geology of Canada 3, pp. 261-291.

Embry, A.F., 1991b. Mesozoic history of the Arctic Islands, In: Trettin, H.P. (Ed.), Geology of the Innuitian Orogen and Arctic Platform of Canada and Greenland, Geological Survey of Canada, Geology of Canada 3, pp. 369-433.

Embry, A.F., Dixon, J., 1992. The breakup unconformity of the Amerasia Basin, Arctic Ocean: Evidence from Arctic Canada. Geological Society of America Bulletin 102, 1526-1534.

Forsyth, D.A., Mair, J.A., Fraser, I., 1979. Crustal structure of the central Sverdrup Basin. Canadian Journal of Earth Science, 16, 1581-1598.

Gabitov, R.I., Watson, E.B., Sadekov, A., 2012. Oxygen isotope fractionation between calcite and fluid as a function of growth rate and temperature: An in situ study. Chemcal Geology, 306-307, 92-102.

German, C.R., Masuzawa, T., Greaves, M.J., Elderfield, H., Edmond, J.M., 1995. Dissolved rare earth elements in the Southern Ocean: Cerium oxidation and the influence of hydrography. Geochimica et Cosmochimica Acta 59, 1551-1558.

Graf, J.L., 1984. Effects of Mississippi Valley-type mineralization on REE patterns of carbonate rocks and minerals, Viburnum Trend, southeast Missouri. Journal of Geology, 92, 307-324.

Haeri-Ardakani, O., Al-Aasm, I., Coniglio, M., 2013. Fracture mineralization and fluid flow evolution: an example from Ordovician-Devonian carbonates, southwestern Ontario, Canada. Geofluids, 13, 1-20.

Haley, B.A., Klinkhammer, G.P., McManus, J., 2004. Rare earth elements in pore waters of marine sediments. Geochimica et Cosmochimica Acta, 68(6), 1265-1279.

Hannigan, R.E. and Sholkovitz, R.E., 2001. The development of middle rare earth element enrichments in freshwaters: weathering of phosphate minerals. Chemical Geology, 175, 495-508.

Harrison, J.C., Ford, A., Miall, A.D., Rainbird, R.H., Hulbert, L.J., Christie, R.L., Cambell, F.H.A., 2013. Geology, Tectonic assemblage map of Aulavik, Banks Island and northwestern Victoria Island, Northwest Territories. Geological Survey of Canada Canadian Geoscince Map 35 (preliminary), scale 1:500 000.

Heaman, L.M., Lecheminant, A.N., Rainbird, R.H., 1992. Nature and timing of Franklin igneous events, Canada: implications for a late Proterozoic mantle plume and the break-up of Laurentia. Earth and Planetary Science Letters, 109, 117-131.

Hynes, A., Rivers, T., 2010. Protracted continental collision – evidence from the Grenville Orogen. Canadian Journal of Earth Sciences, 47, 591-620.

Jober, S., Dewing, K., White, J.C., 2007. Structural geology and Zn-Pb mineral occurrences of northeastern Cornwallis Island: implications for exploration of the Cornwallis Fold Belt, northern Nunavut. Bulletin of Canadian Petroleum Geology 55, 138-159.

Johannesson, K.H., Lyons, W.B., Yelken, M.A., Gaudette, H.E., Stetzenbach, K.J., 1996. Geochemistry of the rare-earth elements in hypersaline and dilute acidic natural terres-

trial waters: Complexation behavior and middle rare-earth element enrichments. Chemical Geology, 133, 125-144.

Jørgensen, B.B., Isaksen, M.F., Jannasch, H.W., 1992. Bacterial sulphate reduction above 100°C in deep-sea hydrothermal vent sediments. Science, 258, 1756-1757.

Kamber, B.S., Webb, G.E., 2001. The geochemistry of late Archaean microbial carbonate: Implications for ocean chemistry and continental erosion history. Geochimica et Cosmochimica Acta 65, 2509-2525.

Kawabe, I., Toriumi, T., Ohta, A., Miura, N., 1998. Monoisotopic REE abundances in seawater and the origin of seawater tetrad effect. Geochem. J. 32, 213-229.

Kerr, J.M., 1967. Nares submarine rift valley and the relative rotation of North Greenland. Bulletin of Canadian Petroleum Geology 15, 483-520.

Kerr, J.M., 1977. Cornwallis Lead-Zinc District; Mississippi Valley-type deposits controlled by stratigraphy and tectonics. Canadian Journal of Earth Science 14, 1402-1426.

Kesler, S.E., Vennemann, T.W., Frederickson, C., Breithaupt, A., 1997. Hydrogen and oxygen isotope evidence for origin of MVT-forming brines, southern Appalachians. Geochimica et Cosmochimica Acta, 61(7), 1513-1523.

Köhler, S.J., Harouiya, N., Chaïrat, C., Oelkers, E.H., 2005. Experimental studies of REE fractionation during water-mineral interactions: REE release rates during apatite dissolution from pH 2.8 to 9.2. Chemical Geology, 222, 168-182.

Kontak, D.J., Jackson, S., 1995. Documentation of variable trace- and rare-earth-element abundances in carbonates from auriferous quartz veins in Meguma Lode-gold deposits, Nova Scotia. The Canadian Mineralogist, 37, 469-488.

Kucha, H., Schroll, E., Raith, J.G., Halas, S., 2010. Microbial sphalerite formation in carbonate-hosted Zn-Pb ores, Bleiberg, Austria: micro- to nanotextural and sulfur isotope evidence. Economic Geology, 105, 1005-1023.

Land, L.S., 1973. Holocene meteoric dolomitisation of Pleistocene limestone, North Jamaica. Sedimentology, 20(3), 411-424.

Land, L.S., 1985. The origin of massive dolomite. Journal of Geological Education, 33, 112– 125.

Lawrence, M.G., Greig, A., Collerson, K.D., Kamber, B.S., 2006. Rare earth element and yttrium variability in South East Queensland waterways. Aquatic Geochemistry, 12, 39-72.

Leach, D.L., Sangster, D.F., Kelley, K.D., Large, R.R., Garven, G., Allen, C.R., Gutzmer, J., Walters, S., 2005. Sediment-hosted lead-zinc deposits; a global perspective. In: Hedenquist, J.W., Thompson, J.F.H., Goldfarb, R.J., Richards, J.P. (eds.) Economic Geology: One hundredth Anniversary, vol. 1905-2005, pp. 561-607.

Leybourne, M.I., Goodfellow, W.D., Boyle, D.R., Gwendy, M.H., 2000. Rapid development of negative Ce anomalies in surface waters and contrasting REE patterns in groundwaters associated with Zn-Pb massive sulphide deposits. Applied Geochemistry, 15, 695-723.

Leybourne, M.I. and Johannesson, 2008. Rare earth elements (REE) and yttrium in stream waters, stream sediments, and Fe-Mn oxyhydroxides: Fractionation, speciation, and controls over REE=Y patterns in the surface environment. Geochimica et Cosmochimica Acta, 72, 5962-5983.

Li, Z.X., Bogdanova, S.V., Collins, A.S., Davidson, A., De Waele, B., Ernst, R.E.,

Fitzsimons, I.C.W., Fuck, R.A., Gladkochub, D.P., Jacobs, J., Karlstrom, K.E., Lu, S., Natapov, L.M., Pease, V., Pisarevsky, S.A., Thrane, K., Vernikovsky, V., 2008. Assembly, configuration, and break-up history of Rodinia: A synthesis. Precambrian Research, 160, 179-210.

Lloyd, R.M., 1966. Oxygen isotope enrichment of sea water by evaporation. Geochimica et Cosmochimica Acta, 30(8), 801-814.

Long, D.G.F., Rainbird, R.H., Turner, E.C., MacNaughton, R.B., 2008. Early Neoproterozoic strata (Sequence B) of mainland northern Canada and Victoria and Banks islands: a contribution to the Geological Atlas of the Northern Canadian Mainland Sedimentary Basin. Geological Survey of Canada, Open File 5700 27p.

Lonnee, J., Machel, H.G., 2006. Pervasive dolomitisation with subsequent hydrothermal alteration in the Clarke Lake gas field, Middle Devonian Slave Point Formation, British Columbia, Canada. AAPG Bulletin, 90(11), 1739-1761.

Lougheed, M.S., Mancuso, J.J., 1973. Hematite framboids in the Negaunee iron formation, Michigan: evidence for the biogenic origin. Economic Geology, 68, 202-209.

Machel, H.G., 1999. Effects of groundwater flow on mineral diagenesis, with emphasis on carbonate aquifers. Hydrogeology Journal 7, 94-107.

Machel, H.G., 2001. Bacterial and thermochemical sulfate reduction in diagenetic settings – old and new insights. Sedimentary Geology, 140, 143-175.

Machel, H.G., Krouse, H.R., Sassen, R., 1995. Products and distinguishing criteria of bacterial and thermochemical sulfate reduction. Applied Geochemistry, 10, 373-389.

Mathieu, J., Turner, E.C., Rainbird, R.H., 2013a. Sedimentary architecture of a deeply karsted Precambrian-Cambrian unconformity, Victoria Island, Northwest Territories. Geological Survey of Canada Current Research 2013-1, 1-15.

Mathieu, J., Kontak, D.J., Turner, E.C., 2013b. A fluid inclusion study of diagenetic fluids in Proterozoic and Paleozoic carbonate rocks, Victoria Island, NWT. Geolfuids, 13(4), 559-578.

McCurdy, M., Rainbird, R., McNeil, R., 2013. Exploring for lead and zinc using indicator minerals with stream silt and water geochemistry in the Canadian Arctic islands: and example from Victoria Island, Northwest Territories, In: Paulen, R.C., McClenaghan, M.B. (Eds.) New frontiers for exploration in glaciated terrain, Geological Survey of Canada Open File 7374, 65-70.

McDonnough, W.F., Sun, S., 1995. The composition of the Earth. Chemical Geology, 120, 223-253.

Miall, A.D., 1976. Devonian geology of Banks Isalnd, Arctic Canada, and its bearing on the tectonic development of the circum-Arctic region. Geological Society of America Bulletin, 87, 1599-1608.

Miall A.D., 1979 Mesozoic and Tertiary geology of Banks Island, Arctic Canada, the history of an unstable craton margin. GSC Memoir 387, 235 p.

Miall, A.D., 1986. Effects of Caledonian tectonism in Arctic Canada. Geology, 14, 904-907.

Miall, A.D., 1991. Late Cretaceous and Tertiary basin development and sedimentation, Arctic islands, In: Trettin, H.P. (Ed.), Geology of the Innuitian Orogen and Arctic

Platform of Canada and Greenland, Geological Survey of Canada, Geology of Canada 3, pp 437-458.

Möller, P., Dulski, P., Morteani, G., 2003. Partitioning of rare earth elements, yttrium, and some major elements among source rocks, liquid and vapour of Larderello-Travale Geothermal Field, Tuscany (Central Italy). Geochimica et Cosmochimica Acta, 67(2), 171-183.

Morris, G.A., Page, L., Martinez, V., 2005. New dates (415 Ma) for the Etive Dyke Swarm and the end of the Caledonian Orogeny in the SW Grampian Highlands of Scotland. Journal of the Geological Society of London, 162, 741-744.

Morrow, D.W. 1990. Dolomitization models and ancient dolostones, In: Morrow, D.W. (Ed.), Diagenesis, Geological Association of Canada publications, pp. 125-140.

Nothdurft, L.D., Webb, G.E., Kamber, B.S., 2004. Rare earth element geochemistry of Late Devonian reefal carbonates, Canning Basin, Western Australie: Confirmation of a seawater REE proxy in ancient limestones. Geochimica et Cosmochimica Acta, 68, 263-283.

Nozaki, Y., Zhang, J., Amakawa, H., 1997. The fractionation between Y and Ho in the marine environment. Earth and Planetary Science Letters, 148, 329-340.

Nozaki, Y., Lerche, D., Alibo, D.S., Snidvongs, A., 2000. The estuarine geochemistry of rare earth elements and indium in the Chao Phraya River, Thailand. Geochimica et Cosmochimica Acta, 64(23) 3983-3994.

Oakley, G.N., Stephenson, R., 2008. Crustal structure of the Innuitian region of Arctic Canada and Greenland from gravity modelling: implications for the Paleogene Eurekan Orogen. Geophysics Journal International, 173, 1039-1063.

Obermajer, M., Dewing, K., Fowler, M.G., 2010. Geochemistry of crude oil from Bent Horn field (Canadian Arctic Archipelago) and its possible Paleozoic origin. Organic Geochemistry 41, 986-996.

Ohfuji, H., Rickard, D., 2005. Experimental synthesis of framboids – a review. Earth Science Reviews, 71, 147-170.

Ohmoto, H., Rye, R.O., 1979. Isotopes of sulfur and carbon, in Barnes, H.L., editor, Geochemistry of Hydrothermal Ore Deposits, 2nd edition, New York, USA, Wiley, p. 509-567.

Okulitch, A.V., Trettin, H.P., 1991. Late Cretaceous – Early Tertiary deformation, Arctic Islands, In: Trettin, H.P. (Ed.), Geology of the Innuitian Orogen and Arctic Platform of Canada and Greenland, Geological Survey of Canada, Geology of Canada 3, pp. 469-490.

Okulitch, A.V., Packard, J.J., Zolnai, A.I., 1991. Late Silurian - Early Devonian deformation of the Boothia Uplift, In: Trettin, H.P. (Ed.), Geology of the Innuitian Orogen and Arctic Platform of Canada and Greenland, Geological Survey of Canada, Geology of Canada 3, pp. 302-307.

Oliver, G.J.H., 2001. Reconstruction of the Grampian episode in Scotland: its place in the Caledonian Orogeny. Tectonophysics, 332, 23-49.

O'Neil, J.R., Clayton, R.N., Mayeda, T.K., 1969. Oxygen isotope fractionation in divalent metal carbonates. Journal of Chemical Physics, 51, 5547-5558.

Pourmand, A., Dauphas, N., Ireland, T.J., 2012. A novel extraction chromatography and MC-ICP-MS technique for rapid analysis of REE, Sc and Y: Revising Cl-chondrite

and Post-Archean Australian Shale (PAAS) abundances. Chemical Geology 291, 38-54.

Qing, H., Mountjoy, E.W., 1994. Rare earth element geochemistry of dolomites in the Middle Devonian Presqu'ile barrier, Western Canada Sedimentary Basin: implications for fluid-rock ratios during dolomitisation. Sedimentology, 41, 787-804.

Qing, H., 1998. Petrography and geochemistry of early-stage, fine- and medium-crystalline dolomites in the Middle Devonian Presqu'ile Barrier at Pine Point, Canada. Sedimentology 45, 433-446.

Qu, Ch., Liu, G., Zhao, Y., 2009. Experimental study on the fractionation of yttrium from holmium during the coprecipitation with calcium carbonates in seawater solutions. Geochemical Journal 43, 403-414.

Rainbird, R.H., 1991. Stratigraphy, sedimentology, and tectonic setting of the upper Shaler Group, Victoria Island, Northwest Territories; Unpublished Ph.D. Thesis, University of Western Ontario, London, Ontario.

Rainbird, R.H., Bedard, J.H., Dewing, K., Hadlari, T., in press. Geology, Minto Inlet, Victoria Island, Northwest Territories. Geological Survey of Canada, Geoscince Map 82 (preliminary) 1:50 000.

Rainbird, R.H., Jefferson, C.W., Hildebrand, R.S., Worth, J.K. 1994. The Shaler Supergroup and revision of Neoproterozoic stratigraphy in Amundsen Basin, Northwest Territories; in Current Research, Part C; Geological Survey of Canada, Paper 94-01C, 61-70.

Rainbird, R.H., Jefferson, C.W., Young, G.M., 1996. The early Neoproterozoic sedimentary Succession B of northwestern Laurentian: Correlations and paleogeographic significance. GSA Bulletin, 108 (4), 454-470.

Rainbird, R.H., McNicoll, V.J., Thériault, R.J., Heaman, L.M., Abbott, J.G., Long, D.G.F., Thorkelson, D.J., 1997a. Pan-continental river system draining Grenville Orogen recorded by U-Pb and Sm-Nd Geochronology of Neoproterozoic Quartzarenites and mudrocks, northwestern Canada. The Journal of Geology, 105, 1-17.

Rainbird, R.H., LeCheminant, A.N., Lawyer, I., 1997b. Geology, Duke of York Inlier, Victoria Island, Northwest Territories (part of NTS 77B), Geological Survey of Canada Open-file 3304, scale 1:100000.

Rayner, N.M., Rainbird, R.H., 2013. U—Pb Geochronology of the Shaler Supergroup, Victoria Island, northwest Canada: 2009-2013. Geological Survey of Canada Open-file 7419, 59 p.

Reid, S., Dewing, K., Sharp, R., 2013. Polaris as a guide to northern exploration: Ore textures, paragenesis and the origin of the carbonate-hosted Polaris Zn-Pb Mine, Nunavut, Canada. Ore Geology Reviews, 51, 27-42.

Rhodes, D., Lantos, E.A., Lantos, J.A., Webb, R.J., Owens, D.C., 1984. Pine Point orebodies and their relationship to the stratigraphy, structure, dolomitisation, and karstification of the Middle Devonian Barrier Complex. Economic Geology, 79, 991-1055.

Riciputi, L.R., Cole, D.R., Machel, H.G., 1996. Sulfide formation in reservoir carbonates of the Devonian Nisku Formation, Alberta, Canada: An ion microprobe study. Geochimica et Cosmochimica Acta, 60(2), 325-336.

Savard, M.M., Kontak, D.J., 1998. $\delta^{13}C$-$\delta^{18}O$-$^{87}Sr/^{86}Sr$ covariations in ore-stage calcite at and around the Gays River Zn-Pb deposit (Nova Scotia, Canada) – evidence for fluid mixing. Economic Geology, 93, 818-833.

Savard, M.M., Chi, G., Sami, T., Williams-Jones, A.E., Leigh, K., 2000. Fluid inclusion and carbon, oxygen, and strontium isotope study of the Polaris Mississippi Valley-type Zn-Pb deposit, Canadian Arctic Archipelago: implications for ore genesis. Mineralium Deposita 35, 495-510.

Sharp, Z.D., Kirschner, D.L., 1994. Quartz-calite oxygen isotope thermometry: a calibration based on natural isotopic variations. Geochimica et Cosmochimica Acta, 58, 4491-4501.

Shotyk, W., Metson, J.B., 1994. Secondary ion mass spectrometry (SIMS) and its application to chemical weathering. Reviews of Geophysics 32, 197-220.

Staude, S., Mordhorst, T., Nau, S., Pfaff, K., Brugmann, G., Jacob, D.E., Markl, G., 2012. Hydrothermal carbonates of the Schwarzwald ore district, southern Germany: Carbon source and conditions of formation using $\delta^{18}O$, $\delta^{13}C$, $^{87}Sr/^{86}Sr$, and fluid inclusions. The Canadian Mineralogist 50, 1401-1434.

Stetter, K.O., Huber, R., Blöchl, E., Kurr, M., Eden, R.D., Fielder, M., Cash, H., Vance, I., 1993. Hyperthermophilic archaea are thriving in deep North Sea and Alaskan oil reservoirs. Nature, 365, 743-745.

Tanaka K., Kawabe, I., 2006. REE abundances in ancient seawater inferred from marine limestone and experimental REE partition coefficients between calcite and aqueous solution. Geochemical Journal 40, 425-435.

Tang, H., Chen, Y., Santosh, M., Zhong, Hong, Yang, T., 2013. REE geochemistry of carbonates from the Guanmenshan Formation, Liaohe Group, NE Sino-Korean Craton: implications for seawater compositional change during the Great Oxidation Event. Precambrian Research, 227, 316-336.

Tegner, C., Storey, M., Holm, P.M., Thorarinsson, S.B., Zhao, X., Lo, C.H., Knudsen, M.F., 2011. Magmatism and Eurekan deformation in the High Arctic large igneous province: 40Ar-39Ar age of Kap Washington Group volcanic, North Greenland. Earth and Planetary Science Letters, 303, 203-214.

Thomson, D., Rainbird, R.H., Dix, D., 2014. Architecture of a Neoproterozoic (Cryogenian) intracratonic carbonate ramp (Wynniatt Formation, Shaler Supergroup) in an immense intracratonic basin: ancestral patterns for Paleozoic platforms. Sedimentary Geology, 299, 119-138.

Thorsteinsson, R., Tozer, E.T., 1962. Banks, Victoria, and Stefansson Islands, Arctic archipelago. Geological Survey of Canada Memoir 330, 85 p.

Tlig, S., M'Rabet, A., 1985. A comparative study of the rare earth element (REE) distributions within the Lower Cretaceous dolomites and limestones of Central Tunisia. Sedimentology 32, 897-907.

Trettin, H.P., 1991. Middle and Late Tertiary tectonic and physiographic developments, In: Trettin, H.P. (Ed.), Geology of the Innuitian Orogen and Arctic Platform of Canada and Greenland, Geological Survey of Canada, Geology of Canada 3, pp 493-496.

Trettin, H.P., Mayr, U., Long, D.G.F., Packard, J.J., 1991. Cambrian to Early Devonian basin development, sedimentation and volcanism, In: Trettin, H.P. (Ed.), Geology of

the Innuitian Orogen and Arctic Platform of Canada and Greenland, Geological Survey of Canada, Geology of Canada 3, pp. 163-238.

Turner, E.C., Dewing, K., 2004. Geology of Little Cornwallis Island and Rookery Creek (Cornwallis Island), Nunavut. GSC Open File 1780, scale 1:50,000.

Turner, E.C., Kamber, B.S., 2012. Arctic Bay Formation, Borden Basin, Nunavut (Canada): Basin evolution, black shale, and dissolved metal systematic in the Mesoproterozoic ocean. Precambrian Research, 208-211, 1-18.

Van Acken, D., Thomson, D., Rainbird, R.H., Creaser, R.A., 2013. Constraining the depositional history of the Neoproterozoic Shaler Supergroup, Amundsen Basin, NW Canada: Rhenium-osmium dating of black shales from the Wynniatt and Boot Inlet Formations. Precambrian Research, 236, 124-131.

Valley, J.W., Graham, C.M., 1991. Ion microprobe analysis of oxygen isotope ratios in granulite facies magnetites; diffusive exchange as a guide to cooling history. Contributions to Mineralogy and Petrology 109, 38-52.

Veizer, J., Lemieux, J., Jones, B., Gibling, M.R., Savelle, J., 1978. Paleosalinity and dolomitisation of a Lower Paleozoic carbonate sequence, Somerset and Prince of Wales Islands, Arctic Canada. Canadian Journal Earth Science 15, 1448-1461.

Veizer, J., Bruckschen, P., Pawellek, F., Diener, A., Podlaha, O.G., Carden, G.A., Jasper, T., Korte, C., Strauss, H., Azmy, K., Ala, D., 1997. Oxygen isotope evolution of Phanerozoic seawater. Palaeogeography, Palaeoclimatology, Palaeoecology, 132, 159-172.

Veizer, J., Ala, D., Azmy, K., Bruckschen, P., Buhl, D., Bruhn, F., Carden, G.A.F., Diener, A., Ebneth, S., Godderis, Y., Jasper, T., Korte, C., Pawellek, F., Podlaha, O.G.,

Strauss, H., 1999. $^{87}Sr/^{86}Sr$, $\delta^{13}C$ and $\delta^{18}O$ evolution of Phanerozoic seawater. Chemical Geology, 161, 59-88.

Ward, W.C., Halley, R.B., 1985. Dolomitization in a mixing zone of near-seawater composition, Late Pleistocene, northeastern Yucatan Peninsula. Journal of Sedimentary Petrology, 55(3), 407-420.

Webb, G.E., Kamber, B.S., 2000. Rare earth elements in Holocene reefal microbialites: A new shallow seawater proxy. Geochimica et Cosmochimica Acta, 64(9), 1557-1565.

Wilkinson, J.J., Crowther, H.L., Coles, B.J., 2011. Chemical mass transfer during hydrothermal alteration of carbonates: Controls of seafloor subsidence, sedimentation and Zn-Pb mineralization in the Irish Carboniferous. Chemical Geology 289, 55-75.

Xiao, S., Schiffbauer, J.D., McFadden K.A., Hunter, J., 2010. Petrographic and SIMS pyrite sulfur isotope analyses of Ediacaran chert nodules: Implications for microbial processes in pyrite rim formation, silicification, and exceptional preservation. Earth and Planetary Science Letters, 297, 481-495.

Young, G.M., 1981. The Amundsen Embayment, Northwest Territories; relevance to the upper Proterozoic evolution of North America; Geological Survey of Canada, Paper 81-10. p. 203-218.

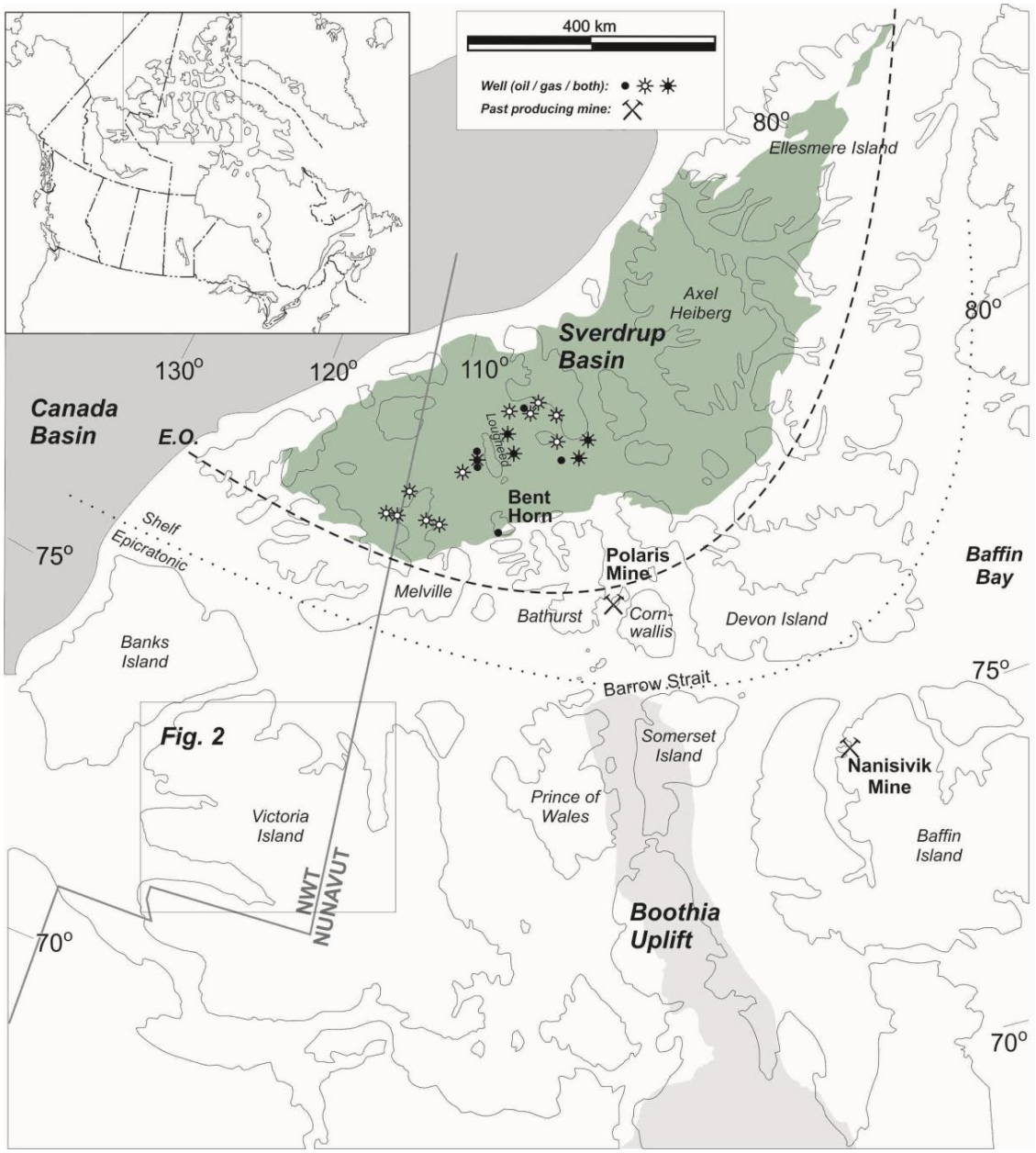

Fig. 4.1. Map of the Arctic archipelago, modified after Dewing et al. (2007a), showing geographic and geological features mentioned in the text. E.O. = southern and eastern extent of Ellesmerian Orogeny.

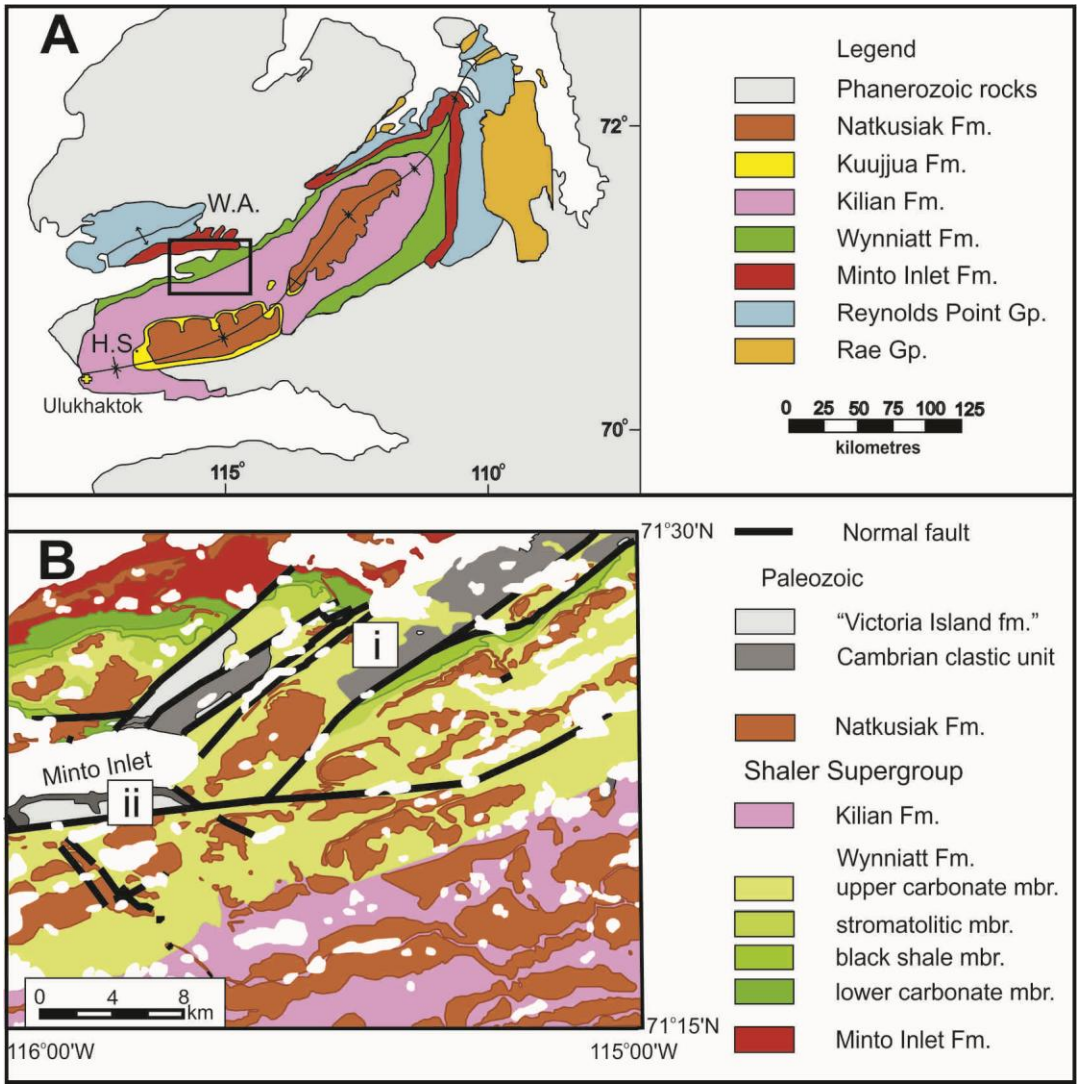

Fig. 4.2. (A) Bedrock geological map of northwestern Victoria Island showing the location of the study area (box for (B)); modified after Thorsteinsson and Tozer (1962). W.A. = Walker Bay anticline, H.S. = Holman Island syncline. (B) Detailed geological map of the study area; modified after Rainbird et al. (in press.). Locations of the samples used in this study: (i) Wynniatt Formation samples, (ii) "Victoria Island formation" samples.

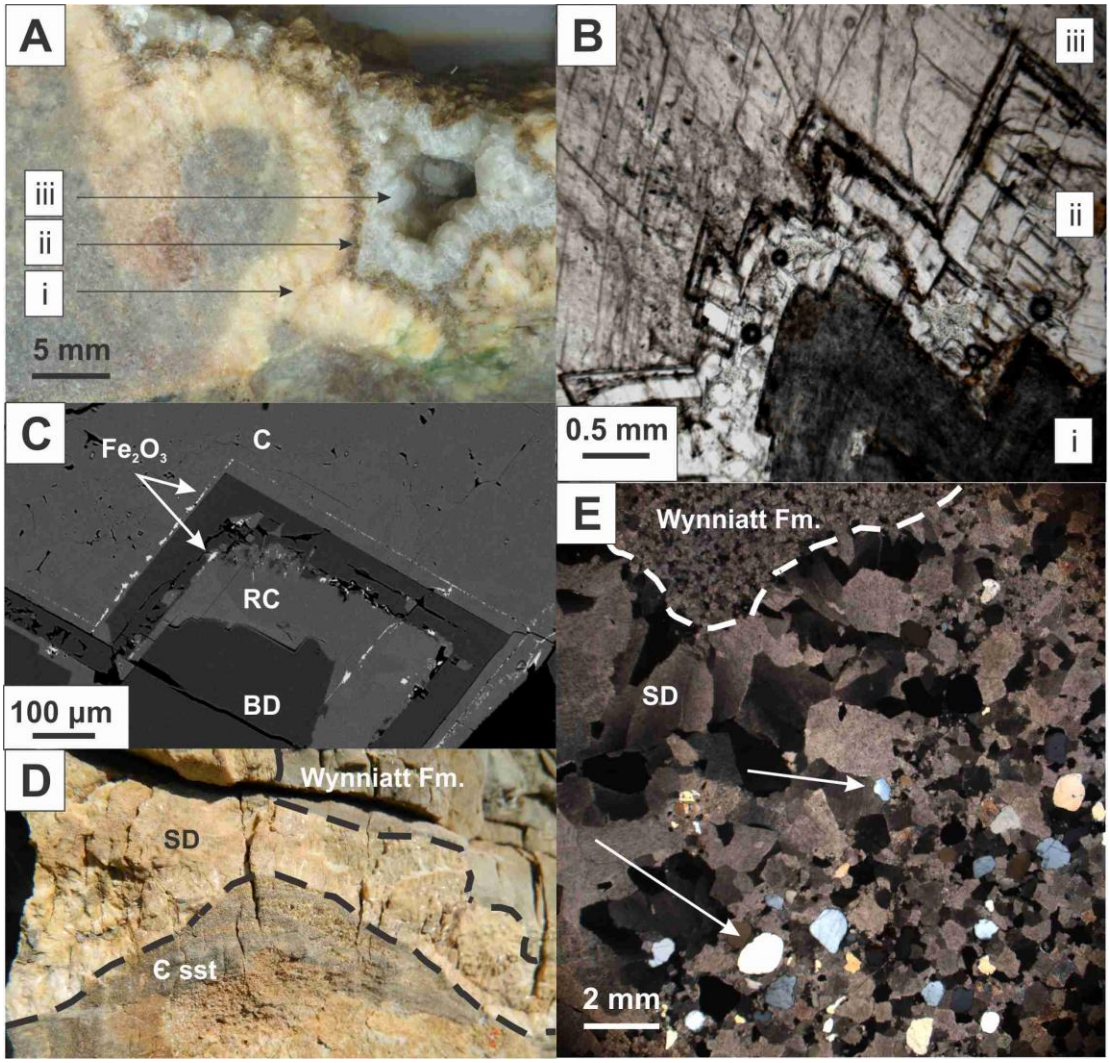

Fig. 4.3. Diagenetic phases of the Wynniatt Formation Upper Carbonate member. (A) Cut slab of a representative sample of Wynniatt Formation dolostone that shows the relationship of the three visible cements: saddle dolomite (SD), brown dolomite (BD), and late-stage calcite (LC). Replacive calcite (RC) is not visible at hand sample scale. (B) Plane-polarised light photomicrograph of the four diagenetic cements. Although BD is colourless, hematite associated with RC results in the brown appearance at hand sample scale (A). (C) Scanning electron microscope image that shows the relationship between RC, BD, hematite, and LC. (D) Hand sample that shows the relationship between Wynniatt

Formation dolostone, SD, and Cambrian sand stone (Ꞓsst). (E) Cross-polarised light photomicrograph that shows Ꞓ detrital quartz grains (arrows) encompassed by SD providing a maximum-age constraint of SD precipitation.

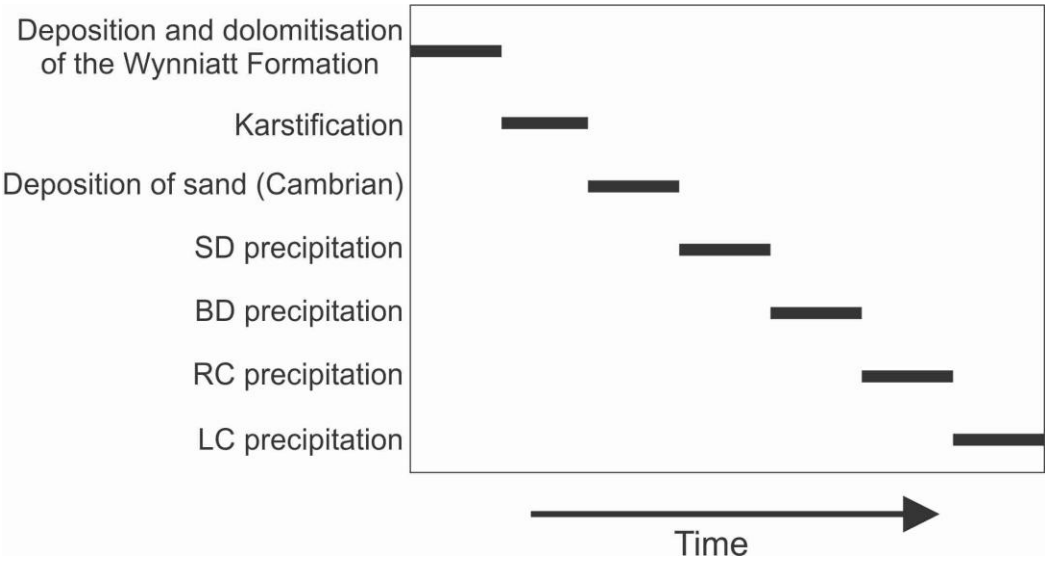

Fig. 4.4. Paragenesis of the Neoproterozoic Wynniatt Formation and its Phanerozoic diagenetic phases. Karsting is inferred to be late Neoproterozoic to Cambrian (Mathieu et al., 2013b). Diagenetic cements have an oldest possible age in the Cambrian as suggested by inclusion of Cambrian clastic sediment by the oldest diagenetic cement (saddle dolomite).

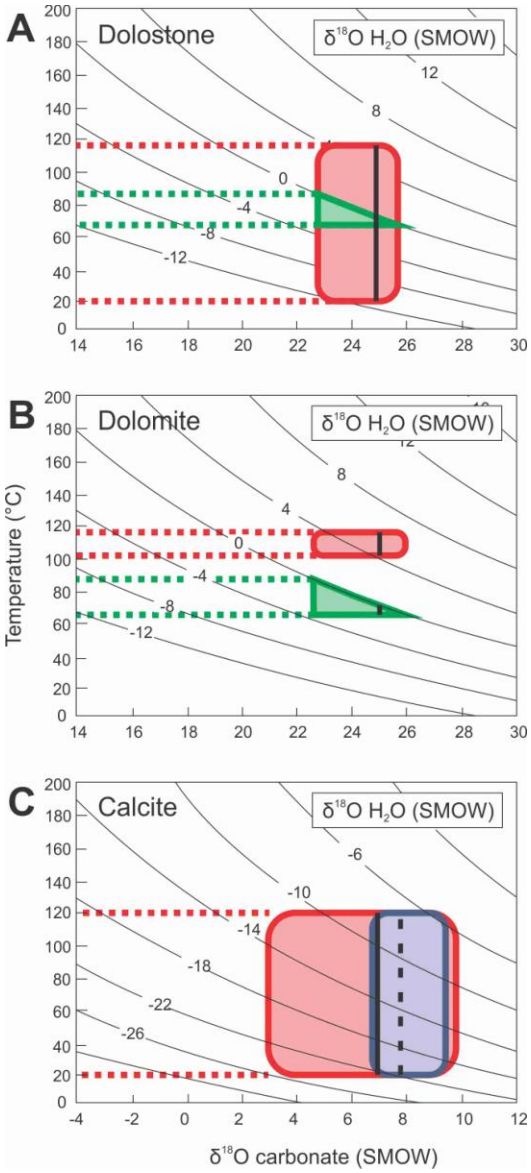

Fig. 4.5. Oxygen isotope diagrams for the Wynniatt Formation show the range of possible $\delta^{18}O_{H2O}$ values for the dolostone and the cement phases. Curved lines are isopleths for $\delta^{18}O_{H2O}$ calculated using the appropriate mineral-water fractionation equations. (A) Possible $\delta^{18}O_{H2O}$ values calculated for Wynniatt Formation dolostone assuming a temperature range of 20°C to 120°C (red field) and temperature range required to produce seawater $\delta^{18}O_{H2O}$ values (green field). (B) Calculated $\delta^{18}O_{H2O}$ values based on the dolomite cements using T_h values from Mathieu et al. (2013a) (red field). A seawater isotopic

composition (green field) would require a temperature of formation below the measured T_h values for fluid inclusions in the cements. (C) Fields for replacive calcite (blue field) and calcite cement (red field) overlap, suggesting that they may have precipitated from the same fluid. Black vertical lines represent average SIMS $\delta^{18}O_{cement}$; solid and dashed black lines in C represent the averages for calcite and replacive calcite, respectively. The fractionation equation from Land (1985) was used for dolomite-water fractionation, whereas the fractionation equation from O`Neil (1969) was used for calcite-water fractionation.

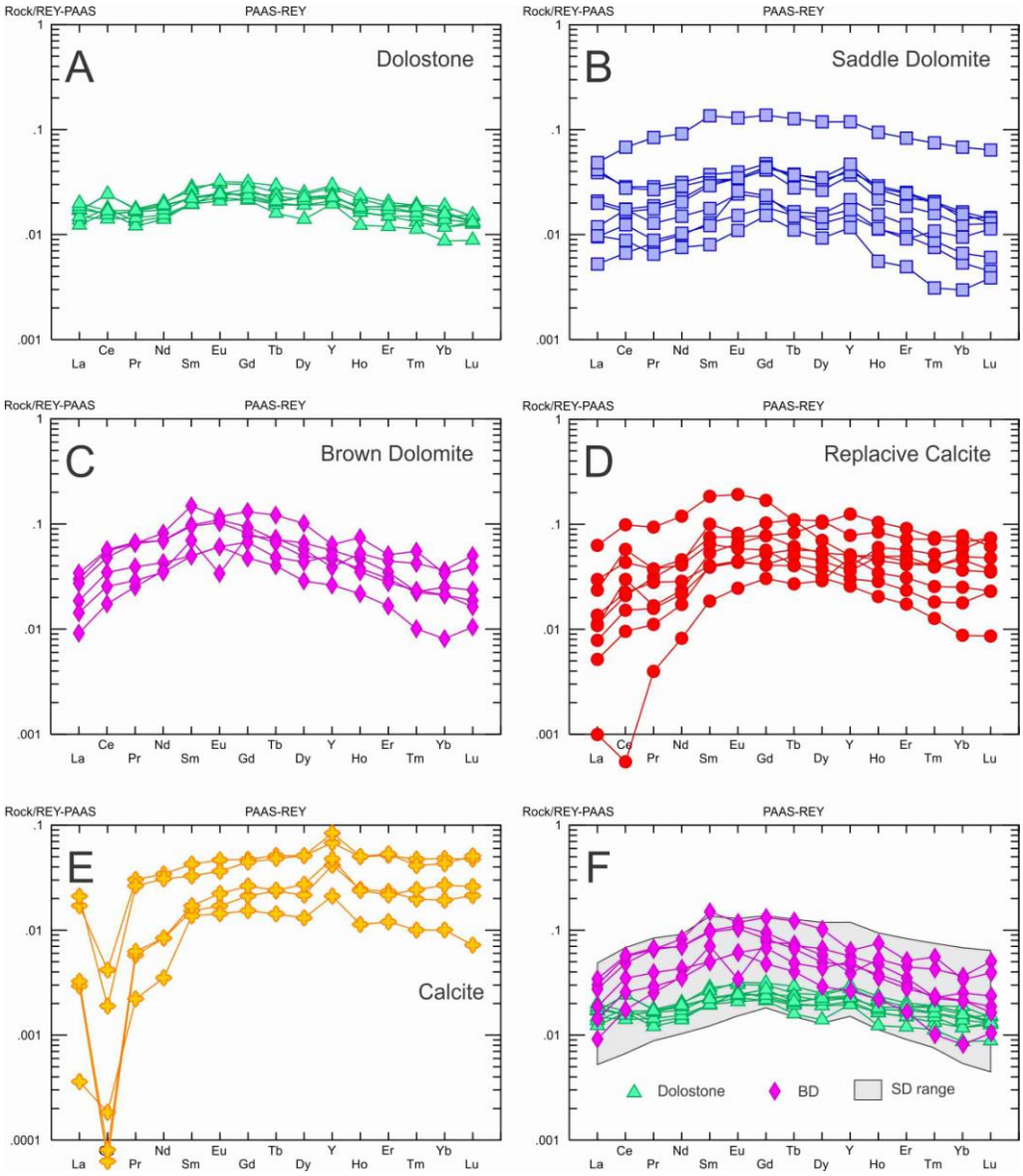

Fig. 4.6. Post Archean Australian Shale (PAAS) normalised REE plots for the Wynniatt Formation dolostone and its diagenetic cements (PAAS values from Pourmand et al., 2012). (A) Recrystallised Wynniatt Formation dolostone. (B) Saddle dolomite cement. (C) Brown dolomite cement. (D) Replacive calcite (dedolomite). (E) Late-stage calcite cement. Note the scale change for this cement stage due to the lower abundances of the

REE. F) Comparison of data for dolostone, saddle dolomite, and brown dolomite cements. The range in saddle dolomite (shaded area) encompasses the datasets for the other two phases, which may suggest that all three phases are related.

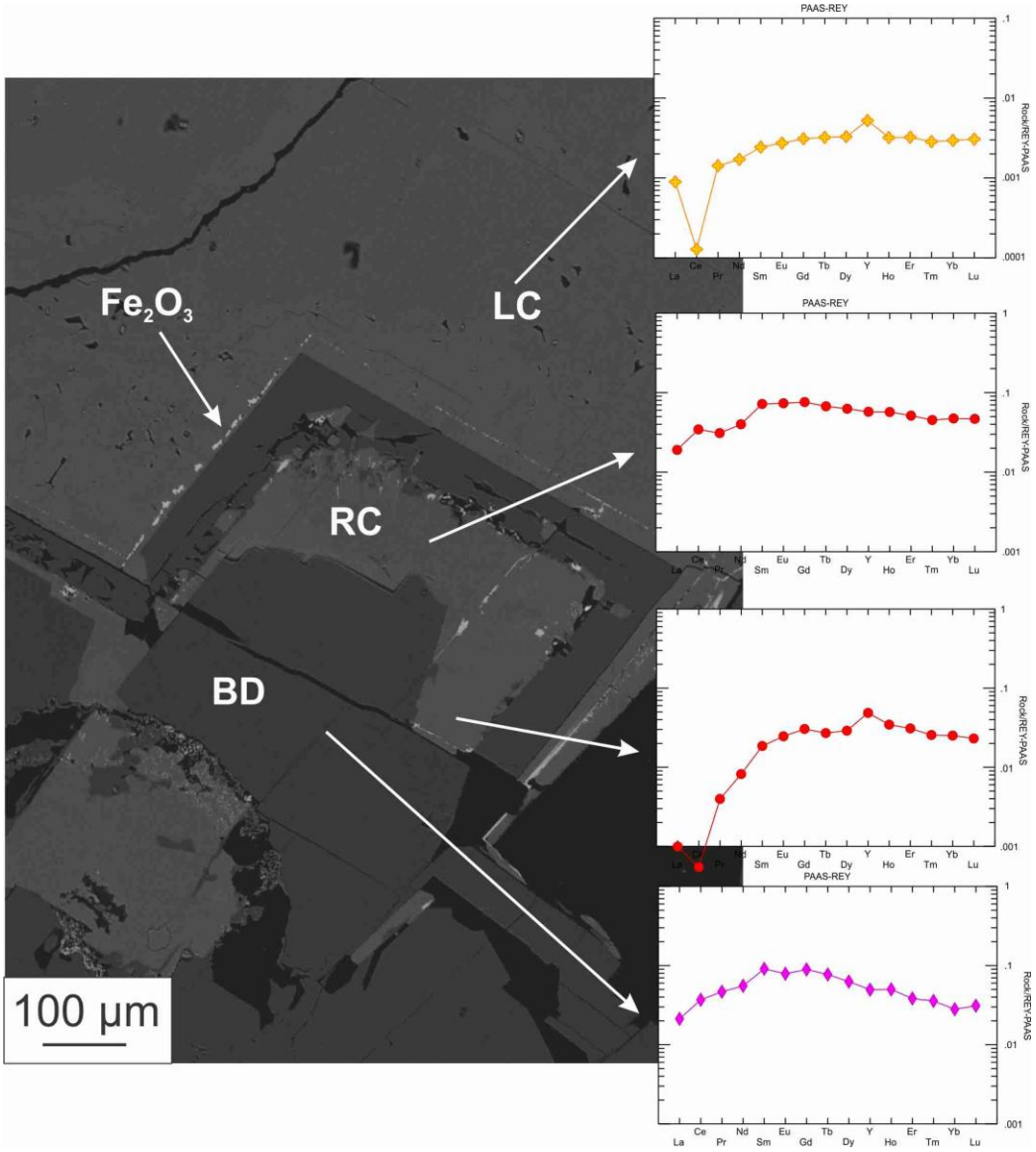

Fig. 4.7. A scanning electron microscope (SEM) image of Wynniatt Formation cements along with their associated average Post Archean Australian Shale (PAAS)-normalised REE diagrams. Note that the replacive calcite (RC) has a REE pattern that is intermediate between those for the brown dolomite (BD) and late-stage calcite (LC).

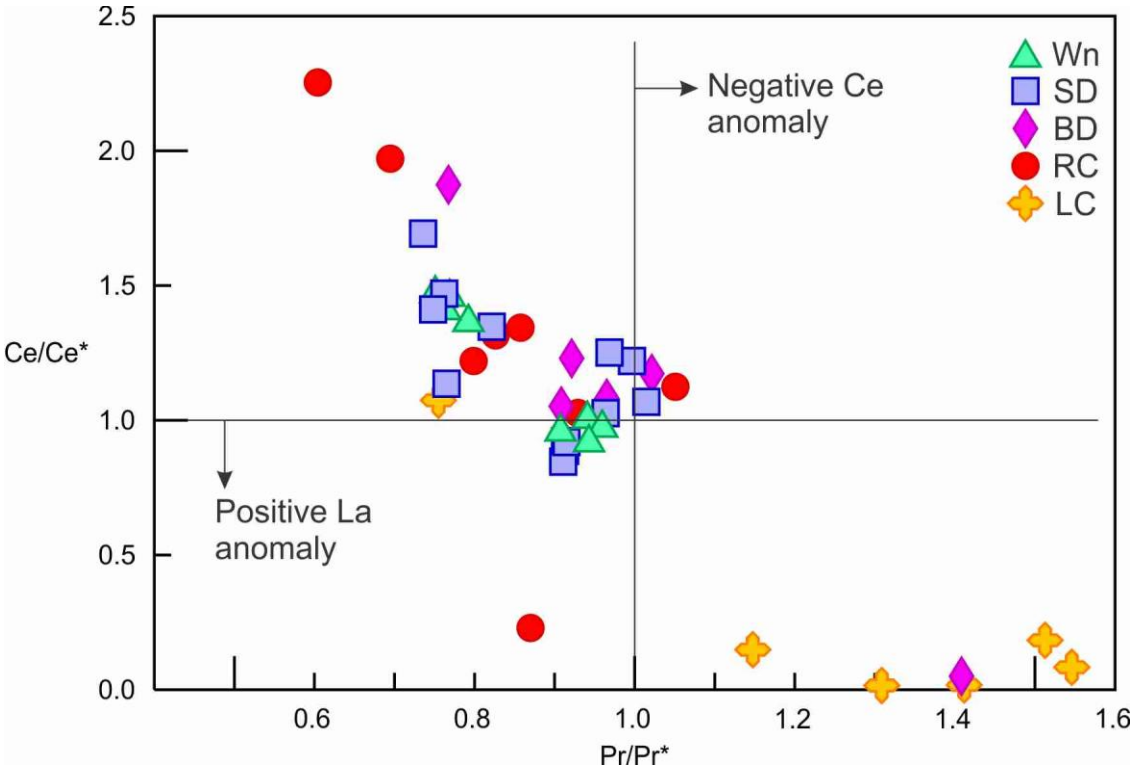

Fig. 4.8. Anomaly discrimination diagram that verifies La and Ce anomalies (after Bau et al., 1997) for Wynniatt Formation phases shows that the majority of phases possess positive Ce and negative La values when normalised to Post Archean Australian Shale (PAAS, subscript SN). Wn= Wynniatt Formation dolostone, SD= saddle dolomite, BD= brown dolomite, RC= replacive calcite, LC= late-stage calcite. $Ce^*=Ce/(0.5*La_{SN}+0.5*Pr_{SN})$. $Pr^*=Pr/(0.5*Ce_{SN}+0.5*Nd_{SN})$.

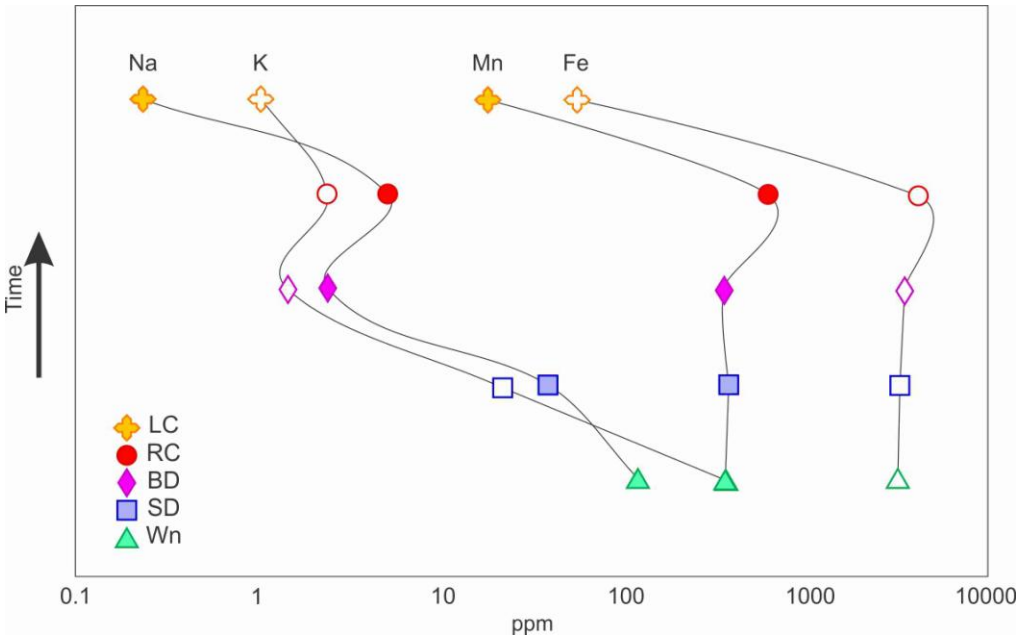

Fig. 4.9. The change in average concentrations of Na, K, Mn, and Fe for the different diagenetic phases in the Wynniatt Formation arranged paragenetically from bottom to top. Wn= Wynniatt Formation dolostone, SD= saddle dolomite, BD= brown dolomite, RC= replacive calcite, LC= late-stage calcite.

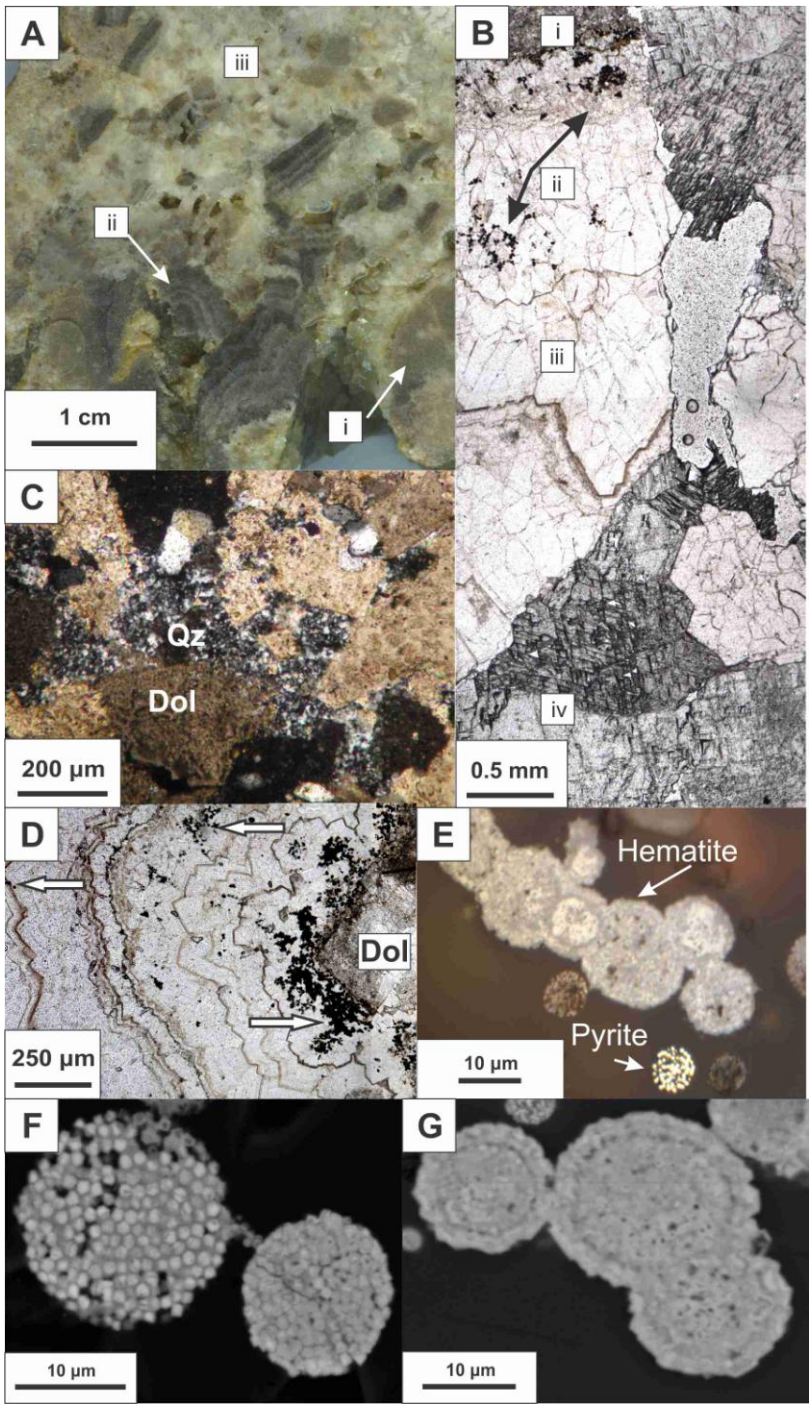

Fig. 4.10. Images of "Victoria Island formation" samples show features and relationships of diagenetic phases. (A) Cut hand sample that shows the brecciated (i) dolostone and (ii) quartz cement being supported by the (iii) dolomite cements (D1 and D2). The zoned tex-

ture of quartz can be seen at the macroscopic level. (B) Plane-polarised light (PL) photomicrograph of: (i) dolostone, (ii) quartz cement, (iii) framboidal pyrite, (iv) and dolomite cements (D1 and D2). (C) Cross-polarised light photomicrograph that shows the silicification and texture of the host dolostone. (D) PL photomicrograph that shows early quartz precipitation was associated with an abundance of early framboidal pyrite (arrows) with diminished quantities during later quartz precipitation. (E) Reflected light photomicrograph of framboidal pyrites hosted by quartz that shows both their fresh (brassy colour) and altered hematite pseudomorphs (grey colour). (F) SEM image of framboid aggregate showing that pyrite framboids contain discrete crystals. (G) SEM image showing alteration of pyrite framboids to hematite with concomitant loss of the framboidal texture.

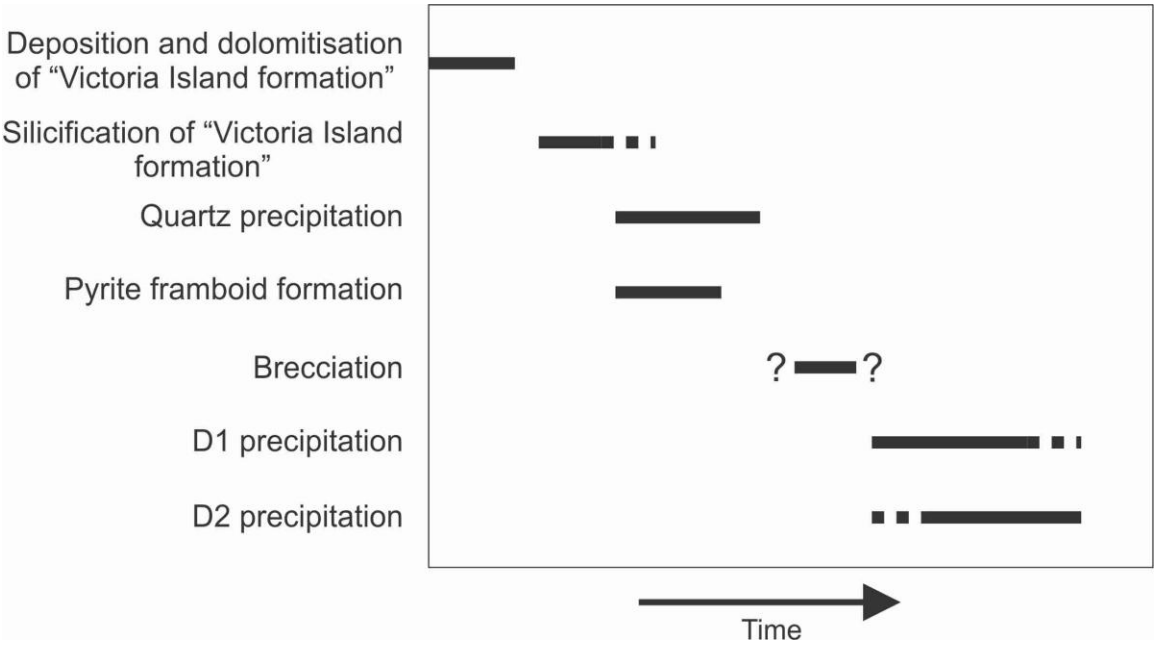

Fig. 4.11. Paragenesis of the Paleozoic "Victoria Island formation" and its diagenetic phases. Silicification may or may not have been related to quartz cement precipitation. Dolomite 1 (D1) cement is suggested to precede dolomite 2 (D2) based on geochemical criteria rather than petrographic criteria.

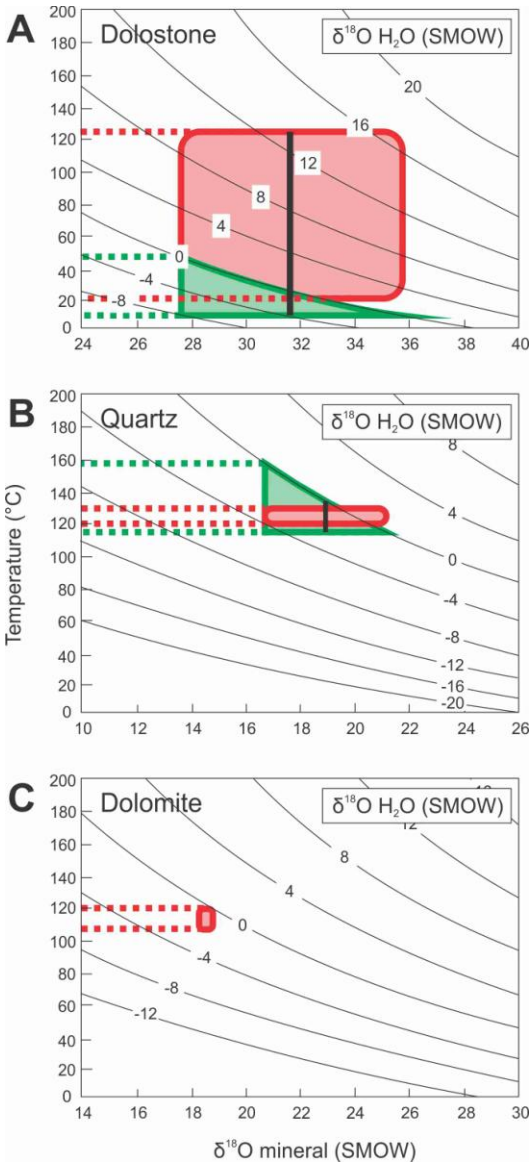

Fig. 4.12. Oxygen isotope diagrams for the "Victoria Island formation" show the range of possible $\delta^{18}O_{H2O}$ values for the dolostone and the cement phases. Curved lines are isopleths for $\delta^{18}O_{H2O}$ calculated using the appropriate mineral-water fractionation equations. (A) Possible $\delta^{18}O_{H2O}$ values calculated for "Victoria Island formation" dolostone assuming a temperature range of 20°C to 120°C (red field) and temperature range required to produce seawater $\delta^{18}O_{H2O}$ values (green field). (B) Calculated $\delta^{18}O_{H2O}$ values based on the quartz cement's T_h values from Mathieu et al. (2013a) (red field). A seawater isotopic

composition (green field) would require a temperature of formation that includes the measured T_h values for fluid inclusions in the cements. (C) Calculated $\delta^{18}O_{H2O}$ values for dolomite cements (D1 and D2) based on T_h values from Mathieu et al. (2013a) indicate that these cements precipitated from seawater. Black vertical lines represent average SIMS $\delta^{18}O_{cement}$. The fractionation equation from Land (1985) was used for dolomite-water fractionation, whereas the fractionation equation from Sharp and Kirschner (1994) was used for quartz-water fractionation.

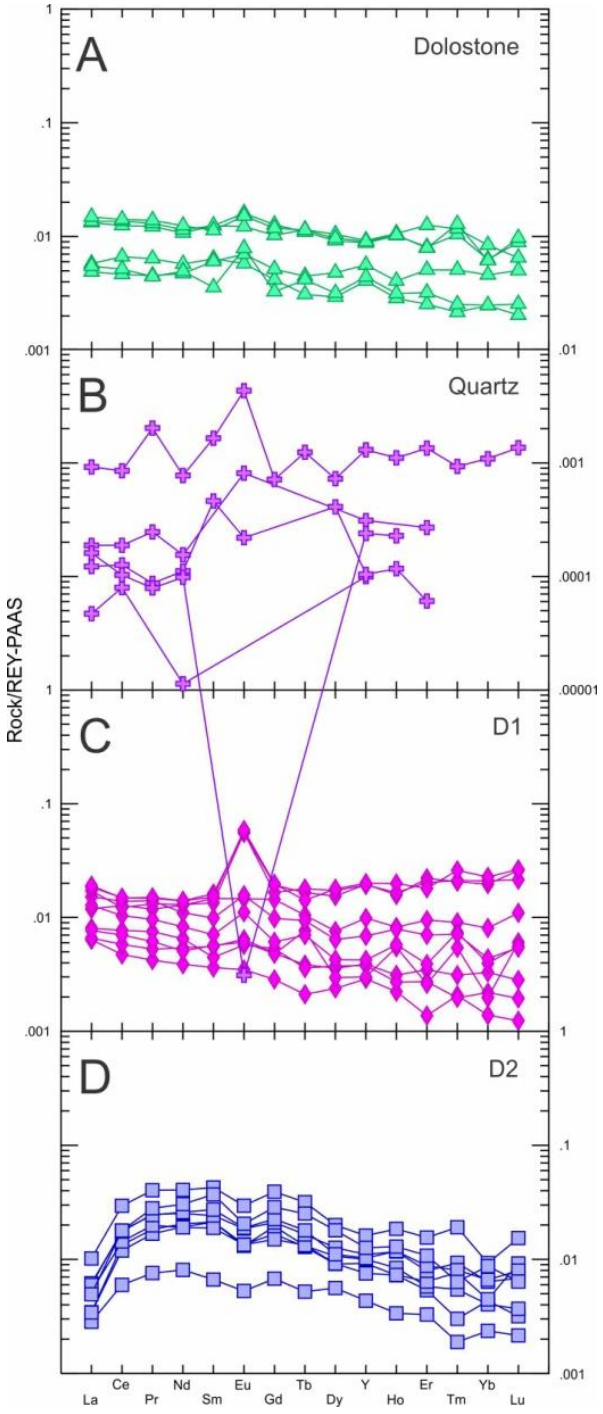

Fig. 4.13. Post Archean Australian Shale (PAAS)-normalised REE plots for the "Victoria Island formation" dolostone and its diagenetic cements (PAAS values from Pourmand et al., 2012). (A) Recrystallised "Victoria Island formation" dolostone. (B) Quartz cement

failed to ablate sufficiently to produce coherent REE diagrams (Note the change in scale for the quartz cement from the dolomite phases). (C) Dolomite 1 cement. D) Dolomite 2 cement.

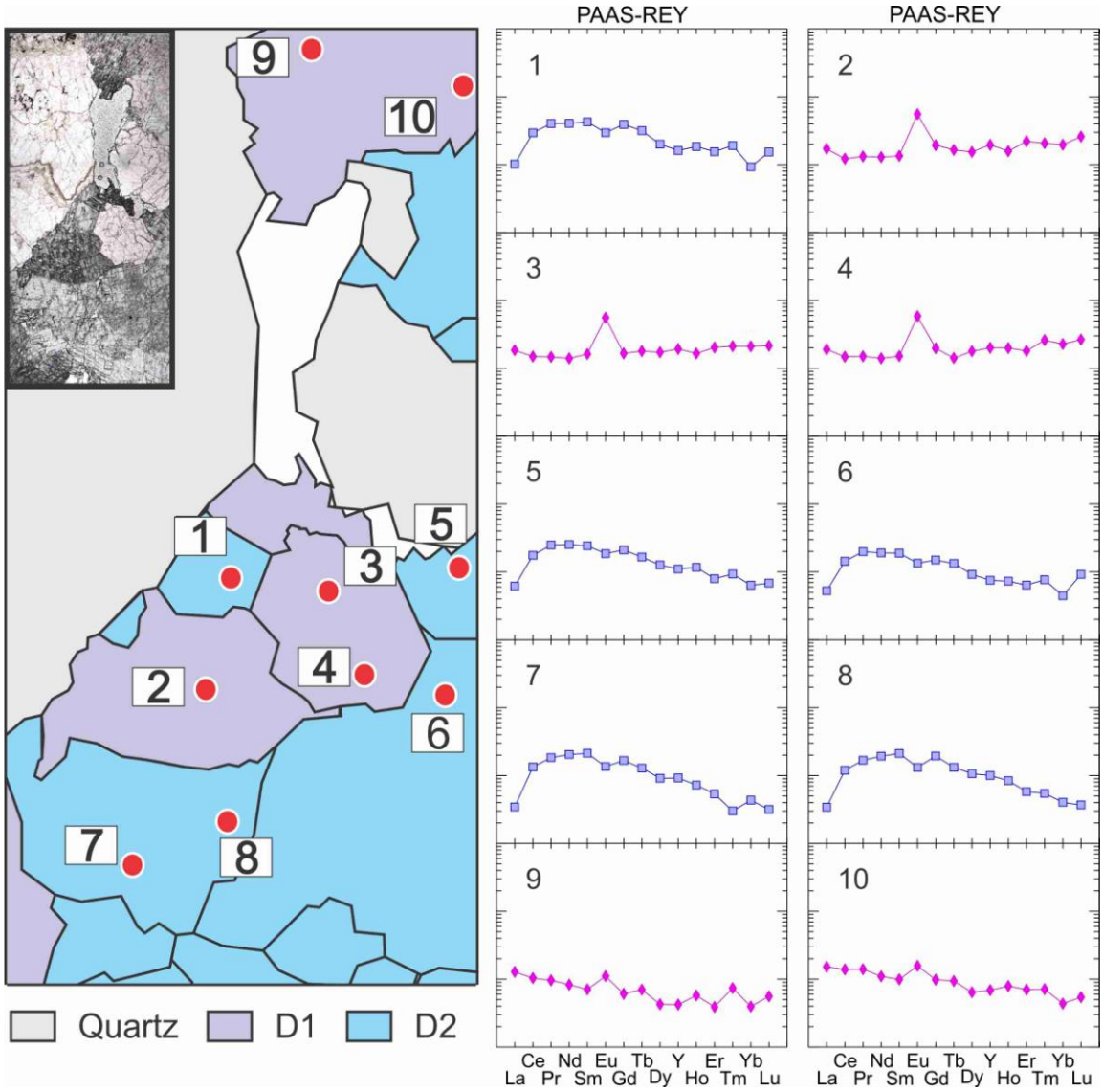

Fig. 4.14. Interpretive diagram of "Victoria Island formation" cements (quartz and dolomite (D1, D2)) along with the locations of the points for LA ICP-MS analysis and the PAAS-normalised REE profiles for these points. Note that points 1, 5, 6, 7 and 8 equate to D2 whereas points 2, 3, 4, 9, and 10 are D1. Inset figure is the plane-polarised light photomicrograph (Fig. 4.10B) represented in the diagram.

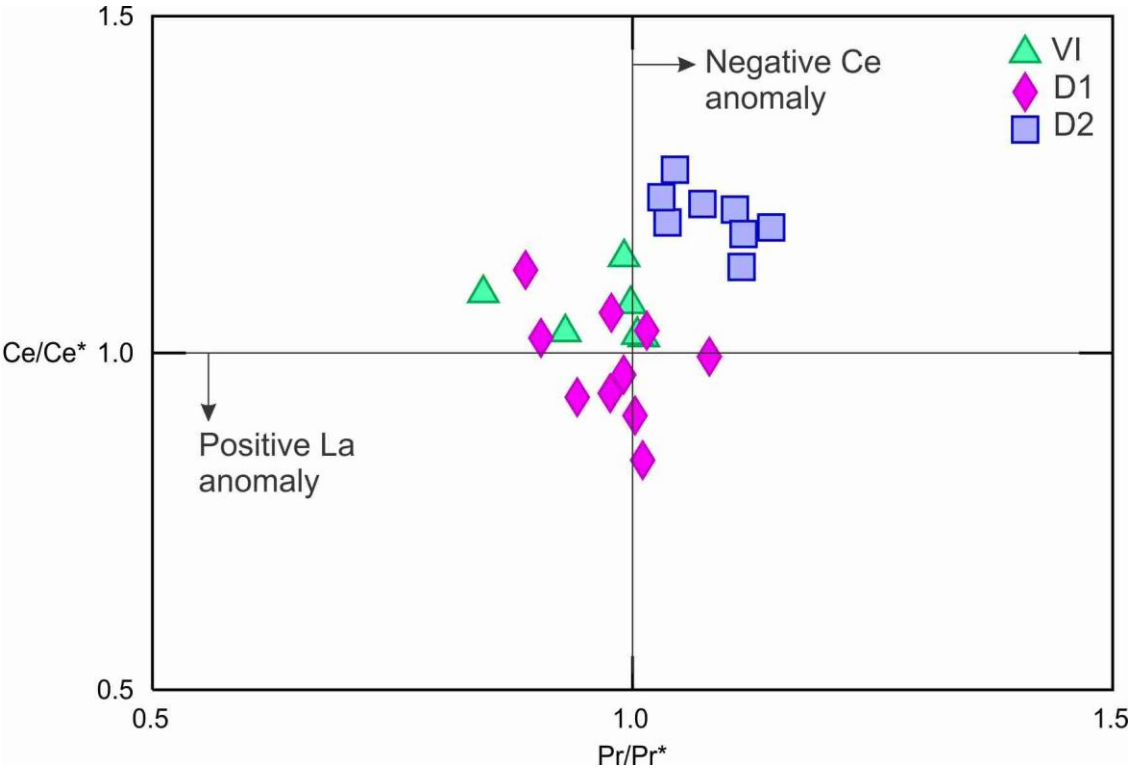

Fig. 4.15. Anomaly discrimination diagram to determine if there are La and Ce anomalies (after Bau et al., 1997) for "Victoria Island formation" indicates that dolostone (VI) and dolomite 1 (D1) lack appreciable Post Archean Australian Shale (PAAS)-normalised anomalies; whereas dolomite 2 (D2) has negative La and Ce anomalies. $Ce^*=Ce/(0.5*La_{SN}+0.5*Pr_{SN})$. $Pr^*=Pr/(0.5*Ce_{SN}+0.5*Nd_{SN})$. SN – shale normalised.

Table 4.1. Summary of average SIMS isotope values for the different phases and precipitating water. Mineral-water oxygen fractionation equations for dolomite, calcite, and quartz are from Land (1985), O'Neil et al. (1969), and Sharp and Kirschner (1994), respectively, were used to calculate the water isotopic composition relative to Vienna Standard Mean Ocean Water (V-SMOW). Homogenisation temperatures (T_h), displayed in parentheses, used in the calculations are from Mathieu et al. (2013b). Wynniatt Formation (WF) dolostone value is from D. Thomson (pers. Comm.). SD – saddle dolomite, BD – brown dolomite, RC – replacement calcite, LC – late-stage calcite, VIf – "Victoria Island formation", D1 – dolomite cement 1, D2 – dolomite cement 2, CDT – Canyon Diablo Troilite.

Host	**Mineral**	**$\delta^{18}O_{V\text{-}SMOW}$ (‰)**	**$\delta^{18}O_{H2O}$ @ 20°C**	**$\delta^{18}O_{H2O}$ @ T_h or 120°C**
WF	Dolostone	24.2	-9.1	5.3
	SD	24.7	--	4.6 (108)
	BD	24.7	--	5.4 (116)
	RC	7.8	-21.9	-7.3
	LC	6.9	-22.6	-8.2
VIf	Dolostone	31.8	-1.5	12.9
	Quartz	18.7	--	-1.3 (125)
	D1 and 2	18.6	--	-0.8 (115)
		$\delta^{34}S_{CDT}$ (‰)		
	Pyrite	-11.1	--	--
		-5.6	--	--
		-6.5	--	--
		-4.3	--	--
		-4.0	--	--
		-11.7	--	--
		-9.1	--	--

Table 4.2. LA ICP-MS analyses of REE for Wynniatt Formation (W) and "Victoria Island formation" (VI) phases (in ppm). Dst - dolostone, SD - saddle dolomite, BD - brown dolomite, RC - replacive calcite, LC - late-stage calcite, Q - quartz, D1 - dolomite 1 cement, D2 - dolomite 2 cement. N.d. – not detected

Table 4.2

Host	W	W	W	W	W	W	W	W	W	W	W	W	W
Phase	Dst	Dst	Dst	Dst	Dst	Dst	Dst	Dst	SD	SD	SD	SD	SD
Na	100.12	76.85	86.76	108.27	97.72	133.38	156.57	163.67	85.50	43.76	65.32	82.06	53.74
Mg	41425.03	40910.52	50564.66	50078.37	31966.60	38420.31	43228.20	48992.56	47317.72	49884.17	61509.85	64337.63	56685.72
Ca	78837.48	78379.97	96390.08	96713.62	56668.06	65966.94	76648.31	85646.25	91493.11	93569.29	107451.72	113244.39	100007.99
Al	110.44	266.87	294.29	234.52	682.92	634.30	337.83	312.10	190.73	13.27	27.58	71.89	21.06
K	108.15	133.05	256.07	135.81	693.82	637.92	457.71	355.65	123.14	24.54	9.69	12.42	21.61
V	1.18	2.39	2.01	1.86	0.36	0.46	0.31	0.30	1.93	0.23	0.08	0.08	0.08
Mn	385.59	464.54	456.34	476.68	217.95	250.09	258.28	300.85	508.25	415.70	335.67	347.83	311.57
Fe	2881.41	4209.58	3581.19	3427.82	2470.15	2537.19	2735.36	3121.01	3697.72	2822.39	2950.30	3089.80	3773.00
Rb	3.13	4.17	3.85	3.75	4.58	5.26	4.87	5.59	4.24	1.93	2.67	2.69	1.96
Sr	15.74	19.92	18.19	17.64	19.87	24.28	24.88	28.56	20.39	9.77	15.79	16.37	11.48
Ba	0.44	0.88	0.70	0.61	1.16	1.19	1.18	1.23	0.70	0.37	0.48	0.58	0.36
La	0.53	0.47	0.65	0.65	0.57	0.67	0.71	0.76	0.67	0.74	1.49	1.59	0.80
Ce	1.41	1.31	1.92	1.93	1.12	1.25	1.23	1.34	1.83	2.99	2.28	2.20	1.39
Pr	0.12	0.11	0.16	0.15	0.13	0.15	0.15	0.15	0.16	0.24	0.25	0.24	0.17
Nd	0.50	0.47	0.68	0.69	0.52	0.58	0.63	0.65	0.65	1.12	1.06	0.98	0.75
Sm	0.11	0.11	0.16	0.15	0.11	0.13	0.12	0.12	0.13	0.26	0.21	0.19	0.17
Eu	0.03	0.02	0.03	0.03	0.02	0.03	0.03	0.03	0.03	0.06	0.04	0.04	0.04
Gd	0.11	0.10	0.14	0.15	0.10	0.11	0.11	0.13	0.14	0.26	0.22	0.19	0.21
Tb	0.02	0.01	0.02	0.02	0.01	0.02	0.02	0.02	0.02	0.03	0.03	0.02	0.03
Dy	0.09	0.07	0.11	0.12	0.09	0.10	0.11	0.11	0.11	0.15	0.15	0.12	0.16
Y	0.56	0.53	0.75	0.79	0.53	0.61	0.64	0.61	0.76	1.11	1.14	0.99	1.07
Ho	0.02	0.01	0.02	0.02	0.02	0.02	0.02	0.02	0.02	0.03	0.03	0.02	0.03
Er	0.04	0.03	0.05	0.06	0.04	0.05	0.05	0.05	0.05	0.06	0.06	0.05	0.07
Tm	0.01	0.00	0.01	0.01	0.01	0.01	0.01	0.01	0.01	0.01	0.01	0.01	0.01
Yb	0.03	0.02	0.05	0.05	0.03	0.04	0.04	0.04	0.05	0.04	0.04	0.04	0.05
Lu	0.01	0.00	0.01	0.01	0.01	0.01	0.01	0.01	0.01	0.01	0.01	0.01	0.01
Pb	0.03	0.08	0.05	0.03	0.78	0.45	0.46	0.50	0.03	0.02	0.03	0.03	0.09
Th	0.06	0.03	0.08	0.07	0.10	0.10	0.10	0.09	0.04	n.d.	0.00	0.00	0.00
U	0.01	0.03	0.03	0.02	0.03	0.03	0.04	0.02	0.02	0.00	0.00	0.00	0.00
Y/Ho	0.24	0.23	0.23	0.22	0.24	0.25	0.23	0.23	0.24	0.21	0.24	0.24	0.22
ΣREE	3.56	3.28	4.75	4.83	3.30	3.77	3.87	4.04	4.63	7.12	7.02	6.69	4.94
ΣREE+Y	4.13	3.81	5.50	5.62	3.83	4.38	4.51	4.65	5.39	8.23	8.16	7.68	6.01

Table 4.2 continued

Host	W	W	W	W	W	W	W	W	W	W	W	W	W
Phase	SD	SD	SD	SD	SD	SD	BD	BD	BD	BD	BD	BD	RC
Na	27.58	1.34	0.69	31.76	69.31	32.73	3.77	1.57	2.94	1.22	n.d.	n.d.	35.35
Mg	57801.46	52412.01	51427.04	47304.67	47371.77	48756.11	40250.67	45907.32	43903.62	44390.61	44746.38	43799.91	42602.90
Ca	100798.78	93701.91	90905.29	86153.92	86061.26	87996.98	94781.44	85037.85	82462.46	79499.89	79570.23	79753.92	92901.57
Al	28.66	38.89	27.24	15.92	20.26	146.15	117.64	16.98	48.10	14.07	3.35	9.26	126.67
K	8.35	1.20	0.15	18.66	36.56	19.41	0.73	1.24	3.32	0.38	n.d.	0.61	18.12
V	0.05	0.26	0.35	0.34	0.37	0.11	3.27	0.66	5.65	5.41	0.40	0.16	6.59
Mn	296.08	347.84	402.05	406.77	440.97	446.84	443.20	218.61	408.88	330.93	173.74	361.83	537.60
Fe	3759.09	4274.38	3050.76	2711.83	2871.25	3878.41	4065.76	2492.11	3752.81	3362.58	2147.98	3046.95	4540.14
Rb	1.57	1.33	1.34	0.02	0.01	0.01	2.22	1.53	n.d.	0.01	n.d.	n.d.	1.83
Sr	9.53	8.21	7.82	15.58	15.88	12.33	11.39	7.69	6.80	5.89	6.27	7.78	8.84
Ba	0.27	0.06	0.02	0.36	0.59	0.31	0.79	0.36	0.77	0.11	n.d.	n.d.	13.66
La	0.76	1.86	0.20	0.45	0.36	0.37	0.55	1.30	1.04	0.35	1.14	0.71	0.43
Ce	1.31	5.42	0.53	1.38	0.99	0.70	2.03	4.53	3.82	1.38	4.42	2.75	1.66
Pr	0.16	0.74	0.07	0.11	0.08	0.06	0.26	0.59	0.58	0.22	0.57	0.35	0.28
Nd	0.69	3.10	0.34	0.51	0.35	0.26	1.18	2.35	2.78	1.22	2.37	1.45	1.47
Sm	0.16	0.75	0.07	0.10	0.07	0.04	0.27	0.53	0.82	0.39	0.54	0.28	0.56
Eu	0.04	0.14	0.02	0.03	0.03	0.01	0.07	0.11	0.13	0.04	0.12	0.07	0.09
Gd	0.20	0.64	0.08	0.10	0.11	0.07	0.31	0.38	0.61	0.36	0.44	0.22	0.48
Tb	0.03	0.10	0.01	0.01	0.01	0.01	0.04	0.05	0.09	0.06	0.06	0.03	0.09
Dy	0.16	0.56	0.06	0.07	0.07	0.04	0.20	0.23	0.47	0.27	0.31	0.13	0.50
Y	1.27	3.21	0.41	0.58	0.47	0.32	1.35	1.24	1.72	1.05	1.51	0.71	2.12
Ho	0.03	0.10	0.01	0.02	0.01	0.01	0.04	0.04	0.08	0.05	0.05	0.02	0.09
Er	0.07	0.24	0.03	0.04	0.03	0.01	0.08	0.09	0.15	0.13	0.10	0.05	0.21
Tm	0.01	0.03	0.00	0.00	0.00	0.00	0.01	0.01	0.02	0.02	0.01	0.00	0.03
Yb	0.04	0.19	0.02	0.02	0.03	0.01	0.06	0.06	0.10	0.10	0.07	0.02	0.19
Lu	0.01	0.03	0.00	0.00	0.00	0.00	0.01	0.01	0.02	0.02	0.01	0.00	0.03
Pb	0.02	0.03	0.01	0.02	0.08	0.05	0.04	0.02	0.08	0.02	0.01	0.01	0.16
Th	0.00	0.00	0.01	n.d.	n.d.	n.d.	0.00	0.00	n.d.	n.d.	n.d.	n.d.	0.02
U	0.00	0.00	0.00	0.00	0.00	n.d.	0.02	0.00	0.01	0.00	n.d.	n.d.	0.04
Y/Ho	0.22	0.24	0.22	0.22	0.22	0.22	0.22	0.25	0.21	0.18	0.24	0.24	0.19
ΣREE	4.93	17.10	1.85	3.43	2.61	1.91	6.44	11.52	12.42	5.64	11.72	6.80	8.21
ΣREE+Y	6.20	20.31	2.26	4.01	3.07	2.23	7.79	12.76	14.14	6.69	13.23	7.50	10.33

Table 4.2 continued

Host	W	W	W	W	W	W	W	W	W	W	W	W	W
Phase	RC	RC	RC	RC	RC	RC	RC	RC	LC	LC	LC	LC	LC
Na	8.62	n.d.	6.25	7.78	n.d.	n.d.	n.d.	n.d.	n.d.	0.24	n.d.	n.d.	n.d.
Mg	1619.78	1813.46	39888.81	36247.97	486.15	183.14	1687.51	44986.74	1349.54	695.76	1367.76	515.73	664.81
Ca	148413.78	148366.05	86412.89	96192.02	158018.88	157167.39	154787.01	79410.71	176877.59	180233.40	162104.50	164230.37	166941.42
Al	793.93	1.98	121.90	57.09	9.30	0.11	0.86	4.29	0.48	0.27	1.10	5.28	0.19
K	3.23	n.d.	1.81	1.17	0.42	n.d.	n.d.	n.d.	0.56	0.54	n.d.	1.56	1.39
V	25.53	0.24	7.79	4.45	0.11	0.01	0.04	0.39	0.06	0.03	0.03	0.13	0.02
Mn	1500.10	584.52	551.65	578.72	609.16	409.41	8.02	108.29	76.66	0.29	3.00	7.95	0.51
Fe	17155.36	147.61	5516.54	4262.17	232.51	189.06	130.78	1614.81	111.40	8.79	22.80	116.25	10.44
Rb	3.42	0.04	0.01	n.d.	0.02	n.d.	0.02	0.00	2.24	7.74	0.01	n.d.	0.00
Sr	16.72	63.93	6.82	8.41	10.11	8.37	23.12	11.02	11.46	37.81	25.37	18.09	29.58
Ba	70.62	0.33	1.35	1.68	0.12	0.02	0.03	n.d.	0.17	0.06	0.08	0.07	0.03
La	0.90	0.41	0.30	0.20	1.14	2.40	0.04	0.52	0.65	0.11	0.01	0.80	0.12
Ce	4.59	2.37	1.21	0.76	3.45	7.86	0.04	1.79	0.33	0.00	0.01	0.15	0.01
Pr	0.33	0.15	0.14	0.10	0.33	0.83	0.04	0.25	0.27	0.05	0.02	0.23	0.06
Nd	1.56	0.80	0.73	0.58	1.39	4.05	0.28	0.97	1.16	0.28	0.12	1.04	0.29
Sm	0.42	0.30	0.22	0.22	0.36	1.02	0.10	0.22	0.24	0.08	0.08	0.18	0.09
Eu	0.08	0.07	0.05	0.05	0.06	0.21	0.03	0.05	0.05	0.02	0.02	0.04	0.02
Gd	0.36	0.36	0.24	0.19	0.26	0.79	0.14	0.19	0.22	0.10	0.07	0.21	0.12
Tb	0.05	0.06	0.04	0.04	0.03	0.08	0.02	0.03	0.04	0.02	0.01	0.04	0.02
Dy	0.25	0.48	0.26	0.21	0.18	0.33	0.14	0.15	0.24	0.10	0.06	0.24	0.13
Y	1.38	3.38	1.06	0.97	0.82	1.36	1.31	0.70	1.83	1.12	0.57	2.27	1.29
Ho	0.05	0.11	0.06	0.05	0.03	0.05	0.04	0.02	0.05	0.03	0.01	0.05	0.02
Er	0.12	0.26	0.16	0.14	0.07	0.13	0.09	0.05	0.15	0.07	0.03	0.15	0.06
Tm	0.02	0.03	0.02	0.02	0.01	0.02	0.01	0.01	0.02	0.01	0.00	0.02	0.01
Yb	0.10	0.22	0.16	0.14	0.05	0.13	0.07	0.02	0.14	0.05	0.03	0.12	0.08
Lu	0.02	0.03	0.03	0.02	0.01	0.02	0.01	0.00	0.02	0.01	0.00	0.02	0.01
Pb	0.69	0.10	0.10	0.08	0.10	0.09	0.01	0.01	0.02	0.01	0.00	0.02	0.01
Th	0.03	n.d.	0.00	0.00	0.01	0.01	n.d.	n.d.	0.00	n.d.	n.d.	n.d.	n.d.
U	0.16	n.d.	0.03	0.03	0.00	n.d.	n.d.	n.d.	n.d.	0.00	n.d.	n.d.	n.d.
Y/Ho	0.21	0.19	0.19	0.17	0.24	0.20	0.13	0.25	0.23	0.18	0.16	0.22	0.19
ΣREE	10.22	9.03	4.70	3.69	8.18	19.27	2.35	4.96	5.40	2.06	1.05	5.57	2.33
ΣREE+Y	11.60	12.41	5.76	4.66	9.00	20.63	3.66	5.66	7.23	3.18	1.62	7.83	3.62

Table 4.2 continued

Host	Vif	Vif	Vif	Vif	Vif	Vif	Vif	Vif	Vif	Vif	Vif	Vif	Vif
Phase	Dst	Dst	Dst	Dst	Dst	Dst	Qz	Qz	Qz	Qz	Qz	D1	D1
Na	34.64	102.98	243.88	72.24	55.49	79.41	262.40	81.28	2112.00	21.82	80.00	33.05	419.67
Mg	33880.26	20977.15	22864.08	49720.03	51555.88	53507.37	69.76	14.08	518.40	2.69	12.29	30392.82	22128.17
Ca	61289.02	38903.07	41917.48	101860.74	109854.87	114763.28	448.00	326.40	1088.00	161.92	225.28	53567.34	41204.17
Al	5.98	175.45	118.89	234.38	346.79	508.86	65.92	59.52	185.60	6.78	26.30	7.26	110.64
K	6.13	67.89	57.16	68.39	110.97	149.19	60.80	43.52	160.00	20.10	39.68	8.70	60.66
V	0.59	4.04	4.42	7.80	8.28	8.92	0.15	0.03	0.09	0.08	0.10	0.50	3.36
Mn	10.74	18.31	17.91	35.58	44.77	56.48	0.12	n.d.	0.71	n.d.	0.12	15.88	16.79
Fe	17.78	205.96	186.72	564.44	994.13	894.36	17.28	4.67	21.63	1.79	74.24	47.87	156.42
Rb	2.30	1.70	2.21	0.19	0.35	0.54	0.12	0.09	0.55	0.03	0.07	1.64	2.40
Sr	11.76	7.36	9.76	23.32	22.46	24.29	0.52	0.19	0.73	0.05	0.10	8.51	11.37
Ba	0.09	0.84	0.91	0.78	1.26	1.36	0.63	0.16	3.58	0.52	0.15	0.18	1.07
La	0.22	0.19	0.21	0.51	0.52	0.57	0.01	0.00	0.04	0.00	0.01	0.24	0.25
Ce	0.53	0.37	0.41	0.99	1.09	1.12	0.01	0.01	0.07	0.01	0.01	0.38	0.46
Pr	0.06	0.04	0.04	0.11	0.12	0.12	0.00	n.d.	0.02	0.00	0.00	0.04	0.05
Nd	0.19	0.16	0.17	0.36	0.39	0.42	0.01	0.00	0.03	0.00	0.00	0.13	0.18
Sm	0.04	0.03	0.02	0.07	0.07	0.06	n.d.	n.d.	0.01	0.00	n.d.	0.02	0.03
Eu	0.01	0.01	0.01	0.02	0.01	0.02	0.00	n.d.	0.00	0.00	0.00	0.00	0.01
Gd	0.02	0.02	0.02	0.06	0.05	0.06	n.d.	n.d.	0.00	n.d.	n.d.	0.01	0.02
Tb	0.00	0.00	0.00	0.01	0.01	0.01	n.d.	n.d.	0.00	n.d.	n.d.	0.00	0.00
Dy	0.01	0.02	0.01	0.04	0.05	0.05	n.d.	n.d.	0.00	0.00	n.d.	0.01	0.02
Y	0.11	0.15	0.12	0.24	0.25	0.24	0.01	0.00	0.04	0.00	0.01	0.08	0.10
Ho	0.00	0.00	0.00	0.01	0.01	0.01	n.d.	n.d.	0.00	0.00	0.00	0.00	0.00
Er	0.01	0.01	0.01	0.02	0.04	0.02	0.00	n.d.	0.00	0.00	n.d.	0.00	0.01
Tm	0.00	0.00	0.00	0.00	0.00	0.01	n.d.	n.d.	0.00	n.d.	n.d.	0.00	0.00
Yb	0.01	0.01	0.01	0.02	0.02	0.02	n.d.	n.d.	0.00	n.d.	n.d.	0.00	0.01
Lu	0.00	0.00	0.00	0.00	0.00	0.00	n.d.	n.d.	0.00	n.d.	n.d.	0.00	0.00
Pb	0.12	0.67	0.63	2.28	4.47	3.47	0.20	0.06	0.36	0.36	0.10	0.24	0.33
Th	0.01	0.20	0.15	0.64	0.74	0.51	0.00	0.00	0.01	0.00	0.00	0.02	0.13
U	0.02	0.71	0.51	2.07	2.55	1.19	0.50	0.40	0.99	1.60	0.40	0.03	0.37
Y/Ho	0.29	0.25	0.23	0.30	0.30	0.29	0.41	NA	0.68	0.20	0.21	0.28	0.25
ΣREE	1.21	1.04	1.03	2.47	2.62	2.73	0.04	0.01	0.21	0.03	0.03	0.93	1.15
ΣREE+Y	1.32	1.19	1.15	2.70	2.87	2.97	0.05	0.01	0.25	0.03	0.03	1.01	1.26

Table 4.2 continued

Host	Vif	Vif	Vif	Vif	Vif	Vif	Vif	Vif	Vif	Vif	Vif	Vif	Vif
Phase	D1	D1	D1	D1	D1	D1	D1	D1	D2	D2	D2	D2	D2
Na	7.96	29.24	115.01	31.72	15.46	33504.28	38109.40	38365.88	110.30	6.86	5.51	14.61	7.25
Mg	30458.72	53206.42	49208.27	51033.80	52280.49	9013.34	9117.94	8863.99	28907.25	41139.38	36885.23	51720.80	48229.43
Ca	55206.42	110914.04	107293.32	103680.40	108908.07	16828.46	17642.82	17620.63	51728.76	75041.27	65785.00	107133.20	95845.46
Al	6.51	8.81	28.95	6.76	15.16	2724.61	2689.85	2802.58	27.01	15.35	13.84	23.46	9.99
K	1.03	5.81	54.80	6.37	0.96	2198.00	3087.78	2994.28	12.55	0.34	1.64	9.23	1.65
V	3.58	1.33	2.85	0.83	9.74	0.33	0.36	0.34	7.53	9.10	8.82	12.04	8.81
Mn	114.22	32.89	30.49	40.32	89.25	11.52	10.25	9.71	65.80	62.47	49.43	78.83	107.85
Fe	563.49	157.73	301.04	78.61	390.47	66.51	59.77	56.59	574.34	826.60	578.00	847.14	1106.44
Rb	3.58	0.01	0.08	0.00	0.02	7.90	10.65	10.23	1.11	1.57	1.40	0.03	n.d.
Sr	17.97	21.81	18.29	22.58	25.70	11.79	12.68	12.94	4.79	7.62	6.77	11.65	9.10
Ba	0.03	0.21	0.77	0.21	0.05	69.45	82.38	82.12	0.21	0.01	0.03	0.08	0.03
La	0.31	0.29	0.45	0.49	0.58	0.66	0.71	0.73	0.11	0.13	0.13	0.39	0.20
Ce	0.61	0.56	1.02	0.83	1.11	0.97	1.19	1.18	0.48	1.06	0.95	2.35	1.14
Pr	0.07	0.05	0.10	0.08	0.12	0.12	0.13	0.13	0.07	0.16	0.15	0.36	0.18
Nd	0.22	0.17	0.44	0.28	0.37	0.44	0.47	0.48	0.27	0.69	0.65	1.38	0.65
Sm	0.02	0.03	0.08	0.04	0.06	0.07	0.09	0.08	0.04	0.12	0.12	0.24	0.10
Eu	0.01	0.01	0.02	0.01	0.02	0.06	0.06	0.06	0.01	0.01	0.01	0.03	0.01
Gd	0.02	0.02	0.07	0.03	0.05	0.09	0.08	0.09	0.03	0.08	0.09	0.18	0.07
Tb	0.00	0.01	0.01	0.01	0.01	0.01	0.01	0.01	0.00	0.01	0.01	0.02	0.01
Dy	0.02	0.01	0.04	0.02	0.03	0.07	0.08	0.08	0.03	0.04	0.05	0.09	0.04
Y	0.10	0.08	0.27	0.11	0.19	0.53	0.52	0.54	0.12	0.25	0.27	0.44	0.20
Ho	0.00	0.01	0.01	0.01	0.01	0.02	0.02	0.02	0.00	0.01	0.01	0.02	0.01
Er	0.01	0.01	0.03	0.01	0.02	0.06	0.06	0.05	0.01	0.02	0.02	0.04	0.02
Tm	0.00	0.00	0.00	0.00	0.00	0.01	0.01	0.01	0.00	0.00	0.00	0.01	0.00
Yb	0.01	0.01	0.02	0.01	0.01	0.06	0.06	0.06	0.01	0.01	0.01	0.03	0.01
Lu	0.00	0.00	0.00	0.00	0.00	0.01	0.01	0.01	0.00	0.00	0.00	0.01	0.00
Pb	0.16	0.33	1.81	0.42	0.08	1.57	2.15	2.20	0.30	0.15	0.03	0.37	0.03
Th	0.03	0.01	0.10	0.01	0.02	0.16	0.17	0.16	0.00	n.d.	n.d.	0.01	0.00
U	0.01	0.01	0.06	0.06	0.00	0.07	0.10	0.09	0.00	0.00	0.00	0.01	0.00
Y/Ho	0.30	0.32	0.24	0.30	0.33	0.27	0.27	0.28	0.24	0.23	0.23	0.26	0.27
ΣREE	1.40	1.26	2.55	1.93	2.57	3.18	3.49	3.54	1.17	2.60	2.48	5.58	2.65
ΣREE+Y	1.51	1.34	2.82	2.05	2.76	3.70	4.01	4.08	1.28	2.85	2.75	6.01	2.86

Table 4.2 continued

Host	Vif	Vif	Vif
Phase	D2	D2	D2
Na	8.11	7.75	0.88
Mg	50677.08	50296.17	48441.98
Ca	104814.66	100899.25	98958.40
Al	13.80	16.19	16.48
K	1.88	2.19	0.85
V	7.88	9.82	8.49
Mn	246.46	80.80	77.60
Fe	3237.49	1061.55	1066.80
Rb	n.d.	0.01	0.01
Sr	9.08	12.60	9.75
Ba	0.03	0.06	0.03
La	0.24	0.23	0.19
Ce	1.40	1.42	1.43
Pr	0.22	0.22	0.25
Nd	0.86	0.88	1.03
Sm	0.13	0.15	0.21
Eu	0.02	0.02	0.02
Gd	0.10	0.11	0.13
Tb	0.01	0.01	0.02
Dy	0.06	0.05	0.08
Y	0.30	0.28	0.34
Ho	0.01	0.01	0.01
Er	0.02	0.02	0.03
Tm	0.00	0.00	0.00
Yb	0.02	0.02	0.02
Lu	0.00	0.00	0.00
Pb	0.09	0.14	0.11
Th	0.00	0.02	0.01
U	0.00	0.00	0.00
Y/Ho	0.26	0.25	0.24
ΣREE	3.39	3.43	3.77
ΣREE+Y	3.69	3.70	4.12

Table 4.3. Summary table of fluid characteristics for the different phases determined using different methods. Homogenisation temperature (T_h) and fluid inclusion information from Mathieu et al., (2013a). Oxygen isotopes of Wynniatt Formation dolostone are from D. Thomson (pers. Comm.). WF – Wynniatt Formation, VIf – "Victoria Island formation", SD – saddle dolomite, BD – brown dolomite, RC – replacement calcite, LC – late-stage calcite, Qz – quartz, D1 – dolomite 1, D2 – dolomite 2, M.W. – meteoric water, S.W. – seawater, HT - hydrothermal. Parentheses indicate less probable sources.

Host	**Mineral**	**T_h (°C)**	**$\delta^{18}O$**	**REE**	**Fluid inclusion**
WF	Dolostone	--	S.W.-Siliciclastic interaction	Reduced, shale-interaction	--
	SD	105-115 Reduced HT	S.W. –Siliciclastic interaction	Reduced, shale-interaction	Siliciclastic/S.W. Assumed saline
	BD	100-117 Reduced HT	S.W.-Siliciclastic interaction	Reduced, shale-interaction	Fluid mixture Different origins/flow paths Siliciclastic-interaction Assumed saline
	RC	--	M.W. (S.W.)	Reduced/oxygenated, shale/M.W. (S.W.)	--
	LC	--	M.W. (S.W.)	Oxygenated, M.W. (S.W.)	M.W.
VIf	Dolostone	--	Siliciclastic	Reduced, shale/sulphide-interaction	--
	Quartz	120-133 Reduced HT	S.W.	Reduced?	Mixed fluid: Sulphur-rich + metalliferous fluid, shale-interaction High salinity
	D1	109-124 Reduced HT	S.W. (M.W.)	Reduced, shale-interaction	Siliciclastic/S.W. Assumed moderately saline
	D2	109-124 Reduced HT	S.W. (M.W.)	Phosphatic/Fe-oxide-rock interaction	Siliciclastic/S.W. Assumed moderately saline

CHAPTER 5 - CONCLUDING REMARKS

Paragenetic differences between chapters 3 and 4 are largely due to finer microanalyses of the different phases. Replacive calcite (RC) in the Wynniatt Formation was only recognised after SEM imagining and analyses had been done in preparation for chapter 4. Dolomite cements in the "Victoria Island formation" were only divisible into two separate cements (D1 and D2) by their different REE abundances and normalised profiles obtained with the LA ICP-MS. The subtle differences in the parageneses of these phases between the two chapters did not affect the overall interpretation of the origin of fluids, but instead helped to refine some of the earlier interpretations. No interpretations of fluid origin could be established for either of the host dolostones in chapter 3; therefore, the diagenetic history of the dolostones was established in chapter 4. Chapter 3 conclusions involved fluid interaction with an unknown terrigeneous clastic unit for the saddle dolomite (SD) and brown dolomite (BD), whereas chapter 4 refined the fluid origin to being possibly seawater that interacted with a phosphatic-shale. In chapter 3, the calcite cement was inferred to have originated from a low-salinity fluid; chapter 4 confirmed the meteoric origin of the calcite-precipitating fluid, with the addition of the inference of a changing fluid:rock ratio involving the dissolution of BD and precipitation of RC. Fluid mixing of a metalliferous fluid with a sulphur-rich fluid was inferred for quartz cement from the "Victoria Island formation" samples in both chapters 3 and 4. Framboidal pyrite associated with quartz precipitation has been inferred to have been precipitated by the mixing of a metalliferous fluid with a sulphur-rich fluid at the site of precipitation in both chap-

ters. Chapter 4 adds to this interpretation that bacterial sulphate reduction was probably the predominant mechanism for sulphate reduction. The dolomite cements in chapter 3 were treated as a single phase because of the lack of distinguishing characteristics, which became apparent after LA ICP-MS analysis. The origin of the dolomite-precipitating fluid was determined in chapter 3 to be a moderately saline, Na-dominant fluid that interacted with a K-rich reservoir (basement granite or siliciclastic equivalent). Chapter 4, with the two dolomite cements, D1 and D2, revealed that the probable source of this fluid was seawater-derived and subsequently interacted with a (phosphatic-) shale unit at depth, and the two REE patterns that distinguish the two cements were the product of changing fluid:rock ratio. The dolomite fluid inclusion data from chapter 3 were assumed to represent both D1 and D2 in chapter 4 because the range in homogenisation temperature (T_h) is seen both within a single crystal and between other crystals; it is assumed that at least some of the fluid inclusion assemblages (FIA) would have been from both cement types.

Both chapters 3 and 4 indicate similarities to known carbonate-hosted MVT deposits with regards to diagenetic setting and history, and suggest that further study of Victoria Island sedimentary rocks may be merited. Further work on outstanding issues could include: (1) better defining whether the cement-precipitating fluid was hydrothermal or not; (2) establishing the genetic relationships between possible fluid-movement mechanisms (e.g., tectonics or thermal); and (3) quantifying with absolute dating the timing of fluid movement and upgrading the burial history of the units studied.

REFERENCES

Adams, J.J., Rostron, B.J., Mendoza, C.A., 2000. Evidence for two-fluid mixing at Pine Point, NWT. *Journal of Geochemical Exploration* **69-70**, 103-108.

Alibo, D.S., Nozaki, Y., 1999. Rare earth elements in seawater: Particle association, shale normalization and Ce oxidation. *Geochimica et Cosmochimica* Acta, **63(3/4)**, 363-372.

Andrews, J.E., Hamilton, P.J., Fallick, A.E., 1987. The geochemistry of early diagenetic dolostones from a low-salinity Jurassic lagoon. *Journal of the Geological Society of London*, **144**, 687-698.

Anglin, C.D., Harrison, J.C., 1999. Mineral and energy resource assessment of Bathurst Island area, Nunavut. *Geological Survey of Canada Open-File* 3714.

Appold, M.S., Wenz, Z.J., 2011. Composition of ore fluid inclusions from the Viburnum Trend, Southeast Missouri District, United States: Implications for transport and precipitation mechanisms. *Economic Geology*, **106**, 55-78.

Bao, S., Zhou, H., Peng, X., Ji, F., Yao, H., 2008. Geochemistry of REE and yttrium in hydrothermal fluids from the Endeavour segment, Juan de Fuca Ridge. *Geochemical Journal* 42, 359-370.

Banner, J.L., Hanson, G.N., Meyers, W.J., 1988. Rare earth element and Nd isotopic variations in regionally extensive dolomites from the Burlington-Keokuk Formation (Mississippian): Implications for REE mobility during carbonate diagenesis. *Journal of Sedimentary Petrology* **58**, 415-432.

Bau, M., Romer, R.L., Luders, V., Dulski, P., 2003. Tracing element sources of hydrothermal mineral deposits: REE and Y distribution and Sr-Nd-Pb isoptopes in fluorite

from MVT deposits in the Pennine Orefield, England. *Mineralium Deposita* **38**, 992-1008.

Bodnar, R.J., 1993. Revised equation and table for determining the freezing point depression of H2O-NaCl solutions. *Geochimica et Cosmochimica Acta*, **57,** 689-684.

Bodnar, R.J. 2003. Introduction to fluid inclusions. In: *Fluid inclusions: Analysis and interpretation* (eds Samson I *et al.*), Short course series vol. 32. Mineralogical Association of Canada, pp. 1-8.

Bril, H., Papapanagiotou, P., Patrier, P., Lenain, J., Beaufort, D., 1996. Fluid-rock interaction in the geothermal field of Chipilapa (El Salvador): contribution of fluid-inclusion data. *European Journal of Mineralogy*, **8**, 515-531.

Bukowski, K., Galamay, A.R., Goralski, M., 2000. Inclusion brine chemistry of Badenian salt from Wieliczka. *Journal of Geochemical Exploration*, **69-70**, 87-90.

Chen, Z., Osadetz, K.G., Embry, A.F., Gao, H., Hannigan, P.K., 2000. Petroleum potential in western Sverdrup Basin, Canadian Arctic Archipelago. *Bulletin of Canadian Petroleum Geology* **48**, 323-338.

Dansgaard, W., 1964. Stable isotopes in precipitation. *Tellus*, **16(4),** 436-468.

Davies, G.R., Nassichuk, W.W., 1991. Carboniferous and Permian history of the Sverdrup Basin, Arctic Islands, In: Trettin, H.P. (Ed.), Geology of the Innuitian Orogen and Arctic Platform of Canada and Greenland, Geological Survey of Canada, Geology of Canada 3, pp 345-368.

De Baar, H.J.W., Bacon, M.P., Brewer, P.G., 1983. Rare-earth distributions with a positive Ce anomaly in the Western North Atlantic Ocean. *Nature* **301**, 324-327.

Dewing, K., Obermajer, M., 2009. Lower Paleozoic thermal maturity and hydrocarbon potential of the Canadian Arctic Archipelago. *Bulletin of Canadian Petroleum Geology* **57**, 141-166.

Dewing, K., Sharp, R.J., Turner, E., 2007a. Synopsis of the Polaris Zn-Pb district, Canadian Arctic Islands, Nunavut, In: Goodfellow, W.D. (Ed.) Mineral Deposits of Canada: A synthesis of Major deposit-types, district metallogeny, the evolution of geological provinces, and exploration methods. Geological Association of Canada, Mineral Deposits division, Special publication 5, pp. 655-672.

Dewing, K., Turner, E., Harrison, J.C., 2007b. Geological history, mineral occurrences, and mineral potential of the sedimentary rocks of the Canadian Arctic archipelago, In: Goodfellow, W.D. (Ed.) Mineral Deposits of Canada: A synthesis of Major deposit-types, district metallogeny, the evolution of geological provinces, and exploration methods. Geological Association of Canada, Mineral Deposits division, Special publication 5, pp. 733-753.

Dewing K, Pratt BR, Hadlari T, Brent T, Bedard J, Rainbird RH (2013) Newly identified "Tunnunik" impact structure, Prince Albert Peninsula, northwestern Victoria Island, Arctic Canada. *Meteorics and Planetary Sciences*, **48,** 211-223.

Dolnicek, Z., Kropac, K., Janickova, K., Urubek, T., 2012. Diagenetic source of fluids causing the hydrothermal alteration of teschenites in the Silesian Unit, Outer Western Carpathians, Czech Repupublic: Petroleum-bearing vein mineralization from the Stribrnik site. *Marine and Petroleum Geology* **37**, 27-40.

Elderfield, H., 1988. The oceanic chemistry of the rare-earth elements. *Philosophical Transactions of the Royal Society of London* A **325**, 105-126.

Embry, A.F., 1991a. Middle-Upper Devonian clastic wedge of the Arctic Islands, In: Trettin, H.P. (Ed.), Geology of the Innuitian Orogen and Arctic Platform of Canada and Greenland, Geological Survey of Canada, Geology of Canada 3, pp. 261-291.

Embry, A.F., 1991b. Mesozoic history of the Arctic Islands, In: Trettin, H.P. (Ed.), Geology of the Innuitian Orogen and Arctic Platform of Canada and Greenland, Geological Survey of Canada, Geology of Canada 3, pp. 369-433.

Embry, A.F., Dixon, J., 1992. The breakup unconformity of the Amerasia Basin, Arctic Ocean: Evidence from Arctic Canada. *Geological Society of America Bulletin* **102**, 1526-1534.

Fischer, B.J., 2012. Carbonate-hosted Zn-Pb mineralization in the Lower Cambrian Sekwi Formation, Mackenzie Mountains, NWT: Stratigraphic, structural, and lithologic controls, and constraints on ore fluid characteristics. Unpublished M.Sc. Thesis, Laurentian University, Sudbury, Ontario, 281 p.

Forsyth, D.A., Mair, J.A., Fraser, I., 1979. Crustal structure of the central Sverdrup Basin. *Canadian Journal of Earth Science*, **16**, 1581-1598.

Gentzis, T., Goodarzi, F., Embry, A.F., 1996. Thermal maturation, potential source rocks and hydrocarbon generation in Mesozoic rocks, Lougheed Island area, Central Canadian Arctic archipelago. *Marine and Petroleum Geology,* **13,** 879-905.

German, C.R., Masuzawa, T., Greaves, M.J., Elderfield, H., Edmond, J.M., 1995. Dissolved rare earth elements in the Southern Ocean: Cerium oxidation and the influence of hydrography. *Geochimica et Cosmochimica Acta* **59**, 1551-1558.

Goldstein, R.H., 1990. Petrographic and geochemical evidence for origin of paleospeleothems, New Mexico: implications for the application of fluid inclusions to studies of diagenesis. *Journal of Sedimentary Petrology*, **60**, 282-292.

Goldstein, R.H., Reynolds, T.J., 1994. Systematics of fluid inclusions in diagenetic minerals. Society for Sedimentary Geology Short Course 31, 199 p.

Grasby, S.E., Chen, A., Dewing, K., 2013. Formation water geochemistry of the Sverdrup Basin: Implications for hydrocarbon development in the High Arctic. *Applied Geochemistry*, **27**, 1623-1632.

Haeri-Ardakani, O., Al-Aasm, I., Coniglio, M., 2013. Fracture mineralization and fluid flow evolution: an example from Ordovician-Devonian carbonates, southwestern Ontario, Canada. *Geofluids,* **13**, 1-20.

Hanor, J.S., 1994. Origin of saline fluids in sedimentary basins. *In* Geofluids: Origin, migration and evolution of fluids in sedimentary basins (J. Parnell, ed.). *Geological Society Special Publication* **78,** 151-174.

Harrison JC (1994) Melville Island and adjacent smaller islands, Canadian Arctic Archipelago. M*ap 1844A* 1:250000 Geological Survey of Canada.

Harrison, J.C., Dewing, K., Lee, C.C., Stasiuk, L.D., 1999. New mineral occurrences on northeastern Ellesmere Island and new opportunities for mineral exploration in Northern Nunavut. *Geological Survey of Canada Open-File Report* 3822, 43 p.

Harrison, J.C., Ford, A., Miall, A.D., Rainbird, R.H., Hulbert, L.J., Christie, R.L., Cambell, F.H.A., 2013. Geology, Tectonic assemblage map of Aulavik, Banks Island and northwestern Victoria Island, Northwest Territories. Geological Survey of Canada Canadian Geoscince Map 35 (preliminary), scale 1:500 000.

Haynes, F.M., Kesler, S.E., 1987. Chemical evolution of brines during Mississippi Valley-Type mineralization: evidence from East Tennessee and Pine Point. *Economic Geology,* **82**, 53-71.

Haynes, F.M., Sterner, S.M., Bodnar, R.J., 1988. Synthetic fluid inclusions in natural quartz. IV. Chemical analyses of fluid inclusions by SEM/EDA: Evaluation of method. *Geochimica et Cosmochimica Acta,* **52**, 969-977.

Heaman, L.M., Lecheminant, A.N., Rainbird, R.H., 1992. Nature and timing of Franklin igneous events, Canada: implications for a late Proterozoic mantle plume and the break-up of Laurentia. *Earth and Planetary Science Letters,* **109**, 117-131.

Heba, G., Princhonnet, G., Albani, A., 2009. Meteoric diagenesis of Upper Cretaceous and Paleocene-Eocene shallow-water carbonates in the Kruja Platform (Albania): geochemical evidence. *Geologica Carpathica*, **60**, 165-179.

Heinrich, C.A., Cousens, D.R., 1989. Semi-quantitative electron microprobe analysis of fluid inclusion salts from the Mount Isa copper deposit (Queensland, Australia). *Geochimica et Cosmochimica Acta*, **53**, 21-28.

Hitchon, B., Krouse, H.R., 1972. Hydrogeochemistry of surface waters of the Mackenzie River drainage basin Canada, III. Stable isotopes of oxygen, carbon, and sulfur. *Geochimica et Cosmochimica Acta*, **36**, 1337-1358.

Jober, S., Dewing, K., White, J.C., 2007. Structural geology and Zn-Pb mineral occurrences of northeastern Cornwallis Island: implications for exploration of the Cornwallis Fold Belt, northern Nunavut. *Bulletin of Canadian Petroleum Geology* **55**, 138-159.

Jones, D.S., Maloof, A.C., Hurtgen, M.T., Rainbird, R.H., Schrag, D.P., 2010. Regional and global chemostratigraphic correlation of the early Neoproterozoic Shaler Supergroup, Victoria Island, Northwestern Canada. *Precambrian Research*, **181**, 43-63.

Jørgensen, B.B., Isaksen, M.F., Jannasch, H.W., 1992. Bacterial sulphate reduction above 100°C in deep-sea hydrothermal vent sediments. *Science*, **258**, 1756-1757.

Kawabe, I., Toriumi, T., Ohta, A., Miura, N., 1998. Monoisotopic REE abundances in seawater and the origin of seawater tetrad effect. *Geochemical Journal*, **32**, 213-229.

Kerr, J.M., 1967a. Stratigraphy of central and eastern Ellesmere Island, Arctic Canada; part 1, Proterozoic and Cambrian. Geological Survey of Canada Paper, 63p.

Kerr, J.M., 1967b. Nares submarine rift valley and the relative rotation of North Greenland. *Bulletin of Canadian Petroleum Geology*, **15**, 483-520.

Kerr, J.M., 1977a. Cornwallis Fold Belt and the mechanism of basement uplift. *Canadian Journal of Earth Science*, **14**, 1374-1401.

Kerr, J.M., 1977b. Cornwallis Lead-Zinc District; Mississippi Valley-type deposits controlled by stratigraphy and tectonics. *Canadian Journal of Earth Science*, **14**, 1402-1426.

Kesler SE, Reich M, Jean M (2007) Geochemistry of fluid inclusion brines from Earth's oldest Mississippi Valley-type (MVT) deposits, Transvaal Supergroup, South Africa. *Chemical Geology*, **237,** 274-288.

Kontak, D.J., 1995. A study of fluid inclusions in sulfide and nonsulfide mineral phases from a carbonate-hosted Zn-Pb deposit, Gays River, Nova Scotia, Canada. *Economic Geology*, **93,** 793-817.

Kontak, D.J., 2004. Analysis of evaporate mounds as a complement to fluid-inclusion thermometric data: case studies from granitic environments in Nova Scotia and Peru. *The Canadian Mineralogist*, **42,** 1315-1329.

Kontak, D.J., 2013. Fluid inclusion evaporate mound analysis: A rapid, efficient and informative means of determining fluid chemistry in hydrothermal systems. *Atlantic Geology*, **49**, p. 34

Kontak, D.J., Jackson, S., 1995. Laser-ablation ICP-MS micro-analysis of calcite cement from a Mississippi-valley-type Zn-Pb deposit, Nova Scotia: Dramatic variability in REE content on macro- and micro-scales. *The Canadian Mineralogist* **33**, 445-467.

Leybourne, M.I., Goodfellow, W.D., Boyle, D.R., Gwendy, M.H., 2000. Rapid development of negative Ce anomalies in surface waters and contrasting REE patterns in groundwaters associated with Zn-Pb massive sulphide deposits. *Applied Geochemistry*, **15**, 695-723.

Lloyd, J.R., Williams, D.R., Macaskie, L.E., 2001. Metal reduction by sulphate-reducing bacteria: physiological diversity and metal specificity. *Hydrometallurgy*, **59**, 327-337.

Long, D.G.F., Rainbird, R.H., Turner, E.C., MacNaughton, R.B., 2008. Early Neoproterozoic strata (Sequence B) of mainland northern Canada and Victoria and Banks islands: a contribution to the Geological Atlas of the Northern Canadian Mainland Sedimentary Basin. *Geological Survey of Canada, Open File* 5700 27p.

Lonnee, J., Machel, H.G., 2006. Pervasive dolomitization with subsequent hydrothermal alteration in the Clarke Lake gas field, Middle Devonian Slave Point Formation, British Columbia, Canada. *The American Association of Petroleum Geologists Bulletin,* **90,** 1739-1761.

Lowenstein, T.K., Timofeef, M.N., Kovalevych, V.M., Horita, J., 2005. The major-ion composition of Permian seawater. *Geochimica et Cosmochimica Acta,* **69**, 1701-1719.

Machel, H.G., 2001. Bacterial and thermochemical sulfate reduction in diagenetic settings – old and new insights. *Sedimentary Geology*, **140**, 143-175.

Machel, H.G., Krouse, H.R., Sassen, R., 1995. Products and distinguishing criteria of bacterial and thermochemical sulfate reduction. *Applied Geochemistry*, **10**, 373-389.

Machel, H.G., Buschkuehle, B.E., 2008. Diagenesis of the Devonian Southesk-Cairn complex, Alberta, Canada: Marine cementation, burial dolomitisation, thermochemical sulfate reduction, anhydritization, and squeegee fluid flow. *Journal of Sedimentary Research,* **78**, 366-389.

Madden, R.H.C., Wilson, M.E.J., 2012. Diagenesis of Neogene delta-front patch reefs: alteration of coastal, siliciclastic-influenced carbonates from humid equatorial regions. *Journal of Sedimentary Research*, **82**, 871-888.

Mathieu, J., Turner, E.C., Rainbird, R.H., 2013a. Sedimentary architecture of a deeply karsted Precambrian-Cambrian unconformity, Victoria Island, Northwest Territories. Geological Survey of Canada Current Research 2013-1, 1-15.

Mathieu, J., Kontak, D.J., Turner, E.C., 2013b. A fluid inclusion study of diagenetic fluids in Proterozoic and Paleozoic carbonate rocks, Victoria Island, NWT. *Geolfuids*, **13**(4), 559-578.

McCaffrey MA, Lazar B, Holland HD (1987) The evaporation path of sea water and the coprecipitation of Br- and K+ with halite. *Journal of Sedimentary Petrology*, **57,** 928-937.

McCurdy, M.W., McNeil, R.J., Day, S.J.A., 2013. Geochemical, mineralogical and kimberlite indicator mineral data for silts, heavy mineral concentrates and waters from two geochemical surveys (2010 and 2011) on Victoria Island, Northwest territories (NTS 87G, 87H, 88A and 88B). *Geological Survey of Canada Open-file* 7198, 16 p.

McNaughton, K., Smith, T.E., 1986. A fluid inclusion study of sphalerite and dolomite from the Nanisivik lead-zinc deposit, Baffin Island, Northwest Territories, Canada. *Economic Geology*, **81**, 713-720.

Miall, A.D., 1976. Devonian geology of Banks Isalnd, Arctic Canada, and its bearing on the tectonic development of the circum-Arctic region. *Geological Society of America Bulletin*, **87**, 1599-1608.

Miall A.D., 1979 Mesozoic and Tertiary geology of Banks Island, Arctic Canada, the history of an unstable craton margin. *GSC Memoir* **387**, 235 p.

Miall, A.D., 1986. Effects of Caledonian tectonism in Arctic Canada. *Geology*, **14**, 904-907.Miall, A.D., 1991. Late Cretaceous and Tertiary basin development and sedimentation, Arctic islands, In: Trettin, H.P. (Ed.), Geology of the Innuitian Orogen and Arctic Platform of Canada and Greenland, Geological Survey of Canada, Geology of Canada 3, pp 437-458.

Moreau, J.W., Weber, P.K., Martin, M.C., Gilbert, B., Huteon, I.D., Banfield, J.F., 2007. Extracellular proteins limit the dispersal of biogenic nanoparticles. *Science*, **316**, 1600-1603.

Morris, G.A., Page, L., Martinez, V., 2005. New dates (415 Ma) for the Etive Dyke Swarm and the end of the Caledonian Orogeny in the SW Grampian Highlands of Scotland. *Journal of the Geological Society of London*, **162**, 741-744.

Nothdurft, L.D., Webb, G.E., Kamber, B.S., 2004. Rare earth element geochemistry of Late Devonian reefal carbonates, Canning Basin, Western Australie: Confirmation of a seawater REE proxy in ancient limestones. *Geochimica et Cosmochimica Acta* **68**, 263-283.

Nozaki, Y., Zhang, J., Amakawa, H., 1997. The fractionation between Y and Ho in the marine environment. *Earth and Planetary Science Letters*, **148**, 329-340.

Oakley, G.N., Stephenson, R., 2008. Crustal structure of the Innuitian region of Arctic Canada and Greenland from gravity modelling: implications for the PAleogene Eurekan Orogen. *Geophysics Journal International*, **173**, 1039-1063.

Obermajer, M., Dewing, K., Fowler, M.G., 2010. Geochemistry of crude oil from Bent Horn field (Canadian Arctic Archipelago) and its possible Paleozoic origin. *Organic Geochemistry*, **41**, 986-996.

Ohfuji, H., Rickard, D., 2005. Experimental synthesis of framboids – a review. *Earth Science Reviews*, **71,** 147-170.

Ohmoto, H., Rye, R.O., 1979. Isotopes of sulfur and carbon, *in* Barnes, H.L., editor, Geochemistry of Hydrothermal Ore Deposits, 2nd edition, New York, USA, Wiley, p. 509-567.

Okulitch, A.V., Trettin, H.P., 1991. Late Cretaceous – Early Tertiary deformation, Arctic Islands, In: Trettin, H.P. (Ed.), Geology of the Innuitian Orogen and Arctic Platform of Canada and Greenland, Geological Survey of Canada, Geology of Canada 3, pp. 469-490.

Okulitch, A.V., Packard, J.J., Zolnai, A.I., 1991. Late Silurian - Early Devonian deformation of the Boothia Uplift, In: Trettin, H.P. (Ed.), Geology of the Innuitian Orogen and

Arctic Platform of Canada and Greenland, Geological Survey of Canada, Geology of Canada 3, pp. 302-307.

O'Leary, M.H., 1981. Carbon isotope fractionation in plants. *Phytochemistry*, **20**, 553-567.

Oliver, G.J.H., 2001. Reconstruction of the Grampian episode in Scotland: its place in the Caledonian Orogeny. *Tectonophysics*, **332**, 23-49.

Orr, W.L., 1974. Changes in sulfur content and isotopic ratios of sulfur during petroleum maturation: Study of Big Horn Basin Paleozoic oils. *AAPG Bulletin*, **58**, 2295-2318.

Pourmand, A., Dauphas, N., Ireland, T.J., 2012. A novel extraction chromatography and MC-ICP-MS technique for rapid analysis of REE, Sc and Y: Revising Cl-chondrite and Post-Archean Australian Shale (PAAS) abundances. *Chemical Geology*, **291**, 38-54.

Qing, H., 1998. Petrography and geochemistry of early-stage, fine- and medium-crystalline dolomites in the Middle Devonian Presqu'ile Barrier at Pine Point, Canada. *Sedimentology*, **45**, 433-446.

Qing, H., Mountjoy, E.W., 1994. Rare earth element geochemistry of dolomites in the Middle Devonian Presqu'ile barrier, Western Canada Sedimentary Basin: implications for fluid-rock ratios during dolomitisation. *Sedimentology*, **41**, 787-804.

Rainbird, R.H., 1991. Stratigraphy, sedimentology, and tectonic setting of the upper Shaler Group, Victoria Island, Northwest Territories; Unpublished Ph.D. Thesis, University of Western Ontario, London, Ontario.

Rainbird, R.H., Jefferson, C.W., Hildebrand, R.S., Worth, J.K. 1994. The Shaler Supergroup and revision of Neoproterozoic stratigraphy in Amundsen Basin, Northwest

Territories; in Current Research, Part C; Geological Survey of Canada, Paper 94-01C, 61-70.Rainbird, R.H., Jefferson, C.W., Young, G.M., 1996. The early Neoproterozoic sedimentary Succession B of northwestern Laurentian: Correlations and paleo-geographic significance. *GSA Bulletin*, **108 (4)**, 454-470.

Rainbird, R.H., LeCheminant, A.N., Lawyer, I., 1997. Geology, Duke of York Inlier, Victoria Island, Northwest Territories (part of NTS 77B), *Geological Survey of Canada Open-file* 3304, scale 1:100000.

Rayner, N.M., Rainbird, R.H., 2013. U—Pb Geochronology of the Shaler Supergroup, Victoria Island, northwest Canada: 2009-2013. *Geological Survey of Canada Open-file* 7419, 59 p.

Reid, S., Dewing, K., Sharp, R., 2013. Polaris as a guide to northern exploration: Ore textures, paragenesis and the origin of the carbonate-hosted Polaris Zn-Pb Mine, Nunavut, Canada. *Ore Geology Reviews*, **51**, 27-42.

Reis, M.A.M., Almeida, J.S., Lemos, P.C., Carrondo, M.J.T., 1992. Effect of hydrogen sulfide on growth of sulfate reducing bacteria. *Biotechnology and Bioengineering*, **40**, 593-600.

Riciputi, L.R., Cole, D.R., Machel, H.G., 1996. Sulfide formation in reservoir carbonates of the Devonian Nisku Formation, Alberta, Canada: An ion microprobe study. *Geochimica et Cosmochimica Acta*, **60(2)**, 325-336.

Roedder, E., 1968. Temperature, salinity, and origin of the ore-forming fluids at Pine Point, Northwest Territories, Canada, from fluid inclusion studies. *Economic Geology*, **63,** 439-450.

Roedder, E., 1984. Fluid inclusions: an introduction to studies of all types of fluid inclusions, gas, liquid or melt, trapped in materials from earth and space, and their application to the understanding of geologic processes (ed Roedder E), Vol. 12. Mineralogical Society of America, Washington, DC, pp. 644.

Roedder, E., Bodnar, R.J., 1980. Geological pressure determinations from fluid inclusion studies. *Annual Review of Earth and Planetary Sciences*, **8**, 263-301.

Sangster, D.F., 1998. Mineral deposits compilation and metallogenic domains, northern Baffin Island and northern Melville Peninsula, Northwest Territories. Geological Survey of Canada Open File 3635, 1:1 000 000.

Savard, M.M., Chi, G., 1998. Cation study of fluid inclusion decrepitates in the Jubilee and Gays River (Canada) Zn-Pb deposits – Characterization of ore-forming brines. *Economic Geology*, **93,** 920-931.

Savard, M.M., Chi, G., Sami, T., Williams-Jones, A.E., Leigh, K., 2000. Fluid inclusion and carbon, oxygen, and strontium isotope study of the Polaris Mississippi Valley-type Zn-Pb deposit, Canadian Arctic Archipelago: implications for ore genesis. *Mineralium Deposita*, **35**, 495-510.

Seal, R.R., 2006. Sulfur isotope geochemistry of sulfide minerals. *Reviews in Mineralogy and Geochemistry*, **61**, 633-677.

Shepherd, T.J., Ayora, C., Cendon, D.I., Chenery, S.R., Moissette, A., 1998. Quantitative solute analysis of single fluid inclusions in halite by LA-ICP-MS and cryo-SEM-EDS: complementary microbeam techniques. *European Journal of Mineralogy*, **10**, 1097-1108.

Stetter, K.O., Huber, R., Blöchl, E., Kurr, M., Eden, R.D., Fielder, M., Cash, H., Vance, I., 1993. Hyperthermophilic archaea are thriving in deep North Sea and Alaskan oil reservoirs. *Nature*, **365**, 743-745.

Tanaka K., Kawabe, I., 2006. REE abundances in ancient seawater inferred from marine limestone and experimental REE partition coefficients between calcite and aqueous solution. *Geochemical Journal*, **40**, 425-435.

Tang, H., Chen, Y., Santosh, M., Zhong, Hong, Yang, T., 2013. REE geochemistry of carbonates from the Guanmenshan Formation, Liaohe Group, NE Sino-Korean Craton: implications for seawater compositional change during the Great Oxidation Event. *Precambrian Research*, **227**, 316-336.

Tegner, C., Storey, M., Holm, P.M., Thorarinsson, S.B., Zhao, X., Lo, C.H., Knudsen, M.F., 2011. Magmatism and Eurekan deformation in the High Arctic large igneous provenince: 40Ar-39Ar age of Kap Waashington Group volcanic, North Greenland. *Earth and Planetary Science Letters*, **303**, 203-214.

Thomson, D., Rainbird, R.H., Dix, G., in press. Architecture of a Neoproterozoic (Cryogenian) intracratonic carbonate ramp (Wynniatt Formation, Shaler Supergroup) in an immense intracratonic basin: Ancestral patterns for Paleozoic platforms. *Sedimentary Geology*, in press. 48 p.

Thorsteinsson, R., Tozer, E.T., 1962. Banks, Victoria, and Stefansson Islands, Arctic archipelago. *Geological Survey of Canada Memoir* **330**, 85 p.

Trettin, H.P., 1991. Middle and Late Tertiary tectonic and physiographic developments, In: Trettin, H.P. (Ed.), Geology of the Innuitian Orogen and Arctic Platform of Canada and Greenland, Geological Survey of Canada, Geology of Canada 3, pp 493-496.

Trettin, H.P., Mayr, U., Long, D.G.F., Packard, J.J., 1991. Cambrian to Early Devonian basin development, sedimentation and volcanism, In: Trettin, H.P. (Ed.), Geology of the Innuitian Orogen and Arctic Platform of Canada and Greenland, Geological Survey of Canada, Geology of Canada 3, pp. 163-238.

Turner, E.C., 2001. Investigation of zinc-lead mineralization on eastern Cornwallis Island, Arctic Archipelago, Nunavut. *Geological Survey of Canada Current Research* 2001-B2, 10p.

Turner, E.C., 2011. Structural and stratigraphic controls on carbonate-hosted base-metal mineralization in the Mesoproterozoic Borden Basin (Nanisivik District), Nunavut. *Economic Geology*, **106,** 1197-1223.

Turner, E.C., Dewing, K., 2004. Geology of Little Cornwallis Island and Rookery Creek (Cornwallis Island), Nunavut. *GSC Open File* **1780**, scale 1:50,000.

Tweedale, F., Hanley, J., Kontak, D.J., Rogers, N., 2013. Evaporate analysis of quartz-hosted fluid inclusions by SEM/EDS: Evaluation and application of the method to assess granite metal fertility. Geological Association of Canada-Mineralogical Association of Canada Annual Meeting, Program with Abstracts, vol. 37.

Valley, J.W., Graham, C.M., 1991. Ion microprobe analysis of oxygen isotope ratios in granulite facies magnetites; diffusive exchange as a guide to cooling history. *Contributions to Mineralogy and Petrology*, **109**, 38-52.

Veizer, J., Bruckschen, P., Pawellek, F., Diener, A., Podlaha, O.G., Carden, G.A., Jasper, T., Korte, C., Strauss, H., Azmy, K., Ala, D., 1997. Oxygen isotope evolution of Phanerozoic seawater. *Palaeogeography, Palaeoclimatology, Palaeoecology*, **132**, 159-172.

Veizer, J., Ala, D., Azmy, K., Bruckschen, P., Buhl, D., Bruhn, F., Carden, G.A.F., Diener, A., Ebneth, S., Godderis, Y., Jasper, T., Korte, C., Pawellek, F., Podlaha, O.G., Strauss, H., 1999. $^{87}Sr/^{86}Sr$, $\delta^{13}C$ and $\delta^{18}O$ evolution of Phanerozoic seawater. *Chemical Geology*, **161**, 59-88.

Wheat, C.G., Mottl, M.J., Rudnicki, M., 2002. Trace element and REE composition of a low-temperature ridge-flank hydrothermal spring. *Geochimica et Cosmochimica Acta,* **66(21)**, 3693-3705.

Wilkinson, J.J., Crowther, H.L., Coles, B.J., 2011. Chemical mass transfer during hydrothermal alteration of carbonates: Controls of seafloor subsidence, sedimentation and Zn-Pb mineralization in the Irish Carboniferous. *Chemical Geology,* **289**, 55-75.

Worden, R.H., Smalley, P.C., 1996. H_2S-producing reactions in deep carbonate gas reservoirs: Khuff Formation, Abu Dhabi. *Chemical Geology*, **133**, 157-171.

Young, G.M., 1981. The Amundsen Embayment, Northwest Territories; relevance to the upper Proterozoic evolution of North America; *Geological Survey of Canada, Paper* **81.** p. 203-218.